Abstract

The supply of nitrogen to the sunlit subtropical Atlantic constrains phytoplankton growth and levels of new production. Over the Atlantic, the traditional supplies of nitrogen to the surface ocean through atmospheric deposition and the vertical supply of nitrate from the deep ocean are insufficient to account for the export production diagnosed from geochemical tracers. The principle aims of this study were to: 1) examine the physical structure and nutrient dynamics of the Atlantic Ocean and 2) assess the alternative supplies of nitrogen to the Atlantic Ocean by: a) N_2 fixation by cyanobacteria, b) horizontal advection of organic nutrients and c) fine-scale upwelling of nutrients from the deep ocean initiated by a variety of mechanisms. This study was performed as part of the Atlantic Meridional Transect (AMT) cruise programme, which samples the Atlantic Ocean during the boreal Spring (April/May) and Autumn (September/October) between the 50ºN and 35ºS on board the *RRS James Clark Ross.*

Using the extensive temperature (T), salinity (S) and density (σ_t) data set collected during the AMT programme since 1995, the spatial and temporal variability of the physical structure of the surface Atlantic (< 250m) was examined. In addition, the mixed layer depth (MLD), Ekman transport, and oceanic boundaries, were also determined. Overall, seasonal rather than interannual variability in T, S and σ_t, the MLD and Ekman transport were more obvious. The mixed layer depth tended to reflect winter mixing during spring and summer stratification during autumn. Comparison of the climatologically diagnosed physical supply of nutrients and phytoplankton biomass revealed that while convection is important in supplying nutrients over the flanks of the gyres, horizontal advection is important in the transferring nutrients into the gyres. Sea surface properties, the mixed layer depth and the Ekman transport field were found to show a weak relationship with the atmospheric North Atlantic Oscillation index. Additionally, the oceanic boundaries tended to vary according to the method used to determine their position.

Nitrate and phosphate data collected during the AMT programme was used to assess if the Atlantic is nitrogen or phosphorus limited. Average nitrate to phosphate ratios and the diagnosed parameter, N*, showed that while there is excess nitrate in the north Atlantic, there is excess phosphate in the south Atlantic. Mechanisms explaining this pattern, such as N_2 fixation and differential remineralision and nitrogen and phosphorus, are discussed. In addition, it was found that the nitrate to phosphate ratio determined by statistical correlations were inaccurate.

Using independent biogeochemical proxies, namely stable nitrogen isotopic composition of phytoplankton (δ^{15}N PON), dissolved organic nutrients, amino acids and phytopigments, the supplies of nitrogen to phytoplankton in the surface Atlantic was assessed using samples collected in AMT 10 during April/May 2000. The later stages of a spring phytoplankton bloom, during which nitrate was in excess, was observed in the northern subpolar region, being dominated by eukaryotic nanoflagellates. Over the northern subtropical gyre, isotopically light phytoplankton, the presence of cyanobacteria and elevated nitrate to phosphate ratios implied a localised region of N_2 fixation. It is speculated that the temporal and spatial distribution of N_2 fixation in this region may be controlled by inputs of aeolian dust from the Sahara, causing iron and possibly phosphorus fertilisation, elements which limit N_2 fixation. Over the remainder of the transect, isotopically heavy PON implies that phytoplankton are utilising a heavy source of nitrogen, probably nitrate from the deep ocean. Over subtropical gyres, this supply is probably achieved by transient, fine-scale upwelling, augmented by lateral transfer over the flanks and convection at high latitudes. Latitudinal variation in DON is inconclusive as no clear gradients were observed. However, sharp gradients in DOP and minima in the north and south subtropical gyres were observed. These contrasting distributions may be explained by the elevation of the DON pool through N_2 fixation or the consequence of any transient upwelling providing an enhanced supply of refractory organic nitrogen. The magnitude of export production sustained by the horizontal advection of inorganic and organic nutrients was also assessed.

Contents

Abbreviations

α	kinetic isotope fractionation factor
A	peak area
ALOHA	A Long Term Oligotrophic Habitat Assessment
AMT	Atlantic Meridional Transect
BATS	Bermuda Atlantic Time Series
BSA	albumin bovine serum
C	concentration
Chl *a*	chlorophyll *a*
CRM	Certified reference materials
CTD	conductivity, temperature, depth
CV	coefficient of variation
$\delta^{13}C$	stable carbon isotope
$\delta^{15}N$	stable nitrogen isotope
D	density
Da	daltons
DCM	deep chlorophyll maximum
DCM	dichloromethane
DCU	data collection unit
DFAA	dissolved free amino acids
DIC	dissolved inorganic carbon
DIN	dissolved inorganic nitrogen
DOC	dissolved organic carbon
DON	dissolved organic nitrogen
DOP	dissolved organic phosphorus
EA-IRMS	elemental analyser-isotope ratio mass spectrometry
EDTA	Ethylenediaminetetra-acetic acid
ε	enrichment factor
ER	equatorial region
GAY	glycine, alanine, threonine
GF/F	glass fibre filters fine (0.7 μm)
GLY	glycine
HOTS	Hawaii Ocean Time Series
HPLC	high performance liquid chromatography
HTCO	high temperature catalytic oxidation
ITCZ	Inter Tropical Convergence Zone
KHP	potassium hydrogen phthalate
L	litres
LNSW	low nutrient seawater
MeOH	methanol
mL	millilitres
μL	microlitres
MLD	mixed layer depth
MM	millimolar
μM	micromolar
μm	micron
MW	molecular weight
N	nitrogen
N_2	dinitrogen

N_2O	nitrous oxide7
NO	nitric oxide
NASG	north Atlantic subtropical gyre
NEED	N-1-Naphthylethylenediamine dihydrochloride
NH_4^+	ammonium
$(NH_2)_2CO$	urea
NO_2^-	nitrite
NO_3^-	nitrate
‰	parts per thousand
OPA	*o*-Phthalaldehyde
POC	particulate organic carbon
PON	particulate organic nitrogen
PO_4^{3-}	phosphate
R_f	response factor
S	salinity
SASG	south Atlantic subtropical gyre
SeaWiFS	Sea-viewing Wide Field-of-view Sensor
SPM	suspended particulate matter
SPR	subpolar region
SRP	soluble reactive phosphate
SSD	sea surface density
SST	sea surface temperature
SSS	sea surface salinity
T	temperature
TDN	total dissolved nitrogen
TDP	total dissolved phosphorus
THAA	total hydrolysable amino acids
TOC	total organic carbon
TOMS	total ozone mapping spectrometry
UV	ultraviolet
UW	underway
V	fraction of unutilised substrate
W	watts
$\bar{x}$	mean
σ	standard deviation
σ_t	density (sigma t)
Z_N	nitracline
Z_P	phosphocline
Z_T	thermocline

1.1. INTRODUCTION

1.1.1. The Marine Nitrogen cycle

Nitrogen is a key element of many biogeochemical processes and an essential macronutrient for growth of marine phytoplankton. Nitrogen (N) enters the marine environment through wet and dry atmospheric deposition (Prospero *et al.*, 1996), biological nitrogen fixation (Lipschultz and Owens, 1996) and through riverine inputs (Walsh *et al.*, 1981). Once in the marine environment, N occurs in 3 states; **1)** gaseous nitrogen as dinitrogen (N_2), nitrous oxide (N_2O) and nitric oxide (NO), **2)** inorganic nitrogen as nitrate (NO_3^-), nitrite (NO_2^-) and ammonium (NH_4^+) and **3)** organic nitrogen as urea ($(NH_2)_2CO$), dissolved organic nitrogen (DON) and particulate organic nitrogen (PON), the latter representing plankton biomass and organic detritus. Chemical and microbially mediated processes transform these N pools by a series of oxidation and reduction reactions (Figure 1.1).

Dinitrogen gas (N_2) is the most abundant form of N in the marine environment, N_2 concentrations ($[N_2]$) in the surface ocean being relatively uniform (~ 1mM; Sharp, 1983) and controlled by temperature, salinity and atmospheric pressure (Scranton, 1983). In general, N_2 is biologically unavailable, except for certain specific groups of N_2-fixing marine organisms, which produce both DON and PON.

Nitrate (NO_3^-) is the most abundant form of reactive N or biologically labile N in the marine environment. NO_3^- concentrations ($[NO_3^-]$) are highest in coastal seas (<200μM; Sharp, 1983) and the sub-thermocline (15-25 μM; Michaels *et al.*, 1996) and lowest in the tropical surface ocean (~ 0.05 μM; Michaels *et al.*, 1996) and are seasonally controlled by biological processes (Mann and Lazier, 1997). NO_3^- is lost from the marine environment through denitrification, the prokaryotic reduction (black arrow; Figure 1.1) of NO_3^- to N_2 (Delwiche, 1970). Denitrification is largely confined to

subsurface waters of the sediments of the continental margins and subsurface waters of the open ocean, where a combination of low O_2 supply and high surface productivity can create anoxic environments.

Nitrite (NO_2^-) is less abundant than NO_3^-, NO_2^- concentrations ($[NO_2^-]$) ranging from 0.1μM to 10 μM in the open ocean and coastal regions, respectively (Sharp, 1983). Subsurface maxima in $[NO_2^-]$ are observed due to the excretion of nitrite by phytoplankton and differential inhibition of nitrification (white arrows; Figure 1.1), the bacterially mediated oxidation of ammonium to NO_3^- (Dore and Karl, 1996). NO_2^- is also an intermediate product of denitrification, and thus, NO_2^- is an important marker for transformation processes.

Ammonium and ammonia concentrations ($[NH_4^+]$ and $[NH_3]$, respectively) are generally low in the open ocean (< 1 μM; Sharp, 1983), increasing in coastal waters (< 100 μM: Sharp, 1983). NH_4^+ is the most biologically available reduced-N species. Oxidised forms of N (*e.g.* NO_3^- and NO_2^-) are transformed through a series of enzymatic reactions involving NO_3^- and NO_2^- reductase (black arrows; Figure 1.1) to NH_4^+ before assimilation by phytoplankton (Falkowski, 1983).

Dissolved organic nitrogen (DON) is the most abundant form of reduced-N in the open ocean (~ 4 to 12 μM; Bronk, 2002), and includes urea, amino acids, humic and fulvic substances (Bronk, 2002) and high molecular weight proteinecous molecules yet to be characterised (McCarthy *et al.*, 1996; McCarthy *et al.*, 1997). Although recent evidence suggests that DON may be directly assimilated by specific groups of phytoplankton (Palenik *et al.*, 1989; Bronk and Glibert, 1993), DON requires prokaryotic breakdown to NH_4^+, called ammonification (grey arrow; Figure 1.1) or

utilisation by higher trophic levels and subsequent exudation of NH_4^+, before it can be assimilated by most phytoplankton species.

Nitrous oxide (N_2O) and nitric oxide (NO) are both found in trace concentrations (nM) in seawater. Both N_2O and NO are intermediate substrates during denitrification, the former also being a product of nitrification (Figure 1.1). Although the role of NO in biological cycling is largely unknown at present, N_2O is known to be a potent greenhouse gas (Crutzen, 1981).

Figure 1.1. Schematic of the nitrogen species involved in the Marine Nitrogen Cycle. Oxidation and reduction reactions are shown. Adapted from Capone (2000).

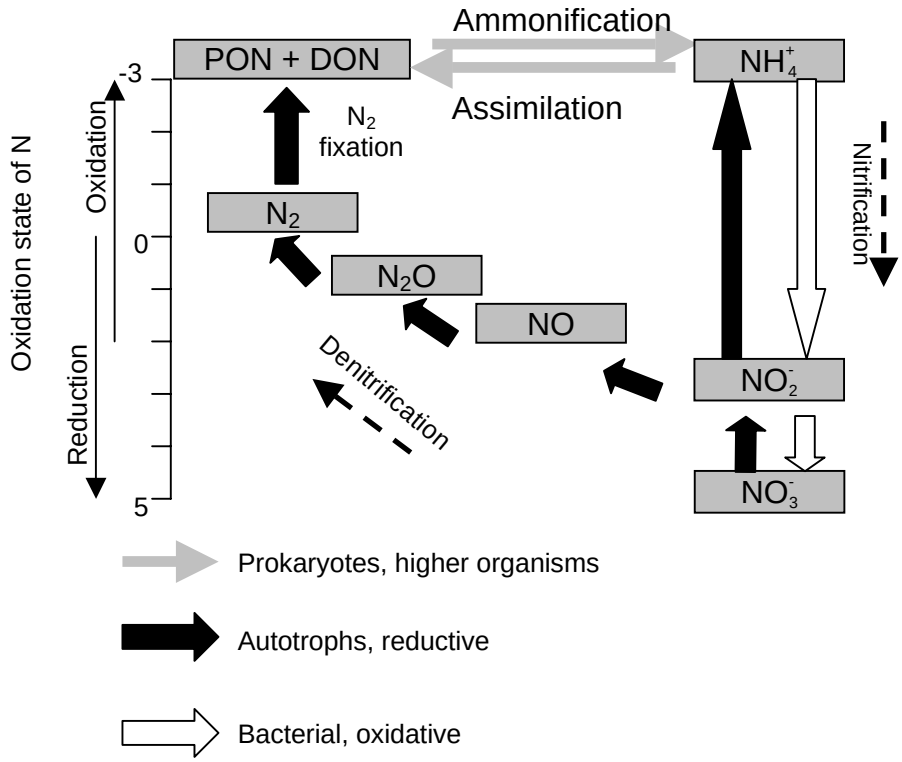

Principle sinks for N are autotrophic and heterotrophic assimilation and subsequent burial.

1.2. SUPPLIES OF NITROGEN TO THE OPEN OCEAN

1.2.1. Introduction and motivation

In the open ocean, primary productivity can be characterised as "new" and "regenerated" production according to the N substrate (Eppley and Peterson, 1979). Nitrate (NO_3^-) is generally considered to fuel "new" production, being transported from the NO_3^--rich deep ocean to the sunlit surface ocean by convection (Marshall and Schott, 1999; Williams *et al*., 2000), advective fluxes during upwelling and vertical mixing (Williams and Follows, 1998), and diffusion across the thermocline (Lewis *et al*. 1986; Planas *et al.,* 1999). In contrast, "regenerated production" is fuelled by ammonium (NH_4^+), a by-product of secondary production and recycling of N in the euphotic zone (Dugdale and Goering 1967; Eppley and Peterson 1979; Glibert, 1982). In a steady state environment, the upward flux of NO_3^- is expected to approximate the loss of N by the downward particle flux from the euphotic zone, that is, export production (Eppley and Peterson, 1979). In contrast, regenerated N is considered to sustain primary production rather than fuelling export production.

Over subpolar regions of ocean and at coastal boundaries, convective mixing and wind-induced upwelling promotes NO_3^- supply to the surface ocean (Williams *et al*., 2000; Dutkiewicz *et al.,* 2001), fuelling primary production (annual primary production estimated to range from 240 to 650 g C m^{-2} y^{-1}; Sathyendranath *et al*. 1995), of which 2 to 17% is exported as organic matter to the deep ocean (Michaels *et al*., 1994: Karl *et al.,* 1996). However, over the extensive subtropical gyres, wind-induced downwelling causes permanent stratification and a deep thermocline, subducting NO_3^- in the ocean interior and causing NO_3^- limitation in the surface ocean. Indeed, these subtropical regions of the ocean are typically oligotrophic or "ocean deserts", surface nutrient (NO_3^-

and NH_4^+) concentrations being typically < 0.1 μM (Rees *et al.* 1999; Lipschultz, 2001). Nevertheless, substantial rates of primary production are still observed over subtropical gyres (annual primary production estimated to range from 60 to 120 g C m^{-2} y^{-1}; Sathyendranath *et al*. 1995; Maranon *et al*., 2000). (It is important to note that estimates of primary production by Sathyendranath *et al*. 1995 represent computations based on latitudinal zones and chlorophyll data. Thus, these estimates of primary production do not include seasonal or interannual variability, but rather represent a broad annual average).

Traditionally, the supply of new N from vertical diffusion of NO_3^- from the deep ocean (0.05 mol N m^{-2} y^{-1}; Lewis *et al.,* 1986; 0.14 ± 0.07 mol N m^{-2} y^{-1}; Planas *et al.*, 1999) and atmospheric deposition of N to the surface ocean (0.005-0.03 mol N m^{-2} y^{-1}; Knap *et al.,* 1986; 0.014-0.05 mol N m^{-2} y^{-1}; Spokes *et al.,* 2000) were considered to fuel phytoplankton growth and export production in these vast subtropical regions. In comparison, export production in the oligotrophic Atlantic is estimated between 0.45 and 0.7 mol of organic N m^{-2} y^{-1}, based on independent geochemical determination employing the seasonal cycle of surface oxygen production and utilisation, residence time of water using ^{3}He and nutrient uptake dynamics (Table 1.1). More recently, sediment trap studies and carbon mass balance models in the subtropical Pacific have supported these previously doubted estimates of export production (0.26 to 0.45 mol N m^{-2} y^{-1}; Emerson *et al.,* 1997). Overall, it appears that the total N inputs (~ 0.015 to 0.14 mol N m^{-2} y^{-1}) are too weak to explain the independently diagnosed levels of export production, implying an imbalance in the N budget over the subtropical North Atlantic (Rintoul and Wunsch, 1991; Sambrotto *et al*. 1993; Michaels *et al*. 1996; Gruber and Sarmiento 1997). It is important to note that the majority of the biogeochemical estimates for export production were performed at the BATS site, which is not

representative of the subtropical Atlantic, or the world's oceans. Few data exists for truly oligotrophic sites. Nevertheless, the close agreement in the geochemical estimates of export production employed by Jenkins *et al.*, using a variety of methods suggests that these values are accurate for the BATS site.

Table 1.1. Estimates of export production (mol N m^{-2} y^{-1}) over the Atlantic Ocean.

METHOD	EXPORT PRODUCTION (mol N m^{-2} y^{-1})	REFERENCE
O_2 utilisation	0.7	Jenkins (1982)
	0.42 ± 0.09	Jenkins and Goldman (1985)
	0.42 ± 0.23	Sarmiento *et al.*, (1990)
	0.48 ± 0.10	Jenkins and Wallace (1992)
O_2 production	0.46 ± 0.09	Jenkins and Goldman (1985)
	0.39 ± 0.16	Spitzer and Jenkins (1989)
	0.51 ± 0.14	Spitzer and Jenkins (1989)
^{3}He flux	0.56 ± 0.16	Jenkins (1988)
	0.70 ± 0.20	Jenkins (1998)
Nitrate uptake	0.35 ± 0.09	Platt and Harrison (1985)
Mean N demand	0.50	

A number of alternative N-supplying processes have been proposed to explain how export production is maintained over oligotrophic gyres; 1) gyre-scale advective transfer and fine-scale eddy and frontal transfer of nutrients (McGillicuddy and Robinson, 1997; Siegel *et al.*, 1999; Mahadevan and Archer, 2000; Uz *et al.*, 2001; Levy *et al.*, 2001), 2) nitrogen (N_2) fixation (Gruber and Sarmiento, 1997) and 3) lateral transport of organic nutrients (Williams and Follows, 1998; Lee and Williams, 2000) (Figure 1.2).

Figure 1.2. Schematic of the alternative N sources to phytoplankton in the surface ocean (*in italics*) by: N_2 fixation (Gruber and Sarmiento, 1997), lateral advection of dissolved organic nitrogen (Williams and Follows, 1998; Lee and Williams, 2000) and supplies of nitrate from the deep ocean through gyre-scale and fine-scale transfer (McGillicuddy and Robinson, 1997; Siegel *et al.*, 1999; Mahadevan and Archer, 2000; Uz *et al.*, 2001; Levy *et al.*, 2001).

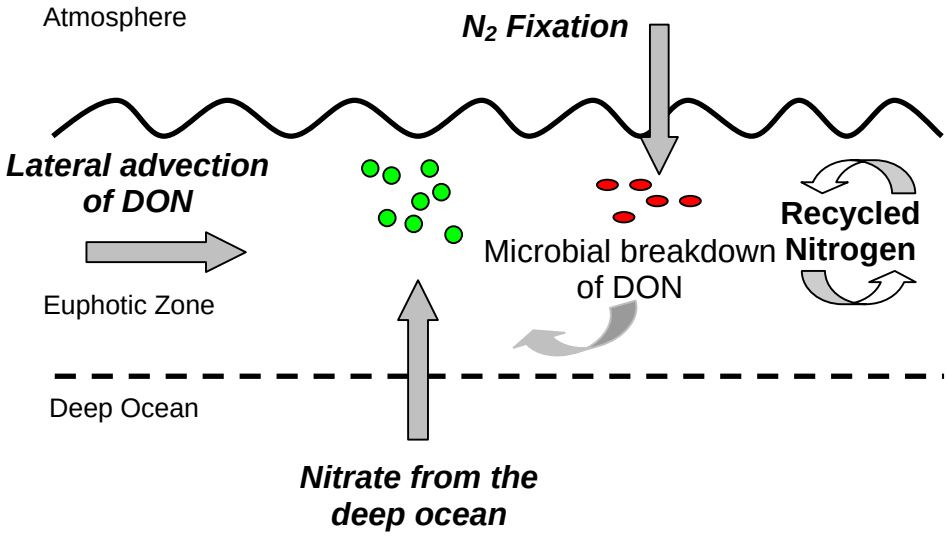

In this study, the distribution and potential of these alternative N sources to phytoplankton in the surface Atlantic are assessed using independent biogeochemical proxies; namely the stable isotopes of nitrogen and dissolved organic nutrients concentrations. In section 1.2.2, a description of the basic kinetics and terminology involved in stable nitrogen isotope biogeochemistry are discussed. In section 1.2.3, the application of stable nitrogen isotopes in solving N supplies to phytoplankton are discussed, as well as the organic nutrient approach.

1.2.2. Methodological approach: the use of Stable Isotopes of Nitrogen

There are several comprehensive reports on the derivation and kinetics of the stable isotopes of nitrogen (Mariotti *et al.*, 1981; Owens, 1987; Altabet, 1996). In the following section, the terminology and description of kinetic isotopic fractionation are reviewed and the application to the present study are discussed. There are numerous adaptations of these equations describing isotope kinetics. The author has used her discretion to define the equations using her own terminology and abbreviations were appropriate.

1.2.2.1. Introduction to Stable Nitrogen Isotope kinetics and Terminology

Nitrogen (N) exists naturally as two stable isotopes, ^{14}N (99.634 %) and ^{15}N (0.366 %) (Wada and Hattori, 1991), the abundance (A) of ^{15}N being expressed in atom percent by the ratio:

$$A = \frac{^{15}N}{^{15}N + ^{14}N} \times 100 \qquad \text{Eq. 1.1}$$

As a convention, the abundance of the heavy isotope, ^{15}N is compared to the abundance of the light isotope, ^{14}N, thus defining a dimensionless parameter, R, where R is described by:

$$R = \frac{^{15}N}{^{14}N} \qquad \text{Eq. 1.2}$$

Natural variations and abundance of ^{15}N relative to ^{14}N in the environment are small and thus, the isotope ratio defined in Eq. 1.2 approximates to:

$$\frac{^{15}N}{^{15}N + ^{14}N} \approx \frac{^{15}N}{^{14}N} \qquad \text{Eq. 1.3}$$

It is analytically challenging to measure the absolute natural abundance of ^{15}N and thus, the isotope ratio, R, is measured against a standard material. The ratio of R to the standard material is expressed in “δ” (delta) notation:

$$\delta = \frac{R_{sample} - R_{standard}}{R_{standard}} \times 1000\ {}^{0}/_{00} \qquad \text{Eq. 1.4}$$

where R_{sample} and $R_{standard}$ is the isotope ratio, as expressed in Eq. 1.2., for a sample and standard, respectively, and δ is expressed in parts per thousand or per mil (‰). The universal standard for N isotope analysis is atmospheric N_2 with a $\delta^{15}N$ of ~ 0 ‰.

1.2.2.2. Kinetic isotope fractionation

Isotope fractionation is the basis for the natural variation in $\delta^{15}N$ in the environment. It is founded on the partitioning of ^{15}N and ^{14}N between two compounds (e.g. within a cell) or phases (e.g. between seawater and organic matter). Chemical fractionation is due to the differences in strength of the N-containing chemical bonds, which are stronger for the heavy isotope (^{15}N) relative to the light isotope (^{14}N), and the probability of reaction (Bigeleisen, 1952). During a unidirectional, irreversible reaction from substrate to product, the rates of reaction of ^{15}N and ^{14}N will differ and are defined as the kinetic isotope fractionation factor (α), described by:

$$\alpha = \frac{R_{product}}{R_{substrate}} \qquad \text{Eq. 1.5}$$

where $R_{product}$ and $R_{substrate}$ are the ratio of ^{15}N to ^{14}N (as defined in Eq. 1.2) for the product and the substrate, respectively. To describe α in terms of the δ notation, the per mil enrichment factor (ε), which is defined as the difference in isotopic composition between the substrate and the product ($\delta_{product} - \delta_{substrate}$), is described by:

$$\varepsilon = (\alpha - 1) \times 1000 \qquad \text{Eq. 1.6}$$

Since rates of reaction are faster for ^{14}N than for ^{15}N, ε is usually positive (in contrast to that originally described by Mariotti *et al.,* 1981, in which $\varepsilon = (1 - \alpha) \times 1000$, thus ε being negative). Subsequently, the product (e.g. phytoplankton) preferentially

incorporates the light isotope, ^{14}N, resulting in the $\delta^{15}N_{product}$ being less than the $\delta^{15}N_{substrate}$, the substrate (e.g. nutrient source) being ^{15}N enriched. In the environment, a substrate or product, which is relatively depleted in ^{15}N, is termed isotopically light, whereas a substance relatively enriched in ^{15}N is termed isotopically heavy. Enrichment factors vary greatly depending on the substrate and ambient nutrient conditions. Enrichment factors during nitrate-based productivity are reported to range between 4 and 9 ‰ in eutrophic oceanic regions (Altabet *et al*., 1991: Voss *et al*., 1996), but up to 12 ‰ in cultures (Pennock *et al*., 1996). Phytoplankton growth on ammonium is accompanied by an enrichment factor of 6.5 to 9 ‰ (Cifuentes *et al*., 1989), but up to 26 ‰ when ammonium concentrations are greater than 20 µM (Pennock et al., 1996).

1.2.2.3. Open and Closed systems

Kinetic isotope fractionation is not only dependent on the $\delta^{15}N_{substrate}$ but also its availability, or more likely, the rate of supply of the substrate. Thus, the terms “open” and “closed” are used to describe a high and low or limiting rate of supply of the substrate, respectively.

Isotope mass balance dictates that the $\delta^{15}N_{substrate}$ increases as a function of its depletion in concentration, as described by Rayleigh fractionation:

$$\delta^{15}N_{substrate(v)} = \delta^{15}N_{substrate(v=1)} - \varepsilon \times ln(v) \qquad \text{Eq. 1.7}$$

where v is the fraction of unutilised substrate ($[N_{observed}]/[N_{initial}]$) and $\delta^{15}N_{substrate\ (v=1)}$ is the initial $\delta^{15}N$ of the substrate.

In an *open* system, where there is an infinite supply (v=1 at all times) of the substrate relative to the product, and the $\delta^{15}N_{substrate}$ remains unchanged despite utilisation, the $\delta^{15}N_{product}$ is described by the instantaneous product equation:

$$\delta^{15}N_{product} = \delta^{15}N_{source} - \varepsilon \qquad \text{Eq. 1.8}$$

In contrast, in a *closed* system, which is defined by a finite substrate pool, v will decrease to very low levels (v=1 → v=0). At any time, the $\delta^{15}N_{product}$ plus $\delta^{15}N_{substrate}$ is equal to the initial $\delta^{15}N_{substrate}$. In a closed system, the $\delta^{15}N_{product}$ is defined by:

$$\delta^{15}N_{product} = \delta^{15}N_{substrate(v=1)} - \varepsilon \times ln\, v - \varepsilon \qquad \text{Eq. 1.9}$$

$$\delta^{15}N_{product} = \delta^{15}N_{substrate(v=1)} - \varepsilon \times \frac{v}{1-v} \times \ln v \qquad \text{Eq. 1.10}$$

where Eq. 1.9 is the instantaneous product equation and Eq. 1.10 is the accumulated product equation. To determine the $\delta^{15}N_{substrate\ (v=1)}$ and ε, a linear curve is drawn between (v/(1-v) x ln v) and $\delta^{15}N_{product}$. The slope represents ε and the y-axis intercept represents $\delta^{15}N_{substrate\ (v=1)}$. Whereas the accumulated product equation describes the $\delta^{15}N_{product}$ over an infinitely long residence time (τ ~ ∝), thus accounting for the substrate used (1-v) and the substrate remaining (v), the instantaneous product equation describes a short-lived relationship between the product and substrate (τ = 0), thus only considering the substrate unutilised (v).

A comparison between the $\delta^{15}N_{substrate}$ and $\delta^{15}N_{product}$ according to the Rayleigh fractionation, instantaneous product and accumulated products, respectively, can be depicted by considering the change in $\delta^{15}N$ during a decrease in the substrate concentration (v), where v=1 is the initial substrate concentration (Figure 1.3). According to the instantaneous product equation, the change in $\delta^{15}N_{substrate}$ and $\delta^{15}N_{product}$ are in parallel, the $\delta^{15}N_{substrate}$ being consistently higher than the $\delta^{15}N_{product}$. According to the accumulated product equation, of the final $\delta^{15}N_{product}$ is 5 ‰ (i.e. ε) greater than the initial $\delta^{15}N_{product}$.

Figure 1.3. Variation in $\delta^{15}N$ (‰) as a function of substrate depletion as predicted by Rayleigh fractionation kinetics, where v is the fraction of unutilised N (v=1). The change in $\delta^{15}N$ for the substrate (dotted line), instantaneous product (dashed line) and accumulated product (solid line) are plotted. An enrichment factor (ε) of 5‰ is employed. Adapted from Altabet (1996).

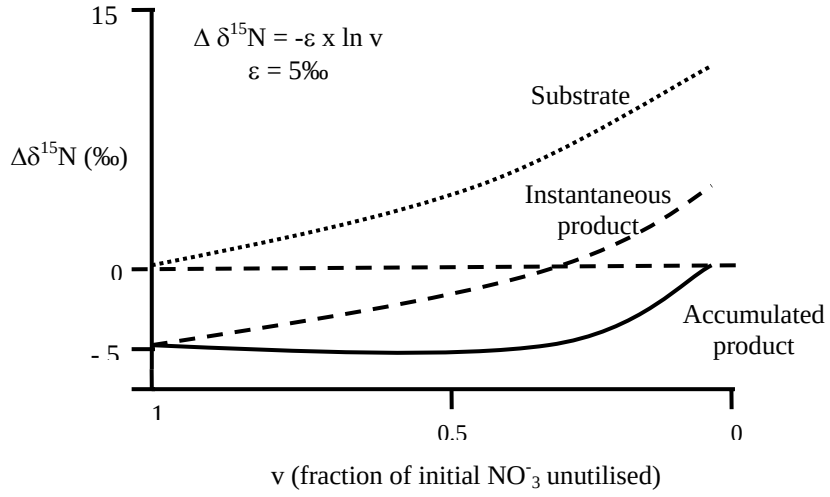

Although knowledge of the mechanics of isotope kinetics, and open and closed systems is useful, an understanding of their application is essential in interpretation of the data to be presented in this thesis. A closed system is one in which nutrients are either depleted or highly limiting to primary production. The highly stratified surface waters of the downwelling oligotrophic gyres can be described as "closed". An open system is one in which the nutrient flux is continuous and infinite. An upwelling regime or the initial stages of a phytoplankton bloom can be described as "open". Closed and open systems represent end members only, with a continuum of states between. Therefore, the stable isotope kinetics in the surface ocean represents an integrated measure over the residence time of the phytoplankton living their.

1.2.3 Stable nitrogen isotope approach to identifying sources of Nitrogen to phytoplankton in the surface Atlantic Ocean

Variations in the natural abundance of the stable isotopes of nitrogen ($\delta^{15}N$) may yield insights into the N cycle on spatial and temporal scales that would be difficult to

study using conventional N tracer (^{15}N) techniques (Altabet and McCarthy, 1985; Horrigan *et al.,* 1990; Montoya *et al.,* 1992).

The stable isotopic composition of phytoplankton, assumed from the particulate organic nitrogen pool ($\delta^{15}N$ PON), is dependent on two factors: 1) the $\delta^{15}N$ of the N source and 2) the isotopic fractionation during uptake and assimilation of N source. The fundamental idea behind this study is to determine the isotopic composition of the phytoplankton in the surface Atlantic and assess the isotopic composition of the possible N sources. By developing a source (N-source) and sink (phytoplankton) map, the distribution and relative importance of the principle N sources can be determined (Figure 1.2). In this section, a brief description of the isotopic composition ($\delta^{15}N$) of the potential N sources to the surface ocean are discussed, as well as the influence of the N sources and isotopic fractionation on the $\delta^{15}N$ of phytoplankton.

1.2.3.1 Supply of nitrate, its N isotope composition and factors which vary its isotope composition

Diffusion of nitrate (NO_3^-) from the deep ocean is too weak to explain the extent of export production observed over much of the Atlantic (see section 1.2.1). Recently, alternative NO_3^- supplying mechanisms have been proposed. On the gyre-scale, Ekman transfer (Williams and Follows, 1998) and convection (Williams *et al.,* 2000) may transport NO_3^- from the productive upwelling regions over the flanks of the subtropical gyre. On the fine-scale, mesoscale eddies (McGillicuddy *et al.,* 1998, 1999; Siegel *et al.,* 1999), planetary waves (Uz *et al.,* 2001) and fine-scale frontal circulations (Mahadavan and Archer, 2000) may inject NO_3^- from the deep to the surface ocean. Thus, NO_3^- is a potential nutrient source even over the subtropical downwelling regions.

The $\delta^{15}N$ of nitrate ($\delta^{15}N\text{-}NO_3^-$) in the deep ocean is relatively constant throughout the worlds oceans, ranging from 4.5 to 6.1 ‰ (Liu and Kaplan 1989; Liu *et al.,* 1996, Sigman *et al.,* 1997), although isotopically heavier NO_3^- (up to 18 ‰) is observed in regions of denitrification (Liu and Kaplan, 1989), which involves strong fractionation (ε from 20 to 40 ‰; Cline and Kaplan, 1975; Liu and Kaplan, 1988; see section 1.2.2.2). In contrast to the deep ocean, the surface ocean experiences large variations in the $\delta^{15}N\text{-}NO_3^-$ ranging from –0.5 to 12 ‰ (Liu and Kaplan, 1989; Altabet, 1988; Liu *et al.,* 1996). This is largely due to partial utilisation of NO_3^- by phytoplankton in an open system (see section 1.2.2.3), which leads to isotopic fractionation during uptake and assimilation of the N source according to the instantaneous product equation (Eq. 1.8; Wada 1980; Altabet *et al.,* 1991; Altabet and McCarthy 1985; Montoya and McCarthy 1995; Wu *et al.,* 1997). The enrichment factor (ε, see Eq. 1.6) for NO_3^- uptake varies between 2 and 9 ‰ (Wada, 1980; Altabet *et al.,* 1991; Sigman *et al.,* 1997; Waser *et al.,* 1998; Waser *et al.,* 1999), higher ε values being observed during culture studies (< 23 ‰; Montoya and McCarthy, 1995). The ε is thought to vary as a function of species (Montoya and McCarthy, 1995), light intensity (Wada and Hattori, 1978), phytoplankton cell status (i.e. previous nutrient conditions) (Waser *et al.,* 1999), culture conditions (Waser *et al.,* 1998) and active N transport (Rau *et al.,* 1998).

As demonstrated in section 1.2.2.2, the $\delta^{15}N_{substrate}$ and $\delta^{15}N_{product}$ vary as a function of substrate concentration, or rather, the fraction of unutilised substrate (v). Over much of the Atlantic, large variations in surface $[NO_3^-]$ are observed, thus altering the $\delta^{15}N\text{-}NO_3^-$. As NO_3^- is assimilated by phytoplankton, the $\delta^{15}N\text{-}NO_3^-$ varies according

to first-order Rayleigh fractionation kinetics (Eq. 1.7). Where [NO_3^-] are high (*i.e.,* an open system, see section 1.2.2.3), the $\delta^{15}N$- NO_3^- remains unaltered, whereas the $\delta^{15}N$-PON decreases to very low values according to the instantaneous product equation (Eq. 1.8; Altabet and McCarthy, 1985; Altabet *et al.,* 1991). Where NO_3^- supply is limited, such as in an oligotrophic gyre (i.e. a closed system, see section 1.2.2.3), the $\delta^{15}N$-NO_3^- becomes enriched in ^{15}N, as phytoplankton initially incorporate ^{14}N over ^{15}N. As phytoplankton drawdown [NO_3^-] to very low levels, the accumulated $\delta^{15}N$-PON resembles the initial $\delta^{15}N$- NO_3^-, according to the instantaneous and accumulated product equations for a closed system (Eq. 1.9 and 1.10). Indeed, large ε values during assimilation of NO_3^- by phytoplankton are a predominant characteristic in the biogeochemistry of ^{15}N in surface water of the NO_3^--rich, high latitude ocean (Wada 1980, Wada *et al* 1987). In contrast, ε tends towards zero in oligotrophic regions (as v tends towards zero in Eq. 1.10), where no net isotopic fractionation is expected (Altabet and McCarthy, 1985; Fogel and Cifuentes, 1993) possibly implying zero N efflux from the cell (Mariotti *et al.,* 1981, Handley and Raven, 1992; Evans *et al.,* 1996). Large variations in $\delta^{15}N$-PON are observed in oligotrophic regions (2-32‰: Saino, 1992; Altabet *et al.,* 1999).

Seasonal variations in $\delta^{15}N$ of PON are strongly associated with the onset of stratification and the removal of NO_3^- from the euphotic zone (Voss *et al.,* 1996; Nakatsuka and Handa, 1997). In general, $\delta^{15}N$ of surface PON decreases from spring-summer to autumn-winter (Wada and Hattori, 1976; Voss *et al.,* 1996; Nakatsuka and Handa, 1997; Waser *et al.,* 2000) in response to the breakdown in stratification from

spring/summer to autumn/winter, increased surface NO_3^- concentrations and thus a progression from a closed to an open system.

In addition to temporal changes, spatial variations in $\delta^{15}N$ are also observed. Many studies have observed a decrease in $\delta^{15}N$ of sinking PON out of the euphotic zone to 1000m (Saino and Hattori 1987; Altabet *et al*., 1991; Nakatsuka *et al.,* 1997); these observations have been attributed to the preferential degradation of amino acids, which are heavier ($\delta^{15}N \sim 3$ ‰) than bulk POM (Macko *et al.,* 1987), zooplankton excretion at depth and subsequent bacterial incorporation of depleted $\delta^{15}N$ ammonium (Checkley and Miller, 1989). In contrast, depth variation in $\delta^{15}N$ of suspended PON exhibits a subsurface minimum around the nitracline and an increase with depth (Saino and Hattori, 1980; Altabet and McCarthy, 1985; Saino and Hattori, 1987; Altabet 1988). Remineralisation (Altabet and McCarthy, 1985; Saino and Hattori, 1987; Checkley and Miller, 1989), oxidative degradation (Saino and Hattori, 1980), ammonification (Minagawa and Wada, 1984) and addition of organic debris from higher tropic levels (Wada *et al.,* 1987, Nakatsuka *et al.,* 1997) may be responsible for such observations. The subsurface minima in $\delta^{15}N$–PON, coincides with a subsurface maximum in [PON] (Altabet and McCarthy 1985; Montoya *et al.,* 1992). This is attributed to the diffusion of deep NO_3^- into the base of the mixed layer promoting phytoplankton growth on high NO_3^- concentrations, which in turn results in isotopic fractionation according to the instantaneous product equation in an open system, *i.e*. $\delta^{15}N$-PON is isotopically light.

In addition, latitudinal variations in $\delta^{15}N$-PON have been observed in response to changes in the ambient nutrients and their concentrations (Waser *et al.,* 2000; Altabet, 2001). A north-south transect across the equatorial Pacific observed a “U” shaped distribution in $\delta^{15}N$-PON around the equator, increasing from ~ 2 ‰ at the

equator to 8 and 16 ‰ north and south of the equator, respectively (Altabet, 2001). Overall, the $\delta^{15}N$ of suspended PON was correlated to surface [NO_3^-]. A west-east transect in the North Atlantic subtropical gyre showed similar trends, with $\delta^{15}N$ of suspended PON ranging from 0.41 to 11.29 ‰ (Waser *et al.*, 2000).

Whereas phytoplankton respond to NO_3^- utilisation integrated over the residence time for phytoplankton in the euphotic zone (Altabet and Francois, 1994), $\delta^{15}N$ NO_3^- can vary more rapidly with changes in both the physical supply and biological uptake (Altabet, 2001).

1.2.3.2. Nitrogen fixation

Biological dinitrogen (N_2) fixation is carried out by some prokaryotic microorganisms (*e.g*. bacteria, cyanobacteria, archea), which have the ability convert N_2 to biologically available substrates, such as dissolved organic nitrogen (e.g. amino acids) and ammonium, using the enzyme nitrogenase (nifH) (Michaels *et al*., 1996; Lipschultz and Owens, 1996; Capone *et al*., 1997; Hood *et al.*, 2000; Mulholland and Capone, 2000). *Trichodesmium* spp., the most studied of the marine N_2-fixers, are largely confined to warm, calm, oligotrophic, tropical waters (Carpenter and Capone, 1992), although it has been suggested that surface NO_3^- (Ohki *et al.*, 1986; Ohki *et al.*, 1991), iron (Howard and Rees, 1996; Falkowski, 1997) and phosphorus (Wu *et al.*, 2000; Sanudo-Wilhelmy *et al.*, 2001) concentrations ultimately control the distribution of *Trichodesmium* spp..

For many years, the contribution of N_2-fixation was considered insignificant (<1%) compared to the total N demand of primary producers in the whole ocean (Carpenter, 1983; Howarth *et al.*, 1988). However, in the past 10 years, scientific evidence has changed this view. In the subtropical North Pacific, Karl *et al*., (1997)

estimates that N_2 fixation may provide up to 25-50% of the N demand of phytoplankton at station ALOHA, similar contributions being found in the Sargasso Sea (> 50%; Michaels *et al.,* 1994). Indeed, nutrient diagnostics predict that the Atlantic is a source of N from N_2 fixation (Gruber and Sarmiento, 1997; Deutsch *et al.,* 2001).

Numerous studies have demonstrated that stable isotope data ($\delta^{15}N$) can provide an independent and integrative measure of the contribution of N_2 fixation to the organic matter in the upper water column (Wada and Hattori 1976; Liu *et al*. 1996; Carpenter *et al.* 1997; Karl *et al*., 1997; Capone, 2001). The $\delta^{15}N$ of dissolved N_2 is ~ 0.6‰, near that of atmospheric nitrogen (~ 0 ‰). During N_2 fixation, the estimated ε is very low (α=1.000; Hoering and Ford, 1960; Minagawa and Wada 1986; Macko *et al.*, 1987; Carpenter *et al.,* 1997). Therefore, the isotopic composition of organic matter containing N derived from N_2-fixation is light, ranging from –2.1 to + 2.9 ‰ (Wada and Hattori, 1976; Macko *et al.,* 1984; Minagawa and Wada 1986; Saino and Hattori, 1987; Carpenter *et al.,* 1997; Carpenter *et al.,* 1999; Kerherve *et al.,* 2001). Indeed, *Trichodesmium* spp. are reported to have the heaviest $\delta^{13}C$ (-12.9 ± 1.1 ‰) and lightest $\delta^{15}N$ among the marine phytoplankton (Wada and Hattori, 1991; Carpenter *et al.,* 1997).

In surface waters, bacterial degradation causes ^{15}N enrichment of PON. Sinking of ^{15}N-enriched PON from the euphotic zone is responsible for the near constant, enriched $\delta^{15}N\text{-}NO_3^-$ (relative to N_2) in the deep ocean (Altabet and McCarthy, 1985; Saino and Hattori, 1987; Checkley and Miller, 1989). In a region of N_2 fixation, sinking and remineralisation of ^{15}N-depleted PON produces isotopically lighter NO_3^- (+1.0 to 4.7 $^{o}/_{oo}$ (Altabet 1988, Liu *et al.* 1996) relative to $\delta^{15}N$ values normally found in the deep ocean (Liu and Kaplan, 1989; Sigman *et al.,* 1997).

1.2.3.3. Recycled N and higher trophic levels

Traditionally, phytoplankton growth in the oligotrophic open ocean is fuelled by regenerated production (i.e. NH_4^+). There are few measurements on the isotopic composition of NH_4^+ (δ^{15}N- NH_4^+) and its fractionation during uptake and assimilation, primarily due to its low concentrations (i.e. < 1-2 μM) and the analytical detection limits for isotopic determination (Waser *et al.* 1999). However, it is known that the δ^{15}N-NH_4^+ is dependent on the δ^{15}N of the grazers excreting the NH_4^+(Minagawa and Wada, 1984, Checkley and Miller, 1989) and the isotope fractionation of 3 ‰ during bacterially-mediated NH_4^+ regeneration by grazers (Hoch *et al.,* 1994). In N replete oceanic conditions, ε is typically 6.5-6.0 ‰ (Cifuentes *et al.,* 1989; Montoya *et al.,* 1991), increasing at higher NH_4^+ concentrations (20-26 ‰; Pennock *et al,* 1996; Waser *et al.,* 1998). However, in severely N-depleted environments, ε is reported to decrease to 0 $^o/_{oo}$ (Hoch *et al.,* 1992; Waser *et al.,* 1998; Waser *et al.,* 1999), possibly due to an NH_4^+ scavenging mechanism (Fogel and Cifuentes, 1992) or decreased NH_4^+ efflux after N-starvation (Waser *et al.,* 1999). Phytoplankton growth fuelled by NH_4^+ in the oligotrophic Atlantic was found to be isotopically light, ranging from –2 to +2 ‰ (Altabet, 1988). Thus, growth on regenerated N appears to be a competing alternative explanation for depleted δ^{15}N PON.

Many studies have identified a "trophic level effect" which causes an average enrichment in the δ^{15}N of PON of 3.4 +/- 0.2 $^o/_{oo}$ per trophic level (Minagawa and Wada, 1984; Minagawa and Wada, 1986; Wada *et al.,* 1987; Fry, 1988), reflecting the net balance of isotopic fractionation during the assimilation and excretion of nitrogen (Montoya *et al.,* 1992). Thus, zooplankton bodies are enriched in ^{15}N and ^{13}C relative to their diet (Wada *et al.,* 1987). Heterotrophic activity also leads to the excretion of

isotopically light ammonia (Checkley and Miller, 1989; Altabet and Small, 1990) and production of faecal pellets enriched by 2.2 ‰ compared to food sources (Altabet, 1988; Altabet and Small, 1990).

1.2.3.4. Dissolved organic nutrients

Dissolved organic nitrogen (DON) is released from phytoplankton cells across a permeable cell membrane by passive or active exudation (Sharp, 1977; Mague *et al*., 1980; Bjørnsen, 1988), by bacterially and virally mediated processes (Bronk and Glibert, 1991; Proctor and Fuhrman, 1991; Carlsson *et al.*, 1993; Suttle, 1994; Fuhrman, 1999), grazing (Lampert, 1978; Miller and Glibert, 1998) and remineralisation of organic aggregates (Smith *et al.*, 1992; Figure 1.4). N_2 fixers are also known to exude 25 to 75% of the recently fixed N (Glibert and Bronk, 1994, Capone *et al*., 1994; Karl *et al.*, 1997).

DON consists of three pools, the labile, semi-labile and refractory DON. Labile DON is considered biologically reactive on time-scales of hours to days (Bronk *et al.*, 1994; Kiel and Kirchman, 1999), whereas semi-labile DON is considered biologically reactive over months to years (Archer *et al*. 1997; Vidal *et al.*, 1999; Carlson, 2002). Much of the refractory DON pool is uncharacterised but is thought to consist of large complex proteinecous molecules, which may remain intact over long time scales.

Figure 1.4. Schematic of the processes involved in the release of dissolved organic nitrogen (DON) in the marine environment, through viral lysis of bacteria or phytoplankton and N_2 fixers, passive and active exudation from bacteria and phytoplankton and N_2 fixers, and sloppy feeding or bacterial activity on zooplankton. Adapted from Bronk (2002).

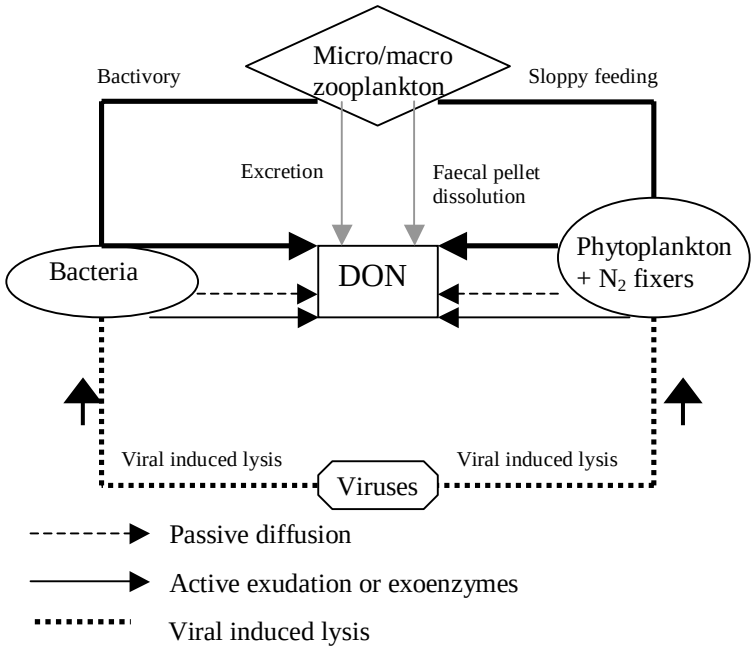

Numerous studies suggest that DON is a potential growth substrate, through bacterial degradation to bioavailable N species, such as NH_4^+ (see section 1.1.1; Berman *et al.,* 1991; Antia *et al.,* 1991; Bronk and Glibert 1993, Jorgensen *et al*. 1994, Kroer *et al*. 1994) and that DON may support up to 30-50% of the daily phytoplankton N demand in the equatorial Pacific (Benner *et al*., 1997). More recently, direct uptake and assimilation of low molecular weight DON compounds (e.g. amino acids, primary amines) by phytoplankton has been demonstrated (Palenik and Morel, 1990; Berman and Chava, 1999; Palenik and Henson, 1997).

DON concentrations tend to exceed inorganic nitrogen by an order of magnitude in the oligotrophic ocean and thus are a potentially important source of N to phytoplankton in the surface Atlantic. An alternative mechanism supplying N to the subtropical gyres is a lateral influx of DON from upwelling zones in the tropics and subpolar gyres (Williams and Follows, 1998; Lee and Williams, 2000; Abell *et al*.,

2000). DON may penetrate further than NO_3^-, which would be rapidly assimilated by phytoplankton in the oligotrophic surface waters.

In a nutrient replete environment where conditions permit phytoplankton growth near maximal rates, the nitrogen to phosphorus ratio (N: P) for dissolved and particulate inorganic and organic is 16.1 (Redfield *et al.,* 1963). N inputs to the surface ocean N_2-fixing organisms are not accompanied by concomitant phosphorus inputs, leading to P limitation (Karl *et al.,* 1997; Karl *et al.,* 2001, Sanudo-Wilhelmy *et al.,* 2001). Thus, elevated N: P ratios in the dissolved inorganic and organic pools may characterise regions of N_2 fixation, although other factors must be considered (Loh and Bauer, 2000).

Dissolved P is partitioned between soluble reactive phosphate (SRP), which includes orthophosphate (PO_4^{3-}) and dissolved organic phosphorus (DOP), species which include nucleotides, phospholipids, sugar phosphates and vitamins (Karl and Bjorkman, 2001). DOP concentrations often exceed SRP in the open ocean, the former comprising 70 to 80 % of the surface total dissolved P pool (Karl and Yanagi, 1997; Karl *et al.,* 2001), and representing a significant fraction of the biologically available phosphorus (Smith *et al.,* 1986; Bjorkman *et al.,* 2000; Karl and Bjorkman, 2001). Horizontal advection may represent a far field source of DOP to subtropical gyres.

Few data exists for the $\delta^{15}N$ of DON due to methodological difficulties. Abell *et al.,* (2000) reported that DON is isotopically light (1 to 2 ‰); in that case, $\delta^{15}N$ DON was determined by $\delta^{15}N$ of NO_3^- before and after ultraviolet oxidation. In contrast, Benner *et al.,* (1997) isolated high molecular weight DON by tangential-flow ultrafiltration and found $\delta^{15}N$ DON from the surface (1m) and deep Atlantic (900 and 2400m) to be isotopically heavy (6.6 to 8.9 ‰). The range in $\delta^{15}N$ DON, which appears

dependent on the method of DON isolation and isotopic analysis, renders its inclusion in an isotopic approach inconclusive. Thus, alternative approaches have been used in this study to assess the potential for DON as a growth substrate to phytoplankton.

1.2.4. The present study.

1.2.4.1. Field work

The Atlantic Meridional Transect (AMT) is a twice-annual sampling programme between the UK (~ 50°N) and the Falklands Islands (~ 52°S), covering a distance of over 13500 km in the Atlantic Ocean (Figure 1.5). Biogeochemical and physical measurements are made along the transect in range of ecosystems from the subtropical north and south Atlantic, the equatorial and coastal upwelling region off northwest Africa and the northern subpolar region. The diversity in oceanic regimes, as indicated by variations in the remotely sensed surface chlorophyll *a* concentrations (SeaWiFS) (Figure 1.5), allows this cruise track to be an ideal platform from which investigate the sources of nutrients to phytoplankton of the Atlantic Ocean. The present study is primarily based upon the Atlantic Meridional Transect in April/May 2000 (AMT 10, see Chapter 4 for details), although data from all AMT cruises is discussed in order to wider provide a context (see Chapter 3).

1.2.4.2. Aims and objectives

The principle aims of this thesis are:

1. to assess the seasonal and interannual variability in the physical structure of the Atlantic along the Atlantic Meridional Transect using temperature, salinity and the derived density data collected on 11 AMT cruises.
2. to determine if the Atlantic Ocean is nitrate or phosphate limited using nutrient data collected on 11 AMT cruises.

3. to assess the role of nitrogen fixation, the horizontal advection of organic nutrients, and gyre and fine scale upwelling of nutrients using the stable nitrogen isotope composition of the N source (N_2, NO_3^-, DON) and surface (7m) phytoplankton.

4. to assess the potential of the horizontal Ekman transport of organic nutrients from productive regions to subtropical gyres in supplying N and P to phytoplankton by determining the meridional distribution of DON and DOP.

Figure 1.5. SeaWiFS ocean colour image of yearly averaged AMT surface chlorophyll *a* concentrations (mg m^{-3}) in the Atlantic Ocean. Image from www.ims.plym.ac.uk/geomatics/amt

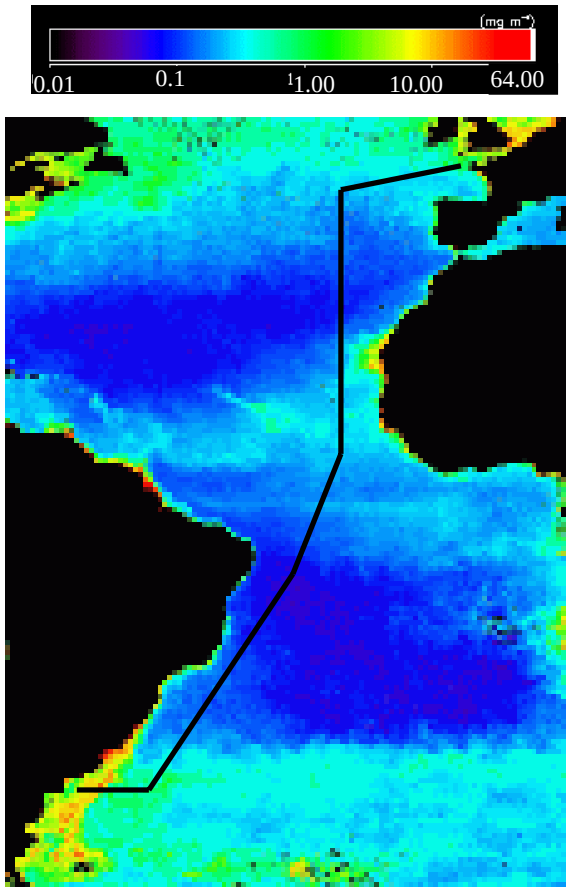

1.2.4.3. Temporal and spatial variability in the physical structure and nutrient dynamics along the Atlantic Meridional Transect

In Part One of Chapter 3, the temporal and spatial variability in the physical structure of the Atlantic, determined from surface and water column temperature, salinity and density, is assessed for biannual AMT cruises since 1995. The responses of

the surface ocean to atmospheric winds and pressure anomalies are also examined. Additionally, oceanic boundaries are defined by a variety of methods.

In Part Two of Chapter 3, the nutrient dynamics along the Atlantic Meridional transect are assessed by examining the relationship between nitrate and phosphate concentrations for cruises since 1995. In addition, climatological diagnostics are applied to compare the Atlantic nutrient dynamics to other data sets and ocean basins.

1.2.4.4.. Nutrients, phytoplankton biomass and species composition.

In Chapter 4, the inorganic nutrient distributions are determined during by analysis of nitrate plus nitrite (nitrate herein) and phosphate concentrations in surface ocean (< 250m). Phytoplankton biomass is determined by analysis of particulate organic carbon and nitrogen (POC and PON, respectively). Phytoplankton pigments are also employed to decipher the dominant phytoplankton functional group dominating the water column.

1.2.4.5. Stable nitrogen isotope approach

In Chapter 4, the $\delta^{15}N$ of suspended PON was determined along the AMT track. By taking into the account the ambient NO_3^- concentrations and the dynamics of the environment (open vs. closed system) it is possible to decipher the dominant N supply (Figure 1.6), based on literature values for the $\delta^{15}N$ of the N sources.

The basis of this studies surrounds the fact that the potential sources of N to phytoplankton in the surface ocean have distinct $\delta^{15}N$ values (Figure 1.6, see section 1.2.3.). For example, NO_3^- from the deep ocean, supplied by gyre-scale and fine-scale processes is isotopically heavier (~ + 5 ‰) than N_2 (~ 0‰), creating two distinct end members. On the other hand, DON derived from an N_2 fixing source (-3 to + 2 ‰) is

markedly different to that derived from a non-N_2 fixing source (4 to 6.5 ‰), the $\delta^{15}N$ of NH_4^+ being around -2 ‰. The $\delta^{15}N$ of phytoplankton utilising NO_3^- from the deep ocean depends on the nutrient dynamics, that is, if NO_3^- is limiting. Thus, isotopic fractionation in either a closed or an open system determines the integrated $\delta^{15}N$-PON (Figure 1.3). In contrast, phytoplankton utilising N derived from N_2 fixation will be ~ 0‰. The $\delta^{15}N$ of DON varies according to its source, that is, if it is derived from a region of N_2 fixation Regenerated production may result in a similar isotopic composition of PON to that produced by N_2 fixation, therefore, other biogeochemical proxies are required to clarify the dominant N source.

Figure 1.6. Schematic showing the $\delta^{15}N$ (‰) of the N sources associated with (i) atmospheric N_2 ([1]Minagawa and Wada, 1986), (ii) DON from an N_2 fixing source ([2] Liu *et al*., 1997; [3] Abell *et al*, 1999), (iii) DON from a non-N_2 fixing source ([4]Benner *et al*., 1997; [5]Knapp and Sigman, 2003), (iv) NO_3^- from the deep ocean ([6]Liu and Kaplan, 1989) and (v) NH_4^+ ([7]Checkley and Miller, 1989) and isotope fractionation during the assimilation of the N source in a closed and open system, where $\delta^{15}N_{Product}$ and $\delta^{15}N_{substrate}$ represents the stable N isotope composition of the product and substrate, respectively (see section 1.2.3. for details).

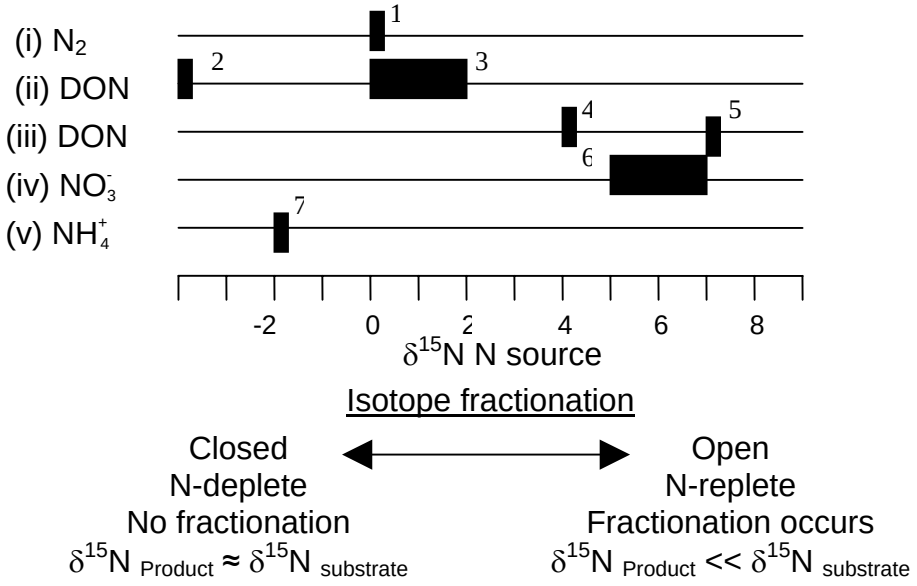

1.2.4.6. Dissolved organic nutrients

In Chapter 4, the latitudinal variation in DON and DOP are determined. If lateral advection is an important process supplying N in the Atlantic, latitudinal gradients in DON and DOP, reflecting a source at the upwelling regions and a sink in the gyres, would be expected. In addition, concentrations of dissolved free and total acid hydrolysable amino acids were determined in order to estimate the fraction of labile or semi-labile DON available to phytoplankton in the surface Atlantic.

2.1 LABORATORY PROTOCOLS AND CHEMICALS

2.1.1. Cleaning protocols

Throughout this study, Milli-Q water (18 mΩ cm^{-1}) was used for rinsing, preparation of standards and reagents and as a medium for the preparation of artificial seawater and throughout dialysis experiments. Glassware and utensils (forceps, spatulas) were meticulously cleaned prior to use following a strict protocol: > 4 h in Decon-90 detergent, rinse with distilled water (3 times), > 4h in 10% hydrochloric acid or 10% sodium hydroxide, rinse with Milli-Q water (> 6 times) and pre-combusted at 450^{o}C for > 4h in a muffle furnace. Glassware and utensils were stored in pre-combusted (450^{o}C for > 4h) aluminium foil. Forceps and spatulas were wiped with dichloromethane (DCM) prior to use.

Glass fibre filters (GF/F) employed throughout this study were pre-combusted prior to use. Filters were wrapped in aluminium foil (10 per pack) and placed in a muffle furnace at 450^{o}C for > 4h.

2.1.2. Materials, Chemicals and their Suppliers

Table 2.1. Chemicals and reagents, their analytical grade and relevant suppliers used in the present study

PURPOSE	CHEMICAL	ANALYTICAL GRADE	SUPPLIER
Cleaning	Decon cleaning reagent	Decon-90	BDH
	Hydrochloric acid	AnalaR sp. gr 1.16	BDH
	Dichloromethane	AnalaR	BDH
	Sodium hydroxide	AnalaR	BDH
Filtration	Glass Fibre filters	GF/F (0.7 μm)	Whatman from BDH
	Glass Fibre filters	GF/F (0.7 μm)	Whatman from BDH
Preservation	Orthophosphoric 85% v/v,	ARISTAR	BDH
Reagents for nitrate analysis	Ammonium chloride	AnalaR	BDH
	Sulphanilamide	AnalaR	BDH
	N-1-Naphthylethylenediamine dihydrochloride (NEED)	AnalaR	BDH
Reagents for phosphate analysis	Sulphuric acid	AnalaR	BDH

	Ammonium molybdate	AnalaR	BDH
	Brij-35 Wetting agent	20%	BDH
	Potassium antimony tartrate	AnalaR	BDH
	Ascorbic Acid	AnalaR	BDH
	SDS wetting agent	AnalaR	BDH
Standards	Potassium nitrate	AnalaR	BDH
	Potassium dihydrogen orthophosphate	AnalaR	BDH
Artificial seawater	Sodium chloride	AnalaR	BDH
	Potassium chloride	AnalaR	BDH
	Magnesium sulphate 7 hydrate	AnalaR	BDH
	Magnesium chloride 6 hydrate	GPR	BDH
	Calcium chloride 6 hydrate	GPR	BDH
	Sodium hydrogen carbonate	AnalaR	BDH
	Boric Acid	GPR	BDH
	Sodium nitrate	AnalaR	BDH
	Sodium hydrogen phosphate 4 hydrate	AnalaR	BDH
	Sodium chloride	AnalaR	BDH
DON experiments	Urea	AnalaR	BDH
	Ethylenediaminetetra-acetic acid (EDTA)	AnalaR	BDH
	BSA	Albumin, Bovine 98% minimum	Sigma
	Hydrogen peroxide	AnalaR	BDH
	Formaldehyde	AnalaR	BDH
HTCO	Aluminium oxide impregnated with 0.5% platinum	TC catalyst set	Shimadzu
	Silver nitrate in 25% phosphoric acid	/	Shimadzu
	Potassium hydrogen phthalate	AnalaR	BDH
	Glycine	AnalaR	BDH
Pigments	Canthaxanthin	/	Water quality institute, Denmark
	Chlorophyll a	From spinach	Sigma Chemical Co.
	Divinyl chlorophyll a	/	R. Bidigare, University of Hawaii
	Divinyl chlorophyll b	/	R. Bidigare, University of Hawaii
	Methanol	HiPerSolv	BDH
	HPLC column	3 µm Hypersil® MOS2 C-8, 120Å pore size, 100 x 4.6mm	Thermo Shandon
	Ammonium acetate	HiPerSolv	BDH
Amino acids	o-Phthaldialdehyde	97%	Sigma
	2-mercaptoethanol	AnalaR	BDH
	Ortho-boric acid	AnalaR	BDH
	Ethanol	ARISTAR 99.7-100%	BDH
	Water	HiPerSolv	BDH
	Toluene	Glass distilled grade	Rathburn Chemical Ltd, Scotland

	Brij 35 solution	30% w/v	Sigma diagnostics
	Sodium Acetate-3-hydrate	HiPerSolv	BDH
	Glacial acetic acid	HiPerSolv 100%	BDH
	HPLC column	5 μm C_{18} adsorbosphere OPA-HR reverse phase, 150mm x 4.6 mm	Alltech
	Methanol	HiPerSolv	BDH
	Tetrahydrofuran	HiPerSolv	BDH
	Hydrochloric Acid	ARISTAR	BDH
	β-alanine	*	Sigma
	α-amino adipic acid	*	Sigma
	γ-amino adipic acid	*	Sigma
	$_{L}$-Arganine Hydrochloride	*	Sigma
	$_{D,L}$-Aspartic Acid	*	Sigma
	Fluorophenylalanine	*	Sigma
	$_{L}$-Glutamic acid	*	Sigma
	Glycine	*	Sigma
	$_{L}$-Histidine	*	Sigma
	Hydroxylysine	*	Sigma
	$_{L}$-Isoleusine	*	Sigma
	$_{L}$-Leusine	*	Sigma
	$_{L}$-Lysine Hydrochloride	*	Sigma
	$_{D,L}$-Methionine	*	Sigma
	$_{L}$-Ornithine Hydrochloride	*	Sigma
	$_{D,L}$-Phenylalanine	*	Sigma
	$_{D,L}$-Serine	*	Sigma
	$_{D,L}$-Threonine	*	Sigma
	$_{L}$-Tyrosine	*	Sigma
	$_{D,L}$-Valine	*	Sigma
Consumables	Dialysis membranes	Spectra/Por ® Cellulose ester membrane, 100 MWCO, flat width 16 ± 1.5mm and 31 ± 0.2 mm	Medicell International Ltd, London
	Dialysis clips	Spectra/Por® Closures, 35mm	Medicell International Ltd, London
	Dialysis clips	/	BDH

* 98 % minimum or higher. Purchased in an amino acid calibration kit, Sigma Aldrich.

2.1.3. Statistical analysis of data

Where replicate (> 3) samples were obtained or replicate analysis was performed, the mean ($\bar{x}$), standard deviation (σ) and standard error (SE) were determined by:

$$\bar{x} = \frac{\sum_i x_i}{n} \qquad \text{Eq. 2.1}$$

$$\sigma = \sqrt{\frac{\sum_i (x_i - \bar{x})^2}{(n-1)}} \qquad \text{Eq. 2.2}$$

$$SE = \frac{\sigma}{\sqrt{n}} \qquad \text{Eq. 2.3}$$

where n is the number of observations. In order to determine the precision of replicate analysis (> 3), the coefficient of variation (CV), as a percentage, was determined by:

$$CV = \frac{\bar{x}}{\sigma} \times 100\,\% \qquad \text{Eq. 2.4}$$

When it was not possible to collect replicate samples or perform replicate analysis, the mean CV was determined for all replicate analyses (>3), and the percentage error applied to samples of less < 3 replicates.

The standard deviation (σ) and CV for data (C) determined by the difference between two measured parameters (e.g. A-B=C, where A and B are the measured parameters) is described by:

$$\sigma_C = \sqrt{\frac{(\sigma_A)^2 + (\sigma_B)^2}{n-1}} \qquad \text{Eq. 2.5}$$

$$CV_C = \sqrt{\frac{(CV_A)^2 - (CV_B)^2}{n-1}} \qquad \text{Eq. 2.6}$$

The 95% confidence limits, used to compare methods or correlations between two data sets, were determined from the mean ($\bar{x}$) and standard deviation (σ) of the sample, as described by:

$$95\%\ \text{confidence interval} = \bar{x} \pm t(\frac{\sigma}{\sqrt{n}}) \qquad \text{Eq. 2.7}$$

where t is obtained from statistical tables (Table 2.3, Miller and Miller, 1993).

The Dixons-Q test was used to exclude outliers from within sample analysis or between-sample analysis, and is described by:

$$Q = \frac{\text{suspect value} - \text{nearest value}}{\text{largest value} - \text{smallest value}} \qquad \text{Eq. 2.8}$$

where the nearest value is closest to the suspect value in size. The value is question was rejected if the calculated value for Q was greater than the critical value of Q, (P=0.05, i.e. 95% confidence) gained from Table A4 in Miller and Miller (1993).

2.2. SAMPLE COLLECTION

2.2.1. Atlantic Meridional Transect

Samples were collected at 23 stations during a research cruise (*RRS James Clark Ross*, 13th April and 6th May 2000), which was part of the Atlantic Meridional Transect programme (AMT 10), between 35° 05'S, 49° 18'W and 49°19'N, 06° 00' W and including the JGOFS site at 47° N, 20° W (Figure 2.1). Discrete depths were sampled using a 12 x 12 L Niskin bottle sampler mounted on a Sea-Bird Electronics 911 Plus Conductivity Temperature Depth (CTD) frame, which provided temperature, density, salinity and fluorescence profiles for each station (see Appendix A). Between 7 and 10 depths were sampled during each CTD cast to a depth of 250m and samples were drawn from all depths in the present study (see Appendix B for sample log). Choice of sampling depths was based on real time fluorescence depth profiles taken at each station, samples taken above and below the deep chlorophyll maximum. One station

(AMT10-7) at -13^{o} 30' N, 32^{o} 19' W was sampled to a depth of 1000m. Date, latitude (°N) and longitude (°W), local time and maximum depth sampled for each station are shown in Table 2.1. Note that samples were not collected at all stations during this study and that samples from certain depths were unavailable (see Appendix B).

Figure 2.1. Atlantic Meridional Transect cruise track and station positions (numbered symbols) from Montevideo (M), Uruguay, to Grimsby, UK., with a port call at Funchal, Madeira. AMT 10 was from 12th April, 2000 to 7th May, 2000 on board the RRS James Clark Ross.

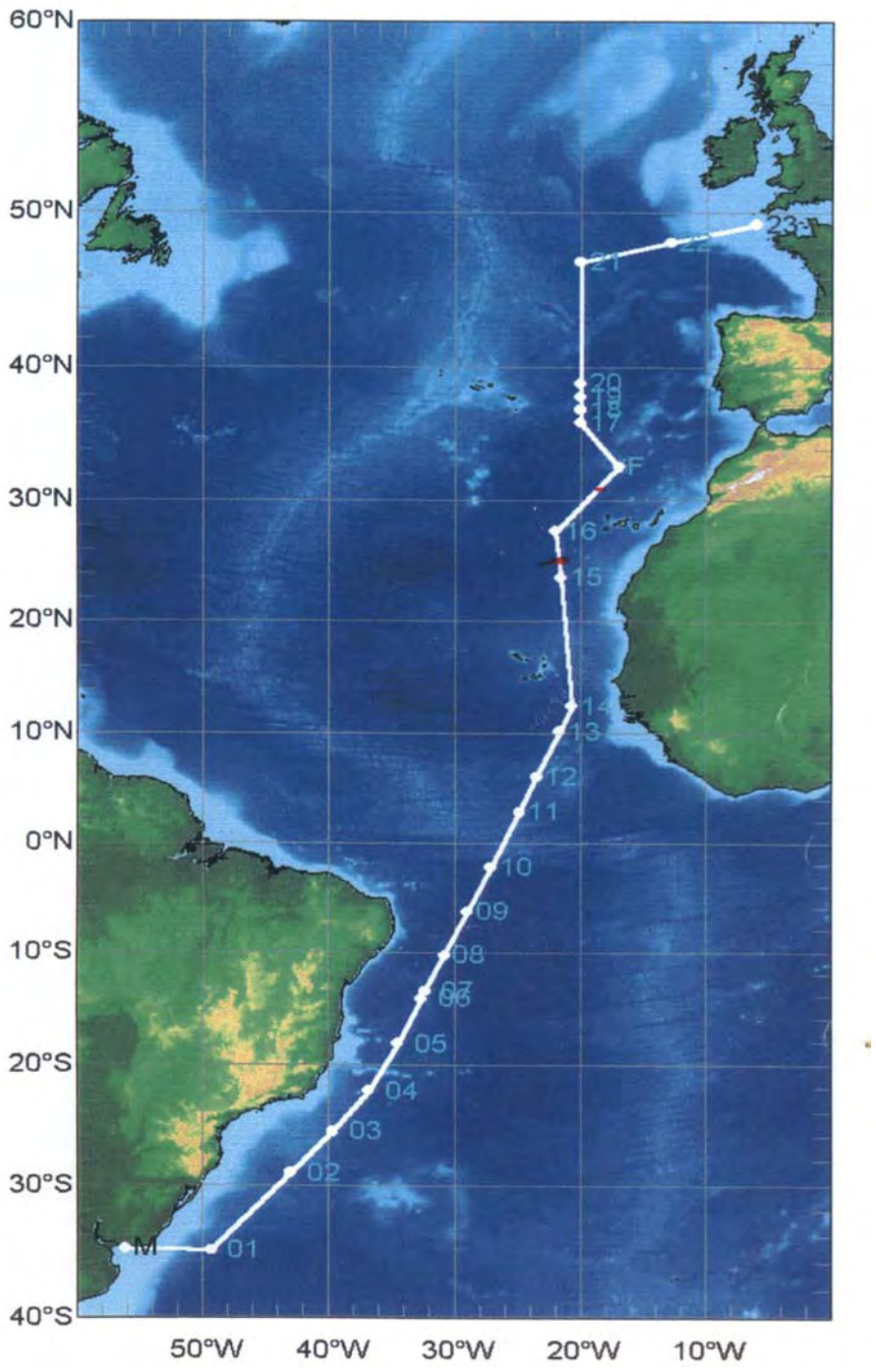

Table 2.2 Station number, date, latitude and longitude, local time of station and the maximum depth sampled for AMT 10 from 12th April 2000 to 7th May 2000 between Montevideo, Uruguay to Grimsby, UK.

STATION NUMBER	DATE DD/MM/YY	LATITUDE (^{O} N)	LONGITUDE (^{O} W)	LOCAL TIME OF STATION	MAX. DEPTH
AMT10-1	13/04/00	- 35 05.3	49 18.0	1530	200
AMT10-2	15/04/00	-29 02.8	43 01.4	1014	200
AMT10-3	16/04/00	-25 40.5	39 41.4	1015	No station
AMT10-4	17/04/00	-22 14.8	36 50.4	1015	250
AMT10-5	18/04/00	-18 09.7	34 32.2	1000	No station
AMT10-6	19/04/00	-14 11.0	32 39.1	1000	250
AMT10-7	19/04/00	-13 30.8	32 19.6	1505	1000
AMT10-8	20/04/00	-10 17.1	30 49.9	1000	250
AMT10-9	21/04/00	-6 20.4	28 59.7	1000	250
AMT10-10	22/04/00	-2 13.5	27 06.0	1000	250
AMT10-11	23/04/00	1 56.5	25 15.1	1000	200
AMT10-12	24/04/00	6 05.9	23 27.0	1000	200
AMT10-13	25/04/00	10 12.2	21 39.3	1000	200
AMT10-14	26/04/00	12 28.1	20 39.4	2359	200
AMT10-15	27/04/00	23 40.9	21 33.8	1455	230
AMT10-16	29/04/00	27 32.0	21 57.7	1000	250
AMT10-17	01/05/00	36 00.0	19 59.7	1600	200
AMT10-18	01/05/00	36 57.6	19 59.6	2200	200
AMT10-19	02/05/00	37 55.0	20 00.2	0400	No station
AMT10-20	02/05/00	38 52.0	20 00.2	1000	200
AMT10-21	04/05/00	46 59.4	20 01.7	0522	200
AMT10-22	05/05/00	48 12.3	12 50.0	1000	150
AMT10-23	06/05/00	49 19.3	06 00.0	1000	100

2.2.2. Collection of samples for analysis of dissolved inorganic and organic nutrients

Samples were collected for the analysis of dissolved inorganic nitrogen (effectively nitrate and nitrite (NO_3^- + NO_2^-), herein NO_3^-), soluble reactive phosphate (PO_4^{3-}), dissolved organic carbon (DOC), dissolved organic nitrogen (DON) and dissolved organic phosphorus (DOP). Due to the low concentrations of the inorganic and organic nutrient pools in oligotrophic regions, it was necessary to follow a rigorous protocol to reduce contamination throughout the preparation, sampling and filtration procedure. Collection vessels and the glass filtration unit were pre-cleaned prior to the cruise and

rinsed (>10 times) between stations with Milli-Q water, wrapped in pre-combusted aluminium foil and oven dried (<60°C) prior to use at each station. The bench area for sample filtration and acidification was kept clean and dust free. Samples were drawn at the earliest opportunity from the recovered CTD (*i.e.* after sampling for trace gases). Polyethylene (powder free) gloves and a laboratory coat were worn throughout the sample collection and filtration procedures.

Samples for dissolved inorganic and organic nutrient analysis were drawn directly from the Niskin bottles (without touching the Niskin bottle spout) into pre-cleaned glass flasks (250mL) with glass stoppers. The glass flasks were rinsed (x 3) in sample seawater prior to sample collection. Seawater from each sampling depth was filtered through a pre-combusted Whatman GF/F filter mounted in a Quick Fit filtration unit. One filter was used per station unless a significant change in pressure was observed due to clogging of the filter. Negligible contamination from GF/F filters has been reported previously (Tanoue, 1992), although they permit passage of bacteria and viruses. Filtration was under positive pressure (high-purity oxygen, < 5 psi). Samples were filtered in order of the maximum depth to the surface. The first 100 mL of each sample was used to rinse the filter and was discarded. 100 mL of sample was subsequently collected in a pre-cleaned amber glass bottle (150 mL) with a Teflon lined cap. Samples were labelled (cruise number, station number, depth, date) and immediately frozen upright at –20^{o}C.

To compare storage vessels and preservation techniques, samples for DOC and DON analysis were also collected, using the same sample collection and filtration technique as above, in pre-combusted 10 mL quartz ampoules. Samples were preserved by acidification to pH <3 with 50 μL of orthophosphoric acid (85% v/v, ARISTAR grade), dispensed using a high precision dispenser with glass nozzle, to approximately 8

mL of seawater sample. This procedure removes DIC and arrests biological processes. However, potential effects of acidification include the production of volatile products from hydrolysis of organic matter, precipitation of macromolecules and for DON absorption of atmospheric ammonium and volatile organic amines (Sharp, 1993) although these have yet to be quantified. Ampoules were sealed using a butane burner and metal forceps. Care was required to ensure all ampoules were sealed correctly. On occasions when adverse weather did not permit immediate sealing, ampoules were covered in combusted foil and stored at < 4^{o}C. After sealing, samples were stored in the dark at < 4^{o}C

Although it is considered unnecessary to filter samples in oligotrophic waters due to the low POM concentrations (Wangersky, 1993), samples were collected from a wide variety of oceanic regimes during the present study, highly oligotrophic to highly productive. Thus, all samples were filtered to ensure a consistent sampling strategy.

2.2.3 Collection of samples for particulate organic matter, phytoplankton pigments and stable isotopic composition of suspended particulate matter.

Samples for particulate organic carbon (POC), nitrogen (PON), phytoplankton pigments and stable nitrogen isotopic composition of suspended PON (δ^{15}N PON) were collected from the uncontaminated seawater supply, pumped from a depth of 7 m through a 6 mm steel mesh filter. Seawater was filtered through pre-combusted (450^{o}C, > 4 hours) Whatman GF/F filters (150 mm) using a Sartorius GmbH filtration apparatus consisting of three 20 L stainless steel cylinders connected to a stainless steel tripod stand with a 150 mm diameter filtration platform (Figure 2.2). Sampling was performed under positive pressure using the on-board compressed air supply. Two in-line scrubbers, activated carbon and silica, were used to remove organic material and water respectively, from the compressed air supply.

Figure 2.2. Schematic of the Sartorius GmbH filtration large volume filtration unit used to filter seawater (200L-100L) from the underway non-toxic supply during AMT 10.

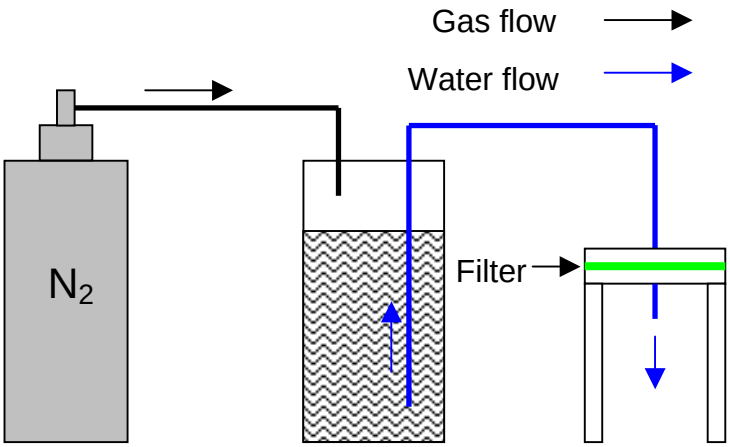

The initial sampling strategy was to filter 1000 L through each filter. This was based on previously AMT PON concentrations (0.1 μM) and the mass of N required for stable isotopic analysis of PON (100 μg N). However, on board determination of chlorophyll *a* concentrations (Welschmeyer, 1994) during the filtration process revealed 60% *in situ* degradation during the time (20 h) to filter 1000 L. Therefore, at each station or underway, only 200 L from the uncontaminated seawater supply was filtered (2 to 4 hours), unless a significant pressure change was observed, indicating high loading of the filter. Filters were then folded in half, wrapped in pre-combusted aluminium foil, labelled and frozen immediately (–20^{o}C). In hindsight, filters should have been stored in liquid nitrogen as it has been shown storage at –20^{o}C is insufficient in preventing pigment degradation (Jeffery *et al.*, 1997).

2.2.4 Collection of samples for stable isotopic composition of dissolved organic nitrogen (δ^{15}N DON)

Large volumes (~ 2 L) of filtered seawater were required for the δ^{15}N DON based on the concentration of DON in the open ocean (~ 5 μM) and the mass of N required for stable isotopic analysis of DON (100 μg). Seawater samples were collected at each station by removing the waste pipe from the tripod of the Sartorius GmbH filtration apparatus (see Figure 2.2) and collecting ~ 2 L of seawater directly into 2.5 L pre-cleaned amber bottles. After collection, the bottles were capped with plastic lids lined with pre-combusted aluminium foil, and were frozen upright at –20^{o}C.

2.3 SAMPLE ANALYSIS

2.3.1 Inorganic nutrient analysis – nitrate plus nitrite and phosphate

Nutrient analysis for samples collected on AMT 10 was performed by the author at Southampton Oceanography Centre. NO_3^- and PO_4^{3-} were analysed using a Skalar Sampler 1000 auto-sampler (maximum 40 samples) and Skalar San^{plus} segmented flow analyser with colourimetric detector (50mm cell). Digital output from the colourimetric detector was collected by a Skalar San^{plus} system data collection unit (DCU) and interpreted using FlowAccess Software on a Dell Laptop computer (Figure 2.3). Standard colorimetric techniques (Kirkwood 1995, Heywood and King 1996) were employed, but are described briefly below.

Figure 2.3. A schematic of the Skalar Sampler 1000 auto-sampler, Skalar San ^{plus} segmented flow analyser, colourimetric detector, data collection unit and computer for data processing used for the determination of nitrate (blue) and phosphate (red) analysis. Not to scale.

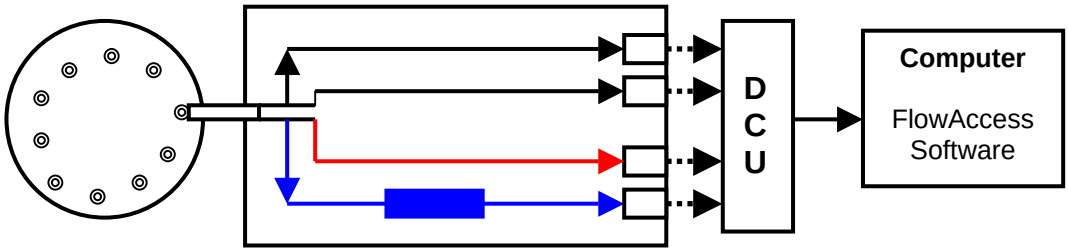

2.3.1.1. Nitrate

For direct colourimetric determination of concentrations of NO_3^- ($[NO_3^-]$), it is necessary to reduce nitrate to nitrite by passing the sample through a copperised cadmium column at a pH of 8 to 8.5, achieved by addition of ammonium chloride buffer. A diazotising agent, sulphanilamide and a coupling agent, N- (1-naphthyl) ethylenediamine dihydrochloride (NEED), are added to form a pink diazo-couple complex with absorbance measured at 543 nm. As the reaction time is critical, tube diameter and mixing spirals on the auto-analyser are adjusted to allow 10 minutes for the reaction to go to completion before absorbance is determined (Figure 2.4). Details of the buffer and combined reagent are shown in Table 2.2. All reagents were stored in labelled black plastic 1 L bottles.

Figure 2.4. Flow diagram of hydraulics for nitrate plus nitrite analysis. Key indicates diameters (mm) of tube required to gain flow rates.

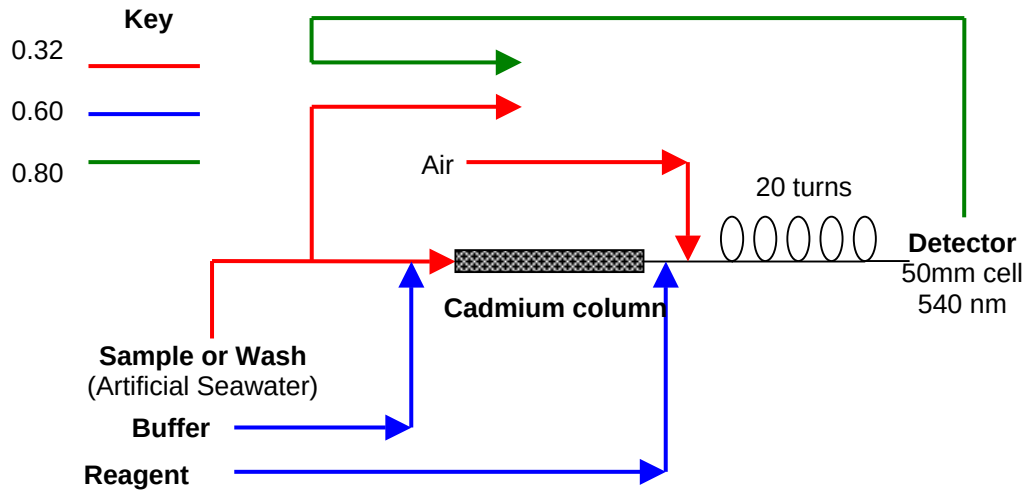

Table 2.3. Details of reagents required for nitrate plus nitrite (NO_3^-) analysis. All reagents are prepared in Milli-Q water.

REAGENT	SOLUTION	MASS IN VOLUME (1 L)	FINAL CONCENTRATION (M)
Buffer	Ammonium chloride	3 g	0.057
Combined	Sulphanilamide	0.5 g*	0.003
reagent	HCl	5 mL*	0.058
	NEDD	50mg*	0.0002
	10% Brij-35 wetting agent	0.5 mL*	N/A

* To be prepared together in 1 L of water

2.3.1.2. Phosphate

Details of the reagents used for phosphate are shown in Table 2.4. Again, all reagents were stored in labelled black plastic 1 L bottles. Phosphate concentrations ($[PO_4^{3-}]$) are determined using the colorimetric method developed by Murphy and Riley (1962). Molybdate, sulphuric acid, potassium antimony tartrate and ascorbic acid are used as reducing agents and absorbance of the final blue solution is measured at 880 nm. Subsequent investigations have altered the method slightly (reagent concentrations), as the acid/molybdenum ratio is crucial and influences the form of final reduced complex and also controls the reaction kinetics. Again, the time for reaction is critical, so tube diameters and mixing spirals are adjusted accordingly (Figure 2.5).

Table 2.4. Details of reagents required for phosphate (PO_4^{3-}) analysis. All reagents are prepared in Milli-Q water.

REAGENT	SOLUTION	MASS IN VOLUME (1 L)	FINAL CONCENTRATION (M)
Reagent 1	Sulphuric acid 5M	400 mL	2
	Ammonium molybdate	9.6 g	0.0078
	Potassium antimony tartrate	0.212 g	0.00065
Reagent 2	Ascorbic Acid	8.4 g	0.047
	SDS wetting agent	0.5 g	N/A

Figure 2.5. Flow diagram of hydraulics for phosphate (PO_4^{3-}) analysis. Key indicates diameters of tubes required to gain flow rates.

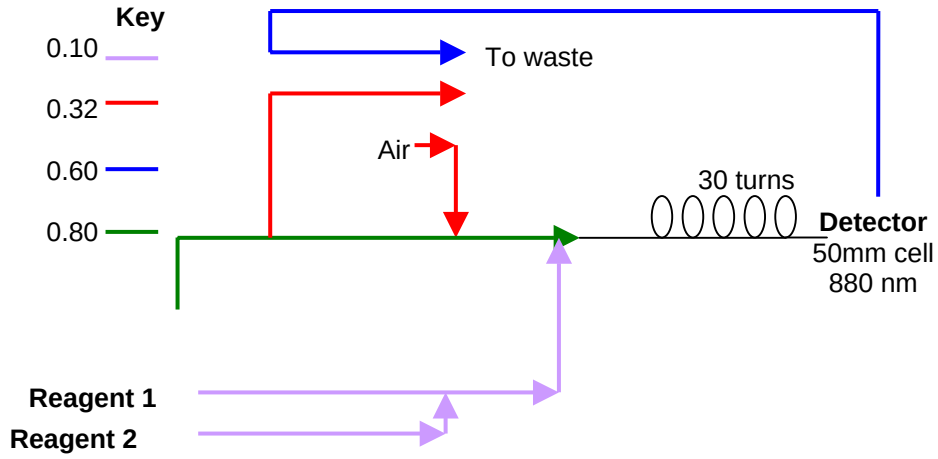

2.3.1.3 Standards

Mixed standards were prepared daily in clean 250 mL plastic volumetric flasks. Primary standards of potassium nitrate (10 mM) and phosphate (10 mM) (Table 2.5) were added to each flask and the volume made up to 250 mL with Milli-Q water. All calibrations were performed using standards ranging in concentration from 0 to 30 µM N and 0 to 3 µM P (Table 2.5). A typical calibration chromatogram and curve are shown in Appendix C.

Table 2.5. Volume of nitrate (Vol. NO_3^-: 10mM) and phosphate (Vol. PO_4^{3-}: 10 mM) stock standards required for daily preparation of mixed standard for final concentrations of NO_3^- ($[NO_3^-]$) and PO_4^{3-} ($[PO_4^{3-}]$) ranging from 0 to 30 µM and 0 to 3µM, respectively. Standards are prepared in Milli-Q water.

FLASK NUMBER	Vol. NO_3^- (µL)	Vol. PO_4^{3-} (µL)	$[NO_3^-]$ (µM)	$[PO_4^{3-}]$ (µM)
0	0	0	0	0
1	125	12.5	5	0.5
2	250	25	10	1.0
3	375	37.5	15	1.5
4	500	50	20	2
5	750	75	30	3

To prevent changes in the refractive index of the flow cell contents, it was imperative that the salinity of the between-sample wash and standards were as close to the salinity of the seawater samples as possible. Artificial seawater (31g NaCl in 1000mL Milli-Q) was used to flush the system, maintain a continuous flow and avoid any optical problems in the flow cell. A salinity match was tested by dropping a few millilitres of artificial seawater into a sample and watching for a "mirror effect".

A typical FlowAccess table of standards and samples is shown in Appendix C. To ensure the baseline and gain or peak height remained constant during daylong analytical work, a wash (W, artificial seawater as above) and drift (D, 10 μM N and 1 μM P mixed standard) were analysed after every 8 samples. Peak areas were recorded and the following equations used to calculate the final concentration of the sample:

a. Wash correction factor (W_f):

$$W_f = \left(N_{sample} - N_{wash}\right) \times \left(\frac{W_2 - W_1}{N_{W2} - N_{W1}}\right) \qquad \text{Eq. 2.9}$$

b. To obtain wash corrected sample peak height (S_w) using W_f:

$$S_w = (\text{Sample} - W_1) - W_f \qquad \text{Eq. 2.10}$$

c. Drift correction factor (D_f):

$$D_f = \left(\frac{D_2 - D_1}{W_2 - W_1}\right) \times (N_{sample} - N_{wash} + 1) + D_1 \qquad \text{Eq. 2.11}$$

d. To correct sample (S_w) for D_f:

$$S_w \times \left(\frac{\text{Sample peak area}}{D_f}\right) \qquad \text{Eq. 2.12}$$

where N_{sample}, N_{wash}, N_{W1} and N_{W2} is the position number of the sample, wash, wash preceding and wash proceeding the sample in question. W_1, W_2, D_1 and D_2 are the peak

areas for the wash preceding and wash proceeding and drift preceding and drift proceeding the sample in question (respectively).

Due to insufficient time, not all samples were analysed in triplicate. Precision was determined from the coefficient of variation (CV, see Eq. 2.4).

Precision was calculated from samples analysed in triplicate or greater and was better than 7.6% for DIN and better than 8.4 % for PO_4^{3-}. Data was evaluated using the Dixon's Q test (see Eq. 2.8) and was rejected if the calculated value for Q was greater than the critical value of Q, (P=0.05, i.e. 95% confidence) gained from Table A4 in Miller and Miller (1993).

Mechanistic or chemical problems caused peak areas to be below the baseline (negative area) during PO_4^{3-} analysis (See Appendix C). The FlowAccess software included negative peak areas in calculating the concentration and thus, SRP accuracy was questionable. Despite washing the PO_4^{3-} lines with 10% sulphuric acid and changing the tubes, this problem could not be rectified during the period allocated for analysis.

The detection limit of the analyses was calculated by 2 methods:

1. Three times the standard deviation of the baseline noise, (Miller and Miller, 1993), calculated from the wash (W) height
2. The baseline noise, calculated from the amplitude of the noise signal.

Large differences were found in the detection limits by applying these methods. The mean detection limits for NO_3^- were 0.29 μM and 0.04 μM using method's 1 and 2, respectively. The mean detection limits for PO_4^{3-} were 0.09 μM and 0.03 μM using methods 1 and 2, respectively. Sanders and Jickells (2000), using this equipment, reported detection limits of 0.1 μM and 0.01 μM for NO_3^- and PO_4^{3-} respectively. An experiment was performed using low nutrient seawater (LNSW) spiked with NO_3^- and

PO_4^{3-} to gain final concentrations between 0.1and 2.5 μM and 0.05 to 1 μM respectively. The detection limits were interpreted to be 0.05 μM for both NO_3^- and PO_4^{3-} (Table 2.6).

Table 2.6. Determined concentrations (det conc., μM) of NO_3^- and PO_4^{3-} from analyses of NO_3^- and PO_4^{3-} -spiked (spk conc, μM) low nutrient seawater (LNSW) for determination of detection limits. Standard deviation (σ) and coefficient of variation (Eq. 2.6) are shown

SPK CONC. (μM)	DET CONC (μM)	σ	CV (%)
NO_3^- LNSW	0.163	0.016	9.91
0.025	-0.008	0.023	14.59
0.05	0.078	0.016	6.46
0.1	0.102	0.039	14.53
0.2	0.139	0.023	7.505
0.4	0.247	0.04	9.652
0.6	0.337	0.023	4.690
PO_4^{3-} LNSW	-0.079	0.203	258.68
0.025	-0.006	0.005	81.21
0.05	0.028	0.001	4.35
0.1	0.082	0.005	6.52
0.2	0.163	0.02	1.52
0.4	0.414	0.11	26.47
0.6	0.587	0.006	0.97

From this experiment, it was also possible to assess the accuracy. The concentration of the spiked LNSW and the measured concentration are plotted in Figures 2.6, a and b for NO_3^- and PO_4^{3-}, respectively. For NO_3^-, the relationship between the spiked and measured concentration was poor (0.5507). In contrast, the relationship between the spiked concentration and measured concentration for PO_4^{3-} was near one-to-one (1.078), despite the mechanistic problems as described above. Finally, commercial standards of nitrate (0.4 μM) and phosphate (0.4 μM) were analysed in replicate (x 4). The results were 0.149 μM and 0.413 μM for NO_3^- and PO_4^{3-}, respectively, confirming that NO_3^- measurements were underestimated.

Figure 2.6 Relationship between (a) LNSW NO_3^-- spiked standards and actual concentration of NO_3^-µM, actual concentration = 0.5507 (LNSW spike standard) + 0.197, R^2 = 0.9573 and (b) LNSW PO_4^{3-} spiked standards and actual concentration of PO_4^{3-} µM, actual concentration = 1.0768 (LNSW spike standard) - 0.0416, R^2 = 0.9915.

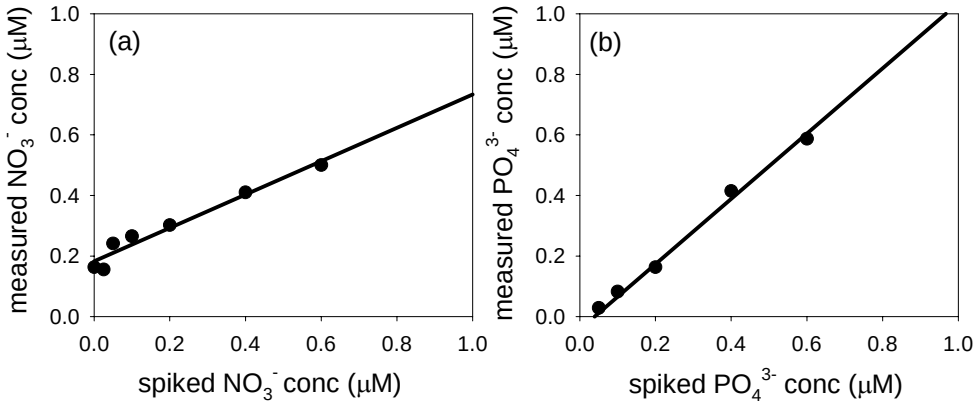

As previously stated, a drift (D) sample (10 µM standard) was analysed after 8 samples to monitor drift during the analytical run. The concentration of each drift was used to assess the precision of repeated analysis on a daily and weekly basis. NO_3^- D (10µM) concentrations ranged from 9.45 µM to 11.52 µM with a precision better than 22.2 %. PO_4^{3-} D (1µM) concentrations ranged from 0.89 µM to 1.25 µM with a precision better than 6.5%. In conclusion, the analysis of PO_4^{3-} was found to be more accurate than NO_3^-.

2.3.2 Organic nutrient analysis

Dissolved organic nitrogen and phosphorus (DON and DOP, respectively), was determined by irradiation (2 hrs) of seawater samples in pre-cleaned (nitric acid and Milli-Q water) quartz glass tubes (10 mL) using a Metrohm 705 UV digestion system at a temperature of > 80^{o}C (Sanders and Jickells 2000). The final [NO_3^-] and [PO_4^{3-}] in the irradiated samples yielded total dissolved N (TDN) and P (TDP). DON and DOP

concentrations were calculated by difference between as TDN and TDP and the initial [NO_3^-] and [PO_4^{3-}], respectively.

Sanders and Jickells (2000) performed a series of experiments using surface Antarctic seawater and urea to investigate the optimal UV oxidation time for analysis of DON. They concluded that 2 hours was sufficient to oxidise 70% of the organic nitrogen to NO_3^-. This experiment was repeated using a seawater sample from AMT 10 (AMT 10, station 23, 80m) and UV oxidation for 0 to 3 h (Figure 2.7). Between 2 and 3 hours, there was a 10% increase in the [NO_3^-]. Despite this increase being within the precision of the analytical method, the author interprets the increase as a suggestion that not all the DON had been oxidised. Although the method employed by Sanders and Jickells (2000) and in this study may be sufficient for processing a large number of samples at sea, it is questionable whether the results accurately reflect [DON] in open ocean samples.

Figure 2.7. Change in NO_3^- concentration ([NO_3^-]) with increasing time of UV oxidation for seawater sample from AMT10, station 23, depth 80m.

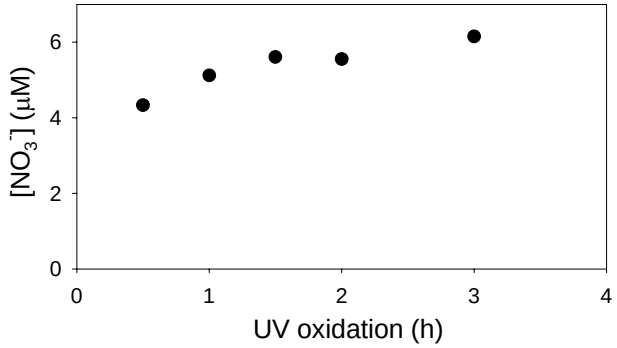

2.3.2.1. Experiments to determine optimum time for UV oxidation for DON analysis.

The chemistry of DON and DOP is complex and little is known about their molecular composition. It is difficult to replicate the lability of the naturally occurring DON and DOP pools to investigate oxidation efficiency and optimum conditions required to completely oxidise DON to NO_3^- and DOP to PO_4^{3-}. Oxidation times vary

between analysts, ranging from 2 hours (Sanders and Jickells, 2000) to 20 hours (Abell *et al.*, 2000). It is also questionable whether DON and DOP should be analysed simultaneously as it is suspected that DOP may be more labile than DON. Although some studies suggested that irradiation for 2 h is sufficient to oxidise DOP (Armstrong *et al.*, 1966, Karl *et al.*, 1993), Ormazagonzalez and Statham (1996) found that polyphosphates may not be completely oxidised after 2 hours UV oxidation. In contrast, Karl and Yanagi (1997) suggest that even 20 min photo-oxidation at < 40°C converts some 60-70% of TOP in surface waters to reactive phosphate. Considering that DON may required up to 20 hours UV oxidation for complete conversion of DON to NO_3^-, simultaneous analysis of DON and DOP should probably be avoided, otherwise losses of P may occur.

During UV oxidation, oxygen becomes limiting. The addition of an oxidising agent, for example, hydrogen peroxide or a persulphate reagent, is also controversial. Sanders and Jickells (2000) discourage the use of reaction initiators, catalysts or oxidants due to high blanks, whereas other analysts use hydrogen peroxide (50 μL per 15mL; Abell *et al.*, 2000) and persulphate reagent (5 ml per 15mL sample; Bronk *et al.*, 2000) on a regular basis.

A series of experiments were performed as part of this study using model N-containing compounds in artificial seawater (see Appendix D), fresh water and seawater samples (Table 2.7) to investigate UV oxidation efficiency. An oxidising agent, hydrogen peroxide, was used throughout the experiment and the temperature maintained at > 75°C throughout the oxidation period.

Table 2.7. Model N-containing compounds, their molecular weight (MW, Da) and their nitrogen content (N %), and freshwater and seawater samples used to investigate the UV oxidation efficiency and addition of an oxidising agent. Throughout the experiments, the initial DON concentration of the commercially available compounds (int. DON, μM) was 10 μM).

SAMPLE	SOURCE	MW	INT. DON (μM)	N %
Urea	BDH	60	10	46
GAY	Sigma Aldrich		10	
EDTA	BDH	292	10	9.58
BSA	BDH	66,000	10	15.9
Coastal	Oban lough, Scotland	/		/
Sea water	Atlantic Ocean	/		/

Initial [NO_3^-] were measured using a Technicon autosampler (maximum capacity 40) attached to a Technicon AutoAnalyser II segmented flow single channel analyser coupled with a Technicon AutoAnalyser S.C. Colourimeter. Data was collected on a Bryans Southern Instruments (Mitcham, England) 28000-chart recorder. The chemistry of the reaction is essentially the same as that detailed in Section 2.3.1.1 above. Calibrations were performed using potassium nitrate (10 mM stock) diluted to final standard concentrations ranging from 0 to 20 μM. Stock solutions of the model-N compounds were prepared and diluted to a final working concentration of 10 μM N.

Model N-containing solutions, fresh water and seawater samples were oxidised in an in-house built UV oxidation kit with an output of 1200 W (Amba lamps) powered by a Pervulux motor. Samples (15 mL) were oxidised in pre-cleaned quartz combustion tubes with Teflon caps, spiked with 100 μL of hydrogen peroxide. After the oxidation period of between 1 and 20 h, the sample was cooled and TDN analyses were performed in triplicate as above. DON concentrations were calculated (DON = TDN- NO_3^-) and percentage yields for model N-containing compounds assessed as:

$$\% \text{ yield} = \frac{\text{Final}[NO_3^-]}{10\mu\text{M}} \times 100 \qquad \text{Eq. 2.13}$$

The results of the experiments are presented in Figure 2.9. Ambiguous data was obtained for urea (Figure 2.8 a) and ethylenediaminetetra-acetic acid (EDTA) (Figure 2.8 b), considered low molecular weight DON, with a large range in recovery for samples oxidised for the same period of time. The tri-peptide, GAY (glycine, alanine, threonine) showed 75% recovery after 4 hours UV oxidation but this decreased to 59% after longer exposure to UV light (6 h, Figure 2.8 c). BSA (albumin bovine serum) was chosen to represent the large, more recalcitrant fraction of DON. Even after exposure to 20 hours UV oxidation, recovery did not exceed 20% (Figure 2.8 d). Freshwater samples obtained from Oban Lough, Scotland, showed maximum concentration after 5 hours UV oxidation (8 hour sample excluded using Dixons-Q test, see equation 2.6) but decreased thereafter (Figure 2.8 e). Seawater samples from AMT 10 (AMT 10 station 17 and AMT 10 station 23) exposed to UV oxidation showed the maximum [NO_3^-] at 8 and 16 hours respectively (17 hour result excluded on AMT 10, station 17). Overall, NO_3^- concentrations tended to remain constant after 12 hours, but decreased after 16 hours exposure to UV light (Figure 2.8, f). A decrease in [NO_3^-] observed with the AMT compounds and other model N-containing compounds may be due to the loss of nitrogen as ammonium (ammonium was not analysed during the experiments). In addition, loss of volume due to the relatively high temperature required for the reaction would also affect the final DIN concentration, creating a more concentrated solution. However, the initial and final volumes were not measured in this study, as the risk of contamination was considered too great during the transfer of the sample.

Figure 2.8. Variation in the percentage (%) recovery (a) urea, (b) ethylenediaminetetra-acetic acid (EDTA), (c) the tripeptide, glycine, alanine, threonine (GAY), (d) albumin bovine serum (BSA), and change in nitrate (NO_3^-) concentration (μM) for (e) coastal water (Oban) and (f) open ocean seawater (AMT 10, station 17) with increasing time to UV oxidation (hours).

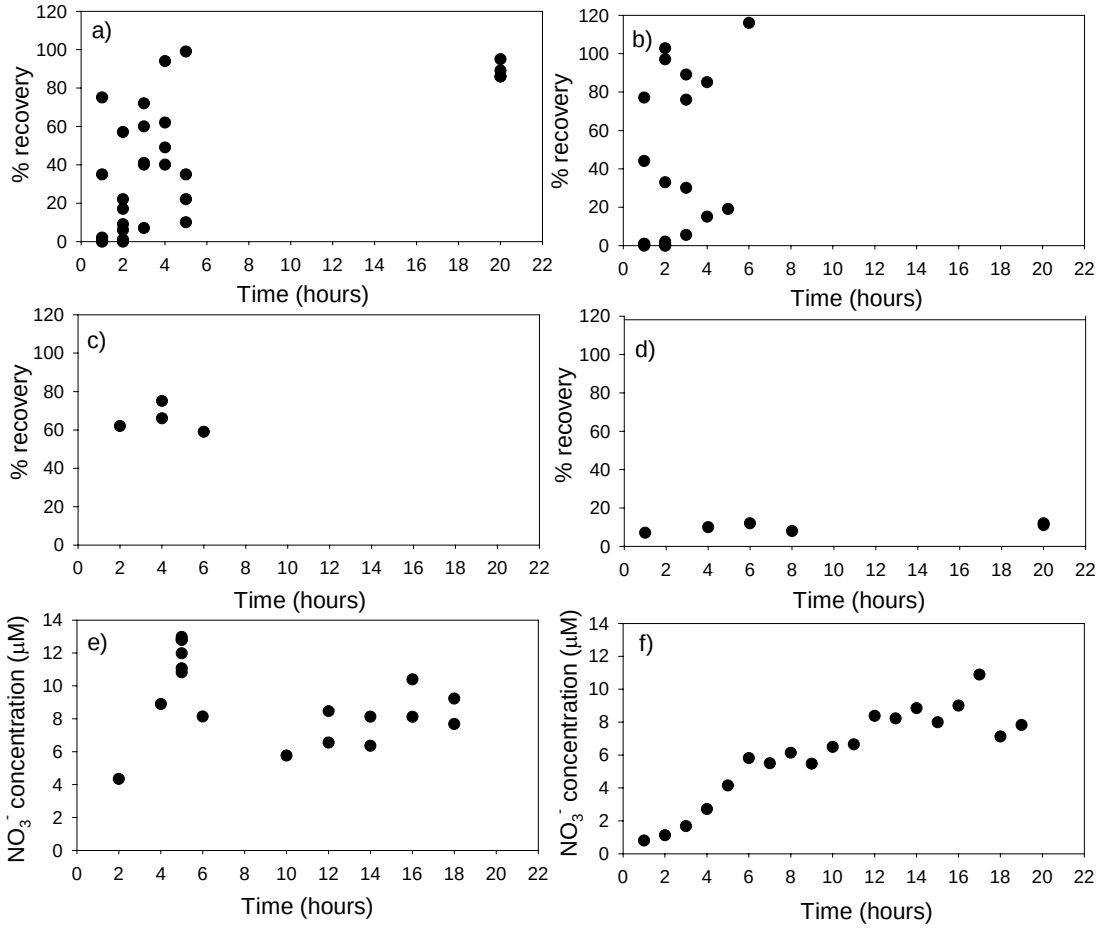

In conclusion, 12 hours UV oxidation with 100μL per 20mL of hydrogen peroxide was deemed sufficient to oxidise DON to NO_3^-. However, 100% recovery of the model-N compounds was not obtained.

In addition to the UV oxidation method, there are 2 alternative methods for the analysis of DON in seawater:

1. Addition of persulphate reagent to oxidise DON to nitrate (Menzel and Vaccaro, 1964; Sharp, 1973; Valderrama, 1981)
2. High temperature catalytic oxidation (HTCO) (Sharp, 1973; Suzuki and Sugimura, 1985).

A comprehensive review (Bronk *et al.*, 2000) and international intercalibration exercise (Sharp *et al.*, 2002) revealed contradictory results; the former study concluded that UV oxidation underestimates [DON] in seawater, whereas the later study concluded that HTCO methods measured the lowest average [DON] and UV oxidation the highest. It is obvious that more activity is required to produce a reliable and reproducible protocol for DON analysis.

2.3.3. Analysis of DOC and DON by High Temperature Catalytic Oxidation

The High Temperature Catalytic Oxidation (HTCO) technique has revolutionised the analysis of DOC and DON (Sugimura and Suzuki, 1988; Tanoue, 1992; Sharp *et al.*, 1993; Wangersky *et al.*, 1993; Peltzer *et al.*, 1996). It is rapid, precise (1-2%) and can be used at sea (Spyres *et al.*, 2000). Seawater samples from AMT 10 were analysed for DOC and DON using the HTCO technique at the University of Plymouth. In order to compare the UV oxidation method and HTCO technique, seawater samples used in the above oxidation efficiency experiment were also analysed for DOC and DON using the HTCO technique. Samples collected on AMT 10 were stored in quartz ampoules, acidified with orthophosphoric acid and flame sealed (see Section 2.1.1). Samples for the method comparison exercise were stored in 150 mL amber bottles with a Teflon lined cap and frozen (-20°C).

2.3.3.1 Principle of operation

The principles of analysis are essentially the same for DOC and DON, except for the methods of detection. Briefly, an aliquot of filtered seawater (200 μL) is directly injected from a *Shimadzu* auto-sampler (maximum capacity 80) into the catalyst filled (aluminium oxide impregnated with 0.5% platinum) oxidation column of the *Shimadzu*

TOC 5000 a analyser. Oxidation takes place at a temperature of 680^{o}C in an atmosphere of high purity oxygen (carbon-free). The sample gas is passed through a series of scrubbers to remove halides (silver nitrate in 25% phosphoric acid, IC reaction vessel), water (electronic dehumidifier) and halogens. Quantitative production of CO_2 and the nitric oxide radical (NO•) gases occurs as follows;

$$DOM\ (DOC + DON) + DIN + O_2 \xrightarrow{680^{o}C,\ Pt\ catalyst} CO_2 + NO\bullet + H_2O \quad \text{Eq. 2.14}$$

The DOC concentration is directly related to the amount of CO_2 produced, which is determined using *a Licor Li 6252*, solid state infrared gas analyser (IRGA) (CO_2-specific wavelength of 4.26 μm).

The quantitatively produced nitrogen oxide radical (NO•) reacts with ozone produced by an in-built ozone generator to form nitrogen dioxide in the excited station (NO_2*), which emits quantifiable light energy (650-900nm) upon decay to ground state:

$$\begin{aligned} NO\bullet + O_3 &\rightarrow NO_2^{*} + O_2 \\ NO_2^{*} + O_3 &\rightarrow NO_2^{o} + h\nu \end{aligned} \quad \text{Eq. 2.15}$$

The light is detected by the photomultiplier tube in a nitrogen-specific chemiluminesence *ANTEK 705D* detector. The light emitted is proportional to the chemically bound N. To calculate DON, it is necessary to have accurate data on the dissolved inorganic N (DIN) pool (nitrate, nitrite, ammonium if available) (TN-DIN=DON). Both the signals from the *Licor* carbon-specific detector and from the *ANTEK* N-specific detector are transferred using data collection units (DCU) to a computer and interpreted using *Shimadzu* TOC and *LabView* software respectively. A schematic of the HTCO system and detectors is shown in Figure 2.9.

Figure 2.9. A schematic diagram of the Schimadzu TOC 5000A, infra-red-gas-analyser (IRGA), Antek Nitrogen specific chemiluminesence detector and data collection units used for the simultaneous analysis of dissolved organic carbon (DOC) and total dissolved nitrogen (TDN).

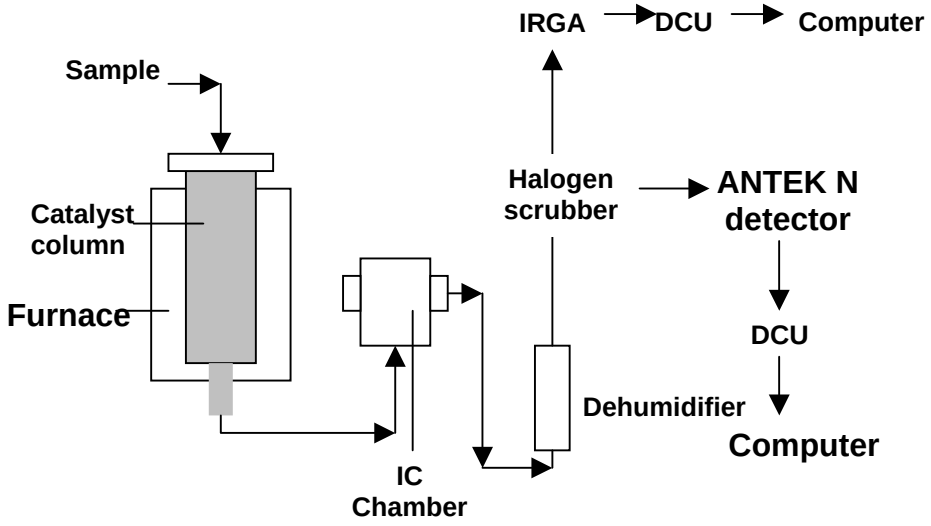

2.3.3.2 Standards, calibrations and certified reference materials

Calibration was performed before and after analysis of ~ 80 samples/standards. Mixed standards were prepared from stock standards of potassium hydrogen phthalate, KHP (100 mM C, $C_8H_5O_4K$) and glycine (GLY; 50 mM N, $C_2H_5NO_2$) for C and N respectively (Table 2.8). A secondary stock solution was prepared with a C: N ratio of 6: 1 (33.33 mL GLY stock + 66.66 mL KHP stock). Daily working standards ranged from 0 to 360 μM and 0 to 60 μM for C and N respectively (Table 2.8).

Table 2.8. Volume (μL) of stock standards of potassium hydrogen phthalate (KHP) and glycine (GLY; $C_2H_5NO_2$) for preparation of daily mixed standards of carbon and nitrogen concentrations ([C] and [N]) ranging from 12 to 360 μM C and 2 to 60 μM N, respectively

VOL. KHP AND GLY (μL)	[C] (μM C)	[N] (μM N)
12	12	2
30	30	5
60	60	10
120	120	20
180	180	30
360	360	60

Standards were poured directly into the pre-cleaned auto-sample vials and placed in the auto-sampler (maximum capacity 72). Calibrations for DOC and DON concentrations ([DOC] and [DON], respectively) were performed at the start of analysis (Figure 2.10i; DOC 1 and DON 1) and after analysis of ~80 samples (Figure 2.10ii; DOC 2 and DON 2). The slope (DOC 1, 105.89 ± 8.53; DOC 2, 98.54 ± 2.26) and intercept (DOC 1, 983.95 ± 1556.77; DOC 2, 1898.05 ± 393.27) for DOC 1 and DOC 2 calibrations were not significantly different (95 % confidence level, n=4)). However, the slope for DON 1 (23.56 ± 0.97) and DON 2 (29.52 ± 0.69) was significantly different (95% confidence level, n=4), indicating a significant change in the detection of nitrogen during the period of analysis. The intercepts for DON 1 (36.97 ± 27.7) and DON 2 (58.65 ± 19.32) were not significantly different.

Figure 2.10. Calibration curves determined at (i) the start of analysis for (a) concentrations of dissolved organic carbon ([DOC], μM) and dissolved organic nitrogen ([DON], μM) and (ii) after analysis of ~ 80 samples for (a) [DOC] (μM) and (b) [DON] (μM). The regression equation and correlation coefficient (R) are noted. The critical correlation coefficient when n=5 is 0.755 (Table C8, Ebdon, 1985).

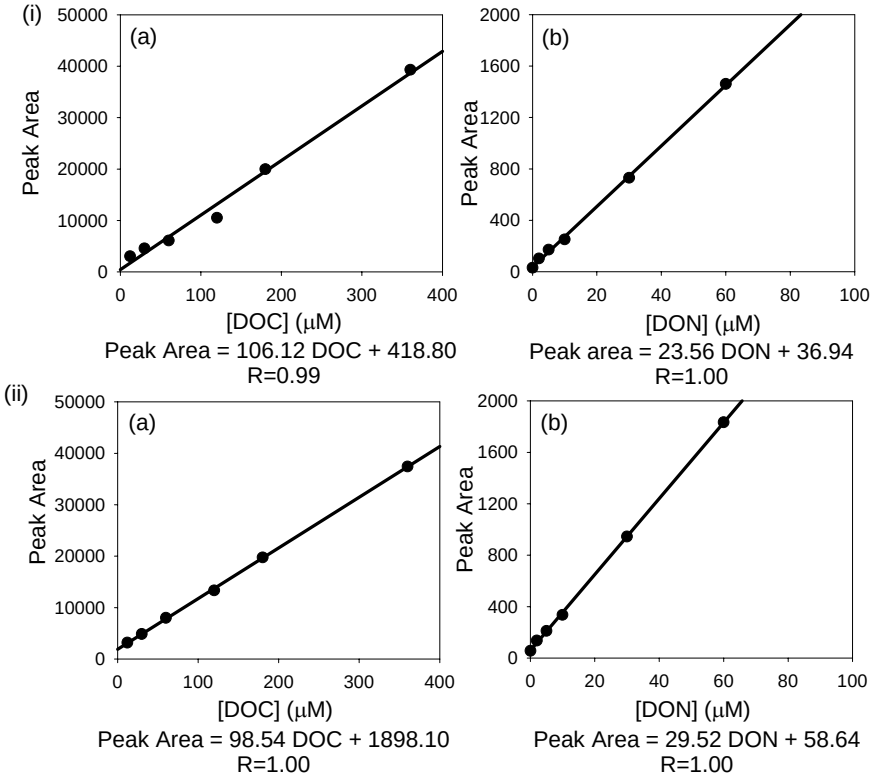

Before opening the sample or reference material ampoules, the neck of each ampoule was cleaned with Milli-Q water and allowed to dry. The seawater sample was poured directly into an pre-cleaned auto-sample vials and placed in the auto-sampler.

DIC concentration is at least an order of magnitude greater that DOC and therefore must be removed before sample analysis. The acidified samples were purged with carbon-free high purity oxygen for 10 minutes in the auto-sampler immediately prior to analysis.

Certified reference materials (CRM) were analysed immediately after calibration and after analysis of 50 to 70 samples. CRM employed were Low Carbon Seawater (LCSW; lot#05/99/01) and Deep Sargasso Sea water (DSS; lot #04/99) distributed by Dennis Hansell at Bermuda Biological Station. [DOC] (56.97 ± 9.33 μM, 95 % confidence level) and [DON] (19.19 ± 1.71 μM) for DSS were lower than concentrations gained during an international calibration exercise ([DOC], 64 μM and [DON], 22.6 ± 0.3 μM; Sharp *et al.*, 2002), respectively. [DOC] (2.79 – 3.26 μM) of LCSW was higher than the certified concentration (2 μM) and [DON] were below the detection limits of the HTCO instrument (~ 1μM, Eric Acterberg, University of Plymouth).

A standard (DOC, 60 or 180 μM; DON, 10 or 30 μM) was injected (x 3) after analysis of 8 samples to monitor drift during the daily analysis (Figure 2.11, a and b). [DOC] standard (60 μM) drifted significantly (95% confidence level), whereas DOC standard 180 μM did not drift significantly, probably due to the close proximity of the injections. Injection 99 was excluded. Drift during DON analysis was not significant (95% confidence level) for both 10 μM and 30 μM standards. Note that analysis of DOC standards 60 and 180 μM yielded actual [DOC] of 82.6 to 140.9 μM and 192.6 to 203.4 μM, respectively (Figure 2.11, a). Analysis of DON 10 μM and 30 μM standards

yielded measured [DON] of 8.8 to 19.5 μM and 37.6 to 38.9 μM, respectively (Figure 2.11, b). This inaccuracy was probably due to the memory effect in the instrument, confirmed by the increase in peak area for Milli-Q water injected throughout the analysis period (Figure 2.12).

Figure 2.11. Variation in concentrations of repeated injections of (a) dissolved organic carbon ([DOC]) standards of 60μM C (white circles) and 180 μM C (white squares) and (b) dissolved organic nitrogen ([DON]) standards of 10μM N (white circles) and 30 μM (white squares). 95% confidence intervals are shown.

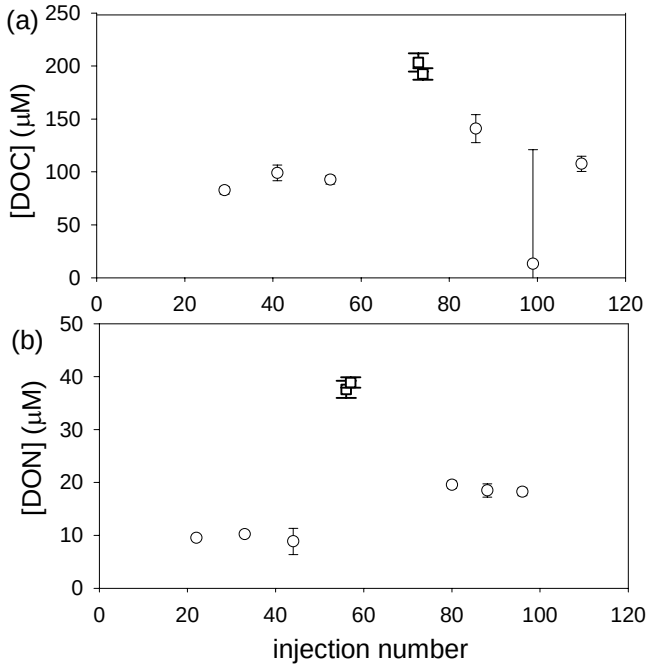

Figure 2.12. Variation in peak height for DOC (black circles) and DON (white circles) for repeated injections of Milli-Q water throughout standard and sample analysis

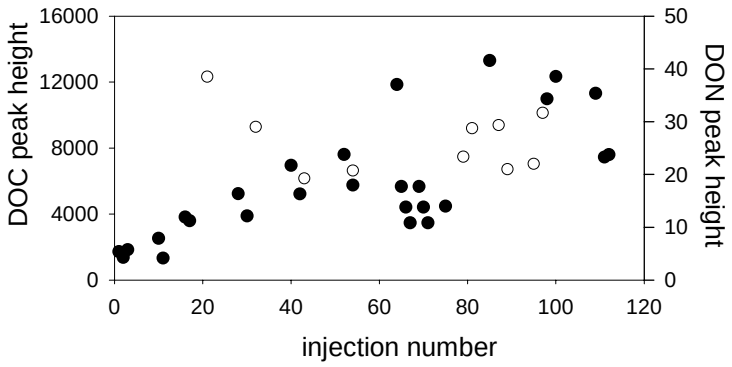

Between-vial (x 3) precision, determined by triplicate injection of seawater samples AMT 10-8-7 and AMT 10-16-7 (stored in amber bottles), was better than 19 % for both DOC and DON (Table 2.9). Within vial precision was better than 19% for DOC analyses, but declined (maximum 288 ‰) during analyses of Milli-Q water or LCSW. Within-vial precision was better than 14% for DON analyses ([DON] > 3μM), but declined to 34 % at low [DON] (< 3 μM). Both observations can probably be explained by analyses near detection limits of the instrument.

Table 2.9. Mean concentration (μM), standard deviation (σ) and coefficient of variation (CV, %) for triplicate analysis of dissolved organic carbon ([DOC]) and dissolved organic nitrogen ([DON]) samples from AMT 10, station 8 at 7m and AMT 10, station 16 at 7m to determine between-vial precision.

SAMPLE	CONCENTRATION (μM)	σ	CV (%)	N
AMT 10-8-7				
DOC	97.83	7.62	7.78	3
DON	6.27	0.45	7.17	3
AMT 10-16-7				
DOC	87.06	16.08	18.47	3
DON	3.03	0.55	18.15	3

During sample collection, storage and decarbonation, there is a high potential for contamination of DOC and DON. Unclean sample collection methods, sample bottles, storage vessels, transfer methods, gases used for decarbonation and lack of gloves and a clean working environment all have the potential of introducing contaminants. In addition, there are a number of inherent problems with the HTCO technique. The most quantitatively significant problems are associated with: (1) mechanical effects associated with the HTCO techniques (e.g. sample injection, salt deposition, memory effects, (2) estimation of the system blank (i.e. carbon emission from the catalyst and components of the analytical hardware) and (3) the oxidation efficiency (Chen *et al.*, 2002). It was beyond the scope of the present study to investigate these parameters.

2.3.4. Phytoplankton Pigment analysis

Photosynthetic and accessory pigments have been widely used to determine the phytoplankton biomass, distribution and composition of phytoplankton assemblages in the marine environment (Jeffrey *et al.*, 1997, Gibb *et al.*, 2000, Barlow *et al.*, 2002). Chlorophyll *a* is the principle photosynthetic pigment used as a unique marker for phytoplankton biomass. Accessory pigments are indicative of specific algal groups (Table 2.10). Therefore, it is possible to deduce which algal group is dominant in the water column depending on the dominant pigment present.

Table 2.10. Marine phytoplankton pigments, pigment abbreviation and representative algal group (compiled from Jeffrey *et al.*, 1997).

PIGMENT	PIGMENT ABBREVIATION	ALGAL GROUP/PROCESS
Chlorophyll c3	Chl c3	Some prymnesiophytes, several diatoms and dinoflagellates
Chlorophyll c1 c2	Chl c1 c2	Most diatoms, dinoflagellates, some prymnesiophytes
Peridinin	Per	Dinoflagellates
19'- Butanoyl-oxyfucoxanthin	But	Prymesiophytes, several dinoflagellates, one chrysophyte
Fucoxanthin	Fuc	Diatoms, prymnesiophytes, chrysophytes, raphidophytes, several dinoflagellates
19'-Hexanoyl-oxyfucoxanthin	Hex	Prymnesiophytes, several dinoflagellates
Violaxanthin	Viol	Green algae, chlorophytes, prasinophytes, eustigmatophytes.
Diadinoxanthin	Diadino	Diatoms, dinoflagellates, prymnesiophytes, chrysophytes, raphidophytes, euglenophytes.
Alloxanthin	Allo	Cryophytes
Diat	Diat	Trace in diatoms, prymnesiophytes and some chrysophytes
Zeaxanthin	Zea	Cyanophytes, prochlorophytes, rhodophytes
Lutein	Lut	Green algae, chlorophytes, prasinophytes
Canthaxanthin	Canth	Internal standard
Divinyl Chlorophyll b	Dv Chl b	Prochlorophytes
Chlorophyll b	Chl b	Green Algae: chlorophytes, prasinophytes and euglenophytes
Divinyl Chlorophyll a	Dv Chl a	Prochlorophytes
Chlorophyll a	Chl a	All photosynthetic microalgae
β Carotene	Car	All algae except cryptophytes and rhodophytes
β Carotene	Car	Green algae, cryptophytes, prochlorophytes, rhodophytes.

[1] includes chlorophytes, prasinophytes and euglenophytes

A suite of filters were selected for phytoplankton pigment analysis (Table 2.11) from each oceanic region sampled during AMT 10 and analysed at Plymouth Marine Laboratory using the method by Barlow *et al*., 1997. An experiment was performed to check if the pigment distribution was homogenous across the 150mm filter (130mm with sample). A strip was removed along the centre of the filter with an area equivalent to a 25mm disc and its chlorophyll *a* concentration determined. Chlorophyll *a* concentrations varied by 11% across the filter. Therefore, to ensure the sample was representative of the whole filter, two strips (4 x 130 mm) were removed from the centre of the filter, each strip being equivalent in area to a 25mm filter (Figure 2.13).

Table 2.11. Filter number, oceanic region, the date sample was collected, average latitude (Lat. ^{o}N) and volume filtered (Vol. L) for samples selected for phytoplankton pigment analysis from AMT 10 cruise. See Appendix B for details of samples.

FILTER	OCEANIC REGION	DATE	LAT. (^{O}N)	VOL (L)
3	Equatorial upwelling	17/04/00	-10	800
4	Equatorial upwelling	20/04/00	-7	920
9	North Africa upwelling	26/04/00	+19	120
14	N. Subtropical gyre	29/04/00	+26	200
18	N. Subtropical gyre	30/05/00	+30	200
23	N. Subtropical gyre	01/05/00	+35	180
27	Subpolar	02/05/00	+38	100
31	Subpolar	03/05/00	+45	160
36	Subpolar	05/05/00	+48	160

Figure 2.13. Filter area removed from 130mm filter for extraction and analysis of phytoplankton pigments. Note that the area removed from the 130mm filter was equal to the area of a 25mm filter.

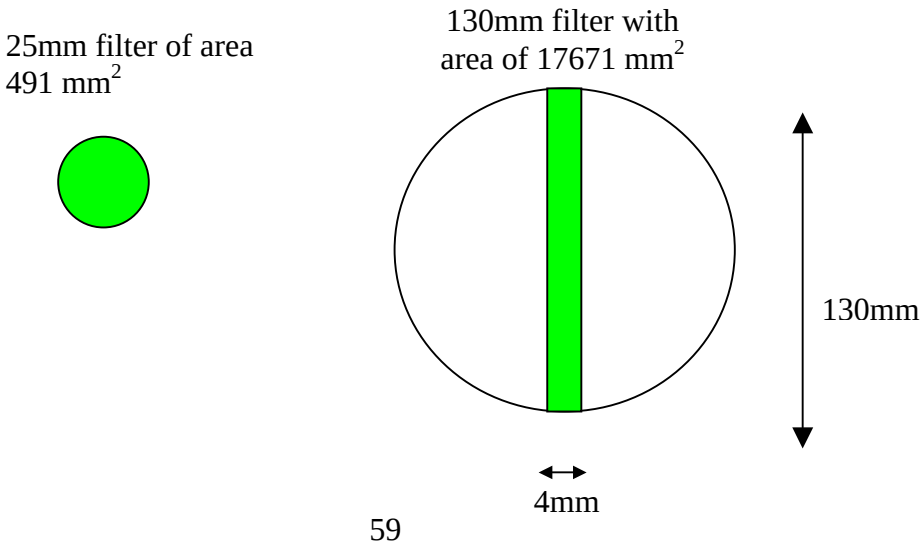

Each strip was placed into a 20 mL plastic tube. Using a pipette, 3 mL of methanol containing an internal standard of canthaxanthin (650 ng ml^{-1} final concentration), was added to plastic tube. The sample was sonicated and macerated to lyse the phytoplankton cells to release pigments. The sample was centrifuged (2000rpm, 4 min) and the final volume of methanol was noted. The supernatant was decanted into micro-centrifuge tubes and samples were centrifuged at high speed for 30 seconds to remove small particles. The supernatant was transferred to 1.5mL amber glass vials and capped with a soft-top lid for automatic injection.

Pigments were analysed using Thermofinnigan auto-sampler mode AS2000 attached to a Thermofinnigan High Performance Liquid Chromatography (HPLC) and fitted with a reverse-phase HPLC column (3 μm Shandon Hypersil ® MOS2 (endcapped), C-8, 120 Å pore size, 100 x 4.6 mm). The mobile phase was ammonium acetate (1 M) and stationary phase, the C8 column. The solvent programme is described in Table 2.12. The Injection volume was 100μL and fluorescence was measured at a wavelength of 440nm. The mean elution times of the each pigment were predetermined (Denise Cummings, PML, personal communication) by co-elution of a mixed standard of pigments listed (Table 2.10). Although the mean retention times varied (± 2 minutes), the elution order of the pigments remains constant. Three chlorophyll *a* standards (monovinyl chlorophyll a standard, Sigma Chemical Co., and divinyl chlorophylls *a* and *b*, University of Hawaii and University of Maryland, respectively, and a canthaxanthin standard (Sigma Chemical Co.) were injected at the start of each sample run. Blanks (methanol) were injected between each sample to wash the column. Reproducibility was 4%.

Table 2.12. Solvent Programme employed for marine phytoplankton pigment analysis at Plymouth Marine Laboratory. Solvent A is 70: 30 Methanol: Ammonium Acetate (1 M). Solvent B is methanol (Barlow *et al.,* 1997).

TIME (min)	SOLVENT A	SOLVENT B	FLOW RATE (ml/min)
0	75	25	1
1	50	50	1
20	30	70	1
25	0	100	1
30	0	100	1
30.1	75	25	1
39	75	25	1
Injection loop volume 100μL, wavelength 440nm			

A chromatograph, retention times of each pigment and area under each pigment peak are reported (see Appendix E).

2.3.4.1. Calculation of pigment concentrations

In order to calculate the concentration of each pigment, the response factors of each pigment relative to canthaxanthin were determined:

$$R_f = \frac{A_{pigment} \times C_{standard}}{A_{standard} \times C_{pigment}} \qquad \text{Eq. 2.16}$$

where $A_{pigment}$ and $A_{standard}$ is the peak area of the pigment and canthaxanthin, respectively, and $C_{pigment}$ and $C_{standard}$ are the concentrations of the pigment and canthaxanthin (650 ng ml^{-1}), respectively. For equal concentrations of pigment and canthaxanthin in the mixed standard, $C_{standard}/C_{pigment}$ is 1. The elution time (min), peak area of each pigment standard and canthaxanthin and response factors (R_f) are shown in Table 2.13.

Table 2.13. Elution time, peak area for calibration and response factors (R_f; Eq. 2.16) of marine phytoplankton pigments determined in this study. See Table 2.10 for pigment abbreviations.

PIGMENT	ELUTION TIME (MIN)	PEAK AREA	R_F
Chlc3	2.6 - 2.7	87362	1.36
Chl c1 c2	3.4 – 3.5	87362	1.36
Per	4.2 – 4.3	37991	0.59
But	5.2	56030	0.87
Fuc	5.51 – 5.57	55871	0.87
Hex	6.2 – 6.3	56838	0.88
Viola	6.5 – 6.6	97366	1.52
Diadino	7.5 – 7.6	89257	1.39
Allo	8.8 – 8.9	78674	1.22
Diato	9.7 – 9.8	58325	0.91
Zea	10.5 – 10.6	72852	1.13
Lut	11.0	83888	1.31
Canth	13.1 – 13.2	64229	1.00
Dv Chl b	18.2 – 18.3	22919	0.36
Chl b	19.2 – 19.3	13690	0.21
Dv Chl a	24.2 – 24.3	33387	0.52
Chl a	24.6 – 24.7	19953	0.31
Car	27.6 – 27.7	56219	0.88

Pigment concentrations (ng L^{-1}) were calculated as follows:

$$\text{Pigment (ng L}^{-1}) = \frac{A_{\text{pigment}}}{R_{\text{f pigment}}} \times \text{Dilution factor} \times \frac{V_{\text{extract}}}{V_{\text{filtered}}} \qquad \text{Eq. 2.17}$$

where A_{pigment} is the peak are of the pigment, $R_{\text{f pigment}}$ is the response factor of the pigment, the dilution factor (2) accounts for the addition of the buffer in the HPLC (0.1 mL buffer and 0.1 mL sample) and V_{extract} and V_{filtered} are the volumes of extract (0.1 x 32 = 3.2 mL) and volume of seawater filtered (mL), respectively. It was later found that the canthaxanthin standard was degraded or contaminated (inconsistent peak areas) and therefore it was deemed necessary to check pigment concentrations from first principles, using the height (H) and width (W) of the pigment peak from the chromatogram (Figure 2.14). This calculation was performed on a selection of pigments to compare methods of determination of concentration.

Figure 2.14. Parameters used to calculate pigment concentrations based on the height (H) and width (W) of the chromatogram peak.

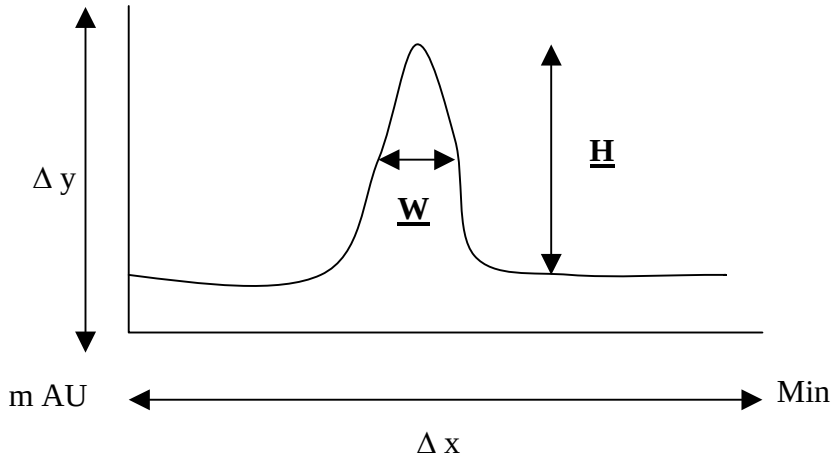

To calculate the concentration of chlorophyll *a*, two steps are required:

1. Area of the pigment peak:

$$\text{Pigment area} = \left(\frac{W \times H \times 1 \times 1}{\Delta y \times \Delta x \times 564 \times 100} \right) \div 5 \qquad \text{Eq. 2.18}$$

where W is the width of the peak (cm) at mid-length of the peak and H is the height of peak (cm) from top to base line. The rate of change of the x and y axis are represented by Δ x, calculated from the change in the x-axis scale per minute (cm/min) and Δ y, calculated by the change in the y-axis scale per minute (m AU/min, note change to cm/AU).

2. Pigment concentrations were calculated by:

$$\text{Pigment (ng L}^{-1}) = \frac{A_{\text{pigment}} \times \text{Dilution factor} \times V_{\text{extract}}(L)}{V_{\text{filtered}}\,(\text{L})} \qquad \text{Eq. 2.19}$$

where the variables are as described for Eq. 2.17. Pigment concentrations in the water column were calculated by considering the ratio between the sub-sample and whole filter (ratio of 12.48).

Pigment concentrations gained for methods described above were comparable and thus the former method was used to calculate the pigment concentration (ng L^{-1}) of particulate matter collected on AMT10.

2.3.5. Particulate organic matter and stable isotopic composition of suspended particulate matter

The chlorophyll *a* concentration across the sample filters was found to vary by 11% and thus it was assumed that the particle distribution across the filter was probably heterogeneous (see Section 2.3.4.). In order to obtain representative samples for determination of POC and PON concentrations and stable nitrogen isotopic composition of PON (δ^{15}N PON), sub-samples (13 mm diameter discs) were randomly cut from the 150 mm filter using a clean (rinsed with dichloromethane and dried) stainless steel core cutter. Between 5 to 10 discs were cut and homogenised to a pulp with Milli-Q (< 4ml) water in a mortar and pestle were and freeze-dried (24 h, – 60°C). The homogeneity of the samples was investigated by analyses (x3) of the homogenised sample for POC and PON using a Carlo Erba Instruments NC 2500 elemental analyser. Samples with greater than 10 % variability were re-homogenised, freeze-dried and re-analysed. Triplicate POC and PON analysis had a precision of better than 12 %. Concentrations of POC and PON in the water column were calculated using the ratio of the area of the subs-sample relative to sample area on the 150 mm filter and the volume filtered as follows:

$$\text{Particulate concentation } (\mu\text{M}) = \left(\frac{\text{A}_{\text{sample}}}{\text{A}_{\text{sub-sample}}} \right) \times \text{V}_{\text{filtered}} \qquad \text{Eq. 2.20}$$

where A_{sample} and $A_{sub\text{-}sample}$ are the areas (mm^{-3}) of the sample filter (150 mm radius) and $V_{filtered}$ is the volume (L) of seawater filtered.

Samples for δ^{15}N PON were analysed at SERC Stable Isotope Laboratory, Florida International University, using an elemental analyser - isotope ratio mass

spectrometer (EA-IRMS). The EA was used to combust the organic material and to reduce the formed gases into N_2, which were measured using a Finnigin MAT Delta C IRMS in continuous flow mode (Owens and Rees, 1989). The isotopic ratio (R) is reported using the standard delta notation:

$$\partial^{15}\,\mathrm{N} = \left(\frac{R_{sample}}{R_{std}} - 1 \right) \times 1000\,‰ \qquad \text{Eq. 2.21}$$

where R is the ^{15}N: ^{14}N ratio and the International standard (std) is atmospheric nitrogen (air N_2). Analytical reproducibility was determined by repeated analyses (x 10) of an commercially available amino acid, glycine, and a laboratory standard, homogenised mangrove leaves. Reproducibility was better than 4 %. Precision was better than 0.4 ‰.

2.3.6 Molecular composition of Dissolved Organic Nitrogen

A great deal of time and attention were devoted to developing a reliable and routine method for isolation of DON from seawater and stable nitrogen isotopic analysis (see Appendix F). Unfortunately, methodological difficulties hampered the development of a successful method for the determination of the $\delta^{15}N$ DON. Therefore, amino acids, being the most accessible and previously studied fractions of DON, were studied. Initially, it was necessary to quantify the dissolved free amino acids (DFAA) and total hydrolysable amino acids (THAA) in the open ocean. Two methods were employed, fluorimetric analysis of DFAA (Parsons *et al*., 1984) and chromatographic analysis of THAA (Cowie and Hedges 1992). The concentrations of DFAA were too low to be detected by the latter method.

2.3.6.1 Analysis of dissolved free amino acids in seawater by fluorimetric techniques.

2.3.6.1.1. Principle of Analysis

Primary amines are reacted with *o*-Phthalaldehyde, a fluoregenic agent, to form a highly fluorescent product in the presence of 2-mercaptoethanol. These fluorescent

products are measured in a 1cm cell with a fluorometer at an optimal excitation (λ_{ex}) and emission (λ_{em}) of 342 nm and 452 nm, respectively.

2.2.6.1.2. Reagents

All reagents were prepared using Milli-Q water. Where possible, either AnalaR or ARISTAR grade reagents were employed to reduce the magnitude of the blank and risk of contamination. An outline of the primary reagents and mixed buffered reagent are described in Table 2.14.

The mixed buffer reagent was prepared by adding 20 mL of *o*-Phthalaldehyde (OPA) solution reagent to 1 mL of mercaptaethanol and 400 mL of borate buffer solution. The solution was ready for use after 12 hours and stable for 2 weeks. On occasions, clear, cuboid crystals were observed in the solution, possibly due to precipitation of the borate buffer. The solution was stored at < 4^{o}C.

Table 2.14 Details for preparation of reagents, o-Phthalaldehyde and borate buffer solutions, used for mixed reagent solution for fluorimetric analysis of amino acids.

REAGENT	CHEMICALS	MASS IN VOLUME	FINAL CONCENTRATION
o-Phthalaldehyde solution	o-Phthalaldehyde 95% ethanol	0.2g in 20mL 95% ethanol	
Borate buffer solution	Ortho-boric acid	24.7g in 1L Milli-Q water[1]	0.4M

[1]Adjust the pH to 9.5±0.02 with 1N NaOH

2.3.6.1.3. Calibration for fluorimetric amino acid analysis

The amino acid, glycine ($C_2H_5NO_2$) was employed as the standard for calibration. A primary standard was prepared by dissolving 0.0751 g of glycine in 100 mL of Milli-Q (1 mM N stock). To prevent bacterial degradation, 1mL of toluene was added to the standard and refrigerated. The standard was stable for many months.

A secondary standard (13.3 μM N) and working standards (0, 0.348, 0.698, 1.046, 1.395 μM N) were prepared on a daily basis from the glycine stock in clean 100 mL volumetric flasks with Milli-Q water. Standards were stored in the fridge when not in use.

2.3.6.1.4. Analysis of amino acids by fluorimetric techniques

Using a pipette and disposable autoclaved tips (140^{o}C for 2 h), 2 mL of sample/standard and 2 mL of mixed buffered reagent were added to clean 8 mL vials, capped, shaken and allowed to stand for 2 min. It was noted that the fluorescence fluctuated greatly if the time of the reaction varied. Therefore, a strict time schedule was employed. A stopwatch was started as soon as the reagent was added to the sample. At 1 min 30 seconds, the sample was transferred to the 1cm glass cuvette (4 mL capacity) and at 1 min 50 seconds, the cuvette was placed into the fluorometer. Fluorescence was determined (λ_{ex} and λ_{em}, 342 nm and 452, respectively) exactly 2 minutes after addition of the reagent to ensure consistency throughout the procedure. Samples were analysed in triplicate and one sample was analysed throughout the analysis period to ensure consistency between days of analysis. The fluorometer was initially zeroed with Milli-Q water.

2.3.6.2. Total hydrolysable amino acids

2.3.6.2.1.Principle of Analysis

Acidic hydrolysis was used to convert proteins/peptides and bound amino acids to the free compounds. The later were separated using reverse phase high performance liquid chromatography (HPLC). The concentrations of individual amino acids were subsequently determined by the fluorescence response of the OPA derivative (Cowie and Hedges, 1992).

2.3.6.2.2. Reagents for chromatographic determination of amino acids

All reagents were prepared in HPLC grade water. To prepare the mixed reagent, 25 mg of OPA was dissolved in methanol (0.5 mL; HPLC grade) in a volumetric flask (5 mL). 30% *Brij* 35 solution (50 μL) and mercaptaethanol (25 μL; HPLC grade) were added to the flask and volume adjusted to 5 mL with 0.8 M borate buffer solution (Table 2.15). The flask was wrapped in aluminium foil to prevent photo-degradation or background fluorescence and stored at < 4^{o}C. The solution was stable after 12 hours.

Table 2.15. Preparation of reagents for amino acid analysis by HPLC techniques

REAGENT	CHEMICALS	MASS IN VOLUME (1000 ML)	FINAL CONCENTRATION
Borate buffer solution	Ortho-boric acid	49.69g in 900mL water[1]	0.8 M
Acetate buffer	Sodium Acetate-3-hydrate	5.44 g in 1 litre water[2] and 50 ml of tetrahydrofuran	40 mM

[1] Adjust to pH 10.5 using sodium hydroxide and adjust volume to 1L
[2] Adjusted to pH 5.8 with glacial acetic acid

2.3.6.2.3. High Performance Liquid chromatography and quantification

The instrument used for HPLC analyses consisted of a Thermoseparation spectra series P2000 pump, a 20 μL rheodyne injection loop, an Alltech C_{18} adsorbosphere OPA-HR reverse phase column (5um, 150mm x 4.6 mm i.d.), an LDC Fluoromonitor III fluorescence detector and a Thermoseparation products data-jet integrator. The solvent programme employed is outlined in Table 2.16, where solvent A is acetate buffer (Table 2.15) and solvent B is methanol (HPLC grade). The acetate buffer was prepared by dissolving 5.44 g of sodium acetate-3-hydrate in 1 L of HPLC grade water (40 mM). The pH was adjusted to 5.8 with glacial acetic acid, then tetrahydrofuran (50 mL; HPLC grade) was added and the solution shaken well. Solvents were degassed

using helium (20 min) and HPLC tubing was purged (flow rate 10mL min^{-1}; 1 min) to remove any air bubbles trapped or in the pump heads.

Table 2.16. Solvent programme used for chromatographic analysis of amino acids. Solvent A is acetate buffer. Solvent B is methanol. See Table 2.14 for detail of reagent preparation.

TIME (min)	SOLVENT A (%)	SOLVENT B (%)	FLOW RATE (ml min^{-1})
0	100	0	1.0
2	100	0	1.0
45	35	65	1.0
46	10	90	1.0
47	2	98	1.0
50	100	0	1.0

In order to identify and quantify individual amino acids, it was necessary to determine the retention time (time of elution for a specific amino acid) and response factors (R_f) (see Eq. 2.10, where pigments are amino acids) of a suite of amino acids and an internal standard. Amino acids, their abbreviation and molecular weight employed in this study are noted in Table 2.17. Hydroxylysine, a non-protein amino acid, was used as the internal standard. A volume of stock hydroxylysine (2 mM) was added to each sample to gain a final internal standard concentration of 20 μM. A mixed standard was prepared (for determination of response factors) by mixing 100μL of each amino acid stock solution (2 mM; see Appendix G for details) and the internal standard, to give a final concentration of 20 μM for each analyte.

Table 2.17. Abbreviations and molecular weight of amino acids and internal standard employed in this study

AMINO ACID	ABBREVIATION	MOLECULAR WEIGHT
β-alanine	BALA	89.09
α-amino adipic acid	AAAA	161.15
γ-amino adipic acid	GABA	103.12
Arganine	ARG	210.67
Aspartic Acid	ASP	133.10
Fluorophenylalanine	FPHE	183.18
Glutamic acid	GLU	147.13
Glycine	GLY	75.06
Histidine	HIS	209.63
Hydroxylysine	HLYS	198.5
Isoleusine	ILE	131.17
Leusine	LEU	131.17
Lysine	LYS	182.65
Methionine	MET	149.20
Ornithine	ORN	168.62
Phenylalanine	PHE	165.19
Serine	SER	105.09
Threonine	THR	119.12
Tyrosine	TYR	181.19
Valine	VAL	117.15

Equal volumes of the mixed amino acid standard (100 μL) and the OPA reagent (100 μL) were transferred to a clean 2 mL vial and shaken for 1 minute prior to injection (20 μL). Analyses were complete in 50 minutes. A typical chromatogram for the amino acid mixed standard is shown in Appendix H. Retention times and response factors are noted in Table 2.18. Retention times varied by ± 2 minutes but the order of elution remained the same. The concentration of individual amino acids (C_{AA}) was calculated as follows:

$$C_{AA} = \frac{A_{sample} \times C_{internal\ standard}}{A_{internal\,standard} \times Rf_{sample}} \qquad \text{Eq. 2.22}$$

where A_{sample} is the area of the sample peak, $A_{internal\ standard}$ is the area of the internal standard peak, $C_{internal\ standard}$ is the concentration of the internal standard (20 μM this study) and Rf_{sample} is the response factor of the sample (Table 2.17).

Table 2.18. Retention times and response factors for amino acid mixed standard and the internal standard, Hydroxylysine

ABBREVIATION	RETENTION TIME	RESPONSE FACTOR (RF_{SAMPLE})
ASP	3.24	10.22
GLU	5.87	8.67
AAAA	12.9	9.16
SER	13.32	4.86
HIS	15.85	4.12
GLY	19.49	4.24
THRE	23.62	8.18
ARG	25.91	6.21
ALA	28.33	6.81
TYR	29.63	3.96
GABA	30.76	0.11
MET	33.01	0.05
VAL	34.00	8.21
PHE	35.62	5.60
ILE+FPHE	38.71	6.07
LEU	39.41	11.95
HLYS	41.13	1.00
ORN	43.20	0.52
LYS	44.57	1.12

2.3.6.2.4. Acid hydrolysis

Using a pipette and disposable autoclaved tips (140°C; 2 h), the seawater sample (900 μL) was mixed with of the internal standard hydroxylysine, (100 μL; 2mM), and 50% HCL (1 mL, *Aristar* grade). Each sample was degassed using a stream of nitrogen through a pre-combusted Pasteur pipette (1 per sample) for 1 min. The tubes were capped immediately and hydrolysed (150°C; 90 min). After cooling for 1 hour, the hydrolysed samples were placed in a freezer (-20°C; 2 h) and freeze-dried (12 h). Water (900 μL; HPLC grade) was added to the dried sample and was then shaken (20 min)

using a Griffin flask shaker. Samples were either analysed immediately or stored (–2°C) until analysis. Blanks were determined by hydrolysing HPLC grade water as above although this cannot be considered a seawater blank. Recovery (%) was also determined by hydrolysing the tri-peptide, GAY (1μM N), as above.

PART ONE

3.1. SEASONAL CYCLE AND PHYSICAL STRUCTURE OF THE ATLANTIC OCEAN

3.1.1. Introduction

Subtropical gyres are vast regions of the open ocean characterised by basin scale, wind-induced downwelling in their centres (McClain and Firestone, 1993). Seasonal changes enforced by a combination of seasonal winds and solar heating are manifested in the temperature (T) and salinity (S) distributions in the surface layers (250 m). Surface T is directly controlled by radiative heating, as well as by the exchange of sensible and latent heat with the atmosphere. Surface S distributions are controlled by air-sea flux (evaporation versus precipitation) over the open ocean. This in turn affects the upper ocean layer density and stratification. Whereas surface T is rapidly modified by surface heating, surface S is modified relatively slowly, so provides a memory and records the effects of atmospheric and mixing events (*e.g.* convection).

The surface ocean experiences seasonal variation in response to atmospheric forcing. Late spring/early summer conditions represent the legacy of winter cooling and the onset of summer warming, causing weak stratification. In contrast, autumn/early winter conditions represent the legacy of summer warming and the beginning of winter cooling and will therefore be more strongly stratified. The Atlantic Meridional Transect (AMT) cruises during April and May capture spring in the northern hemisphere (weakly stratified) and autumn in the southern hemisphere (summer stratification; Figure 3.1, a). AMT cruises in September-October capture autumn in the northern hemisphere (summer stratification) and spring in the southern hemisphere (weak stratification; Figure 3.1, b: see Appendix A for cruise dates and tracks). For convenience, the April-May AMT transect will be referred to as the Spring AMT and the September-October AMT transect will be referred to as the Autumn AMT. Overall, an asymmetrical

structure of the surface ocean would be observed during the Atlantic Meridional transect due to the seasonal differences between hemispheres.

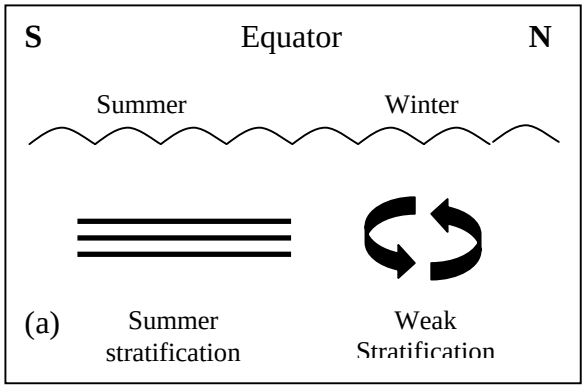

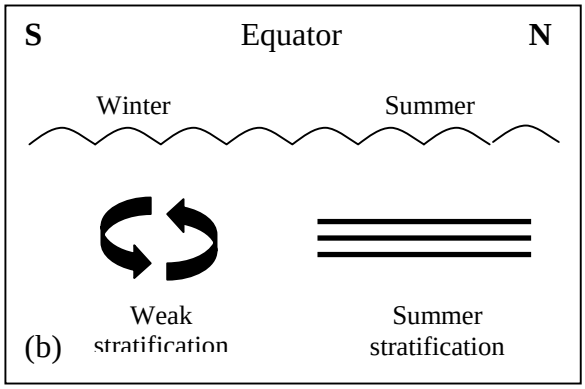

Figure 3.1. Schematic representing the winter mixing and summer stratification in the upper ocean during (a) Spring AMT cruises in April-May and (b) Autumn AMT cruises in September-October in the Atlantic Ocean. Note that in (a) it is spring in the northern hemisphere and autumn in the southern hemisphere and in (b) it is autumn in the northern hemisphere and spring in the southern hemisphere.

In this chapter, the latitudinal variation in surface ocean properties and vertical structure of the Atlantic Ocean is assessed to identify the seasonality and evaluate interannual variability in the physical structure of the Atlantic Ocean. T and S data was collected between 35°S and 50°N during AMT 1 to 11. Autumn AMT cruises (1, 3, 5, 7, 9 and 11) were from the 50°N southwards in September/October and thus represent autumn in the northern hemisphere and spring in the southern hemisphere (Figure 3.2). Spring AMT cruises (2, 4, 6, 8 and 10) were from 35°S northwards and thus represent autumn in the southern hemisphere and spring in the northern hemisphere (Figure 3.3). See Appendix A for individual cruise details.

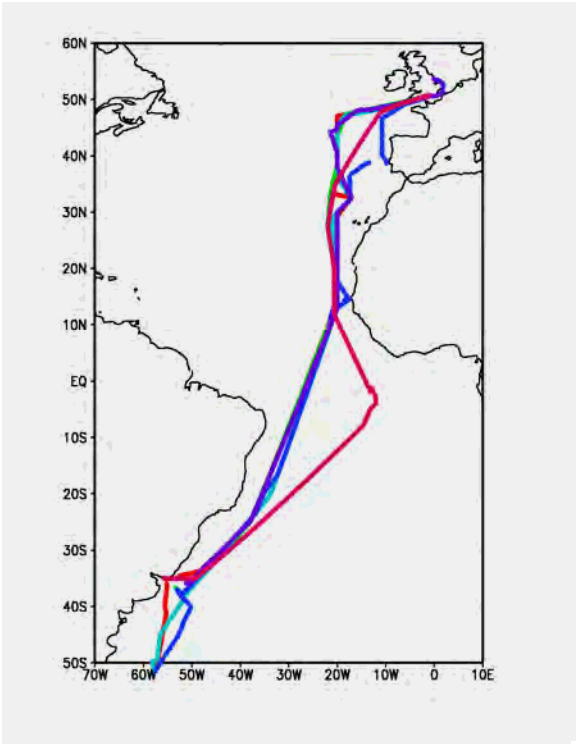

Figure 3.2. Atlantic Meridional Transect cruise tracks for Autumn sampling between 50°S and 50°N in the Atlantic Ocean. Lines are AMT 1 (red line), AMT 3 (green line), AMT 5 (cyan line), AMT 7 (blue line), AMT 9 (purple line) and AMT 11 (magenta line). Autumn AMT cruises sailed southwards from UK, via Montevideo, Uruguay, to the Falkland Islands. AMT 7 called to port at Lisbon and Dakar. See Appendix A for cruise dates

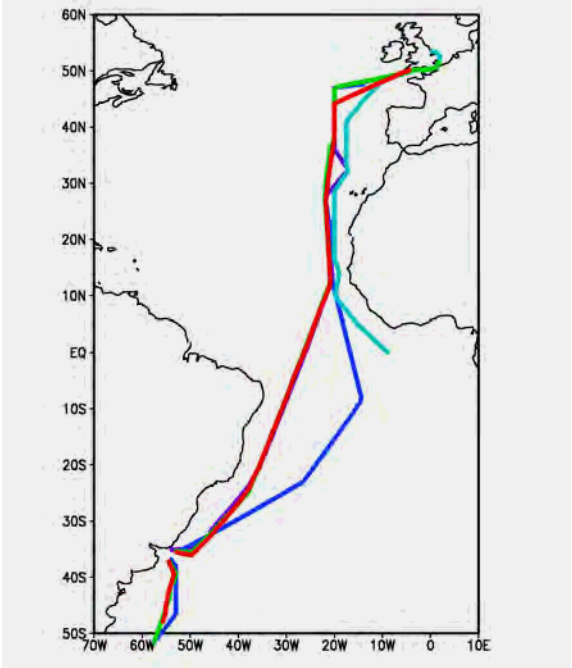

Figure 3.3. Atlantic Meridional Transect cruise tracks for Spring sampling between 50°S and 50°N in the Atlantic Ocean. Lines are AMT 2 (red line), AMT 4 (green line), AMT 6 (cyan line), AMT 8 (blue line) and AMT 10 (purple line). Spring AMT cruises sailed northwards from the Falkland Islands, except AMT 10 which sailed from Montevideo. AMT 6 did not stop at Montevideo. See Appendix A for cruise dates.

3.1.2. Methods and Data acquisition

Surface T and S data was obtained from water drawn into the underway non-toxic system (7m). Data was quality assessed and interpolated at BODC (Alison Fairclough) according to reliability and suspect data was omitted. Sea surface salinities

less than 33 (probably due to the influence of river run off in near-coastal regions) were also omitted, as this study is primary concerned with the subtropical open ocean.

Depth profiles of T and S data were obtained from the SeaBird SBE 911 plus Conductivity Temperature Depth (CTD) profiler attached to a rosette frame at each station sampled between the surface and a maximum depth of 250m. T and S were binned into 1 m intervals and density (σ_t) calculated using the SBE Data Processing (Win 32) programme.

3.2. TEMPERATURE, SALINITY AND DENSITY IN THE ATLANTIC OCEAN

3.2.1 Seasonal and interannual variation in sea surface temperature, salinity and density

3.2.1.1. Background state

In general, sea surface temperature (SST; Figure 3.4, a) gradually increases from the temperate, high latitudes to the subtropical and tropical low latitudes due to increased insolation. However, latitudinal variation in sea surface salinity (SSS; Figure 3.4, b) is more complex, increasing rapidly from the high latitudes to a maxima at ~ 20°S and ~ 30°N, decreasing to a minima just north of the equator (5°N). The SSS distribution is attributed to the balance between upwelling of more saline water and increased precipitation over evaporation at the equator (Aiken *et al*., 2000), high rates of evaporation over precipitation in the subtropical regions, driven by the atmospheric Hadley cell, and high precipitation at high latitudes.

Sea surface density (SSD; Figure 3.4, c) reflects the combined effects of SST and SSS in the surface ocean, SST being the dominant parameter. In general, SSD decreases gradually from the high latitudes to the low latitudes, with a minima at ~ 5°N.

Figure 3.4 Latitudinal variation in the a) sea surface temperature (SST), b) sea surface salinity (SSS) and c) sea surface density (SSD) during autumn (black circles) and spring (white triangles) AMT cruise

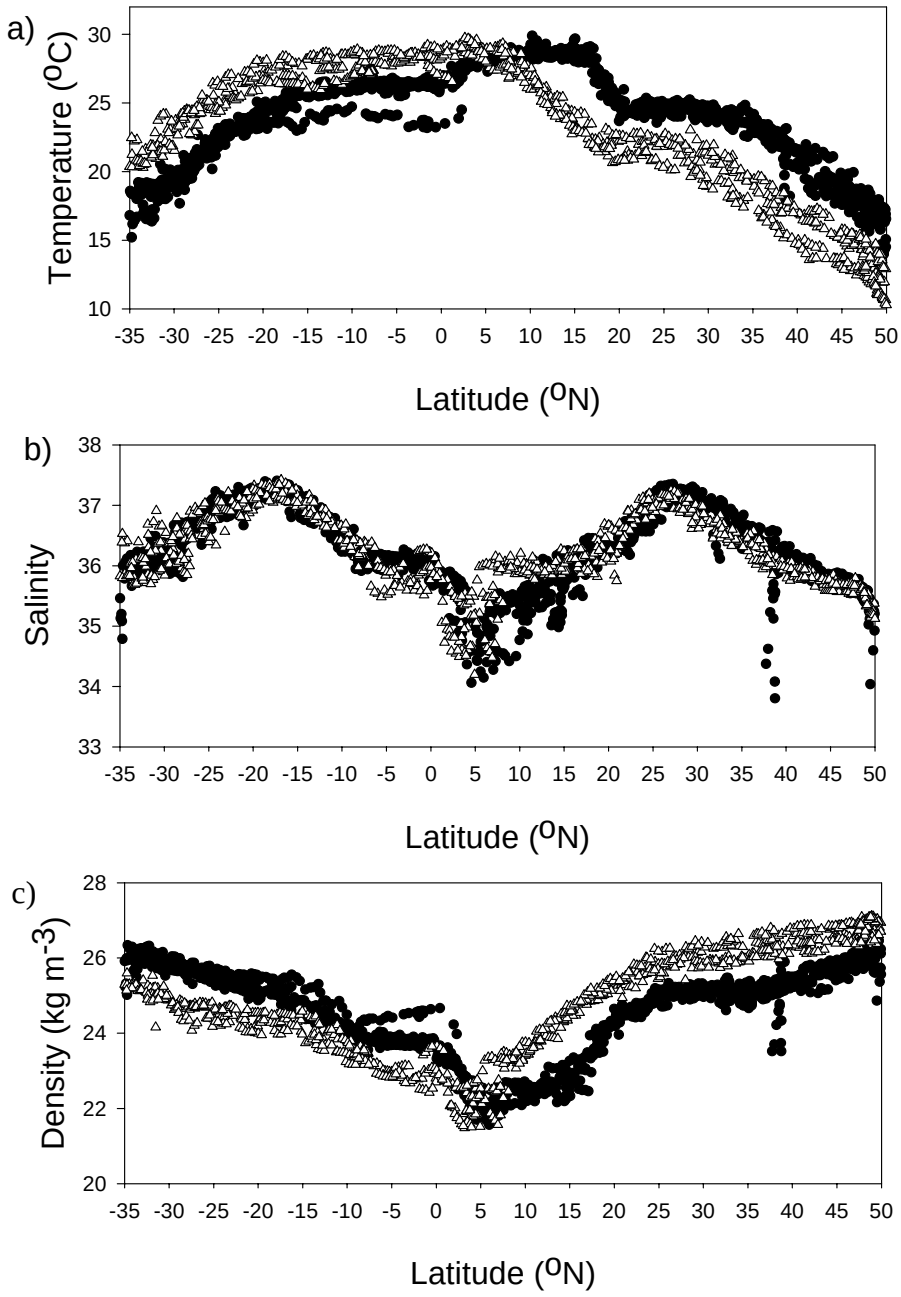

3.2.1.2 Seasonality

SST tends to be higher in the northern hemisphere during autumn cruises, and higher in the southern hemisphere during spring cruises (austral autumn) (Figure 3.4, a), spring SST being a legacy of winter cooling and autumn SST being a legacy of summer heating. Overall, SST in autumn tends to have a symmetrical distribution around 10°N whereas SST in spring is asymmetrical.

Seasonal variations in SSS are observed around the equatorial and coastal upwelling region (Figure 3.4, b), SSS being higher between 5°N and 10°N during Spring AMT's than autumn, and lower between 5°S and the equator. This may be due to the seasonal shift in the Inter Tropical Convergence Zone (ITCZ), which tends to be north of the equator in summer and to the south of the equator in winter. The ITCZ is associated with high rates of precipitation and upwelling of saline water under its path, the relative intensity defining the surface salt properties. During the spring cruise, (which will reflect effects of winter time position of the ITCZ), stronger upwelling over precipitation to the south of the equator transfers more saline water to the surface ocean as observed (Figure 3.4, b). During autumn cruises (which will reflect the effects of the summer position of the ITCZ), when precipitation tends to be dominate (Duce *et al.*, 1991), fresher surface waters are observed to the north of the equator (Figure 3.4, b).

Higher SSD is observed in the northern hemisphere during spring AMT's and in the southern hemisphere during autumn AMT's (Figure 3.4, c), reflecting temperature dependence of SSD. Minima in SSD appear to be at ~ 5°N during both autumn and spring.

3.2.1.3 Interannual variability

In order to examine interannual variability in sea surface properties, SST, SSS and SSD were seasonally divided into Autumn (Figure 3.5) and Spring (Figure 3.6) AMT cruises.

In general, variability in SST was lower (~ 2°C) at low latitudes than at high latitudes (~ 2.5°C) during both Autumn and Spring AMT's (Figure 3.5, a and 3.6, a, respectively) which was probably due to convection. SSS variability tended to be higher in the tropics and high latitudes (~1.3) compared to the subtropical gyres (~ 0.3) during

Spring and Autumn AMT's (Figure 3.5, b and 3.6, b, respectively). SSD is more variable in the tropics (< 1.25 kg m^{-3}) than in subtropics and higher latitudes (< 0.74 kg m^{-3}) during Spring AMT's (Figure 3.5, c), but less variable between autumn cruises (Figure 3.6, c).

During AMT 7 and 11, significant variations in SST, SSS and SSD were observed around the equatorial region and 40°N, respectively (Figure 3.5, a, b and c). The AMT 11 cruise entered the South Atlantic gyre proper (Figure 3.2) thus sampling more saline, stratified waters, leaving the equatorial region further east than previous transects. The anomalously lower SST and SSS observed during AMT 7 were due to a port call at Lisbon (Figure 3.2), thus sampling fresher, cooler coastal waters.

Figure 3.5. Latitudinal variation in a) sea surface temperature (SST), b) sea surface salinity (SSS) and c) sea surface density (SSD) during Autumn AMT cruises between 35°S and 50°N in the Atlantic Ocean. Symbols are AMT 1(red circle), AMT 3(green square), AMT 5 (cyan triangle), AMT 7(blue diamond), AMT 9 (black hexagon) and AMT 11(triangle down triangle).

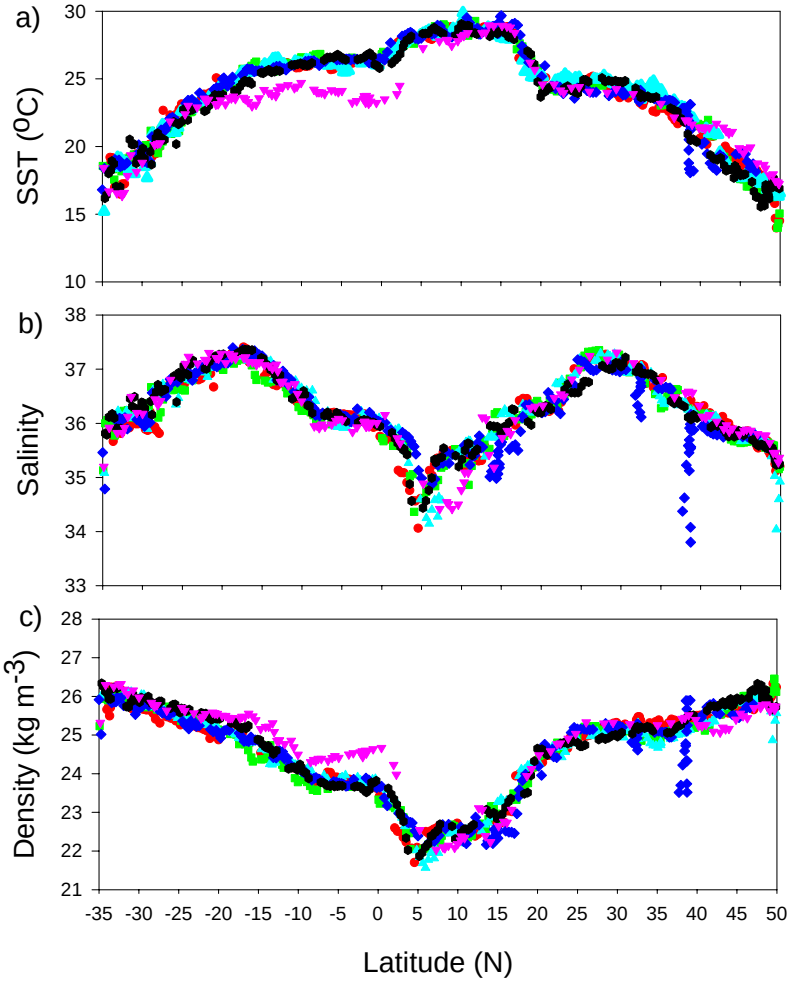

During AMT 10, SST was the lower than previous Spring AMT's (Figure 3.6, a). Anomalously strong winds and frequent storms were probably responsible, wind speeds reaching a mean of 29.5 knots (not corrected for ships speed) over the North Atlantic, in comparison to a mean of 19.5 knots during AMT 2 (Figure 3.7). Around the equatorial region, lower SST (Figure 3.6, a) and higher SSS (Figure 3.6, b) during AMT 4 may have been possibly due to the intensity of upwelling delivering cold water to the surface (see section 3.3.1). Overall, seasonal variability in SST, SSS and SSD was more apparent than interannual variability.

Figure 3.6. Latitudinal variation in a sea surface temperature (SST), b) sea surface salinity (SSS) and c) sea surface density (SSD) during Spring AMT cruises between 35°S and 50°N in the Atlantic Ocean. Symbols are AMT 2 (red open circles), AMT 4 (green open squares), AMT 6 (cyan open triangle), AMT 8 (blue open diamond) and AMT 10 (black open hexagon).

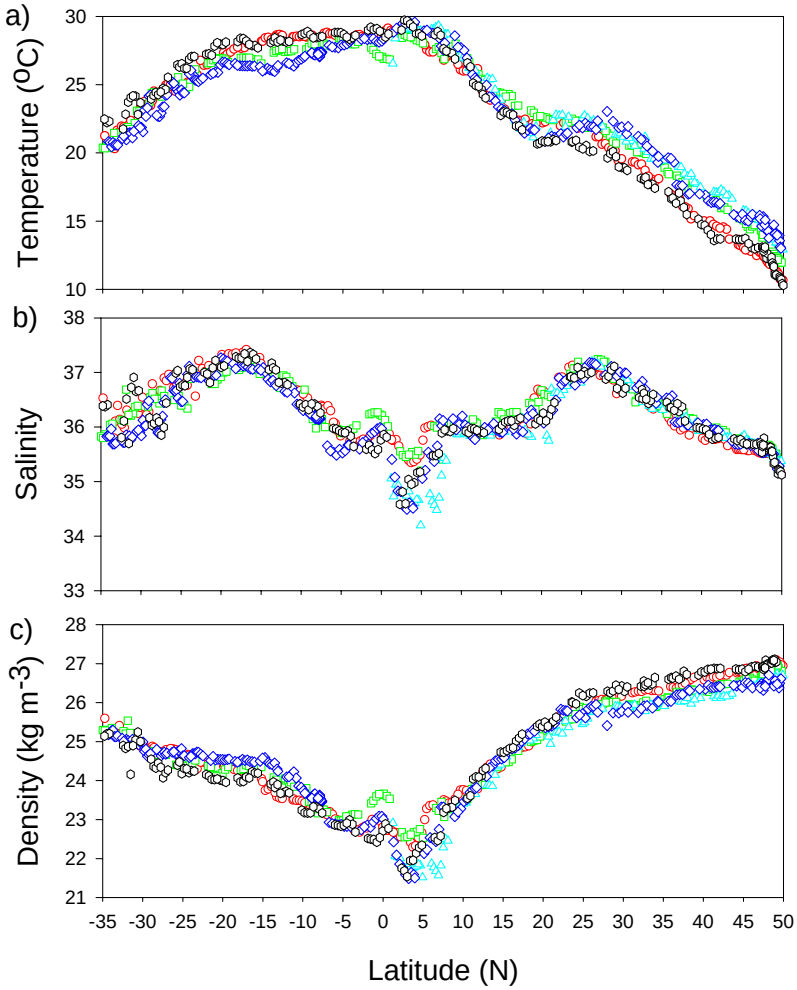

Figure 3.7. Latitudinal variation (35°S to 50°N) in wind speed (knots) from the RRS James Clark Ross during AMT 10 from 12th April to 7th May 2000 in the Atlantic Ocean (Gallienne, 2000)

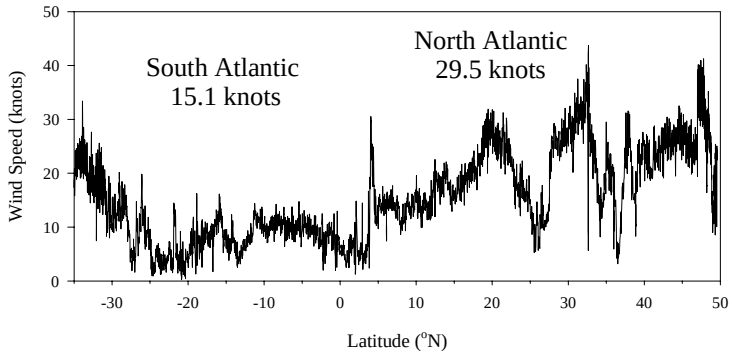

3.2.2 Seasonal and interannual variability in the Latitudinal and depth variation in SST, SSS and SSD

Latitudinal and depth variations (cross-sections) in SST (see Appendices), SSS (Figure 3.8 and 3.9) and SSD (Figure 3.10 and 3.11) reveal persistent features and variations in basin scale vertical structure rather than surface properties. A number of cross-sections were chosen to represent typical and anomalous SSS and SSD distributions.

3.2.2.1 Salinity

Persistent features in basin scale salinity are observed during all AMT transects (Figure 3.8 and 3.9). Upwelling of fresher water around the banded equatorial region (10°S to 10°N) is highlighted by the migration of the 35.8 halocline into the surface waters. In addition, the thick, highly saline, stratified subtropical gyres north and south of 20°N and 10°S, respectively, are persistent, creating symmetry around the equator. However, a number of variations, seasonally and interannual, are observed.

During Autumn AMT cruises (Figure 3.8), except AMT 7 (Figure 3.8, c), a band of low salinity water is observed between the equator and 10°N. During Spring cruises (Figure 3.9), this low saline structure is either shifted southwards or split into two bands. AMT 10 is an exception (Figure 3.9, d) as a surface skin (10 –20m) of fresher

water is observed between 5°S and 10°N. This variation in surface (50m) salinity is probably due to a combination of the seasonal shift in the ITCZ (see section on surface salinity) and a change in upwelling intensity or position (see Ekman section).

Over the north Atlantic, the 35.8 halocline was shallower (< 250m) during AMT 7 (Figure 3.8, c) than other AMT cruises. Over the south Atlantic, the 35.8 halocline during AMT 1 (Figure 3.8, a), 2 and 10 (Figure 3.9, a and d, respectively) was deeper (> 250m) than other AMT cruises. Around the equatorial region, the 35.8 halocline migrated closer to the surface during AMT 3, 7, 9, and 11 (Figure 3.9 a, b, c, d and e) than during AMT 1 and 5. This probably reflects a change in the stratification and convection.

3.2.2.2 Density

In order to compare basin scale density structure, the 23, 25 and 26 kg m^{-3} isopycnals are highlighted (Figure 3.10 and 3.11). The increase in density from the surface to the deep ocean is a manifestation of a decrease in temperature and increase in salinity with depth. Overall, the South Atlantic is persistently stratified during Spring and Autumn AMT cruises. In contrast, the North Atlantic tends to be stratified during autumn cruises, but mixed or weakly stratified during spring cruises, probably reflecting the previous winter mixing.

Density illustrates the banded structure of the equatorial region, which tends to dominate the surface hydrography, defined by light surface waters and sharp gradients in density (*i.e.*, tightly packed isopycnals). Two dominating currents are evident from density profiles, the westward flowing North Equatorial Counter (NEC, north of 10°N) and South Equatorial Current (SEC, 3°N to 15°S), both being highly seasonal broad, uniform structures. During autumn (Figure 3.10), the NEC strengthens and is

characterised by a band of low-density water between 3°N and 9°N (100m) (Aiken *et al.*, 2000). The 23 kg m^{-3} isopycnal probably defines the NEC. During Autumn AMT's, the NEC is generally between the equator and 10°N whereas during Spring AMT's (Figure 3.11), the NEC tends to be less well defined and south of 5°N. In contrast, the latitudinal limits of the SEC are poorly defined by the density structure, although the depth to which it penetrates is defined by tight isopycnals observed at depth (70-100 m) between the equator and 10°S. During AMT 11 (Figure 3.10, e), the approach to the equatorial region was from the interior of the gyre. The density structure observed during AMT 11 (Figure 3.10, e) clearly marks both the SEC and NEC as the cruise track left the equatorial region into the south Atlantic gyre proper (Figure 3.2).

Doming of the isopycnals around 10°N, known as the (Guinea Dome), is a persistent feature during all AMT cruises and is attributed to the equatorial current regime (Aiken *et al*., 2000). However, the doming appears more intense (sharper gradients) during AMT 4, 8, 10 (Figure 3.11 b, c and d, respectively) and AMT 3, 7, 9 and 11 (Figure 3.10 b, c, d and e). Indeed, upwelling appears to be stronger during Spring than Autumn around the equatorial region (Figure 3.21 and 3.22).

In general, the 25 and 26 kg m^{-3} isopycnals tend to outcrop further north in the North Atlantic (> 35°N) during Autumn AMT cruises (Figure 3.10) than Spring AMT cruises (Figure 3.11), reflecting how Autumn transects reveal the relic of summer stratification and Spring transects reveal the relic of winter mixing.

A localised decrease or outcrop in density (100-200 m) around 20°S during AMT 1, 3, and 9 (Figure 3.10 a, b and d), 2 and 8 (Figure 3.11 a and c) is associated with a submarine, shallow seamount (Hooker *et al*., 2000).

Figure 3.8. Latitudinal (35°S to 50°N) and depth (< 250m) variation in salinity during Autumn AMT's in the Atlantic Ocean: (a) AMT 1, (b) AMT 3, (c) AMT 5, (d) AMT 7, (e) AMT 9 and (f) AMT 11. The 35.8 halocline is highlighted (white solid line) and the mixed layer depth (Hooker *et al.*, 2000) included (white dashed line). White areas within the graph are depths where there is no data. MLD is recalculated using a density gradient 0.1 (red dashed lines) and 0.5 (yellow dashed lines).

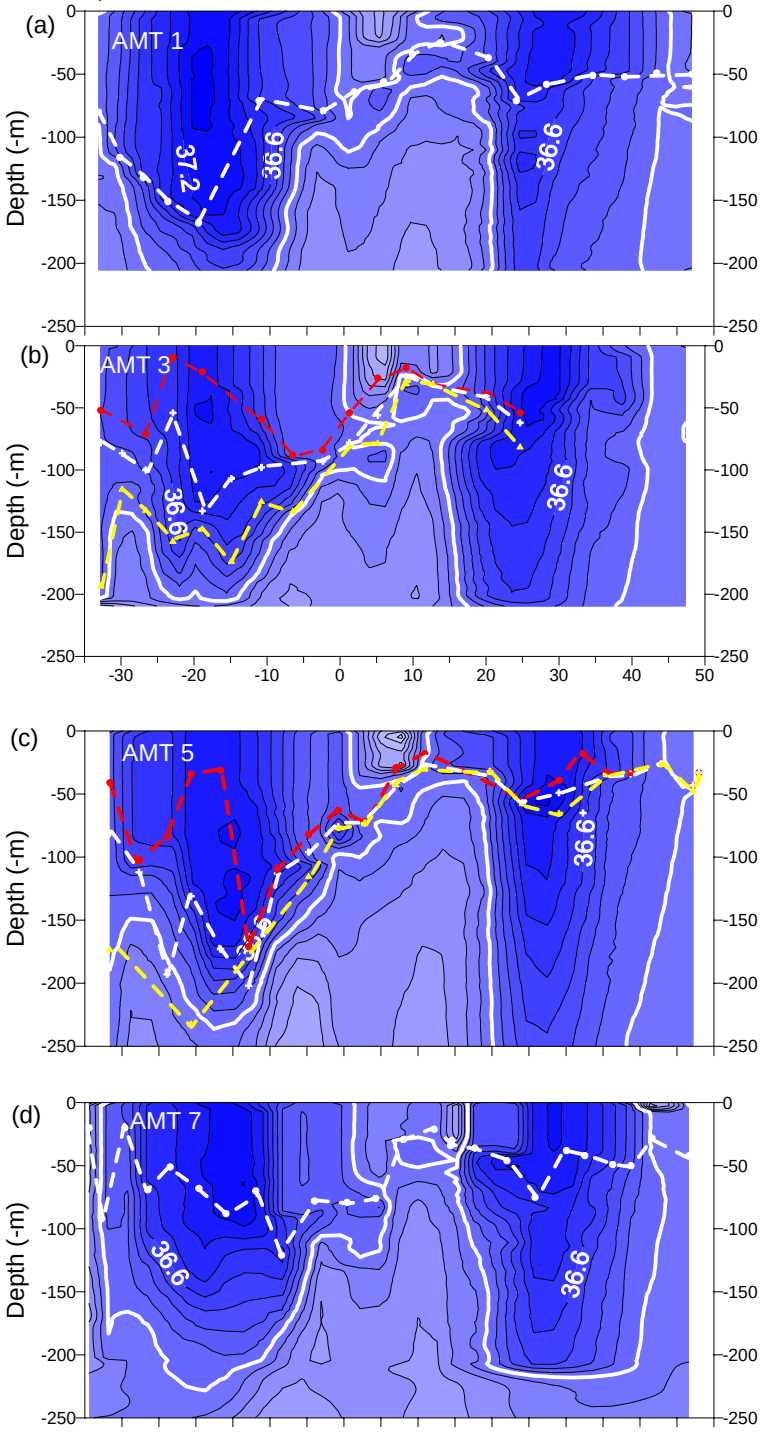

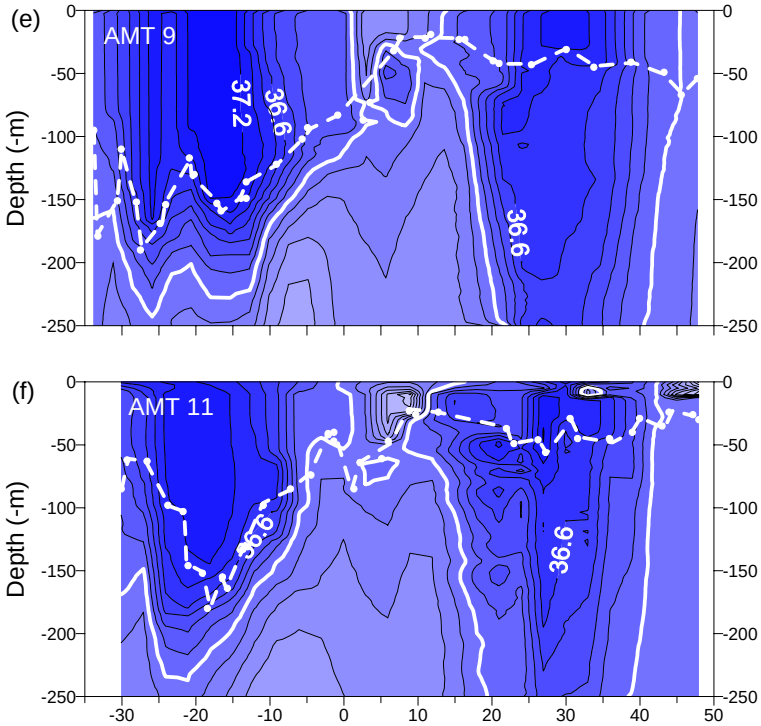

Figure 3.9. Latitudinal and depth (< 250m) variation in salinity during Spring AMT's between 35°S and 50°N in the Atlantic Ocean: (a) AMT 2, (b) AMT 4, (c) AMT 8 and (d) AMT 10. The 35.8 halocline is highlighted (white solid line) and the mixed layer depth (Hooker *et al.*, 2000) included (white dashed line). White areas within the graph are depths where there is no data.

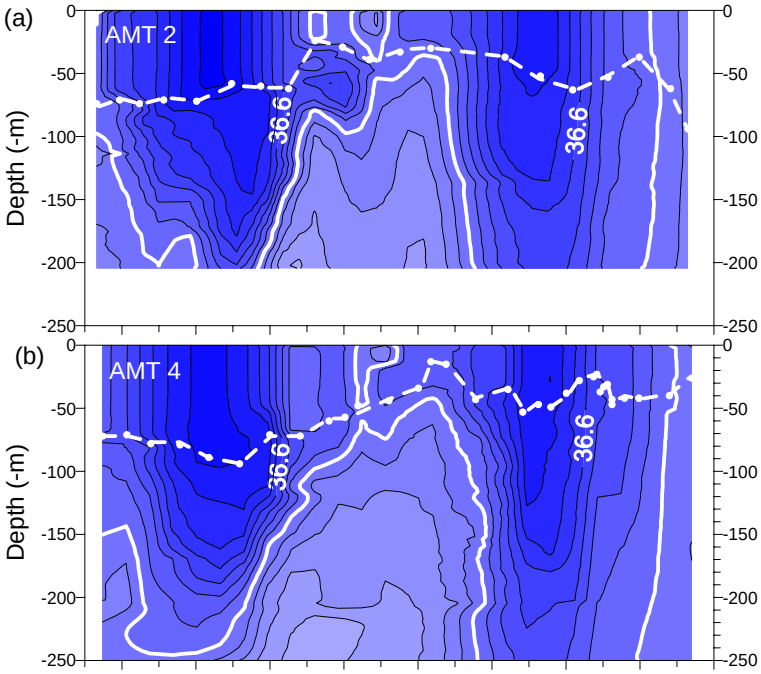

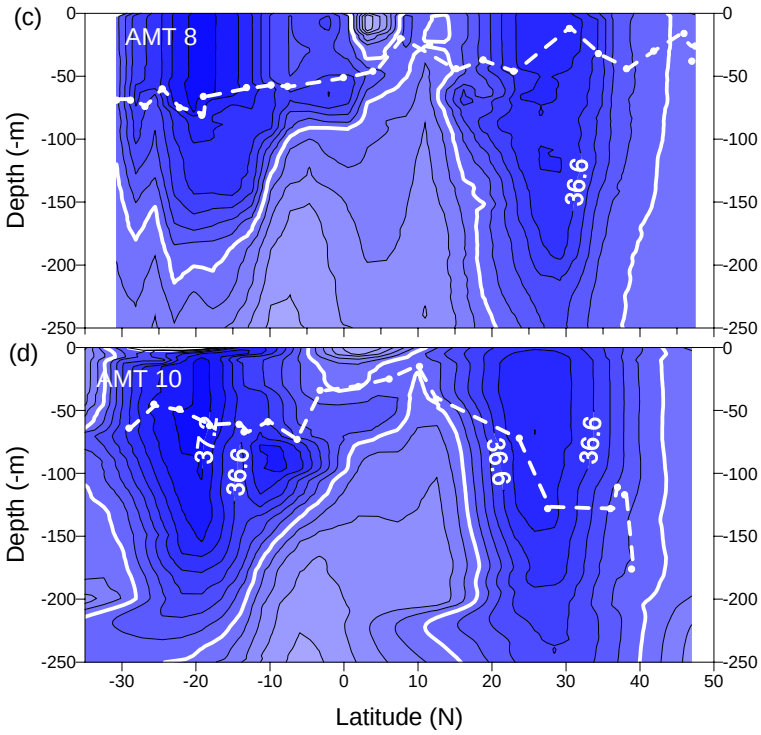

Figure 3.10. Latitudinal and depth (< 250m) variation in density during Autumn AMT's between 35°S and 50°N in the Atlantic Ocean: (a) AMT 1, (b) AMT 3, (c) AMT 5, (d) AMT 7, (e) AMT 9 and (f) AMT 11. The 35.8 halocline is highlighted (white solid line) and the mixed layer depth (Hooker *et al.*, 2000) included (white dashed line). White areas within the graph are depths where there is no data. MLD is recalculated using a density gradient 0.1 (red dashed lines) and 0.5 (yellow dashed lines).

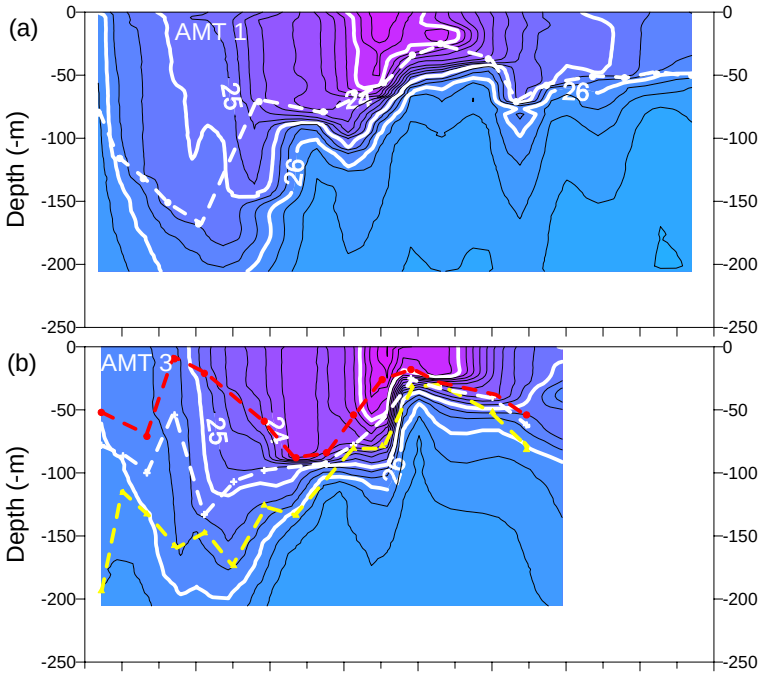

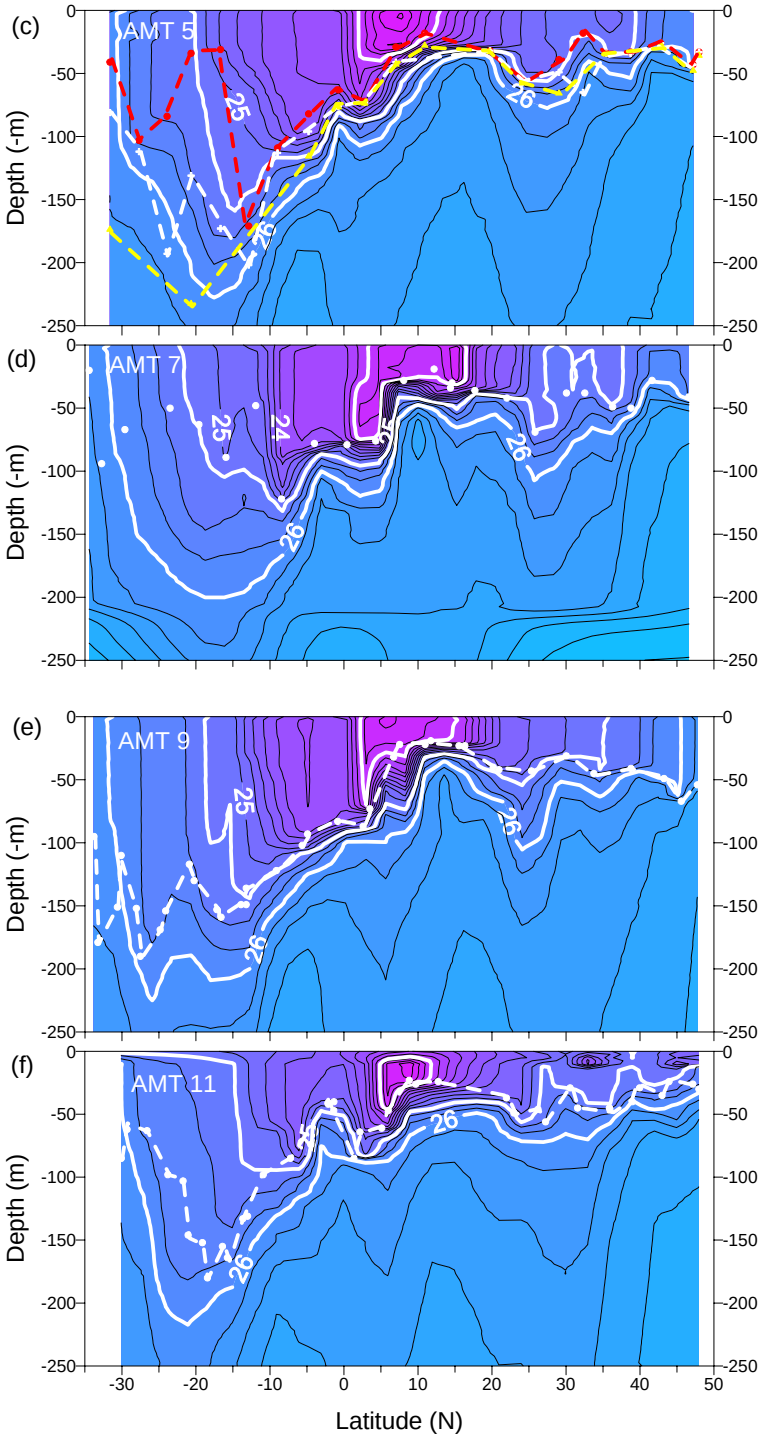
(c)
AMT 5
(d)
AMT 7
(e)
AMT 9
(f)
AMT 11
Depth (-m)
Depth (m)
Latitude (N)
0
-50
-100
-150
-200
-250
-30
-20
-10
0
10
20
30
40
50
24
25
26

Figure 3.11. Latitudinal and depth (< 250m) variation in density during Spring AMT's between 35°S and 50°N in the Atlantic Ocean: (a) AMT 2, (b) AMT 4, (c) AMT 8, and (d) AMT 10. The 35.8 halocline is highlighted (white solid line) and the mixed layer depth (Hooker *et al.*, 2000) included (white dashed line). White areas within the graph are depths where there is no data.

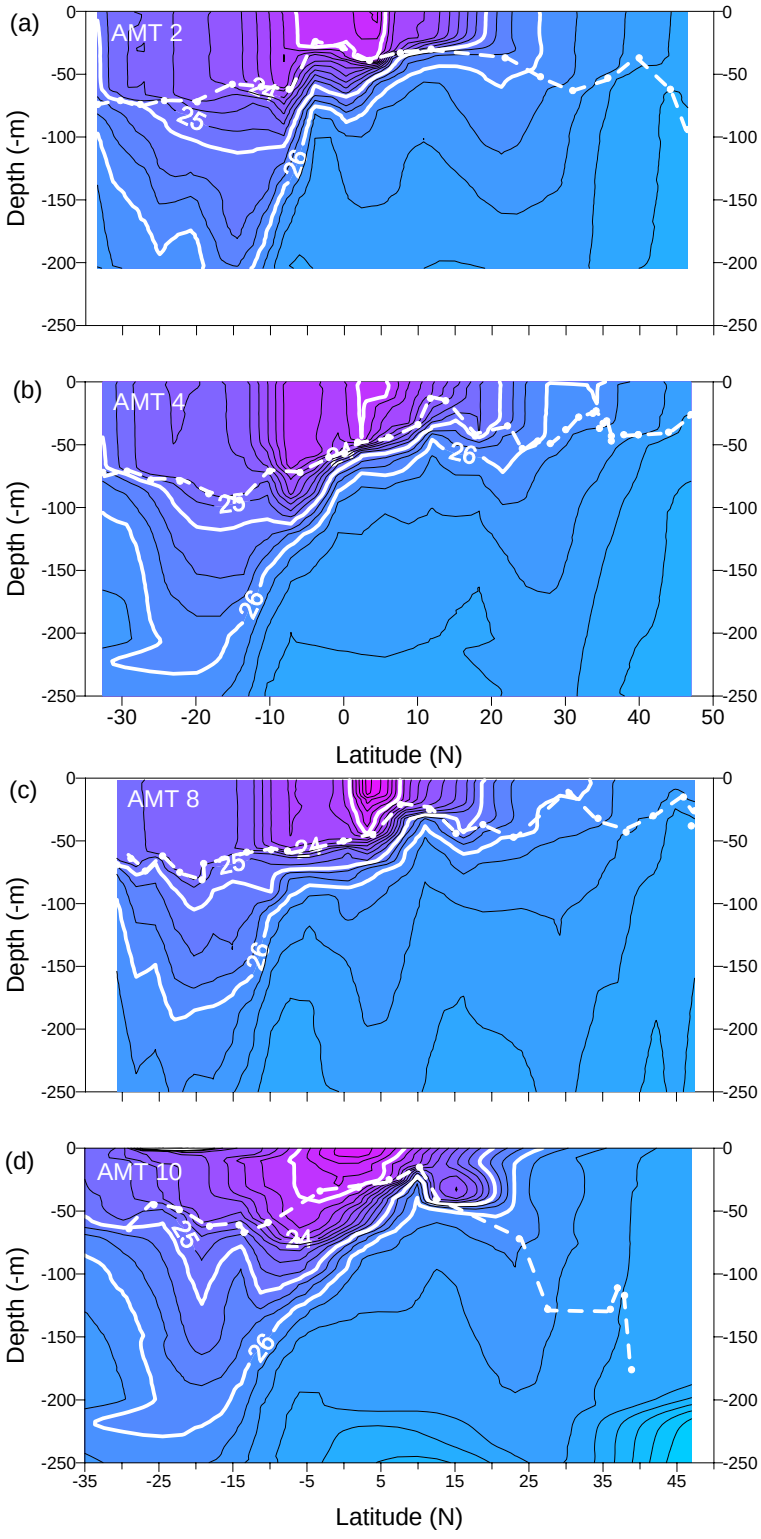

3.2.3 Mixed Layer Depth and Thermocline

3.2.3.1 Introduction

The mixed layer depth (MLD) is typically a vertically homogenous layer in surface ocean which is principally controlled by the surface forcing. Increased surface heating or freshwater inputs tend to stratify the surface ocean, whereas atmospheric cooling or wind mixing tends to deepen the MLD (Mann and Lazier, 1996). Below the MLD, there is a layer in which the temperature decreases or salinity increases most rapidly with depth. This zone is called the thermocline (Z_T). The MLD can be defined from density profiles as the depth where the greatest density gradient is observed. Underlying the MLD, the Z_T can be defined as a layer in which the temperature changes from typical surface to deep ocean values (5 to 8 °C). Unfortunately, the AMT cruise series rarely samples below the 250m and thus it is difficult to define the Z_T, which usually extends depths of 1 to 2 km in subtropical regions. Thus, temperature gradients observed during AMT merely reflect the intrusion of the thermocline into the upper 250m surface waters.

The MLD (and Z_T) varies latitudinally and seasonally (Figure 3.12i from AMT 10 and Figure 3.12ii from AMT 11). During Spring, in the subpolar region (46.98°N, 20°W; Figure 3.12i, a) and northern subtropical Atlantic (27.53°N, 21.90°W; Figure 3.12i, b), there is little depth variation in T and σ_t distribution due to winter mixing and thus weakly defined MLD and Z_T. This is typical for temperate high latitude regions where wind-induced mixing and surface cooling promote a thick homogenous surface layer. However, conditions in the northern subtropical Atlantic are probably storm induced (see section 3.2.1.3, Figure 3.7). During spring in the equatorial region (1.35°S, 14.89°W; Figure 3.12 ii, c), sharp gradients in both T and σ_t define a MLD extending to ~ 75 m, with a shallow intrusion of the underlying Z_T (~ 30m), probably due to the combined effects of upwelling and increased insolation at the tropics. In the

south Atlantic subtropical gyre (23.80°S, 31.13°W; Figure 3.12 ii, d), a thick MLD (~ 100m) and thermocline (~ 100m) are apparent but not well defined, due to previous winter mixing and cooling of the surface waters.

During autumn, surface waters in the subpolar region (47.14°N, 11.59°W; Figure 3.12ii, a) are strongly stratified with a thin MLD (~ 20-30 m) and shallow change in temperature (~ 30 m). In the northern subtropics, surface waters are also stratified but the MLD is thick (60m), with temperature becoming relatively constant below 100m (27.25°N, 21.97°W; Figure 3.12 ii, b). In the equatorial region (1.94°S, 25.26°W; Figure 3.12i, c), there are weak gradients in T and σ_t, defining shallow MLD at ~ 40m, temperature becoming almost constant below ~ 100m. In the southern subtropical downwelling region (22.25 °S, 36.84°W; Figure 3.12i, d), sharp changes in both T and σ_t are observed (~ 50m), creating a shallow MLD. Stratified surface waters during autumn are a relic of summer heating, with deepening of the MLD being promoted by convection and wind-driven mixing.

Atmospheric variability has been directly linked to changes in biological primary production through modification of the depth of the mixed layer (Polovina *et al.*, 1995). Here, the MLD is defined during Spring and Autumn AMT cruises to assess the latitudinal, seasonal and interannual variability in the surface mixed layer.

Figure 3.12. Depth variation (< 300 m) in temperature (T, °C; dashed line) and density (σ_t, kg m^{-3}; solid line) at during (i) the austral spring, AMT 10 (a) 46.98°N, 20°W, (b) 27.53°N, 21.96°W, (c) 1.94°S, 25.26°W and (d) 22.25°S, 36.84°W and (ii) during the austral autumn, AMT 11 (a) 47.14°N, 11.59°W, (b) 27.55°N, 21.97°W, (c) 1.35°S, 14.89°W and (d) 23.80°S, 34.13°W. The mixed layer depth (MLD), defined by a sharp gradient in density and the intrusion of the thermocline (Z_T), defined by a change in the temperature from surface to deep values, are noted

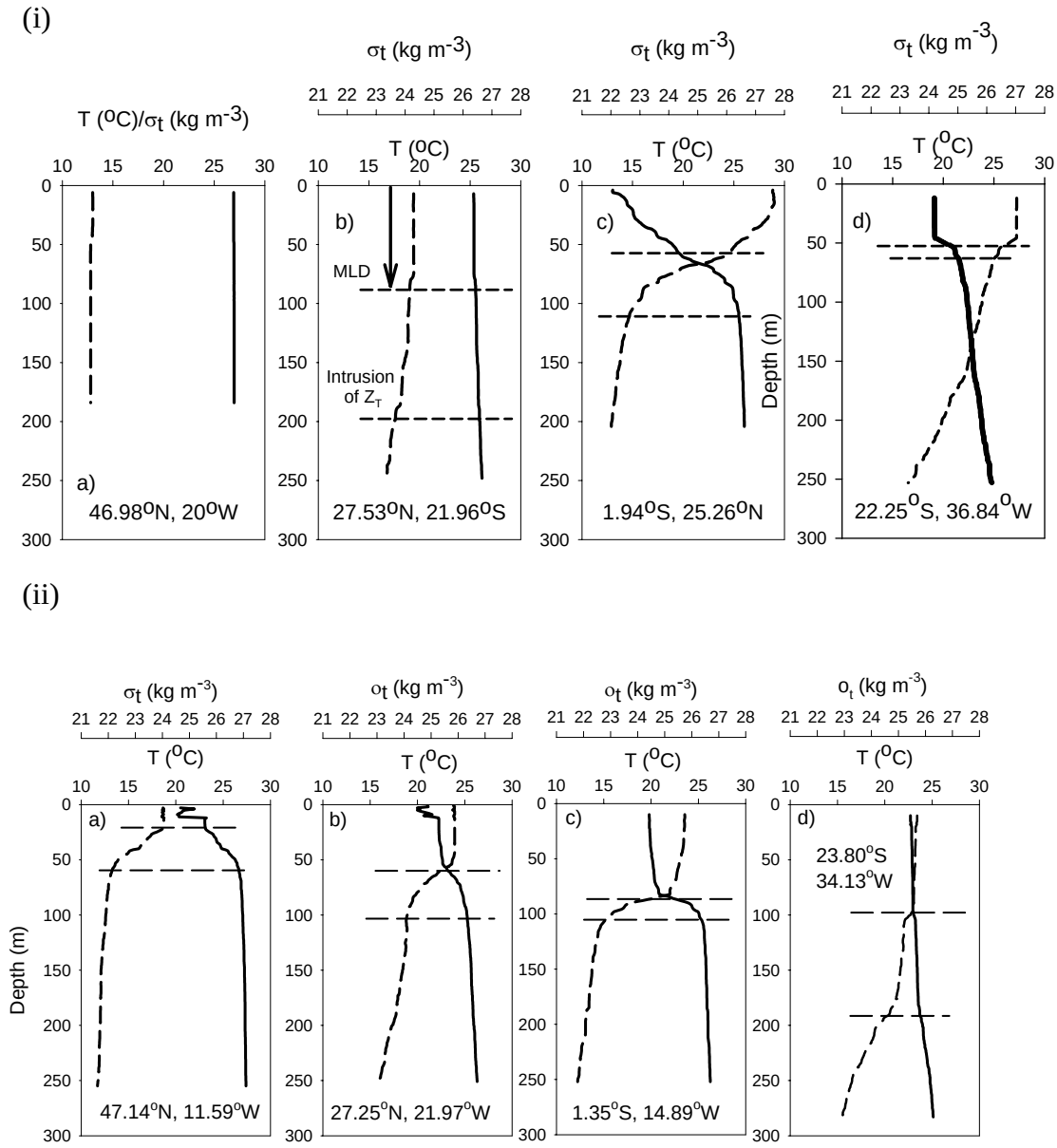

3.2.3.2. Defining the mixed layer depth

There is no universally accepted method of determination of the mixed layer depth (which represents the top of the thermocline) from hydrographic measurements,

both temperature (Polovina *et al*. 1995) and density (Hooker *et al.*, 2000) being used to define the MLD. In the present study, density (σ_t), calculated from T and S (Millero *et al.*, 1980), was used to define the mixed layer depth (MLD) using two methods;

METHOD 1. Depth at which 3 out of 4 consecutive gradients in σ_t ($\Delta\sigma_t/\Delta Z$, where Z is depth in m) are greater than 0.035 kg m^{-3} ($MLD_{density}$) or ($0.1^oC\ m^{-1}$ for T; $MLD_{temperature}$) (Hooker *et al.*, 2000). If the pycnocline or thermocline is not identified, then a change of 0.1 kg m^{-3} or 0.5^oC in σ_t or T, respectively, identifies the $MLD_{density}$ and $MLD_{temperature}$, respectively.

METHOD 2. Depth at which there was the maximum gradient in σ_t ($\Delta\sigma_t/\Delta Z$) (Figure 3.12; $MLD_{max\ gradient}$).

Using method 1, a significant positive correlation between MLD calculated from T and σ_t was observed (Figure 3.13, a; R=0.99, significant at the 95% confidence level), showing that σ_t or T provide consistent definitions and that salinity makes only a minor contribution. However, there was a weaker, but significant relationship between the MLD derived from methods 1 and 2 (Figure 3.13, b; R= 0.84). Comparison of the predicted mixed layers and hydrographic sections showed that the later method is more robust in defining the MLD as it ignores outliers or spikes in the data, requiring consecutive gradients at successive depths.

To illustrate the importance in the choice of gradient used to define the MLD, a $\Delta\sigma_t/\Delta Z$ of 0.1 and 0.5 were applied to AMT 3 and AMT 5, which appeared to have large spikes in the MLD, especially in the south Atlantic (Figure 3.10 c and d; red (0.1) and yellow (0.5) line, respectively). In the equatorial region and where MLD is shallow in the North Atlantic, the gradient in σ_t is large and therefore the MLD is well defined. In contrast, when the gradient in σ_t is lower, such as in the South Atlantic, a smaller gradient in σ_t is more appropriate in defining the MLD.

Figure 3.13 Relationship between a) mixed layer depth defined by temperature ($MLD_{temperature}$) and density ($MLD_{density}$) and b) $MLD_{temperature}$ and MLD defined by the maximum gradient in density ($MLD_{max\ gradient}$) for all AMT cruises.

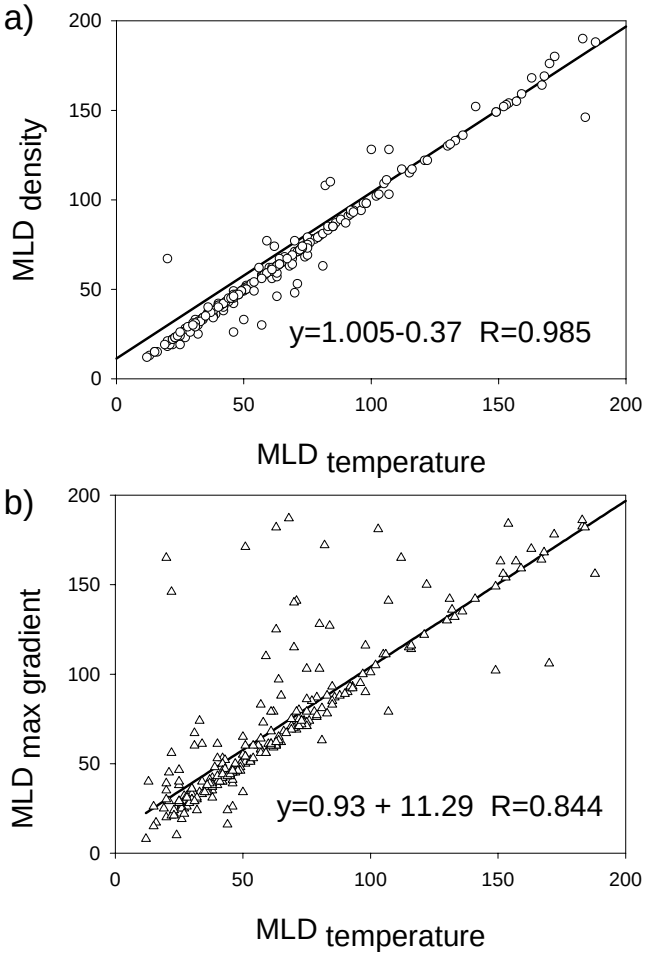

3.2.3.2.1. Temporal variability in the MLD

Solar heating promotes stratification of the surface ocean. Hence, there is reduced variability in the MLD after summer heating, as observed during Autumn sampling in the Northern Hemisphere (black circles) and Southern Hemisphere (white circles; Figure 3.14). MLD during Spring tends to be more variable, especially in the southern hemisphere, being attributed to cooling of the sea surface and increased mixing.

Figure 3.14. Seasonal variation in the mixed later depth (MLD, m) between Autumn (black circles) and Spring (white circles) AMT cruises between 35°S and 50°N.

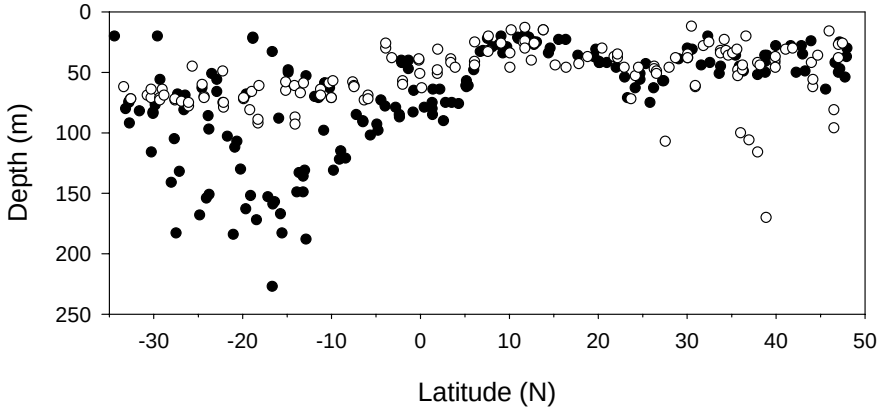

Between Autumn AMT's, there is little interannual variability (~ 30m) north of 10°N, again, due to summer heating stratifying the surface layers (Figure 3.15, a), a slight increase in MLD thickness being observed north of 40°N. However, greater interannual variability (20m to 200m) were observed south of the equator (Figure 3.15, a), probably due to winter mixing being manifested in the southern hemisphere.

Between spring AMT cruises, the MLD varies by ~ 50 m south of the equator (Figure 3.15, b). North of 10°N, larger variations in MLD are observed (AMT 2, 4, 6, and 8; 12 to 96m) with a deepening of the MLD north of 40°N. Indeed, the maximum MLD usually occurs at the end of winter and defines the extent of the seasonal boundary layer. However, during AMT 10, the MLD was much deeper (to 170m) than previous AMT cruises, due to the anomalously strong winds and storms observed in April-May 2000 (see Figure 3.7).

It is necessary to note that the MLD defines a homogenous layer at the surface of the ocean in which chemical and most biological properties are well mixed by physical forcing. In section 4.2.4, the vertical distribution of dissolved organic nutrients is compared to the MLD.

Figure 3.15. Latitudinal variation (35°S-50°N) in the MLD (m) in a) autumn and b) spring AMT cruises.

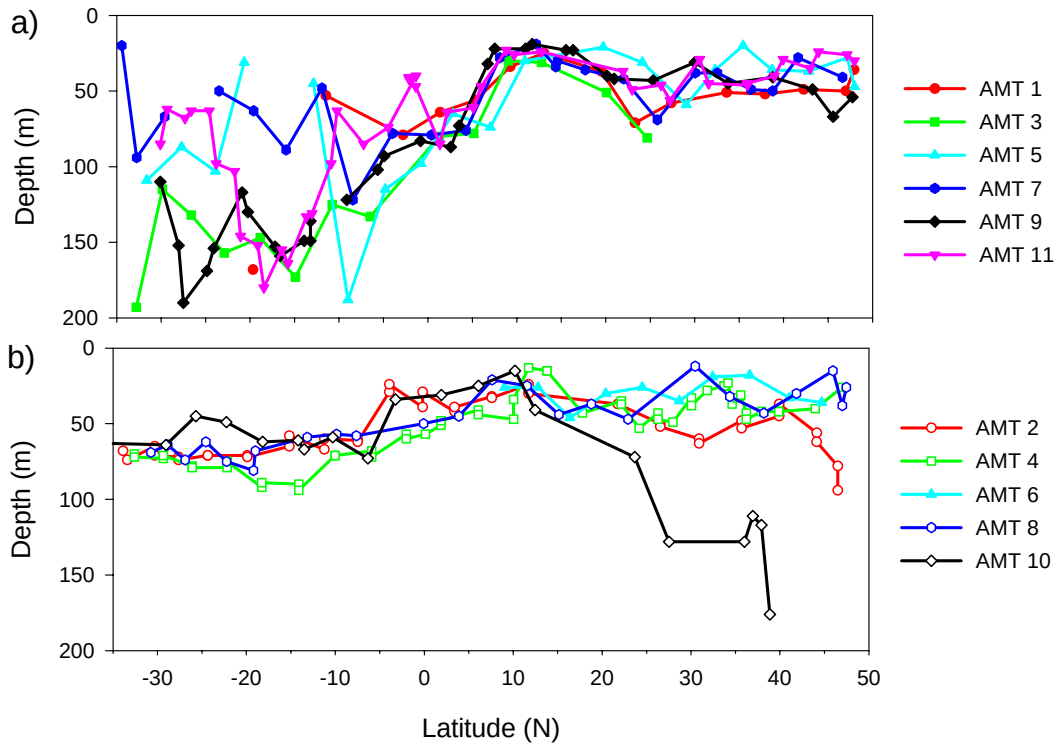

3.3 PHYTOPLANKTON BIOMASS AND PHYSICAL INTERACTION

3.3.1. Comparison of phytoplankton biomass and physical transport of nutrients

Concentrations of the photosynthetic pigment, chlorophyll *a*, in the surface ocean has long been used as a proxy for phytoplankton biomass (Platt and Sathyendranath, 1988; Longhurst *et al.*, 1995; Gibb *et al.*, 2000). In the Atlantic, large variations in phytoplankton biomass can be inferred from remotely sensed chlorophyll *a* distributions in the surface ocean (SeaWiFS), phytoplankton biomass being highest over the high latitude subpolar regions, along coastal boundaries and the equatorial upwelling, and lowest over the vast subtropical gyres (Figure 3.16). These large scale variations in phytoplankton biomass over the Atlantic imply basin scale variations in the supply of nutrients to the surface ocean, given the nutrient requirements of phytoplankton for primary production and growth. Here, physical process supplying nutrients to the surface Atlantic are assessed and compared to the distribution of

phytoplankton biomass. Note that surface chlorophyll *a* concentrations do not always represent the depth of highest productivity or biomass (see section 3.5.1.2 on the deep chlorophyll maximum).

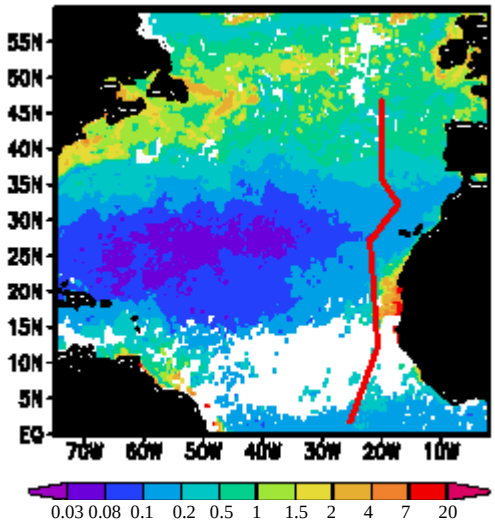

Figure 3.16. SeaWiFS image of remotely sensed annual chlorophyll *a* concentration over the North Atlantic Ocean (0° to 60°N) where blue signifies low chlorophyll a concentrations and green to red high chlorophyll a concentrations (mg m^{-3}).

3.3.1.1 Convection

Convection is the transfer of fluid caused by the thickening of the surface mixed layer, due to a combination of surface buoyancy loss and wind mixing (Marshall and Schott, 1999; Williams and Follows, 2002). Wind-induced convection causes deepening of the mixed layer and entrainment of nutrients and trace metals to the euphotic zone, initiating a biological response which will vary with latitude (Williams *et al.*, 2000). In the subpolar region, the strength of the response is inversely proportional to the strength of the wind, as increased mixing means that phytoplankton remain in the well lit surface layers for less time, thus being light limited. In contrast, in the subtropical regions, primary production and both wind strength and heat flux are positively correlated, the phytoplankton response only being limited by the magnitude of nutrient entrainment (Dutkiewicz *et al.*, 2001; Follows and Dutkiewicz, 2002).

Estimates of the convection over the North Atlantic show highest fluxes of nitrate north of ~ 50°N (> 1 mol N m^{-2} y^{-1}), decreasing over the flanks of the north

Atlantic subtropical region (0.4-0.8 mol N m^{-2} y^{-1}) and being lowest in the subtropical gyre (< 0.2 mol N m^{-2} y^{-1}; Figure 3.17, a). In general, convection tends to increase polewards as the MLD thickens (See section 3.2.3).

Convective fluxes of nitrate over the North Atlantic (Figure 3.17, a) are seemingly in accord with phytoplankton biomass distribution (Figure 3.16), implying that convection asserts a strong influence on phytoplankton production. However, interannual variability in primary production is probably also responds to changes in convection, the standard deviation of convective nitrate fluxes being relatively large over the north east Atlantic (~ 0.1). However, over the subtropics, less interannual variability linked to convection is inferred, the standard deviation being relatively small.

a) Climatological convective nitrate flux

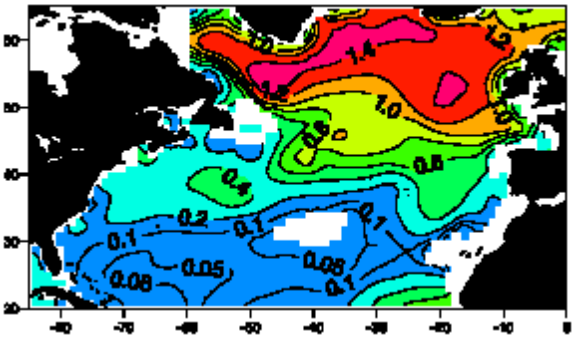

b) Standard deviation

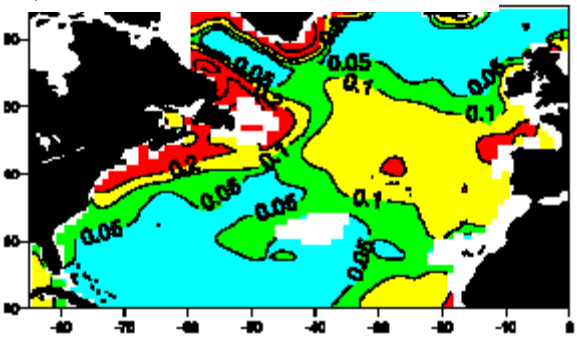

Figure 3.17. Diagrams of (a) annual mean convection of nitrate (mol N m^{-2} y^{-1}) derived from a climatological model from 1968 to 1993 in the North Atlantic Ocean and (b) standard deviation from annual contribution (from Williams *et al.*, 2000).

3.3.1.2. Ekman transport

Atmospheric winds induce a horizontal (Ekman) transfer of the surface layer of the ocean, directed to the right of the wind stress in the northern hemisphere and to the left in the southern hemisphere, inducing upwelling and lateral transfer of the surface

water at variable rates (Figure 3.18). In the subpolar region and tropical upwelling region, vertical Ekman transport supplies nutrients from the deep ocean to the euphotic zone. Along the flanks of subtropical gyres, horizontal Ekman transport supplies nutrients from the subpolar gyre and tropics into the mixed layer of the subtropical gyre, where convergence of surface water causes downwelling and a nutrient depleted surface ocean (Figure 3.18; Williams and Follows, 1998; Williams and Follows, 2002). Overall, a positive Ekman transport implies upwelling and a negative Ekman transport implies downwelling.

Figure 3.18. Schematic meridional section describing wind induced divergence or upwelling over the tropics and subpolar region and convergence or downwelling in the subtropics in the Ekman layer. Upwelling delivers nitrogen (N) to the surface ocean and downwelling creates a N depleted surface ocean. Arrows into the page denote the direction of the wind.

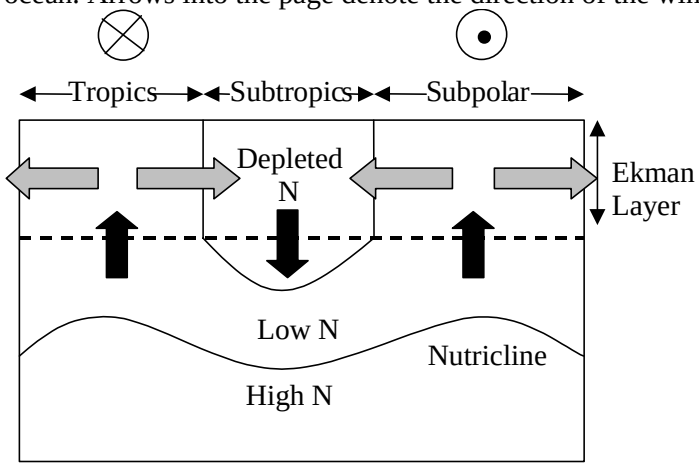

Estimates of the vertical Ekman flux over the North Atlantic Ocean in April shows that there is a strong vertical Ekman transport of nutrients (> 200 mmol N $m^{-2}y^{-1}$) north of 50 °N over the subpolar region (Figure 3.19, a). South of 50°N, vertical supply of nutrients tends to be almost zero or negative, implying a loss of nutrients from the euphotic zone through downwelling. Estimates of the horizontal Ekman flux of nitrate over the North Atlantic indicate a loss of nutrients (negative flux) over the northern subpolar region and equatorial and coastal upwelling region around NW Africa. This is due to biological utilisation of the nutrients, as well as advection of nutrients from these

nutrient rich regions into the euphotic zone of the subtropical gyre, where the horizontal supply tends to be relatively high (> 100 mmol Nm^{-2} y^{-1}). Note the high horizontal fluxes at 45°N and 20°N along the 20°W transect.

Figure 3.19. The supply of nitrate (mmol N m^{-2} y^{-1}) to the euphotic zone in April for (a) vertical Ekman flux and (b) horizontal Ekman flux over the North Atlantic. Diagnostics are based on climatological analysis (Williams and Follows, 1998).

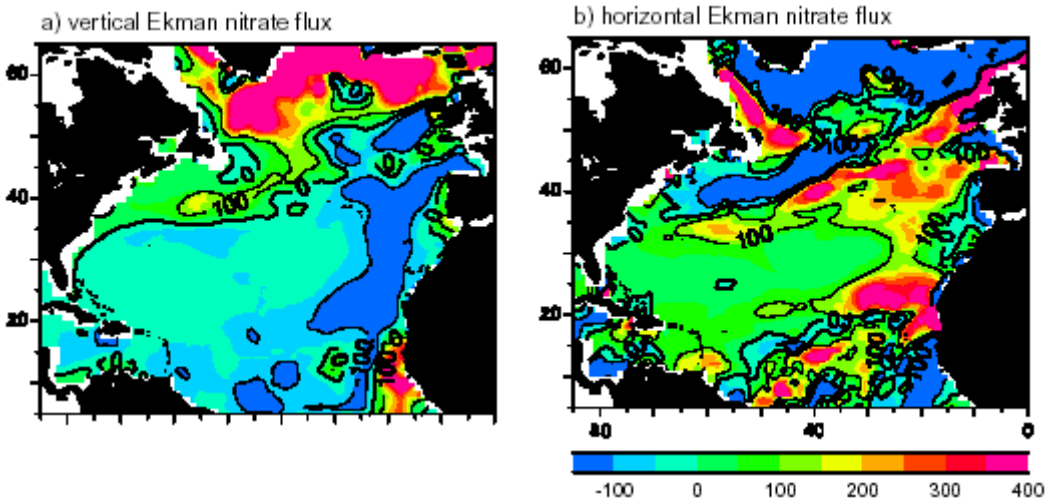

So how does the Ekman transport of nutrients compare with the spatial variation in phytoplankton over the Atlantic? In Figure 3.20, the Ekman pumping field from January to May, 2000 and surface chlorophyll *a* concentrations diagnosed from a SeaWiFS satellite image for the same period are compared (represents timing of AMT 10). Seemingly, over the subtropical gyre, there is a net loss through vertical Ekman transport coinciding with the regions of the lowest phytoplankton biomass (Figure 3.20, purple-blue; chlorophyll *a* concentrations < 0.1 mg m^{-3}). However, over the flanks of the northern and southern subtropical gyres, at 40°N, 20°N and 38°S, the Ekman pumping field indicates regions of downwelling (Figure 3.20), yet phytoplankton biomass remains relatively high (green-yellow-red; chlorophyll *a* concentrations > 1 mg m^{-3}). Nutrients are probably supplied to this region through a combination of convection (Figure 3.17) and horizontal Ekman transfer (Figure 3.19, b).

Figure 3.20 Comparison of Ekman pumping field (white contours) diagnosed from climatology and chlorophyll *a* concentrations (mg m^{-3}) diagnosed from a SeaWiFS ocean colour for the period January to May 2000. Zero contours represent the boundary between upwelling (positive Ekman) and downwelling (negative downwelling). The AMT 10 cruise track is noted (red line). Image produced by Dr. Vassil Rousenov

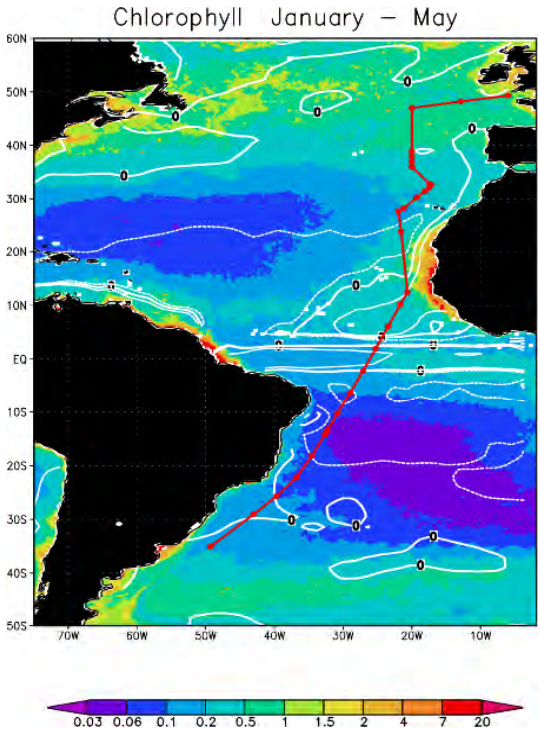

Overall, a combination of convection, horizontal and vertical Ekman transport supply of nutrients to the surface ocean and thus act to sustain the patterns of circular phytoplankton biomass observed (Figure 3.16). However, detailed budgets for the N supply to the euphotic zone suggests that these traditional N sources are too small to explain the levels of export production (see review by McGillicuddy *et al.*, (1999) and Chapter 4 of this study). In section 3.3.2, the seasonal and interannual variability in Ekman transport is assessed throughout the AMT programme. In section 4.5.1 of Chapter 4, the Ekman transport field diagnosed for AMT 10 and inorganic and organic nutrient concentrations are used to gain an estimate of the horizontal Ekman transport to the subtropical gyres of the North and South Atlantic.

3.3.2. Seasonal and interannual variability in Ekman transport during AMT

3.3.2.1. Introduction

In this study, Ekman pumping was calculated by Dr. Vassil Rousennov, using surface wind data (u and v components, 10m above surface), skin temperature and air temperature from NCEP Reanalysis data set (www.cdc.noaa.gov/cdc/data). Ekman pumping is defined as:

$$w = \frac{1}{\rho_0}\left(\frac{\partial}{\partial x}\left(\frac{\tau^y}{f}\right) - \frac{\partial}{\partial y}\left(\frac{\tau^x}{f}\right)\right) \qquad \text{Eq. 3.1}$$

where ρ_0 is the reference density, $f=2\Omega\sin\theta$ is the Coriolis parameter, τ^x and τ^y are the wind stresses in the x and y directions (eastwards and northwards). The Ekman pumping field was calculated for each AMT cruise using data from 3 months prior to and after the cruise month (Spring, January to July; Autumn, June to December; Figure 3.18, a - k). A positive Ekman pumping implies upwelling (green to red regions), whereas a negative Ekman implies downwelling (blue to purple regions), the magnitude of Ekman being relative to the strength of upwelling or downwelling. In this study, zero Ekman was assumed to define the inter-gyre boundary. The along track Ekman pumping was also calculated for Spring and Autumn transects.

3.3.2.2. Background state

The annual mean Ekman pumping field (Figure 3.21, a) clearly depicts the vast regions of strong downwelling over the north and south subtropical Atlantic Ocean (Figure 3.21, a; blue-purple), the most intense downwelling being diagnosed over the south Atlantic gyre between the equator and 20°S. Less intense downwelling is diagnosed north of ~ 30°N and south of ~ 25°S (Figure 3.21, a; green). Regions of strong upwelling are diagnosed over the tropical equatorial region and northwest

African upwelling region, with less intense upwelling being observed at higher latitude (Figure 3.21, a; yellow-red).

In the North Atlantic, upwelling commences further south at ~ 35°N in the West Atlantic compared to the east Atlantic, where annual downwelling extends to ~ 50°N.

Figure 3.21 Ekman pumping field (m y^{-1}) for the Atlantic Ocean averaged over; (a) annual timescale, (b) Autumn (June to December) and (c) Spring (January to July).

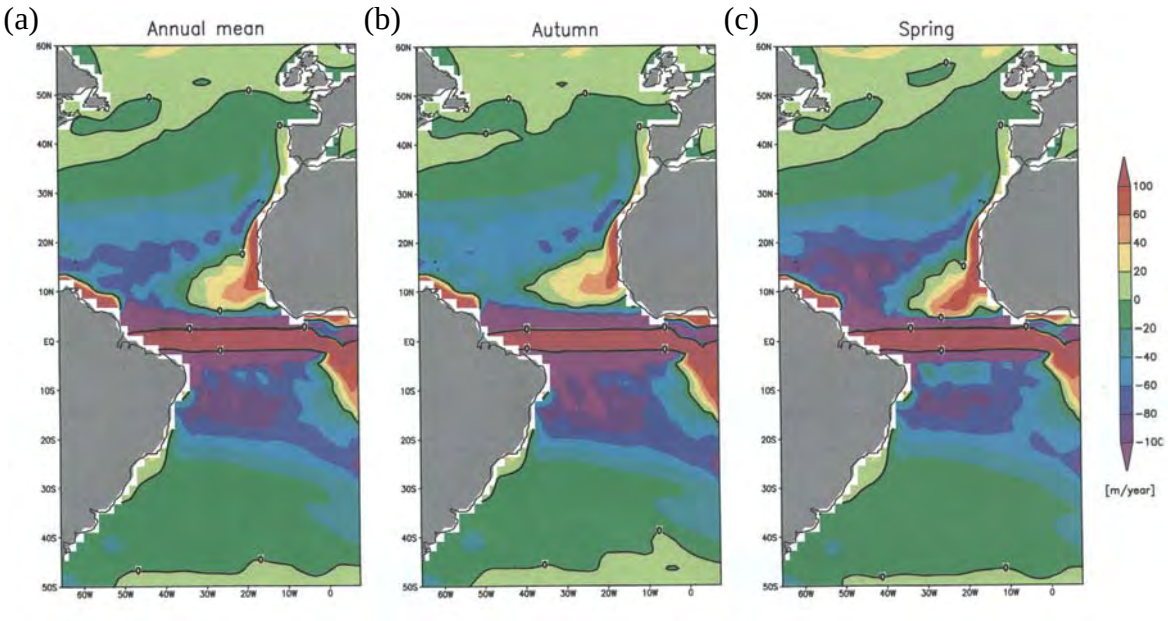

3.3.2.3. Seasonality

In general, the strong downwelling (> 100 m y^{-1}) was diagnosed over a larger region during spring, thus over the southern hemisphere during Autumn AMT cruises (Figure 3.21, b) and over the northern hemisphere during Spring AMT cruises (Figure 3.21, c). In the North Atlantic, downwelling extended further north (north of 50°N) in spring than autumn (~ 45°N), whereas in the South Atlantic, little seasonal variation is seen at high latitudes. This seasonal pattern is due to the stronger zonal winds in winter than summer, induced by the stronger pole-equator T gradient.

From the along track Ekman pumping, regions of downwelling are diagnosed between ~ 25°S and 5°S, and 20°N to 40°N during autumn cruises (Figure 3.22; white

triangles) and between ~ 25°S and 5-8°S and between ~ 15°N and 40°N during spring cruises (Figure 3.22; white circles).

Figure 3.22 Seasonal variation in the along track Ekman pumping (m y^{-1}) between autumn (white triangles circles) and spring (white circles) AMT cruises between 35°S and 50°N in the Atlantic Ocean.

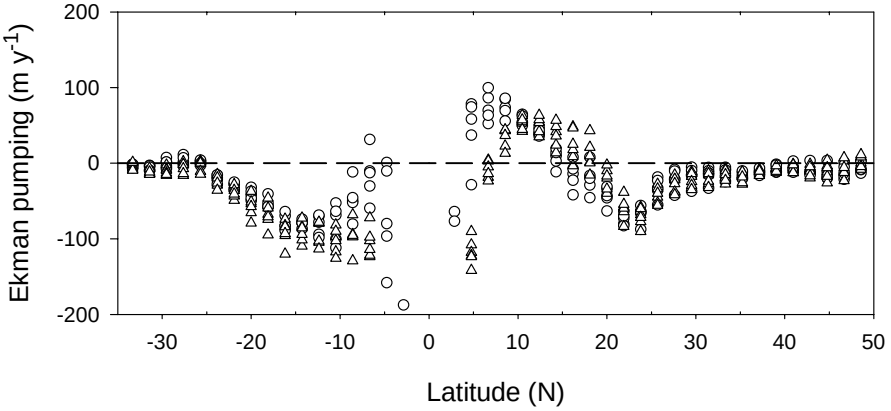

In general, upwelling is diagnosed between 4°S and 20°N, with high values diagnosed between 4°N and 4°S due to calculation of the Ekman field near the equator (*i.e*. θ tends towards zero in the Coriolis parameter) (Figure 3.22). In spring, equatorial upwelling tends to be located further south (5°N) and stronger (100 m y^{-1}) than during autumn, which tends to be more northern (10°N) and weaker (60 m y^{-1}). Persistent downwelling was diagnosed south of the equator until 30°S during autumn cruises, whereas during spring, there was a narrow band of upwelling between 5 and 10°S. In general, north of 20°N, there was persistent downwelling.

3.3.2.4 Interannual variations

3.3.2.4.1 Autumn

Overall, little interannual variability is observed in the diagnosed Ekman pumping field during Autumn AMT cruises, especially in the southern hemisphere where downwelling is intense during all Autumn AMT's (austral spring; see Appendix H for images). In the northern hemisphere, downwelling is less intense, downwelling being strongest during AMT 5 and 11 (Appendx H, H1, c and f). There is southward

shift in the northern flanks of the North Atlantic subtropical gyre during AMT 5 (~ 40°N; Appendix H, H1 c) compared to other AMT's, where the northern gyre boundary extends to ~ 50°N. Interannual variability in the equatorial and coastal upwelling region is small, as implied from the gyre-scale Ekman field.

Again, little interannual variability in the along track Ekman pumping was diagnosed during Autumn AMT's (Figure 3.23, a). Localised and non-persistent upwelling is diagnosed between 26° and 30°N during AMT 1, 2, 3 and 7 (Figure 3.23, a) and north of 43°N during AMT 1, 5 and 11 only. Upwelling diagnosed between 5°N and ~ 20°N was most intense during AMT 7 and 11, with downwelling beginning more equatorward during AMT 9.

Figure 3.23 Interannual variability in along-track Ekman pumping during a) autumn AMT's and b) spring AMT's between 35°S and 50°N in the Atlantic Ocean. Zero Ekman is marked (dashed line).

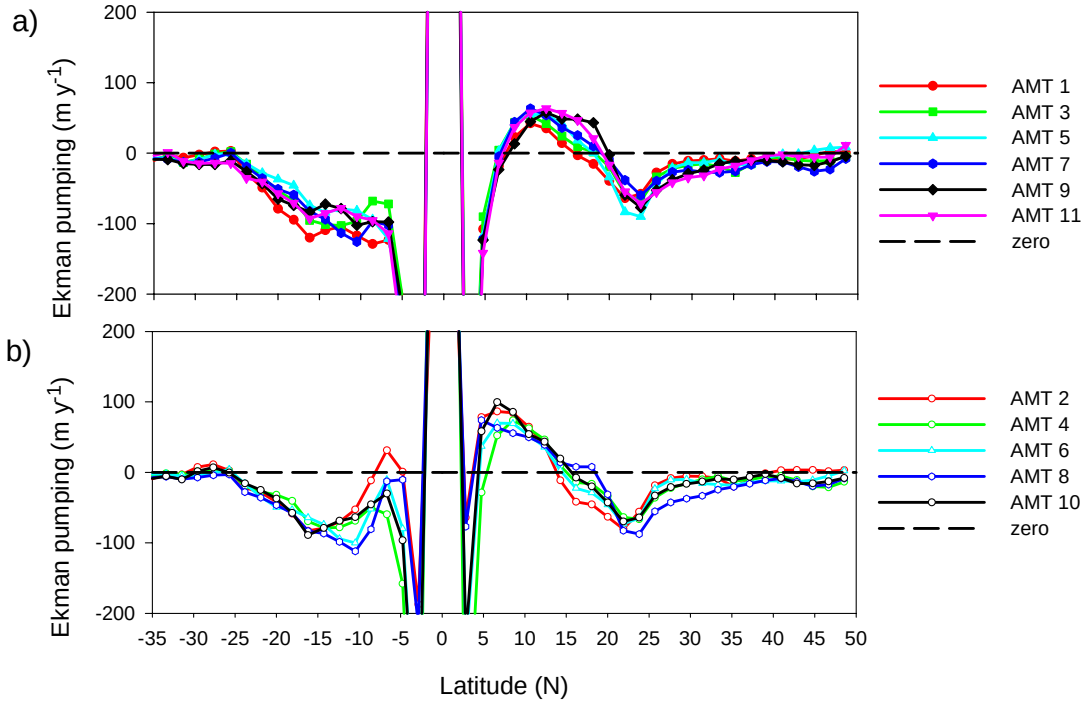

3.3.2.4.2 Spring

Again, little interannual variability in the Ekman pumping field data is diagnosed during Spring AMT cruises. A southward shift in the northern flanks of the North Atlantic gyre is diagnosed during AMT 2 (~ 40°N; See Appendix H, H2, a) and AMT 4 (~ 45°N; Appendix H, H2, b). During spring AMT's, more widespread downwelling is observed in the North Atlantic during AMT 10 (Appendix H, H2, e) than previous AMT's, especially in the west Atlantic. Upwelling around the equatorial region appears more widespread during AMT's 8 and 10 (Appendix H, H2, d and e, respectively).

Localised and non-persistent upwelling is diagnosed (between 28° to 30°S) during AMT 2, 4, and 10 (Figure 3.23, b) and north of 40°N during AMT 2 only. Southwards equatorial upwelling (i.e., > 0) is diagnosed for AMT 2 only although north of 5°N, upwelling is most intense during AMT 10. In the northern subtropical gyre, downwelling began more equatorward during AMT 2 and more poleward during AMT 8.

3.3.3 North Atlantic Oscillation

The dominant mode of atmospheric variability in the North Atlantic region throughout the year is the North Atlantic Oscillation or NAO index. This phenomenon has been defined as the sea-level pressure anomaly between the Icelandic low and the Azores high (van Loon and Rogers; 1978; Hurrell, 1995). Complementary changes in the westerlies over the North Atlantic and in the Trade winds over the tropical Atlantic, heat flux and SST anomalies characterise the two NAO phases (Cayan, 1992; Wallace *et al*., 1992). During a negative NAO phase, the jet stream follows a more southern path, whereas in a positive NAO phase, the Jet Stream follows a more northern path and is stronger. These changes in wind field lead to changes in the heat exchange and

convection, which vary regionally over the North Atlantic. During a negative NAO phase, there is intense convection over the Greenland Sea, but weak convection over the Labrador Sea and Sargasso Sea (Dickson *et al.*, 1996). During a positive NAO phase, the reverse pattern is observed, with intense convection being observed over the Labrador Sea and Sargasso Sea but weak convection over the Greenland Sea (Dickson *et al.*, 1996).

The NAO phase was identified for each AMT cruise in order to assess if changes in SST, SSS and SSD can be explained by this atmospheric forcing.

Table 3.1 Monthly, 3-month mean and previous winter North Atlantic Oscillation (NAO) index for spring (2, 4, 6, 8 and 10) and autumn (1, 3, 5, 7, 9 and 11) AMT transects. Data retrieved from www.cdg.ucar.edu/~jhurrell/nao.html.

		NORTH ATLANTIC OSCILLATION INDEX		
AMT cruise	Season/Year	Month	3 Monthly Mean	Winter NAO
AMT 1	Autumn/1995	-0.1	-0.6	2.4
AMT 2	Spring/1996	-0.9	-1.10	-2.4
AMT 3	Autumn/1996	-0.6	0.73	-2.4
AMT 4	Spring/1997	-2.1	1.43	-0.45
AMT 5	Autumn/1997	-0.8	0.70	-0.45
AMT 6	Spring/1998	0.6	0.70	0.05
AMT 7	Autumn/1998	-3.2	-0.03	0.05
AMT 8	Spring/1999	-0.2	0.87	1.73
AMT 9	Autumn/1999	2.8	-0.73	1.73
AMT 10	Spring/2000	-3.1	0.37	1.55
AMT 11	Autumn/2000	0.8	-1.0	1.55

The monthly NAO index was most negative during AMT's 4, 7 and 10 and most positive during AMT 9, the remaining transects being near zero. Indeed, during AMT 10, low SST, deep MLD (> 150m) and the highest Ekman pumping around the

equatorial region were observed. MLD during AMT 10 was significantly deeper than previous AMT transects and the SST was lower across the northern gyre as predicted. However, no inferences could be made between NAO index and other AMT's.

A number of studies have found correlations between the NAO index and physical and biogeochemical properties over the West Atlantic Ocean (Aebischer *et al*., 1990; Williams *et al.,* 2000; Bates, 2001). Indeed, observations at the Bermuda Atlantic Time Series (BATS) found that cooler surface temperatures, thicker mixed layer depth and increased primary production were correlated with the negative NAO phase. However, Williams *et al.,* (2000) observed a poor correlation between the NAO index and convective and Ekman nitrate flux in the eastern Atlantic (correlation coefficient, 0-0.2 at 97.5 ‰ confidence level) compared to the western Atlantic (correlation coefficient > 0.4 at 97.5 % confidence level). Thus, the lack of coincidence of sea surface and basin-scale properties examined in this study with monthly, seasonal or annual NAO can be explained by differences in response of the east Atlantic and west Atlantic to this pressure oscillation. Indeed, the NAO only captures one third of the atmospheric variability over the Atlantic Ocean (Dickson, 1997).

3.4 BOUNDARIES

3.4.1 Introduction

Intergyre boundaries are regions of sharp contrasts in temperature and salinity across a short distance, i.e., a front. Partitioning ocean regions to define their large-scale characteristics have been done using both biological and physical characteristics (Longhurst *et al.*, 1995; Hooker *et al.*, 2000). In this study, SST and SSS, the along track gradient in SSD (Hooker *et al.,* 2000) and diagnosed Ekman pumping (see section 3.3) are used to define oceanic boundaries and examine their seasonal and interannual variability.

3.4.1.1 SST and SSS

On the basin-scale view, oceanic regions can be broadly characterised according to the surface T and S properties (Figure 3.24 and 3.25). Subtropical gyre regions are defined by an increase in temperature and salinity relative to the cold and more less saline subpolar regions, causing a small decrease in density (Figure 3.24 and 3.25; grey area). The equatorial region is defined a high in SST (due to high solar heating and upwelling of colder water) and a low SSS (due to precipitation and upwelling), leading to a minimum in SSD (Figure 3.24 and 3.25; white area).

On a finer scale, fronts (sharp gradients in T and S) can be used to identify bands within these larger regions (Figure 3.24 and 3.25). Sharp equatorward increases in temperature and salinity around 30°S mark the southern boundary of the south Atlantic subtropical gyre (Figure 3.24 and 3.25; black arrow, A). A decrease in SSS defines the southern extent of the South Equatorial Current (SEC) around 5°-15°S (Figure 3.24 and 3.25; black arrow, B). The northern extent of the North Equatorial Current (NEC) is defined by a polewards decrease in SST, a small polewards increase in SSS, causing a large decrease in SSD around 10°- 20°N (Figure 3.24 and 3.25; black arrow C). However, some boundaries are not well defined (Figure 3.24 and Figure 3.25, question mark "?").

Comparison of the latitudinal variation in SST, SSS and SSD between autumn (Figure 3.24) and spring (Figure 3.25) AMT cruises shows that the boundaries are less well defined in spring than autumn. SST forms a more prominent maximum around the equator in autumn than spring, during which variations in SST tend to be less sharp diffuse than in autumn. Overall, there is little interannual variation (2-4°) in the position of the boundaries between oceanic regions as defined by SST, SSS and SSD.

Figure 3.24 Latitudinal variations (35°S to 50°N) in SST (red), SSS (blue) and SSD (green) for Autumn AMT's (a) AMT 1, (b) AMT 3, (c) AMT 5, (d) AMT 7, (e) AMT 9 and (f) AMT 11. White area defines the equatorial region (increase SST, decrease SSS). Grey shading defines north and south subtropical gyres (decrease SST and increase SSD). "A" defines the southern extent of the south Atlantic subtropical gyre (sharp increase in SST and SSS). "B" defines the south equatorial current (decrease SSS). "C" defines the north equatorial current (poleward decrease in SST, small increase in SSS). "?" notes boundaries which are not possible to define.

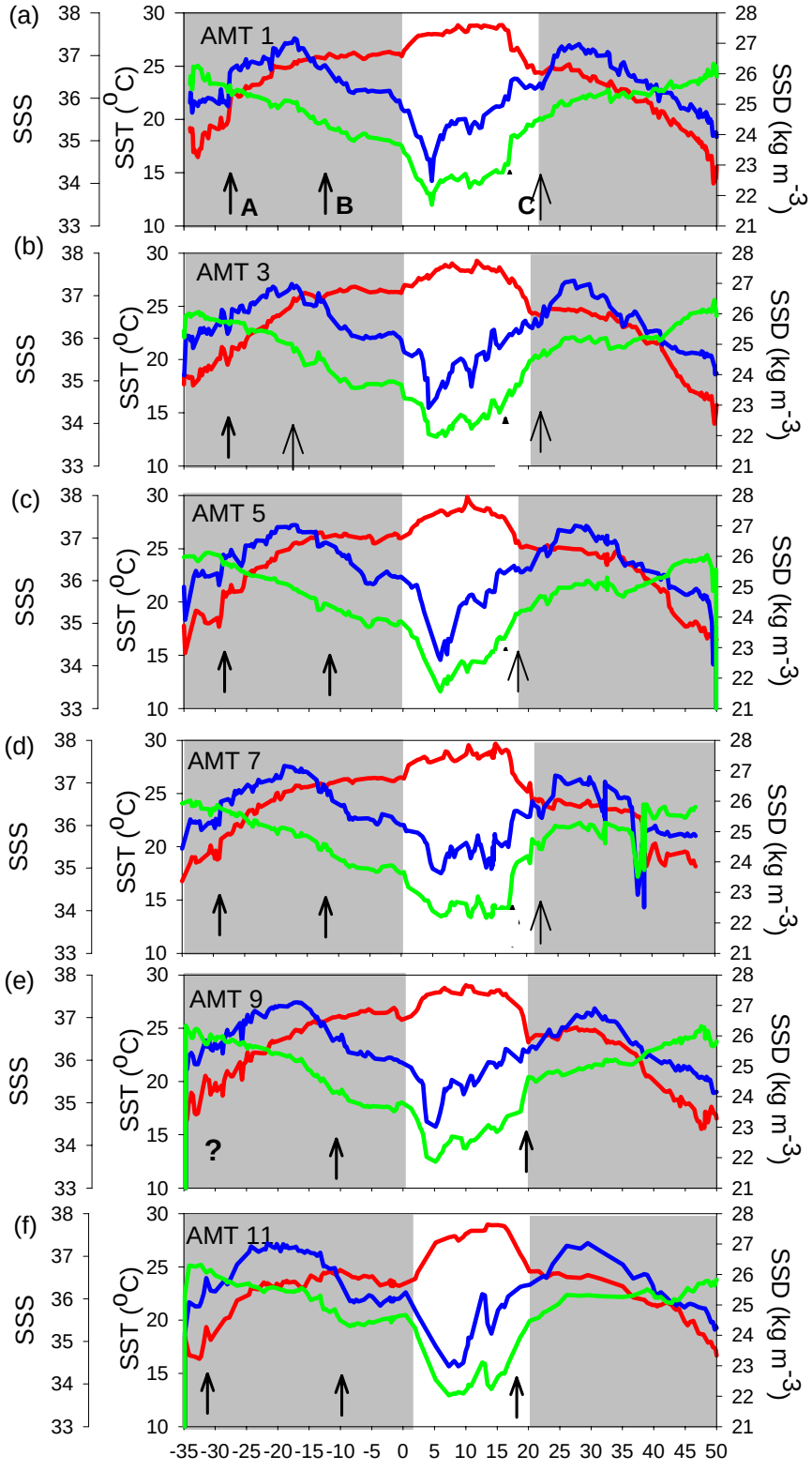

Figure 3.25 Latitudinal variation (35°S to 50°N) in SST (red), SSS (blue) and SSD (green) for Spring AMT's (a) AMT 2, (b) AMT 4, (c) AMT 6, (d) AMT 8 and (e) AMT 10. White area defines the equatorial region (increase SST, decrease SSS). Grey shading defines north and south subtropical gyres (decrease SST and increase SSD). "A" defines the southern extent of the south Atlantic subtropical gyre (sharp increase in SST and SSS). "B" defines the south equatorial current (decrease SSS). "C" defines the north equatorial current (poleward decrease in SST, small increase in SSS). "?" notes boundaries which are not possible to define.

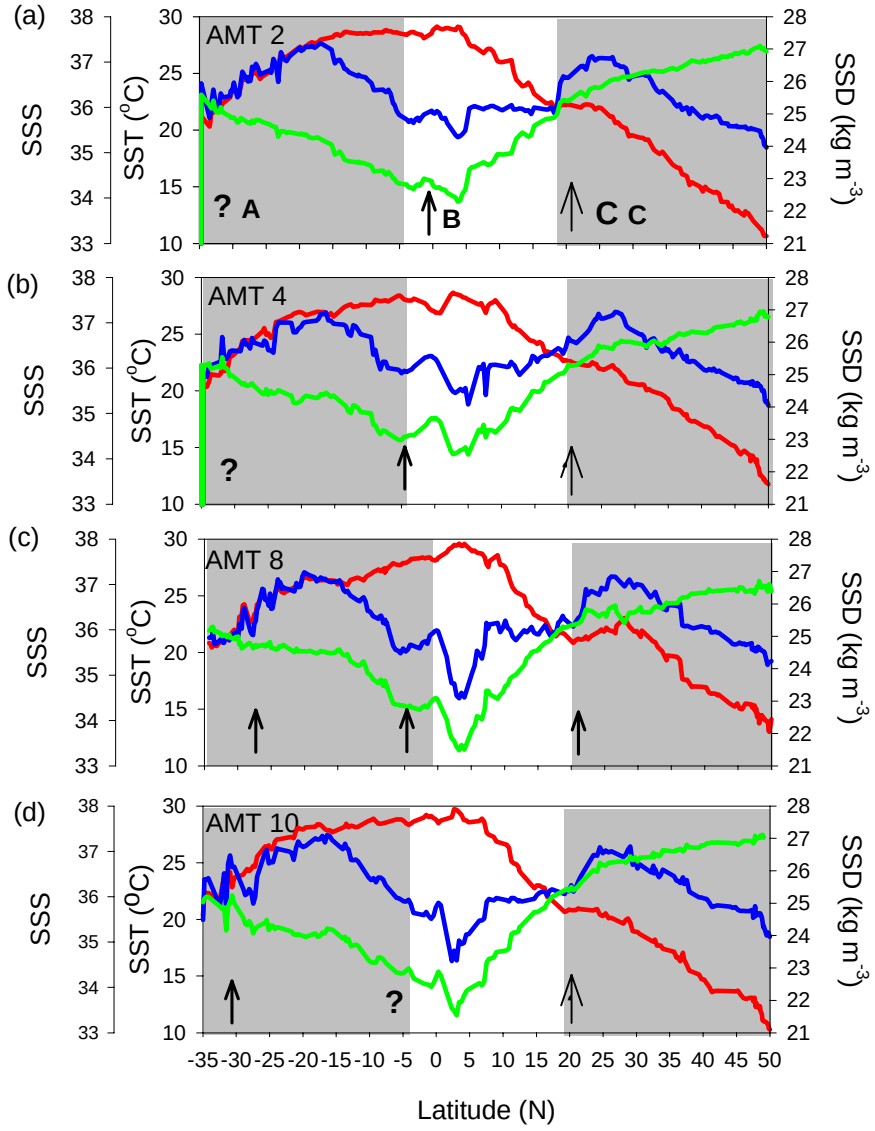

3.4.1.2 Sea surface density

The combined effects of T and S are represented in density (σ_t) and thus fronts can be identified by the change in density (Hooker *et al.*, 2000, Rudnick *et al.*, 2002). The gradient in density was determined by calculating the first spatial derivative in density in the along-track direction (y km), similar to that described by Hooker *et al.*, (2000). Firstly, the mean density was calculated in 200 km boxes (m). Then, the

gradient in density was calculated from one box preceding and proceeding box "m", as described by;

$$\frac{d\sigma_m}{dy} = \frac{\sigma_t^{m+1} - \sigma_t^{m-1}}{y^{m+1} - y^{m-1}} \qquad \text{Eq. 3.2}$$

A Fortran routine was prepared by Dr. Chris Wilson to perform this gradient function and files were run by the author. A maximum in the gradient or equivalently a zero in the second derivative, defines the boundary:

$$\frac{d}{dy}\left(\frac{d\sigma^m}{dy}\right) \qquad \text{Eq. 3.3}$$

Interannual variations (~5° of latitude) in the ocean boundaries (defined by the zero second derivative) are observed during both Autumn and Spring transects (Figure 3.26, a and b, respectively). Variation in the northern boundaries of the equatorial region is more apparent during Autumn than Spring.

Figure 3.26 Latitudinal variation in the second derivative of surface density for (a) Autumn AMT cruises and (b) Spring AMT cruises. Zero intercept defines the ocean boundary

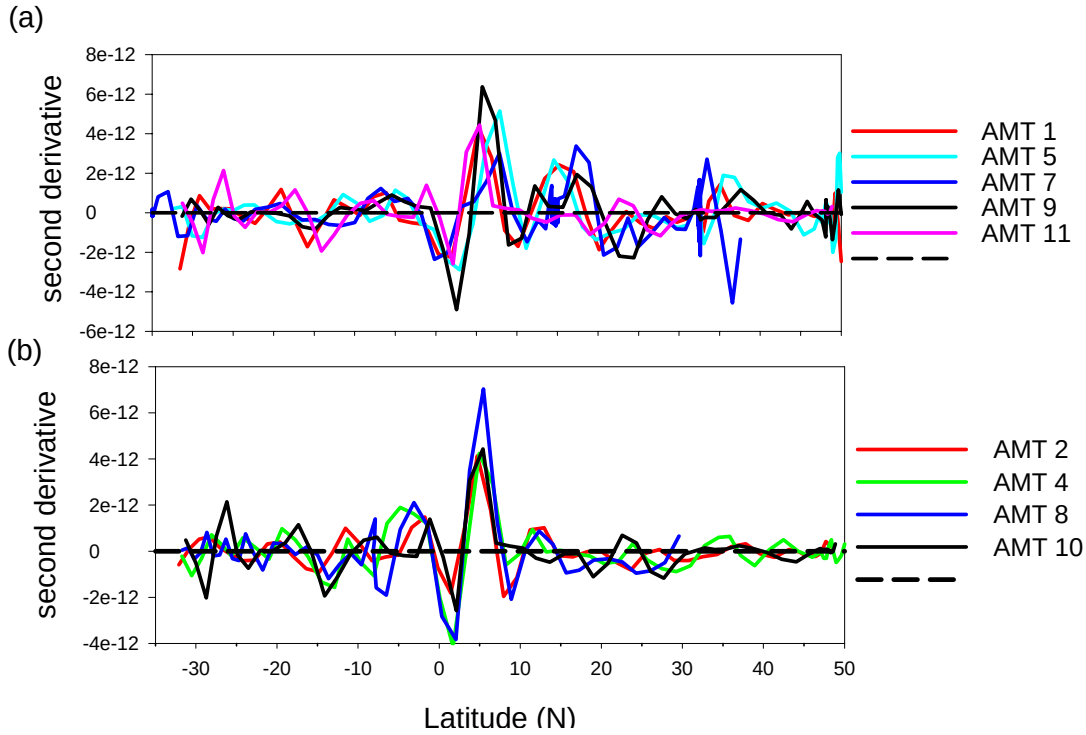

In order to validate this method, fronts identified using a zero second derivative, SST and SSS were compared for data from AMT 1, 2, 5 and 10 only (Figure 3.27, a-d). In most cases, there is good agreement (black arrows) between boundaries using these two related methods.

In this study, the number of boundaries identified using the second derivative (dashed lines) is much greater than those identified by Hooker et al., (2000). Indeed, Hooker *et al.*, (2000) named and defined 14 provinces from data collected during AMT 1 and 2, possibly discounting other boundaries as minor or insignificant.

Figure 3.27 Latitudinal variation (35°S to 50°N) in the second derivative (black line) of along track surface density, sea surface temperature (SST; red line) and sea surface density (SSD; blue line) for Autumn AMT 's (a) AMT 1, (b) AMT 5, and Spring AMT's (c) AMT 2 and (d) AMT 10. Black arrows mark fronts. "?" marks unknown fronts.

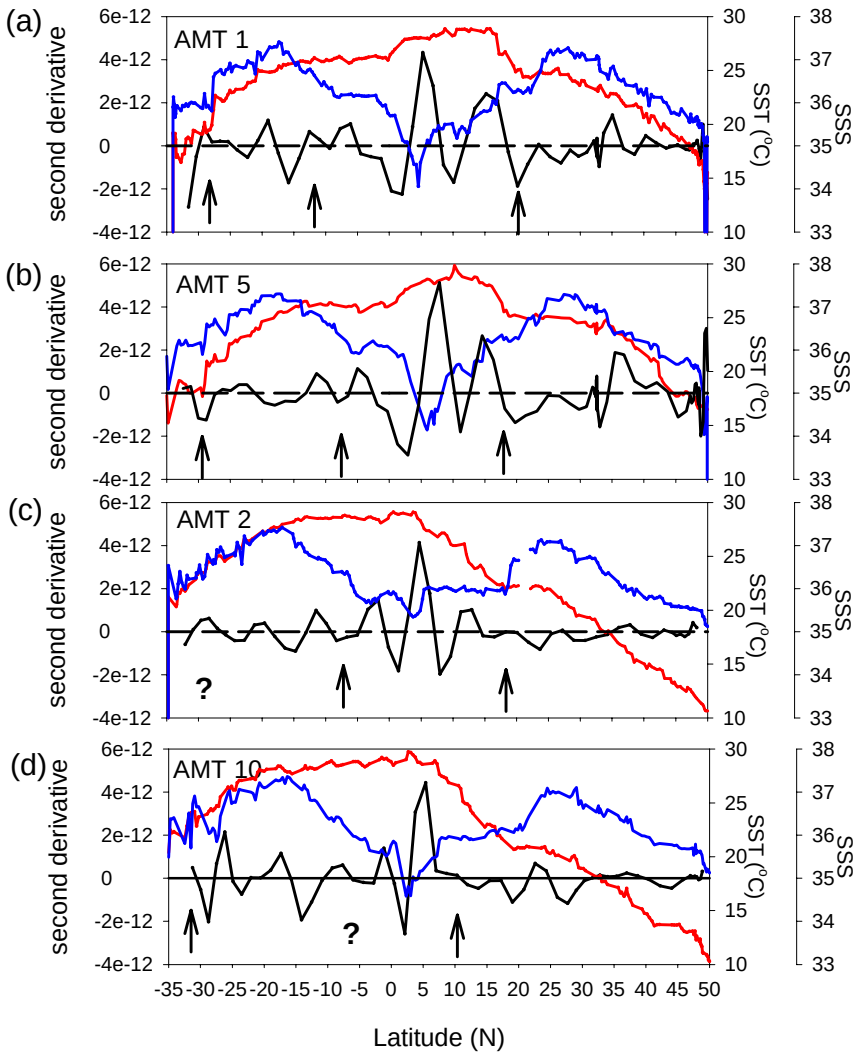

3.4.1.3. Comparison of sea surface properties and Ekman pumping in defining oceanic boundaries

Ekman pumping defines regions of upwelling and downwelling and therefore provides an alternative definition of gyre scale ocean provinces. Comparing SST, SSS and SSD reveals that zero Ekman broadly coincides with a rapid increase in SST and SSS around 30°S (southern extent of southern subtropical gyre), a constant SST and large increase in SSS around 4-8°N, an decrease in SSS and increase in SST around 18-20°N (NEC) during autumn and spring transects. In addition, during AMT 2, zero Ekman at 5-10°N, coincided with a near constant SST and decreasing SSS, thus defining the southern extent of the SEC.

There is a coincidence in identifying fronts using sea surface properties and the Ekman pumping field. However, no such relationship was found between the latter two methods and those identified using the gradient in sea surface density (Hooker *et al.*, 2000; Figure 3.28, black arrows). Thus, it is difficult to determine if variations in ocean regions are attributed to methods used to define the fronts or an actual seasonal or interannual shift in their boundaries. In addition, the variation in the cruise track during the AMT programme further complicates the validation of methods used to define ocean boundaries.

Figure 3.28 Latitudinal variation (35°S to 50°N) in the along track Ekman pumping field (red line) and second derivative (black line) of along track surface density for Autumn AMT 's (a) AMT 1, (b) AMT 5, and Spring AMT's (c) AMT 2 and (d) AMT 10. Black arrows mark fronts. "?" marks unknown fronts.

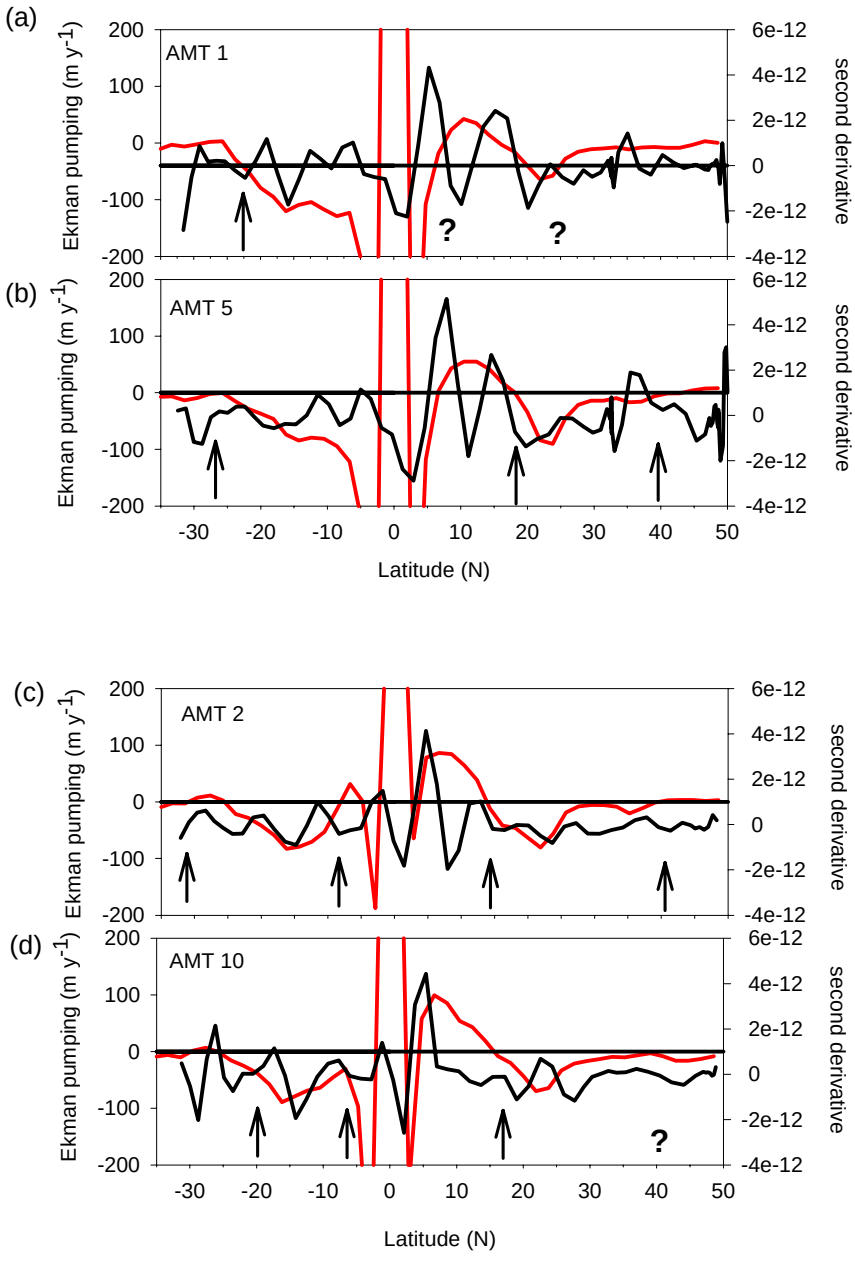

3.5. Conclusions; Physical properties of the Atlantic

1. Seasonal rather than interannual variations in sea surface T, S and σ_t are more apparent. However, interannual variability is evident, being greater for SSS than SST, probably due to the combined effects of the precipitation (addition of freshwater) and upwelling (of highly saline water).

2. Distinct gyre structures are apparent from basin scale T, S and σ_t, showing a persistent pattern with little seasonal and interannual variability. The equatorial and coastal upwelling regions appear more variable, the upwelling region being more distinct during Spring than Autumn, when upwelling is weak.

3. Seasonal variations in MLD conform to the expected response to changes in solar radiation and wind-driven mixing. Spring and autumn AMT's capture the legacy of winter and summer conditions, respectively. Defining the MLD is dependent on the density gradient employed.

4. The convective transport and Ekman flux of nutrients to the euphotic zone strongly influences the distribution of phytoplankton. While convection and the vertical Ekman transport of nutrients are important over the high latitude subpolar region, horizontal Ekman transport is important over the flanks of the subtropical gyres, where wind-induced downwelling creates a nutrient depleted surface ocean.

5. In agreement with basin scale T, S and σ_t, the Ekman pumping field shows that upwelling is stronger in Spring than Autumn in the Atlantic. In addition, interannual variability in Ekman pumping is observed during both Spring and Autumn transects in the northern and southern hemispheres.

6. A negative NAO index may explain the lower SST and deep MLD observed during AMT 10. However, no other surface or basin scale properties can be correlated with NAO, supporting suggestions by Williams *et al.*, (2000) that NAO is correlated with physical properties in the West and central Atlantic, rather than the East Atlantic.

7. Identifying gyre boundaries is complex and dependent on the parameters set to define the boundaries. Frontal regions defined by sea surface properties and by the Ekman pumping field agreed well on the gyre scale. However, fronts defined by along track density gradients were numerous and coincided only occasionally with fronts defined by surface properties and the Ekman field. Therefore, it was difficult to conclude whether these gyre boundaries were changing on a temporal scale or if the changes observed were dependent on the method used to define the boundary. However, within the same method, boundaries did vary by approximately ~ 5°, although no clear pattern was observed.

8. Separating the signatures of seasonal and interannual variability is made difficult through the different choices in cruise track and the exact timing of the AMT cruises (during the transition between heating and cooling seasons), as well as the limited depth range (only the upper 250m).

PART TWO

3.6 IS THE ATLANTIC OCEAN NITROGEN OR PHOSPHATE LIMITED?

3.6.1. Introduction

Carbon, nitrogen and phosphorus are essential elements for phytoplankton in the marine environment. In 1963, Redfield *et al.*, proposed an important unifying concept regarding the stoichiometry of dissolved and particulate carbon (C), nitrogen (N) and phosphorus (P) in the marine environment, concluding that in phytoplankton, there is an elemental ratio of C:N:P of 106:16:1, classically referred to as the "Redfield ratio". Studies concerning phytoplankton growth and nutrient dynamics, where there are significant deviations from Redfield stoichiometry below or above the proposed N: P ratio of 16: 1, were considered indicative of N or P limitation, respectively (Ryther and Dunstan, 1971; Jackson and Williams, 1985; Downing, 1997). However, the bioelemental stoichiometry of phytoplankton is known to change as a function of substrate quality light availability and ambient nutrient concentrations of both macro and trace nutrients (Sakshaug and Holm-Hansen, 1977; Rhee, 1978; Laws and Bannister, 1980; Tett *et al.,* 1985; Letelier *et al.,* 1996; Sterner and Grover, 1998; Touratier *et al.,* 2001). Physiological adaptations, such storage of lipids (Napolitano, 1994; Karl and Tien, 1997), carbohydrates (Fraga *et al.,* 1999; Fraga, 2001) and phosphate sparing (the ability to grow with altered P cell quota by reduction of intracellular nucleotide pools and lower nucleic acid content ; Karl *et al.,* 1998) may also be responsible for the export of organic matter from the euphotic zone with C:N:P ratios significantly different to 106:16:1 (Karl *et al.,* 1996; Christian *et al.,* 1997). Additionally, numerous studies have also shown significant deviations from Redfield stoichiometry in the dissolved organic pool (Sanders and Jickells, 2000; Abell *et al.,* 2000; Karl *et al.,* 2001)

In order to understand N and P dynamics and improve interpretations based on Redfield stoichiometry, the concept of N* was developed (Michaels *et al.,* 1996) which described the concentration of nitrate in excess of that expected from remineralisation of phosphate at Redfield stoichiometry. Using the extensive GEOSECS nutrient data set, and applying Redfield stoichiometry globally, N* was defined as:

$$N^* = [NO_3^-] - 16 \times [PO_4^{3-}] + 2.72 \qquad \text{Eq. 3.4}$$

where $[NO_3^-]$ and $[PO_4^{3-}]$ are the concentrations of nitrate and phosphate in a specific water sample, respectively. The offset of 2.72 μmol kg^{-1} was included to set the global ocean mean N* to zero, implying that global denitrification exceeds N_2 fixation (Michaels *et al.,* 1996). Thus, N* exceeding 2.72 μmol kg^{-1} implies excess N. N* was later derived from the stoichiometric balance of nitrification, denitrification and remineralisation of N rich organic matter from N_2 fixation (Gruber and Sarmiento, 1997). Using this balance, N* was redefined as;

$$N^* = (0.87[NO_3^-] - 16[PO_4^{3-}] + 2.9)\ \mu mol\ kg^{-1} \qquad \text{Eq. 3.5}$$

Again, the constants (relationship between NO_3^- and $16PO_4^{3-}$, 0.87 and intercept when N* is zero, 2.9) force the global N* to zero, implying net global denitrification. Thus, according to Gruber and Sarmiento's diagnostics, N* exceeding 2.5 μmol kg^{-1} implies excess N or P limitation.

Sources of phosphate to the open ocean are primarily rivers (through continental weathering of crustal material) and the atmosphere to the coast and open ocean, respectively (Benitez-Nelson, 2000; Herut *et al.,* 2002). P is removed from the marine system through sedimentary burial (organic, sorption on clays, phosphorite burial and hydrothermal processes; Follmi, 1996; Delaney, 1998) and has a relatively long residence time (50,000 years; Van Cappelan and Ingel, 1994). In contrast, the N cycle is

more complex, having many more sources and sinks (see section 1.1) and its residence time much is shorter than P (5000 years; McElroy, 1983). Numerous authors believe that the balance between N_2 fixation (N source) and denitrification (N sink) ultimately controls which element, N or P, limits primary production (Ganeshram *et al.,* 1995, Codispoti, 1995; Tyrrell, 1999; Benitez-Nelson, 2000), more N_2 fixation inducing a P limited environment. Indeed, there is an ongoing debate in the oceanographic community regarding which nutrient ultimately limits phytoplankton growth in the open ocean, NO_3^- or PO_4^{3-} (or possibly iron).

Using the extensive inorganic nutrient data set collected between 35°S and 50°N in the Atlantic during 9 AMT transects (AMT 7 and 8 excluded due to unreliable nutrient data) the vertical and horizontal distribution of NO_3^- and PO_4^{3-} are assessed in section 3.5.1.2., and compared to the vertical distribution of the deep chlorophyll maximum (DCM) and mixed layer depth (MLD). In section 3.5.1.2., temporal (seasonal and interannual) and spatial (depth and oceanic province) variations in the NO_3^- to PO_4^{3-} ratio and N* ratio are assessed for 9 AMT cruise data sets. In section 3.5.4, the relationship between dissolved organic nitrogen and phosphorus (DON and DOP, respectively) is assessed for data collected during AMT 10.

3.6.1.1. Data management

Nutrient data presented in this thesis was includes AMT 1 to 11. Personnel involved in the collection and analysis of the nutrient data are listed in Table 3.2. Nutrient concentrations (nitrate plus nitrite, nitrate herein ($[NO_3^-]$) and phosphate ($[PO_4^{3-}]$) were determined by standard colourimetric methods (Woodward and Rees, 2001). Nutrient concentrations for AMT 10 were determined by the author at Southampton Oceanography Centre under the supervision of Dr. Richard Sanders (see section 2.3.1).

Quality assessment was performed by the AMT data manager (Dr. Alison Fariclough) at the British Oceanographic Data Centre (BODC). Linear regression analysis (SigmaPlot) was performed to determine the statistical significance of the N: P relationship.

Table 3.2. Summary of personnel and research institution involved in collection of samples and colourimetric determination (Woodward and Rees 2001) of nutrient concentrations (nitrate plus nitrite, nitrate herein ($[NO_3^-]$) and phosphate ($[PO_4^{3-}]$) during AMT 1 to 11. Note AMT 6 is excluded due to a change in cruise track.

CRUISE NUMBER	DATES	INSTITUTE	PERSONNEL
1	Autumn 1995	PML	M. Woodward
2	Spring 1996	PML	M. Woodward
3	Autumn 1996	PML	M. Woodward
4	Spring 1997	PML	M. Woodward
5	Autumn 1997	PML	M. Woodward
7	Autumn 1998	PML	N. Lefevre, J. Aiken, M. Lucas
8	Spring 1999	PML	M. Woodward
9	Autumn 1999	PML/Newcastle	V. Kitidis
10	Spring 2000	Liverpool/SOC	C. Mahaffey
11	Autumn 2000	PML	M. Woodward

Although samples were collected and analysed by numerous investigators, data less than or greater than the Redfield stoichiometry (N: P ~ 16: 1) were not excluded. However, the limitations of the data set must be recognised. Surface $[NO_3^-]$ and $[PO_4^{3-}]$ are often reported to be below the detection limits or statistically indistinguishable from zero. Therefore, surface $[NO_3^-]$ and $[PO_4^{3-}]$ are generally reported as zero, which hampers interpretation of surface ocean nutrient dynamics.

The nitracline (Z_N) and phosphocline (Z_P) were defined by an intermediate depth between successive depths that displayed the maximum gradient in $[NO_3^-]$ or $[PO_4^{3-}]$:

$$\frac{\partial N}{\partial Z} = \left(\frac{N_2 - N_1}{Z_2 - Z_1} \right) \qquad \text{Eq. 3.6}$$

where N_1 and N_2 are $[NO_3^-]$ or $[PO_4^{3-}]$ at depth Z_1 and Z_2 respectively, where Z_1 and Z_2 are successive depths in the water column. At stations where $[NO_3^-]$ or $[PO_4^{3-}]$ did not reach concentrations expected for the sub-surface (usually > 200m) ocean (in comparison to adjacent stations), the maximum depth of the CTD cast was noted.

The deep chlorophyll maximum (DCM) is a layer in the water column where phytopigment concentrations are highest. Fluorimetric data was collected on each sampling cast using a fluorometer (Wet Labs inc.) attached to the CTD frame during all AMT cruises. Fluorescence was binned into 1 m intervals using the SBE Data Processing (Win 32) programme and the depth of maximum fluorescence determined. Note that fluorescence was used for qualitative rather than quantitative assessment of the DCM as the fluorometer was not calibrated against chlorophyll *a* concentrations during some AMT cruises.

Dissolved organic nutrient concentrations for samples collected on AMT 10 were determined by inorganic nutrient analysis prior to and after UV digestion (see section 2.3.2.).

3.6.1.2. Ocean province and depth distribution of nitrate and phosphate

The horizontal distributions of nutrients and phytoplankton biomass in the open ocean are partly controlled by physical processes such as convection and Ekman transport (see section 3.3). In the vertical, $[NO_3^-]$ and $[PO_4^{3-}]$ tend to be low in surface waters and increase with depth, the gradient and depth of increase varying with latitude and season. Figures 3.29 and 3.30 depict characteristic depth profiles of $[NO_3^-]$ (black) and $[PO_4^{3-}]$ (red) during AMT 10 (Spring) and AMT 11 (Autumn), respectively. With respect to seasons, Figure 3.29i, a and b, and Figure 3.30i, c and d represent spring

conditions, whereas Figure 3.29i, c and d, and Figure 3.30i, a and b, represent autumn conditions.

Daily AMT stations typically sample to a maximum depth of 150 to 250 m. Over this depth range during spring, [NO_3^-] and [PO_4^{3-}] tend to be relatively uniform (to a depth of 150m, ~ 5μM and 0.25μM, respectively) at a typical northern subpolar station (46.98°N, 20°W; Figure 3.29i, a). In the north and south Atlantic subtropical regions (27.53°N, 21.90°W; Figure 3.29i, b and 23.80°S, 31.13°W; Figure 3.30i, a, respectively), [NO_3^-] and [PO_4^{3-}] are uniform with depth but at near zero concentrations (27.53°N, 21.90°W; Figure 3.29i, b). In the equatorial region (1.35°S, 14.89°W, Figure 3.30i, c), [NO_3^-] and [PO_4^{3-}] are relatively low in surface waters (~ 2 μM and ~ 0.2 μM, respectively) but increases rapidly at ~ 50 m, becoming uniform below 100m (~ 20 μM and ~ 1 μM, respectively).

During autumn, [NO_3^-] and [PO_4^{3-}] are ~ 3 to 5 μM and 0.2 to 0.3 μM, respectively in the northern subpolar gyre (47.14°N, 11.59°W; Figure 3.30i, a), [NO_3^-] and [PO_4^{3-}] increasing below ~ 50 m (~ 10 μM and ~ 5 μM, respectively). In the north and south Atlantic subtropical gyres (27.55°N, 21.97°W and 22.25°S, 36.84°W; Figure 3.29i, b and d, respectively), [NO_3^-] and [PO_4^{3-}] remain near zero concentrations to 100m and ~ 200m depth, respectively, where a slight increase in both [NO_3^-] and [PO_4^{3-}] is observed. In the equatorial region during autumn (1.94°S, 25.26°W; Figure 3.29i, c), [NO_3^-] and [PO_4^{3-}] concentrations are near zero but increase sharply at ~ 50m to near constant concentrations (~ 20μM and > 1 μM, respectively).

Figure 3.29. Depth variation in nitrate (NO_3^-; black; μM) and phosphate (PO_4^{3-}; red; μM) during Spring AMT cruise (AMT 10) in (i) characteristic profiles from (a) a subpolar region (46.98°N, 20°W), (b) north Atlantic subtropical gyre (27.53°N, 21.90°W), (c) equatorial region (1.94°S, 21.90°W) and (d) the south Atlantic subtropical gyre (22.25°S, 36.84°W). (ii) all station data for AMT 10 for (a) subpolar region (50°N-38°N), (b) north Atlantic subtropical gyre (38°N-20°N), (c) equatorial region (20°N-5°S) and (d) south Atlantic subtropical gyre (5°S-35°S).

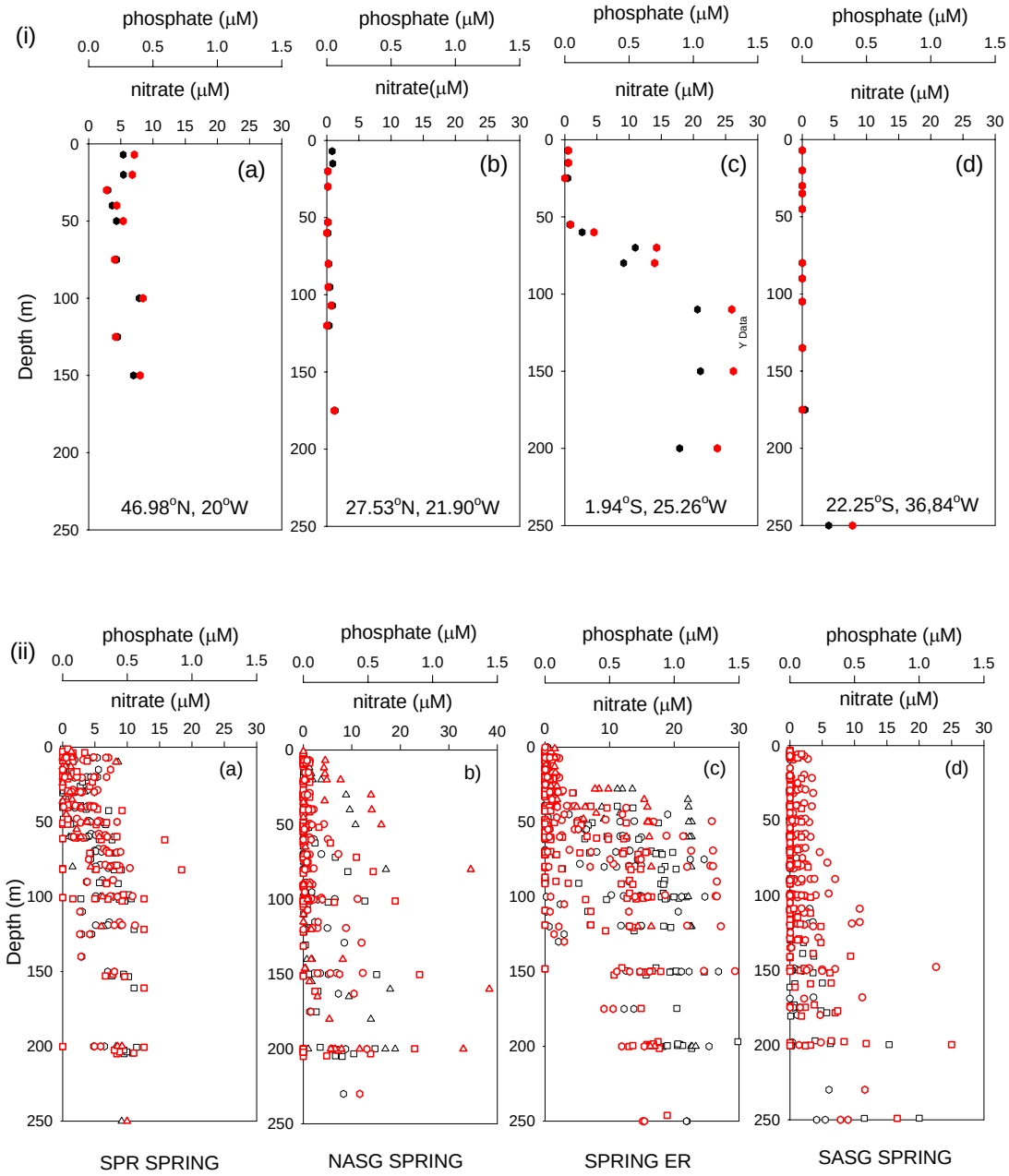

Figure 3.30. Depth variation in nitrate ([NO_3^-]; black) and phosphate ([PO_4^{3-}]; red) concentrations (μM) during Autumn AMT cruise (AMT 11) for (i) characteristic profiles from (a) a subpolar region (47.14°N, 11.59°W), (b) north Atlantic subtropical gyre (27.55°N, 21.97°W), (c) equatorial region (1.35°S, 14.89°W) and (d) the south Atlantic subtropical gyre (23.80°S, 34.13°W) and (ii) all station data for AMT 11 for (a) subpolar region (50°N-38°N), (b) north Atlantic subtropical gyre (38°N-20°N), (c) equatorial region (20°N-5°S) and (d) south Atlantic subtropical gyre (5°S-35°S).

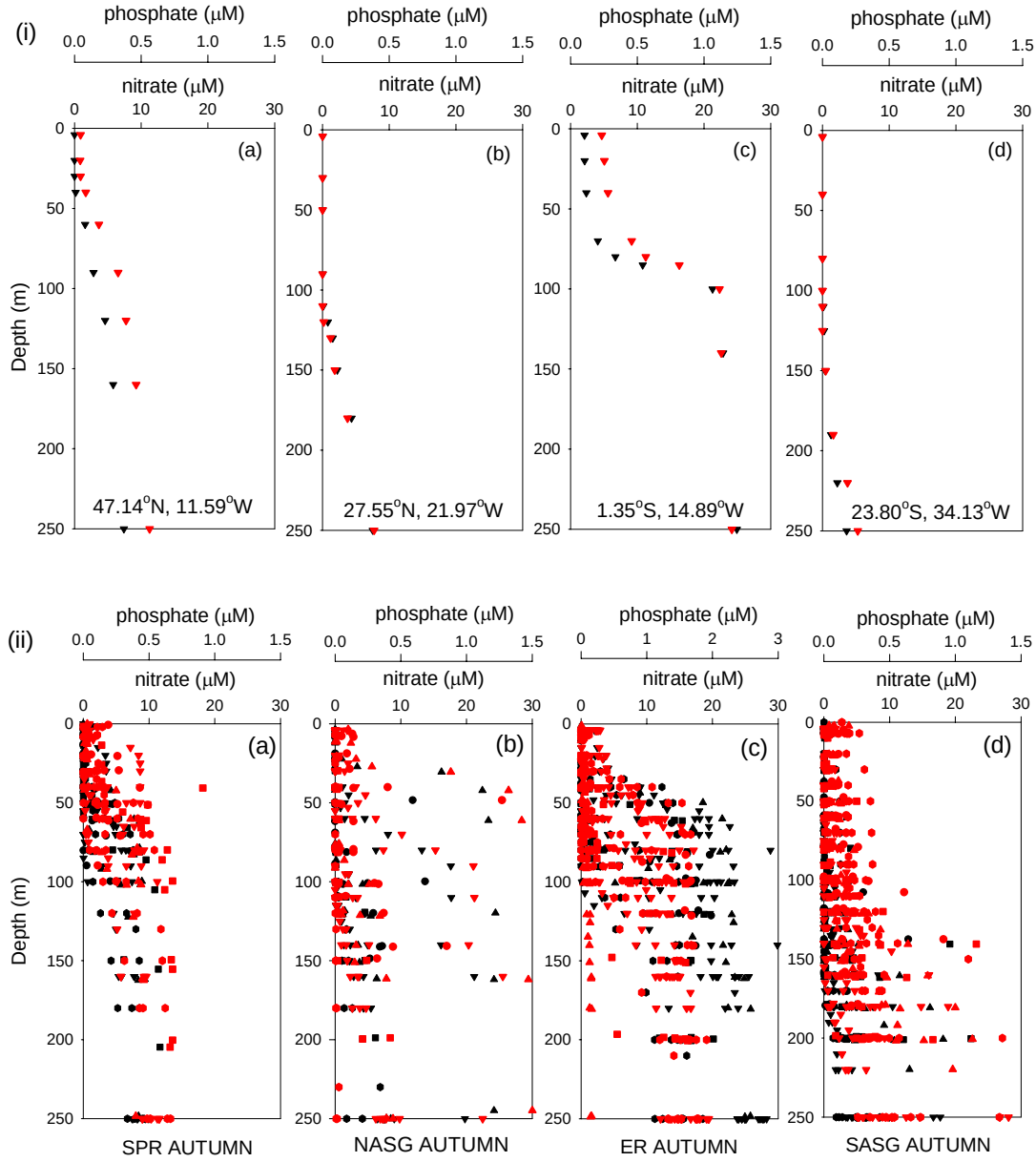

Overall, surface [NO_3^-] and [PO_4^{3-}] tend to be more depleted during autumn than spring in all oceanic regions, reflecting the drawdown of nutrients by phytoplankton in stratified summer waters. However, the subtropical gyres remain nutrient depleted

throughout the spring and autumn to depths greater than 100m, due to consumption by phytoplankton and the net downward vertical Ekman transport of nutrients diagnosed over these regions (see section 2.3.2). In the equatorial region, sharp, near surface gradients in [NO_3^-] and [PO_4^{3-}] reflect net upward vertical Ekman transfer of nutrients. Interannual variability in nutrient concentrations is observed, reflected by the scatter in [NO_3^-] and [PO_4^{3-}] during both Spring (Figure 3.30ii) and Autumn (Figure 3.30ii) AMT transects, respectively.

The vertical distributions of NO_3^- and PO_4^{3-} observed during the AMT programme are typical of the seasonally or permanently stratified tropical and subtropical ocean (Karl *et al.,* 2001; Cavender-Bares *et al.,* 2001). Such nutrient depleted surface waters impinge on the horizontal and vertical distribution of phytoplankton in the water column, which rely on a combination of diffusive fluxes, convection and Ekman transport of nutrients across the thermocline into the euphotic zone (Lewis *et al.,* 1986; Planas *et al.,* 1999), which may explain the tendency for phytoplankton to remain deep in the water column to exploit such fluxes. On the other hand, the light requirement of phytoplankton restricts their position to within the photic zone (> 1% light; Falkowski and Raven, 1997). Additionally, phytoplankton are physically constrained by the seasonal pycnocline and permanent halocline (Anderson, 1969). Thus, a compromise between their nutrient and light requirements, and the physical structure of the water column maintains phytoplankton in a well-defined region called the deep chlorophyll maximum (DCM; Figure 3.31), where chlorophyll *a* concentrations can be up to 50 fold greater than surface waters in typically oligotrophic environments (Agusti and Duarte, 1999). Indeed, the DCM typically coincides with the 3% light level (Agusti and Duarte, 1999). Although the DCM represents a maximum in phytopigment concentration, it does not necessarily represent a maximum in

phytoplankton biomass (Maranon *et al.*, 2000). Rather, photoacclimation of phytoplankton cells (*i.e.* increase in chlorophyll *a* concentrations per cell) at low light levels is a possible explanation for the DCM (Cullen, 1982; Taguchi *et al.*, 1988). Additionally, increased primary production near the nitracline and thermocline (Le Bouteiller, 1986; Pingree *et al.*, 1975), trapping of sinking material and low grazing rates (Longhurst, 1976) and differential degradation of phytopigments (Gieskes *et al.*, 1978) are factors which may enhance the DCM. Thus, the DCM may also represent a water column maximum in productivity, thus raising caution to using surface chlorophyll *a* concentrations as an indicator for water column primary production.

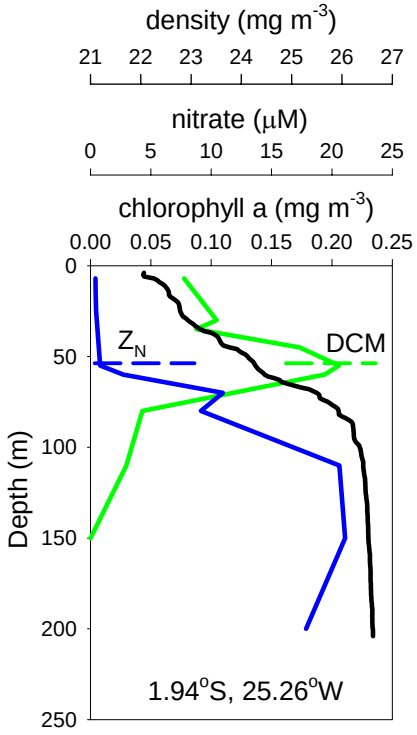

Figure 3.31. Typical depth profiles of nitrate concentrations (μM; blue solid line) and density (mg m^{-3}; black line) and chlorophyll *a* concentrations (μg L^{-1}) from the equatorial region (1.94°S, 25.26°W) during AMT 10 in the Atlantic Ocean. Note the coincidence of the deep chlorophyll maximum (DCM), with the top of the nitracline (sharp increase in nitrate concentrations). At this depth, phytoplankton compromise between nutrient fluxes from the deep ocean and light penetration from the surface. Chlorophyll *a* concentrations are courtesy of Dr. Victoria Hill.

Latitudinal variations in the mixed layer depth (MLD, black line; Hooker *et al.*, 2000), the DCM (green line), the depth of the nitracline (Z_N; red circles) and phosphocline (Z_P; blue circles) indicate distinct regional variations in the interaction between the physical (MLD) and biological (DCM, Z_N and Z_P) controls (Figure 3.32 and 33). During Autumn AMT cruises, in the northern subpolar and subtropical regions, the MLD is consistently shallower than the DCM, the depth of the DCM generally

coinciding with the Z_N and Z_P (Figure 3.32 and 3.33). This probably indicates that nutrients are a greater limiting factor than light at the end of the summer period. In the equatorial region, close vertical proximity of the MLD, DCM, Z_N and Z_P reflects the upwelling of nutrients into the sunlit surface ocean. In the south Atlantic subtropical gyre (representing austral spring), there is tight coupling between the MLD, DCM, Z_N and Z_P during AMT's 1, 9 and 11 (Figure 3.32, a, d and e), the thick MLD reflecting winter mixing and maintaining phytoplankton deep in the water column. However, large deviations in the MLD are observed during AMT 3 and 5, possibly due to the method of defining the MLD or through stochastic fine-scale upwelling events (see section 4.3.3.3.). The lack of simultaneous response of the Z_N and Z_P means that the deviations in MLD are probably attributed to the former scenario.

During Spring AMT transects, the DCM is generally shallower than the MLD, Z_N and Z_P during AMT's 2 and 4, probably due to light limitation in early spring (Figure 3.33). In the northern subtropical region, the MLD is above the DCM during AMT's 2 and 4, again indicating nutrient limitation dominating over light limitation. In the equatorial region tight coupling between MLD, DCM and Z_N and Z_P are observed during AMT's 4 and 10 (the variation in depth of the DCM for AMT 2 is to be trated with caustion, since it appears constant over the subtropics and tropics). In the south Atlantic, MLD is above the DCM and Z_N and Z_P, again implying nutrient limitation over light limitation in the subtropics.

Figure 3.32. Latitudinal variation (35°S to 50°N) in the mixed layer depth (MLD; black line), deep chlorophyll maximum (DCM; green line), depth of the nitracline (Z_N; red circles) and phosphocline (Z_P; blue circles) for Autumn AMT cruises; (a) AMT 1, (b) AMT 3, (c) AMT 5, (d) AMT 9 and (e) AMT 11. The maximum depth of the CTD cast represents profiles where Z_N and Z_P could not be diagnosed (red empty square and blue empty circle respectively).

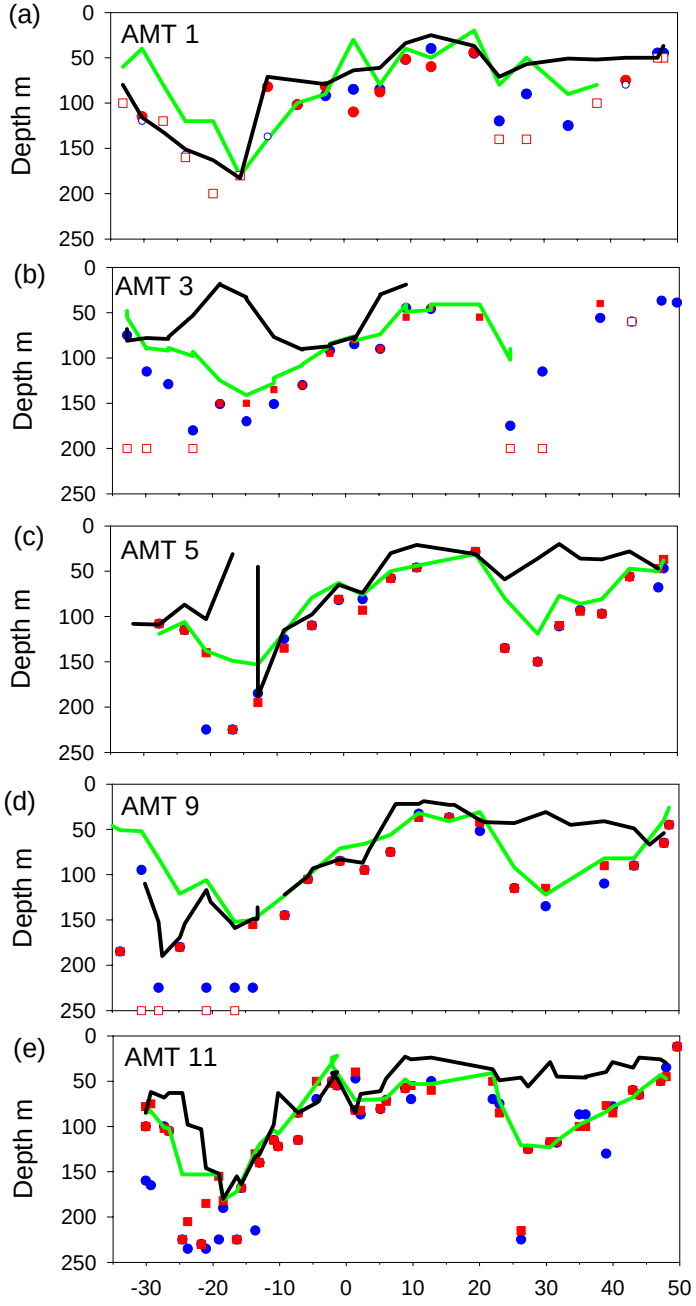

Figure 3.33. Latitudinal variation (35°S to 50°N) in the mixed layer depth (MLD; black line), deep chlorophyll maximum (DCM; green line), depth of the nitracline (Z_N; red circles) and phosphocline (Z_P; blue circles) for Spring AMT cruises; (a) AMT 2, (b) AMT 4 and (c) AMT 10. The maximum depth of the CTD cast represents profiles where Z_N and Z_P could not be diagnosed (red empty square and blue empty circle respectively). Note that the depth of the DCM for AMT 2 is to be treated with caution, as it appears constant over the tropics and subtropics.

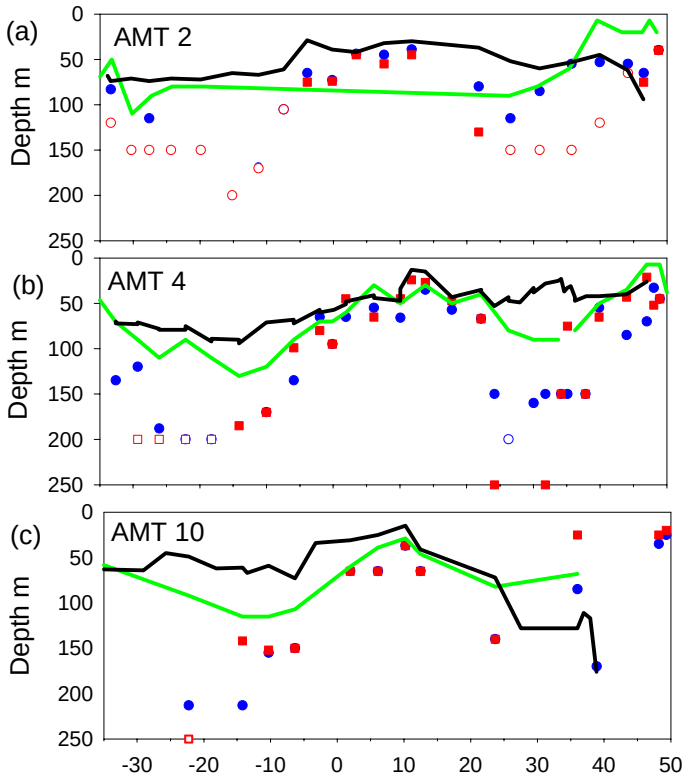

3.6.2. Relationship between Nitrate and Phosphate

3.6.2.1. Seasonality and interannual variability in Nitrate and Phosphate

The correlations between nitrate (NO_3^-) and phosphate (PO_4^{3-}) during Autumn (Figure 3.34, a; NO_3^-=13.7 (± 0.35) PO_4^{3-} – 0.36 (± 0.20), R^2=0.82, n=1280; values in brackets represent the 95% confidence interval of the slope and intercept respectively) and Spring (Figure 3.34, b; NO_3^- = 12.6 (± 0.25) PO_4^{3-} + 0.07 (± 0.16), R^2 = 0.82, n=1072) AMT cruises were highly significant (Pearson's critical correlation coefficient, n > 100, 0.195; Table C8, Ebdon, 1985) at the 95% confidence level and less than the Redfield ratio (16:1). However, the NO_3^-:PO_4^{3-} ratio during Autumn is significantly

higher than during Spring AMT's, implying an excess NO_3^- relative to PO_4^{3-} in Autumn compared to Spring. .

Figure 3.34. Relationship between nitrate (NO_3^-, μM) and phosphate (PO_4^{3-}, μM) for all AMT data collected during a) Autumn transects (NO_3^-=13.70 PO_4^{3-} –0.36, R=0.91, n=1280) and b) Spring transects (NO_3^-=12.60 PO_4^{3-} + 0.07, R=0.94, n=1072), between 35°S and 50°N in the Atlantic Ocean. The dashed line represents the Redfield ratio of 16:1. The ratio between NO_3^- and PO_4^{3-} is significant during (a) Autumn and (b) Spring (critical Pearson's correlation coefficient, R = 0.19).

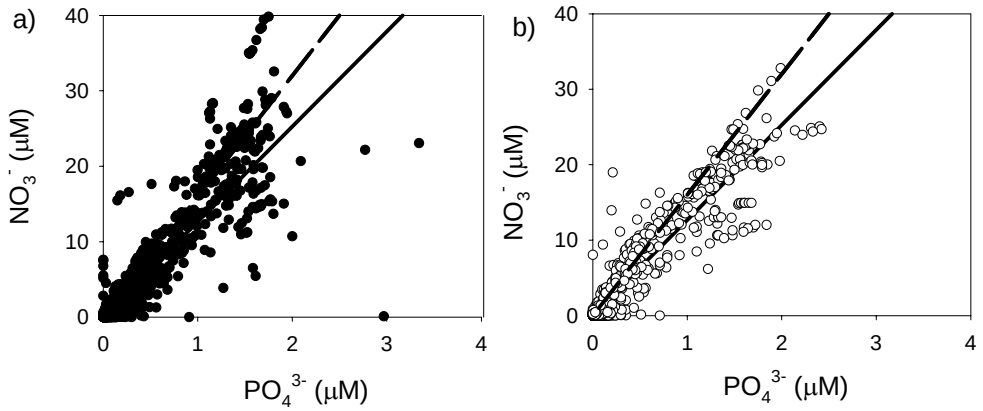

In order to determine temporal differences in the dissolved inorganic N:P ratio, the relationship between NO_3^- and PO_4^{3-} were assessed during Autumn (Figure 3.35i, a-e) and Spring (Figure 3.35ii, a-d) AMT cruises. The correlations between NO_3^- and PO_4^{3-} were significant (at the 95% confidence level) for each AMT data set, the correlation coefficients being greater than the critical value (critical correlation coefficient, 0.196, n > 100; Figure 3.35; Table A1, Miller and Miller, 1993). The N:P ratio was highest during AMT 3, 5, 11 (Autumn) and 10 (Spring) (Figure 3.35i, b, c and ii, d, respectively) and lowest during AMT 1, 9 (Autumn) and 2 (Spring) (Figure 3.35i, a and d, and ii, a, respectively). However, the N:P ratio was significantly lower than Redfield stoichiometry for all AMT data sets except AMT 3, 5 and 11 (Figure 3.36). There was no apparent trend indicating seasonal or interannual variability in the N:P ratios between AMT cruises.

Figure 3.35. Correlation between nitrate (NO_3^-) and phosphate (PO_4^{3-}) concentrations during (i) Autumn AMT's; a) AMT 1, b) AMT 3, c) AMT 5, d) AMT 9 and e) AMT 11 and (ii) Spring AMT's; (a) AMT 2, (b) AMT 4, (c) AMT 6 and (d) AMT 10. The slope, intercept and Pearson's correlation coefficient (R) for each data set are included. The dashed line represents the Redfield ratio of 16:1. The ratio between NO_3^- and $PO_4^{3-}$are significant, critical Pearson's correlation coefficient, R = 0.196, n> 100.

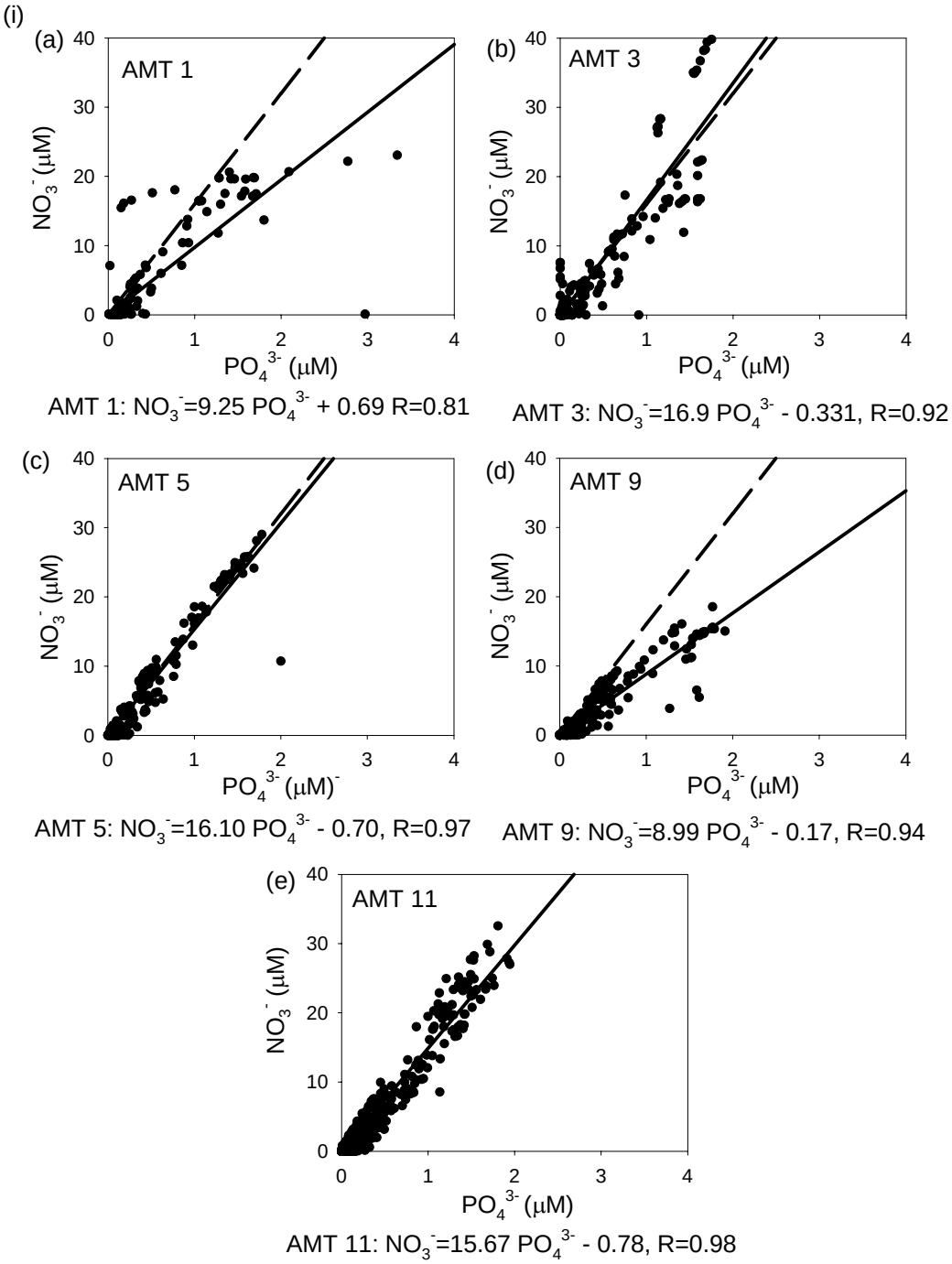

AMT 1: NO_3^-=9.25 PO_4^{3-} + 0.69 R=0.81

AMT 3: NO_3^-=16.9 PO_4^{3-} - 0.331, R=0.92

AMT 5: NO_3^-=16.10 PO_4^{3-} - 0.70, R=0.97

AMT 9: NO_3^-=8.99 PO_4^{3-} - 0.17, R=0.94

AMT 11: NO_3^-=15.67 PO_4^{3-} - 0.78, R=0.98

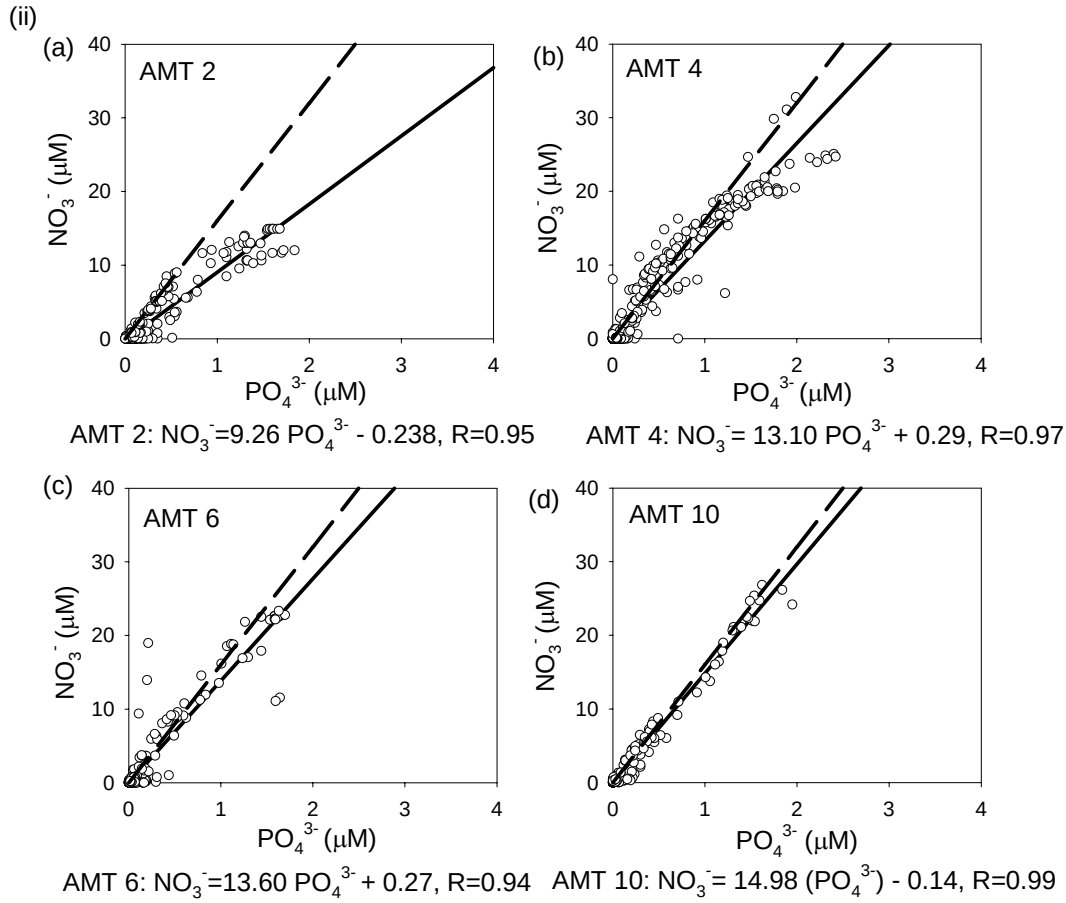

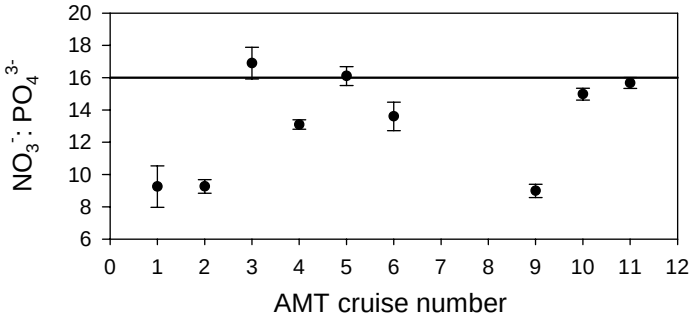

Figure 3.36. Variation in the NO_3^- : PO_4^{3-} ratio for all AMT cruises. 95 percent (%) confidence intervals and Redfield ratio (a, black line) are shown. The intercept of the correlation is forced through zero.

3.6.2.2. Spatial variability in the relationship between nitrate and phosphate

The AMT covers 85° of latitude of 14 oceanic regions (according to Hooker *et al.*, 2000), sampling in diverse oceanic regions with very different physical structure and nutrient dynamics (see section 3.3). Additionally, significant variations in the NO_3^- :PO_4^{3-} ratio are observed during Autumn and Spring AMT cruises (Figure 3.35, a and b).

Thus, plotting overall NO_3^-:PO_4^{3-} over different biogeochemical provinces and seasons may be misleading. Thus, NO_3^- and PO_4^{3-} data were broadly separated according to biogeochemical provinces defined as; (a) subpolar region (38°N to 50°N, SPR), (b) North Atlantic subtropical gyre (20°N to 38°N, NASG), (c) Equatorial and coastal upwelling region (5°S to 20°N, ER) and (d) South Atlantic subtropical gyre (35°S to 5°S, SASG; Figure 3.37 a-d).

The relationship between NO_3^- and PO_4^{3-} was significant at the 95% confidence level in all regions (Pearson's critical correlation coefficient (R) of 0.205, n > 90; Table A2, Miller and Miller, 1993). The NO_3^-:PO_4^{3-} ratio was significantly higher (95 % confidence level) during Autumn than Spring in the SPR, and significantly lower during Spring than Autumn in the ER (Figure 3.37, a and c, respectively). There was no significant difference in the NO_3^-:PO_4^{3-} ratio between Spring and Autumn AMT's in the NASG and SASG (Figure 3.37, b and c, respectively). In general, the NO_3^-:PO_4^{3-} was highest in the SPR (mean 15.68) and NASG (mean 14.44), lower in the ER (mean 13.57) and lowest in the SASG (mean 11.69). Overall, the NO_3^-:PO_4^{3-} ratio was significantly lower than Redfield stoichiometry in all oceanic regions (black circles; Figure 3.38), except during Autumn in the SPR.

Analysis at or near the detection limits of any chemical methods greatly reduces the accuracy of the result, which is amplified when determining ratios. Therefore, data at depths less than 100m were excluded (*i.e.*, to include relatively high nutrients concentrations only) and at [NO_3^-] concentrations less than 0.1 μM (*i.e.*, below the detection limits).

Figure 3.37 Correlation between NO_3^- and PO_4^{3-} in the a) Subpolar region (50°N to 38°N; SPR), b) North Atlantic subtropical gyre (38°N to 20°N; NASG), c) Equatorial region (20°N to 5°S; ER) and d) South Atlantic subtropical gyre (5°S to 35°S; SASG) during all AMT cruises. The slope, intercept and correlation coefficient (R) for each data set are included. The dashed line represents the Redfield ratio of 16:1. The intercept of the correlation is forced through zero.

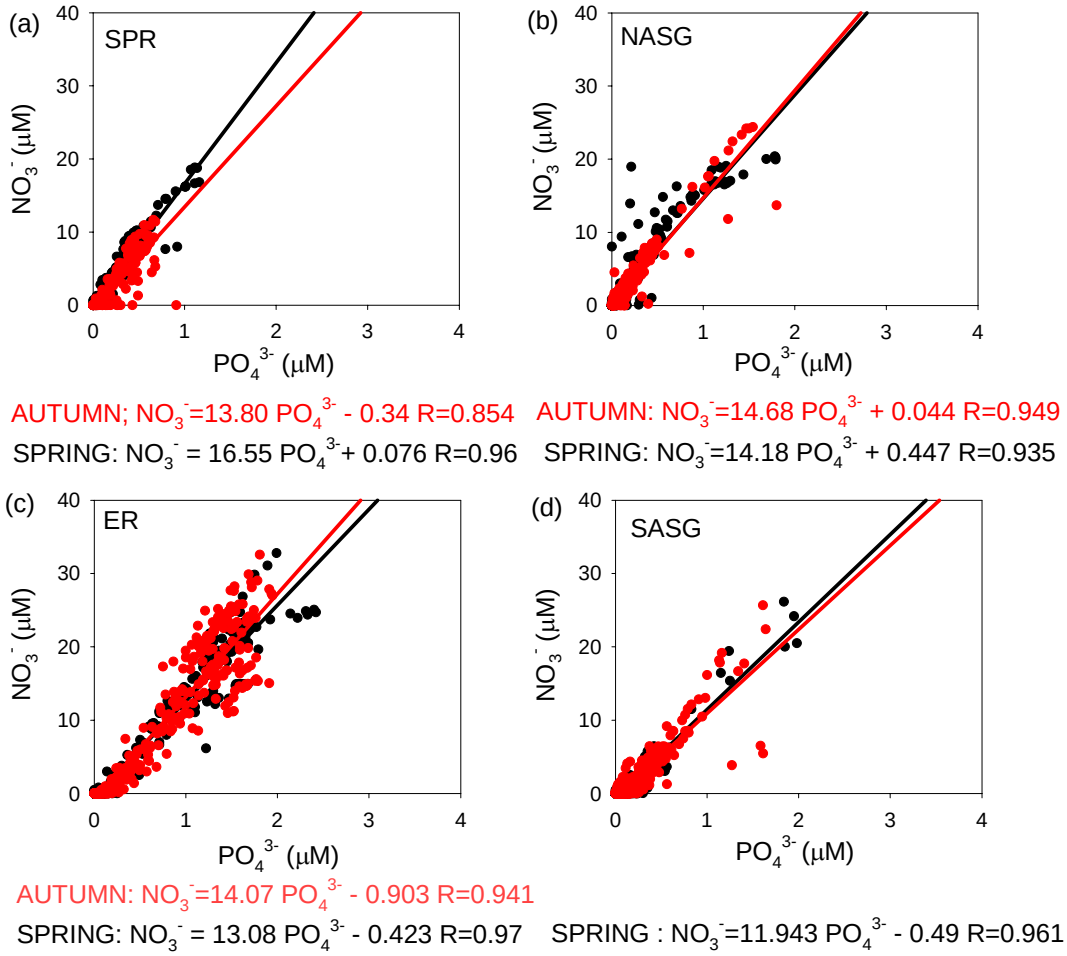

Overall, there was no significant difference (at the 95 % confidence level) in the NO_3^-:PO_4^{3-} ratio determined using all the AMT data (black circles; Figure 3.38), data collected at depths > 100m (white squares; Figure 3.38) and data in which [NO_3^-] were less than 0.1 µM (grey triangles; Figure 3.38). There was also no clear pattern in the NO_3^-:PO_4^{3-} according to the method of determination. Overall, the NO_3^-:PO_4^{3-} ratios in the SPR during Spring and Autumn AMT's, and in the NASG during autumn, were not significantly different from Redfield stoichiometry.

Figure 3.38. Variation in NO_3^-:PO_4^{3-} ratio for all AMT nutrient data (black circles), for nutrient data below 100m (white squares) and NO_3^- greater than 0.1 μM (grey triangles) in the subpolar region (SPR), north Atlantic subtropical gyre (NASG), equatorial region (ER) and south Atlantic subtropical gyre (SASG). The 95% confidence limits are shown. The intercept of the correlation is forced through zero.

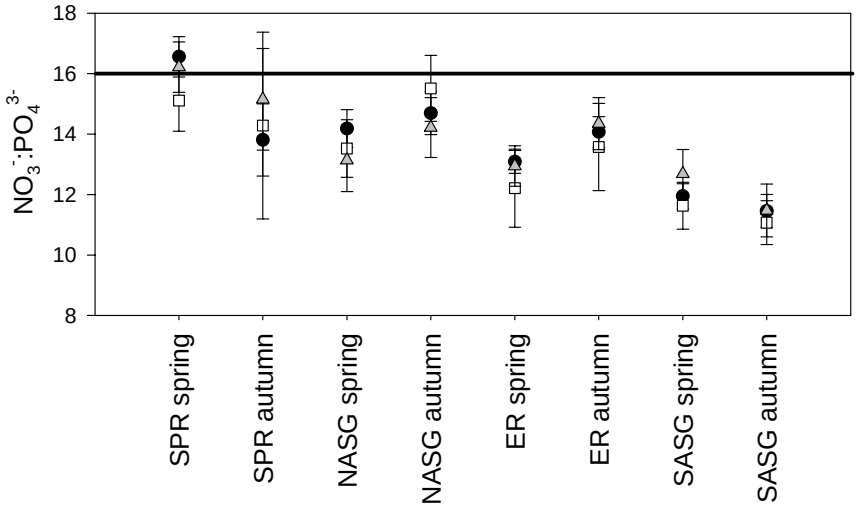

3.6.3. Assessment of N* over the Atlantic meridional transect

N* was determined using NO_3^- and PO_4^{3-} data from depths > 100m in order to determine the nutrient dynamics during remineralisation and avoid [NO_3^-] and [PO_4^{3-}] near the limits of detection in surface waters.

*3.6.3.1. Seasonal variation in N**

N* tends to be higher during autumn (grey triangles) than spring (white circles) over much of the Atlantic meridional transect (Figure 3.39). During Spring, N* is more negative, particularly around the equatorial region. Persistently elevated (>2.5μmolkg^{-1}) N* is observed over both the north Atlantic subtropical gyre and subpolar region (north of 20°N) during Spring and Autumn, but elevated over the equatorial region (5°S-10°N) during Autumn only. South of ~ 10°S, N* is relatively low (< 2.5 μmol kg^{-1}) during both spring and autumn. Overall, the range in N* at depths of > 100m is in accord with that found by Gruber and Sarmiento (1997) along a transect at 30°W in the North Atlantic.

Figure 3.39 Latitudinal variation (35°S-50°N) in N* between autumn (grey triangles) and spring (white circles) determined from AMT nutrient data at depths > 100m.

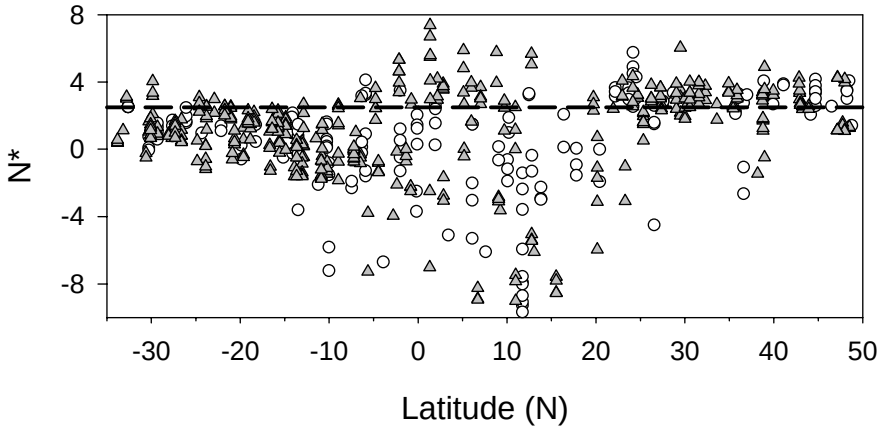

*3.6.3.2. Interannual variability in N**

During Autumn, there is little interannual variability between AMT cruises in the south Atlantic, N* generally being between – 2 and + 4 μmol kg^{-1} (Figure 3.40, a). In the equatorial and coastal upwelling region, there is large interannual variability in N* ranging from – 10 to + 8 μmol kg^{-1}, being highest during AMT 11 (black diamond; Figure 3.40, a). North of 20°N, little interannual variability was observed, N* generally being > 2.5 μmol kg^{-1}.

During Spring AMT cruises (Figure 3.40, b), a similar pattern is observed, interannual variability being low in the south Atlantic and north of 20°N, and high around the equatorial region. N* was more elevated during AMT 4 (green unfilled square; Figure 3.40, b) and 10 (black unfilled diamond; Figure 3.40, b) and relatively low during AMT 2 (red unfilled circle; Figure 3.40, b).

The latitudinal variations in N*, both seasonal and interannual, suggest that there is excess NO_3^- relative to PO_4^{3-} around the equatorial region, especially during Autumn, and in northern subtropics during Spring and Autumn.

Figure 3.40 Latitudinal variation (35°S to 50°N) in N*, defined as N*=0.87(NO_3^-- 16 PO_4^{3-}+ 2.9) μmol kg^{-1}) using nitrate (NO_3^-) and phosphate data (PO_4^{3-}) collected at depths > 100m during a) Autumn AMT and (b) Spring AMT cruises. N* at Redfield stoichiometry (2.523) is marked (black dashed line).

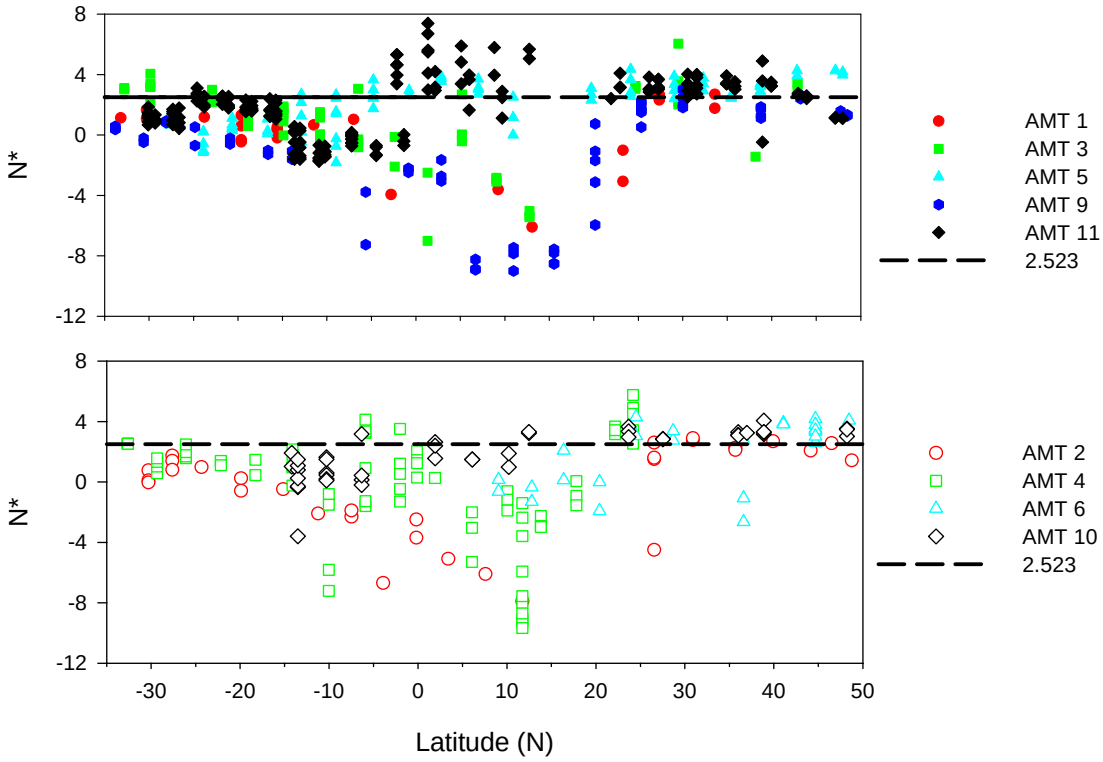

3.6.4. Organic nutrients

Numerous studies have concluded that the N: P ratio tends to be elevated in the organic nutrient pool relative to the inorganic pool, DON: DOP ratios ranging from 30 to 63 (Karl *et al.*, 1997; Vidal *et al.*, 1999; Cavender-Bares *et al.*, 2001). In this study, the relationship between DON and DOP is significant (R=0.55, n=124, critical R of 0.196 at the 95% confidence level; Figure 3.41). However, the DON: DOP ratio (13.70) observed during AMT 10 is substantially lower than found in other studies (Karl et al., 1995; Vidal *et al.*, 1999; Karl *et al.*, 1999; Cavender-Bares *et al.*, 2001). Again, considering the biogeochemical provinces sampled during the Atlantic meridional transect, the data were separated into oceanic provinces as previously defined above (Figure 3.37).

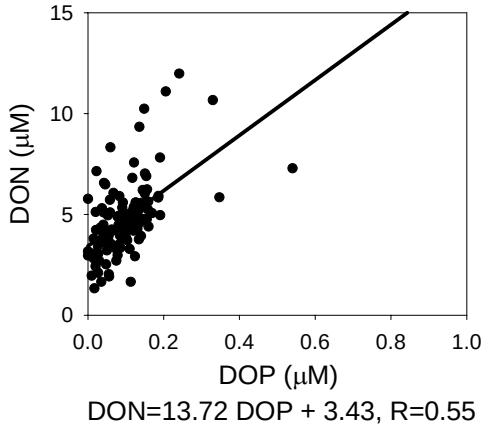

Figure 3.41. Relationship between dissolved organic nitrogen (DON, µM) and dissolved organic phosphorus (DOP, µM) observed on AMT 10 between 35°S and 50°N at all depths.

Figure 3.42. Relationship between dissolved organic nitrogen (DON, µM) and dissolved organic phosphorus (DOP, µM) in the a) subpolar region (SPR), b) north Atlantic subtropical gyre (NASG), c) equatorial region (ER; outliers circled in red) and d) south Atlantic subtropical gyre (SASG) between 35°S and 50°N in the Atlantic Ocean.

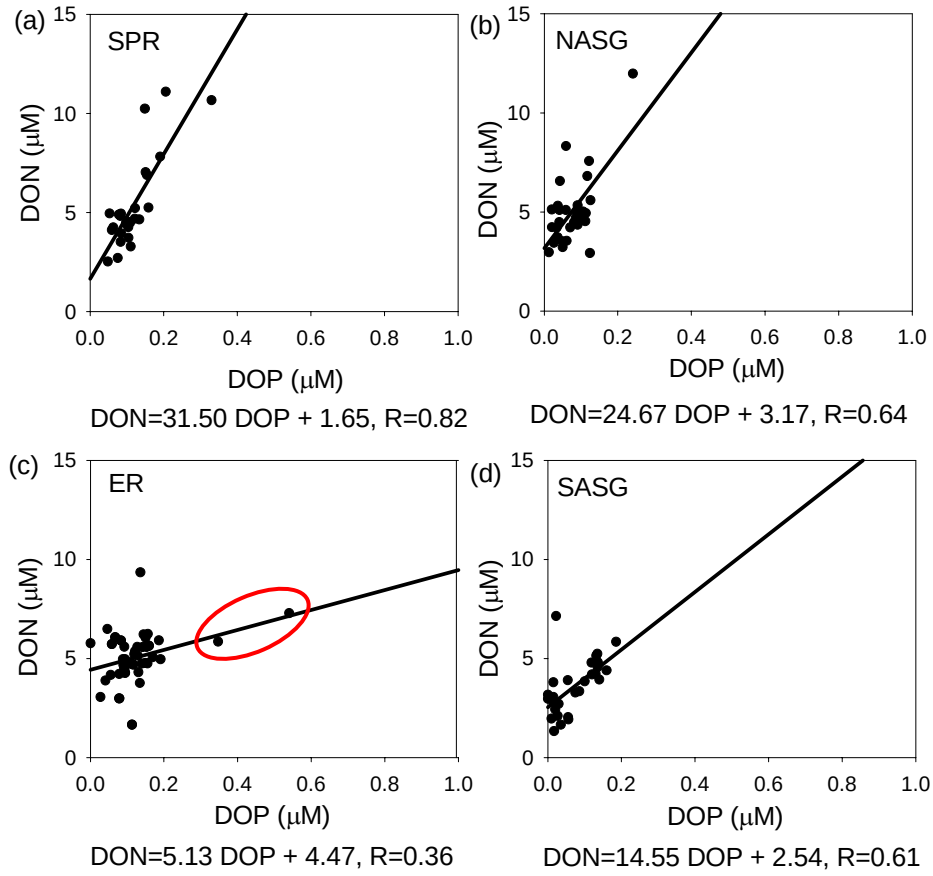

The DON:DOP ratio in the northern subpolar region (31.51; Figure 3.42, a) and subtropical region (24.67; Figure 3.42; b) is higher than the DON: DOP ratio for all data (Figure 3.41), whereas the DON:DOP ratio in the southern subtropics (14.55; Figure

3.42, d) is similar to that of all data. Although the relationship between DON and DOP in the tropics is marginally significant (R=0.36, n=40, critical value of 0.304, Table C8, Ebdon, 1994), the ratio (4.95) is unusually low (Figure 3.42, c). When outliers are removed (Fiure 3.42, c, outliers circled in red; DON=4.68 DOP + 4.59), the correlation coefficient, R, reduces to 0.02. Therefore, the data is treated with suspicion (see Appendix J for further data analysis.

3.7. Discussion and conclusions

Regional comparison of the NO_3^-:PO_4^{-3} ratio and N* reveal inconsistencies in their signals. For example, low NO_3^-:PO_4^{-3} (as diagnosed from the regression analysis) in the north Atlantic subtropical gyre (Spring, 14.18, Autumn, 14.68, mean 14.43; Figure 3.37), classically implies N-limitation. This coincides with a region where elevated N* (> 2.5 μmol kg^{-1}) implies excess N relative to P. Evaluation of the NO_3^-:PO_4^{-3} ratio determined using the individual data points (i.e. N and P at each depth in this region) and from the mean N and P concentrations (mean N and P calculated from all data in this region) reveal that the NO_3^-:PO_4^{-3} ratio determined by regression analysis is consistently lower in all oceanic regions (Table 3.3). In the north Atlantic subtropical gyre, the NO_3^-:PO_4^{-3} changes from 14.43 to 19.27, determined by individual data points, and 16.97, determined using the mean N and P concentration. This illustrates that the determination of NO_3^-:PO_4^{-3} ratios from regression analysis is misleading and simply due to the mathematical derivation of NO_3^-:PO_4^{-3} from correlation statistics which consider the best fit of the data, rather than the individual data points. Indeed, latitudinal variations in the NO_3^-:PO_4^{-3} ratio of individual data points reveals a similar pattern to N*

(Figure 3.43). Therefore, throughout this section, the NO_3^-:PO_4^{-3} ratio determined using the individual data points is discussed (Table 3.3).

Table 3.3. Evaluation of the nitrate to phosphate concentrations ([NO_3^-] and [PO_4^{-3}]), respectively, and ratios (NO_3^-: PO_4^{-3}) for each oceanic region; subpolar gyre (SPR), north Atlantic subtropical gyre (NASG), equatorial region (ER) and south Atlantic subtropical gyre (SASG), diagnosed from individual data points, and for the mean NO_3^- and PO_4^{-3} determined from the individual data points. NO_3^-: PO_4^{-3} ratios from regression analysis (Figure 3.38) and the mean NO_3^-: PO_4^{-3} for individual data points are determined. The mean [NO_3^-], mean [PO_4^{-3}], their ratio and mean N* was determined. Data collected at depths > 100m was used throughout.

REGION	INDIVIDUAL DATA POINTS		MEAN N AND P		
	Correlation NO_3^-:PO_4^{-3}*	NO_3^-:PO_4^{-3}	[NO_3^-] /[PO_4^{-3}]	NO_3^-:PO_4^{-3}	Mean N*
SPR	15.17	17.42	8.34/0.49	16.99	2.95
NASG	14.43	19.27	4.51/0.26	16.97	2.75
ER	13.56	12.03	16.05/1.21	13.24	-0.39
SASG	11.69	10.42	2.43/0.66	9.12	0.93

*average Spring and Autumn correlation

Figure 3.43. Latitudinal (35°S to 50°N) variation in the NO_3^-:PO_4^{3-} ratio, determined using data at depths greater than 100m during Autumn AMT's (white triangles) and Spring AMT's (white circles).

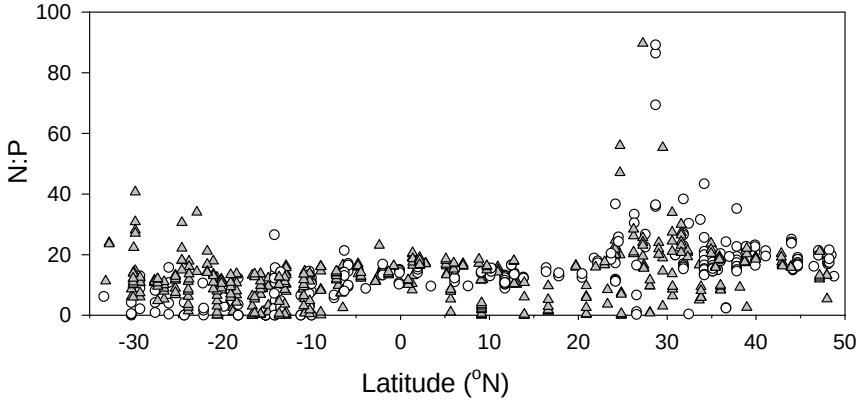

Growth of phytoplankton at Redfield stoichiometry is only achieved during maximal cell growth rates under nutrient sufficient conditions (Goldman *et al.,* 1979; Laws and Bannister, 1980). Thus, the significant deviations in the NO_3^-:PO_4^{3-} ratio from the proposed 16:1 observed throughout this study implies nutrient limitation (or energy

limitation, although not assessed in this study). This appears to vary regionally, the SASG (10.42) and ER (12.03) being more NO_3^- depleted than the SPR (17.42) and NASG (19.27; Table 3.3). Indeed, elevated NO_3^-:PO_4^{3-} ratios in the north Atlantic observed in this study, imply excess NO_3^-, suggesting that PO_4^{3-} is the limiting phytoplankton growth. Indeed, this finding is in agreement with previous observations in the west Atlantic based on PO_4^{3-} budgets, cellular carbon, nitrogen, phosphorus and iron quotas (Wu *et al.,* 2000; Sanudo-Wilhelmy *et al.,* 2001) and N* diagnostics (Gruber and Sarmiento, 1997) but in contrast to PO_4^{3-} assimilation studies (Canellas *et al.,* 2000). The NO_3^-:PO_4^{3-} ratio observed at two subtropical, open ocean time-series sites, Bermuda Atlantic Time Series (BATS; Sargasso Sea) and Hawaii Ocean Time Series (HOTS; northern subtropical Pacific), reveals P-limitation at the former (NO_3^-:PO_4^{3-}; 17.22) and N-limitation at the latter (NO_3^-:PO_4^{3-}; 14.27-15.04) (Wu *et al*., 2000). In this study, the NO_3^-:PO_4^{3-} ratio in the north Atlantic is in agreement with observations at BATS, again implying P-limitation over much of the eastern North Atlantic. In contrast, NO_3^-:PO_4^{3-} ratios in the equatorial region and south Atlantic are less than the NO_3^-:PO_4^{3-} observed at HOTS, implying N limitation over these regions of the eastern Atlantic Ocean.

In accord with the NO_3^-:PO_4^{-3} ratios, elevated N* (> 2.5 μmol kg^{-1}) north of the equator suggests an excess of NO_3^- over much of the North Atlantic (Michaels *et al*., 1996; Gruber and Sarmiento, 1997). However, the interpretation of N* has its limitations. Elevated N* represents net N_2 fixation over denitrification according to the mass balance derivation (Gruber and Sarmiento, 1997; Karl *et al.,* 2001). Thus, in a region where N_2 fixation and denitrification occur simultaneously, N* will

underestimate the extent of N_2 fixation in comparison to direct field observations. Additionally, the ratio of N to P, in the dissolved inorganic and organic pool can be altered by factors other than N_2 fixation. Preferential remineralisation of P relative to N (and C) in the particulate and dissolved organic pools tend to sequester N in DON or PON, thus decreasing the N:P ratios (Loh and Bauer, 2000; Karl *et al.*, 2001). Indeed, significant deviations from Redfield stoichiometry have been observed in the dissolved organic pool, despite N:P in the dissolved inorganic pool being close to 16:1 (Cavender-Bares *et al,* 2001). In contrast, Wu *et al.,* (2000) explain the coincidence of N_2 fixers and an elevated NO_3^-:PO_4^{3-} ratio (17.22) by the preferential conversion of inorganic nitrogen to refractory dissolved organic nitrogen through microbially-mediated recycling in the stratified surface waters of the Sargasso Sea. In addition, atmospheric inputs with elevated N:P (Herut *et al.,* 2002) may also lead to elevated N:P ratios in the dissolved inorganic pool through dissolution of atmospheric fallout.

If we are to assume that elevated N* reflects net N_2 fixation (which is particularly true in the Atlantic, in which denitrification is considered negligible (Michaels *et al.,* 1996), then the seasonal variation in N* observed in this study suggests that during Autumn AMT's, N_2 fixation is important over the equatorial region, but is not a persistent feature. In contrast, elevated N* over the northern subtropics is a persistent feature, both seasonally and interannually. Therefore, elevated N* over much of the Atlantic Meridional Transect suggests that the North Atlantic is PO_4^{3-} limited. Low N* and N:P ratios in the south Atlantic may be explained by the lack of iron inputs, thus limiting N_2 fixation, allowing the accumulation of P.

DON accumulation relative to DOP observed during AMT 10 in spring (April-May), 2000 is probably due to the drawdown of NO_3^- during phytoplankton spring production and DON exudation. Stratification would cause accumulation of DON

throughout the summer months due to slow regeneration, whereas DOP may be more rapidly recycled in the euphotic zone, thus causing a seasonal increase in the DON: DOP ratio. Redfield stoichiometry may be restored in winter, when water column mixing would cause a downward flux of DON and DOP (> 16:1) to depths and an upward flux of NO_3^-: PO_4^{3-} (~ 16:1) to the surface. (Indeed, such a seasonal accumulation and return to Redfield stoichiometry has been observed in the northern subtropical Pacific (Karl *et al.*, 2001) and at BATS (Hansell and Carlson, 2001)). However, there is not yet any DON and DOP data from an Autumn AMT cruise to test this hypothesis.

Indeed, the regions of elevated DON:DOP ratios (Figure 3.43 a and b, respectively) correspond to the region of elevated N*. This signal implies that N_2 fixation is probably the primary source of DON in this region. In contrast, the low N* observed in the south Atlantic coincides with a low DON:DOP ratio (Figure 3.43, d).

3.8. Conclusions: Nutrient distribution in the Atlantic

1. The vertical distribution of nitrate and phosphate during the AMT program is typical of tropical and subtropical regions, with nutrient depleted surface waters and concentrations increasing at depths greater than 100m. Higher surface nutrient concentrations observed in the high latitudes during Spring, and drawdown during summer, creating a nutrient depleted surface ocean in Autumn.

2. NO_3^-:PO_4^{3-} ratios in the equatorial region and south Atlantic subtropical gyre are generally lower than in the northern subtropical gyre and northern subpolar region, reflecting excess N over P over much of the North Atlantic.

3. Seasonally, N:P is higher in Autumn than Spring in the North Atlantic subtropical gyre and the equatorial region, but higher in Spring in the northern subpolar region and south Atlantic region. However, these seasonal differences are only

statistically significant (95% confidence level) over the northern subpolar region and equatorial region.

4. N* is elevated in the equatorial and coastal upwelling region during autumn AMT's only, but is persistently elevated in the north Atlantic (north of 20°N) during both spring and autumn AMT cruises. This signal implies a persistent excess of N and hence P-limitation of much of the North Atlantic.

5. Large seasonal variability in N* is observed between Spring and Autumn AMT cruises, reflecting the changing N dynamics.

6. DON: DOP ratios during AMT 10 were less than 16:1. However, large variations are observed between oceanic regions, DON: DOP being highest over the northern subpolar region (31.51) and north Atlantic subtropical gyre (24.67) and lower over the south Atlantic subtropical gyre (13.04).

3.9. Conclusions to Chapter 3.

1. Simultaneous analysis of T, S and σ_t data, and inorganic and organic nutrient concentrations from the AMT programme have shown the importance of physical forcing in controlling the distribution of biological (phytoplankton distribution in the vertical and horizontal scale) and chemical (inorganic and organic nutrients) parameters over seasonal and interannual timescales.

2. While sea surface properties (both physical, chemical and biological) are valuable in assessing basin-scale variations, they do not reflect the water column dynamics and thus should be treated with caution.

3. Throughout this chapter, the need for repetitive cruise tracks, consistent sampling regime (discrete sampling and maximum depth sampled) and methods of analysis are clearly evident

4.1. PHYSICAL STRUCTURE AND PHYTOPLANKTON BIOMASS OF THE ATLANTIC OCEAN DURING MARCH-APRIL 2000

4.1.1. Introduction

The hydrography, biomass and community structure along the "Atlantic Meridional Transect" (AMT) as determined during the long-term AMT programme have been described previously (Robins and Aiken, 1996; Zubkov *et al*., 1998; Maranon and Holligan, 1999; Aiken *et al*., 2000; Gibb *et al., 20*00; Maranon *et al*., 2000). In this Chapter, the specific conditions during a cruise transect along AMT in April-May 2000, referred to as AMT 10, are reported. Temperature and density distributions (Figure 4.1 a and b, respectively) identify the extensive downwelling zones of the South Atlantic subtropical gyre and the eastern flanks of the North Atlantic subtropical gyre, south of 5^{o}S and north of 20^{o}N, respectively. The shallowing mixed layer depth (MLD, white dashed line) defines the equatorial and coastal upwelling region from 5°S to 20°N, with deepening MLD defining the northern flanks of the northern subtropical gyre and subpolar region north of 35°S.

During AMT 10, significant variations in surface chlorophyll *a* (Chl *a*), particulate organic carbon and nitrogen concentrations ([POC] and [PON], respectively) were observed (Figure 4.2.a), indicating large variations in phytoplankton biomass. A summary of data collected from seawater and particulate samples can be found in Tables 4.1 and 4.2, respectively.

Figure 4.1. Latitudinal (35°S to 50°N) and depth (<250m) variation (a) temperature (°C) and (b) density (kg m^{-3}) during AMT 10 (12th April to 7th May, 2000) in the Atlantic Ocean. White dashed lines define the mixed layer depth (Hooker *et al.*, 2000).

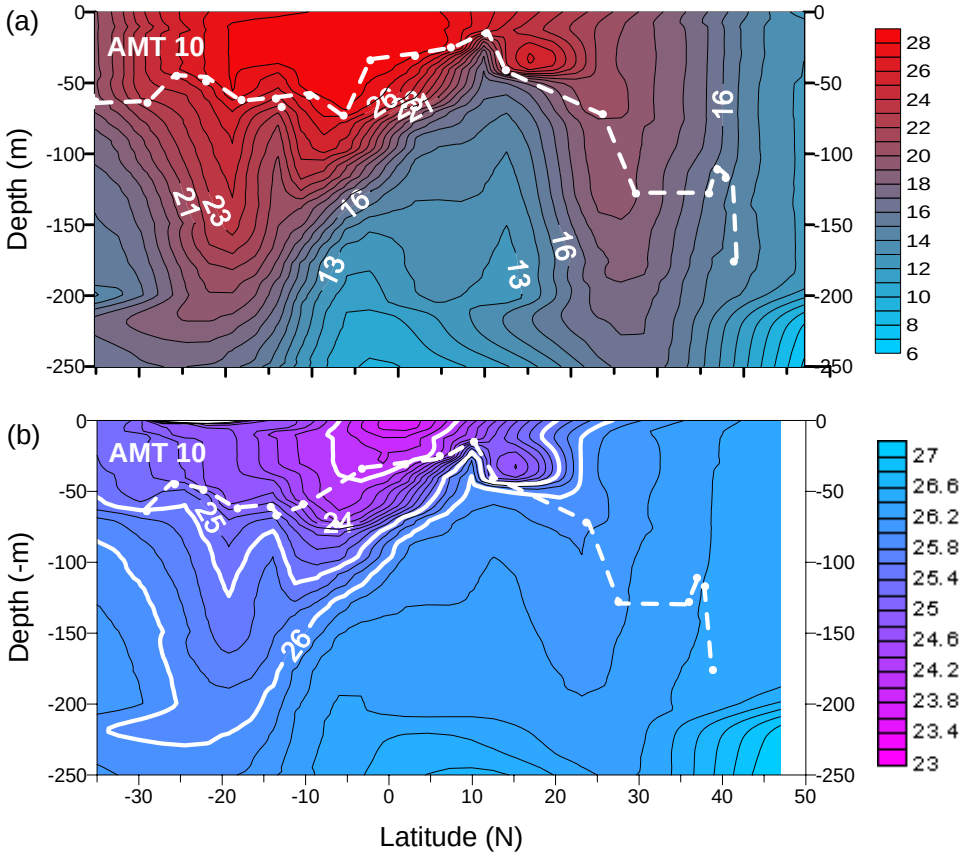

4.1.2. South Atlantic Subtropical Gyre

Slightly elevated Chl *a* (0.24 mg m^{-3}), POC (4.7 ± 0.54 to 9.60 ± 1.11μM) and PON (0.44 ± 0.05 to 0.56 ± 0.06 μM) (Figure 4.2.a) concentrations were observed at the southern flanks of the south Atlantic subtropical gyre, although the concentrations of dissolved inorganic nitrogen ($[NO_3^-]$) (0.28 ± 0.02 μM) and soluble reactive phosphate ($[PO_4^{3-}]$) (0.05 ± 0.003 μM) were relatively low (Figure 4.2 b). The remainder of the south Atlantic subtropical gyre was typically oligotrophic, $[NO_3^-]$ and $[PO_4^{3-}]$ in the mixed layer being less than 0.21 ± 0.02 μM and below detection limits (< 0.05 μM), respectively (Figure 4.2 b). [POC] (1.01 ± 0.12 to 6.91 ± 0.80 μM) and [PON] (0.10 ± 0.01 to < 0.55 ± 0.06 μM) decreased into the subtropical gyre, low Chl *a* concentrations

(< 0.11 mg m^{-3}) confirming low phytoplankton biomass in surface waters (Figure 4.2 a). A peak in Chl *a* was observed at ~ 19°S (0.19 mg m^{-3}).

Figure 4.2 Latitudinal variation (35°S to 50°N) in (a) chlorophyll *a* concentrations (mg m^{-3}; black line), particulate organic carbon (POC, white circles, μM) and particulate organic nitrogen (PON, grey squares, μM) concentrations and (b) depth averaged nitrate (NO_3^-), black squares and phosphate (PO_4^{3-}, white circles) concentrations. The 95% confidence limits are shown. NO_3^- and PO_4^{3-} are averaged above the mixed layer (see section 3.2.3; Hooker *et al.*, 2000). Vertical dotted lines broadly define the south Atlantic subtropical gyre (A), equatorial and coastal upwelling region (B), north Atlantic subtropical gyre (C) and northern subpolar region (D). Underway chlorophyll a data courtesy of Dr. Alex Poulton and Mr. Tim O'Higgins.

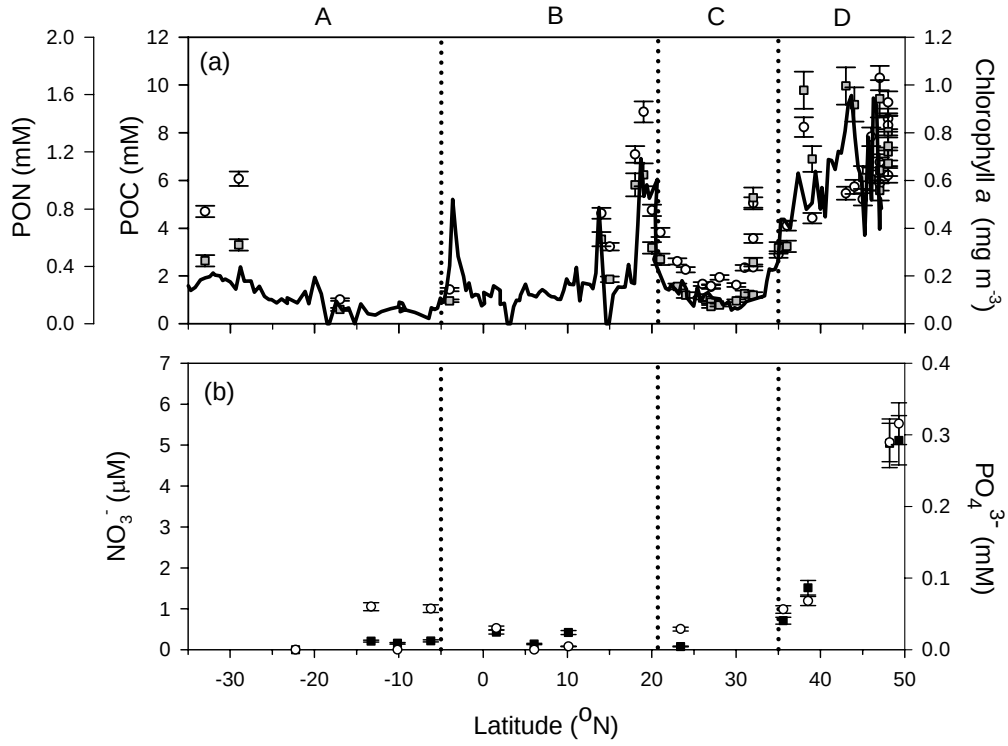

4.1.3. Equatorial Region

The equatorial region is defined by the vertical transport of nutrient rich deep ocean water to the surface. Shoaling surface seawater temperature (Figure 4.1 a) and density contours (Figure 4.1 b) between 5°S to 15°N and 17°N and 21°N are associated with the equatorial current systems and the influence of the West African coastal upwelling and the Mauritanian upwelling. However, surface chlorophyll *a* concentrations indicate that rather than a widespread increase in phytoplankton biomass in the surface ocean, the equatorial region is characterised by a series of localised

upwelling regions indicated by peaks in Chl *a* concentrations (> 0.5 mg m^{-3}), [POC] (4.62 ± 0.53 to 13.81 ± 1.60 μM) and [PON] (0.55 ± 0.06 to 1.33 ± 0.14 μM) at 3.63°N, 13.72°N, 18.69°N and 20.64°N (Figure 4.2 a). Despite low Chl *a* concentrations (0.2 mg m^{-3}) between 4°S and 13.72°N, [POC] and [PON] remain relatively high. The relatively low [NO_3^-] (0.14 ± 0.01 to 0.43 ± 0.03 μM) and [PO_4^{3-}] (< 0.05 μM) observed in the equatorial upwelling region implies rapid utilisation of NO_3^- by phytoplankton in the euphotic zone (Figure 4.2 b).

4.1.4. North Atlantic Subtropical Gyre

Phytoplankton biomass was apparently relatively low over the North Atlantic subtropical gyre, [POC] (1.94 ± 0.22 to 3.57 ± 0.41 μM, 7.14 ± 0.82 maximum, see section 4.2.1.1), [PON] (0.16 ± 0.02 to 0.43 ± 0.04 μM, 0.57 ± 0.07 μM maximum, see section 4.2.1.1) and Chl *a* concentrations (0.06 to 0.18 mg m^{-3}) were similar to or lower than those observed in the South Atlantic subtropical gyre. Adverse weather conditions permitted only one station to be sampled in the north Atlantic subtropical gyre. Surface [NO_3^-] and [PO_4^{3-}] were near detection limits (0.05 μM) (Figure 4.2.b).

Along the northern flank of the subtropical gyre (north of 35°N), increases in Chl *a* concentrations (> 0.69 mg m^{-3}), [POC] (5.04 ± 0.58 to 8.24 ± 0.95 μM) and [PON] (0.88 ± 0.09 to 1.66 ± 0.17 μM) were observed (Figure 4.2.a). Increasing [NO_3^-] and [PO_4^{3-}](1.51 ± 0.10 μM and 0.07 ± 0.004 μM, respectively) were probably responsible for the elevated phytoplankton biomass (Figure 4.2.b)

4.1.5. Northern Subpolar Region

Chl *a* concentrations (0.69 to 0.96 mg m^{-3}), [POC] (5.21 ± 0.60 to 19.05 ± 2.20 μM) and [PON] (0.93 ± 0.09 to 1.86 ± 0.19 μM) indicate the highest phytoplankton

biomass observed during AMT 10 (Figure 4.2. b). Elevated [NO_3^-] (5.04 ± 0.35 μM to 5.11 ± 0.35 μM) and [PO_4^{3-}] (0.28 ± 0.02 μM to 0.32 ± 0.02) probably fuelled primary production in this region (Figure 4.2. b).

4.2. VARIATION IN PHYTOPLANKTON SPECIES AND NUTRIENT DYNAMICS

4.2.1 Distribution of phytoplankton pigments

Determination of pigment concentrations was determined by the author at Plymouth Marine Laboratory. Absolute concentrations of pigments were deemed unreliable due to degradation or contamination of the internal standard, canthaxanthin. Nevertheless, it was assumed that the relative abundance of each pigment (per sample) was reliable and therefore, the relative contribution of each pigment to total pigments (expressed as percentage) was calculated (Table 4.3; see Table 2.7 for pigment abbreviations). Accessory pigments provided chemotaxonomic information on the range of phytoplankton groups that define the community structure (Jeffrey *et al.*, 1997; Gibb *et al.*, 2000). In addition, three chemotaxonomic marker pigment groups (Gibb *et al.*, 2000) were used to determine the dominant group in the water column, the relative abundance of each group being determined as (Figure 4.3):

[Fuc + Per]: large eukaryotes, i.e. diatoms and dinoflagellates

[But + Hex + Chl *b*]: eukaryotic nanoflagellates, i.e. chrysophytes, prymnesiophytes and chlorophytes

[Zea + dv Chl *a*]: prokaryotic picoplankton, i.e. cyanobacteria and prochlorophytes

(See Table 2.7 for pigment abbreviations)

Table 4.3. Pigment distribution, expressed as the percentage pigment to total pigments (1 decimal place) for particulate samples collected from 7m depth during AMT 10 from 10°S to 48°N during April/May 2000. See Table 2.10 for pigment abbreviations.

PIGMENT	10°S	7°S	19°N	26°N	30°N	35°N	38°N	45°N	48°N
T Chl a	50.3	34.3	47.0	54.5	51.3	52.7	47.0	44.3	52.3
Chl a	39.7	30.3	37.7	36.7	47.2	50.8	44.7	41.9	46.6
Dv Chl a	10.6	4.3	9.3	17.8	4.1	1.9	2.3	2.4	5.7
Chl b	0.0	0.0	5.7	0.0	0.0	1.9	4.3	5.3	3.4
Dv Chl b	0.0	0.9	1.9	0.0	0.0	0.0	1.1	2.1	1.4
Chl c3	0.7	0.7	1.5	2.8	2.7	2.5	2.5	1.9	0.0
Chl c1 c2	1.9	3.8	5.5	5.0	5.8	9.2	7.9	7.8	8.8
Allo	0.0	1.7	1.7	0.4	0.0	2.1	2.3	3.4	4.3
But	0.8	2.1	3.4	2.3	3.5	2.3	5.7	4.1	2.9
Car	4.1	4.7	3.9	4.4	2.8	1.8	1.0	1.5	1.4
Diato	0.3	1.0	0.6	0.2	0.0	1.5	1.4	0.4	0.2
Diadino	3.1	3.5	1.5	1.9	2.2	3.2	2.6	2.4	1.6
Fuc	2.4	4.4	4.3	2.7	1.9	13.9	7.4	8.1	8.8
Hex	6.2	11.3	7.9	7.5	8.4	5.7	13.3	11.9	9.4
Lut	0.0	0.0	0.0	0.0	0.0	0.1	0.2	0.2	0.2
Per	1.9	2.4	1.5	1.8	2.3	0.6	1.2	3.3	4.2
Viola	0.4	1.3	0.5	0.2	0.4	0.2	0.6	0.8	0.3
Zea	27.9	27.6	13.1	16.1	18.6	3.4	1.6	2.5	0.8

Chl *a* was the most abundant pigment over the AMT 10 transect, comprising 30.3 to 50.8 % of the total pigment distribution (Table 4.3). In the south Atlantic subtropical gyre (10°S), Zea (27.9 %), dv Chl *a* (10.6 %) and Hex (6.2 %) are the dominant pigments. [Zea + Dv Chl *a*] dominated the chemotaxonomic groups (Figure 4.3), indicating that prokaryotic picoplankton, i.e. cyanobacteria and prochlorophytes, dominated the surface phytoplankton community.

Just south of the equatorial upwelling region (7°S), Zea (27.6 %), Hex (11.3 %) and Car (4.7 %) were the most abundant pigments (Table 4.3). Again, prokaryotic

picoplankton were the most abundant phytoplankton in surface waters, indicated by dominance of [Zea + dv Chl *a*] (Figure 4.3), although the contribution from Hex indicated a substantial prymnesiophyte contribution to the phytoplankton community.

Figure 4.3. Latitudinal variation (35°S to 50°N) in chemotaxonomic pigment biomarkers for identification of the dominant phytoplankton community in the surface ocean (7m) during AMT 10. Groups identified are prokaryotic picoplankton (Zea and dv chl *a*; white squares, black lines), eukaryotic nanoflagellates (But + Hex + Chl *b*; grey triangle, dotted line) and large eukaryotes (Fuc + Per; black circles, dashed line)

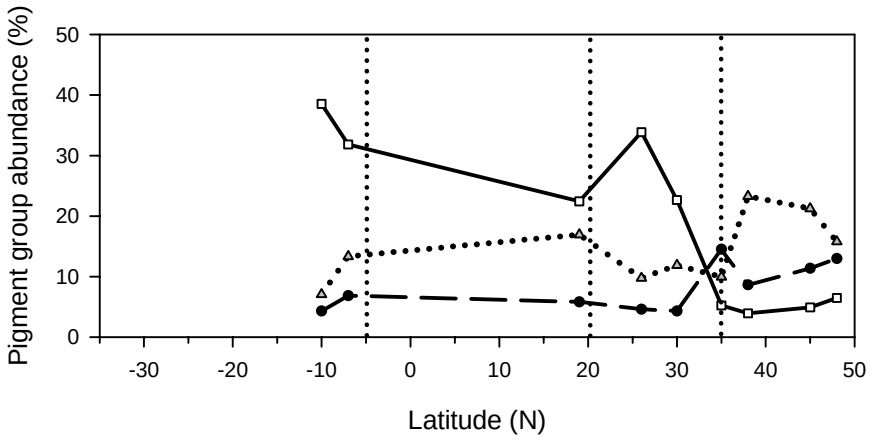

At the northern edge of the coastal and equatorial upwelling region (19°N), [Zea + dv Chl *a*] dominated the phytopigments (Table 4.3), although [But + Hex + Chl *b*] was also relatively high (Figure 4.3), indicating the importance of both prokaryotic picoplankton and prymnesiophytes in this region.

At the northern subtropical gyre (26°N and 30°N), the pigment distributions varied between the two sites sampled (26°N, dv Chl a (17.8 %), Zea (16.1 %), Hex (7.5 %); 30°N, Zea (18.6 %), Hex (8.4 %), Chl *c1 c2* (5.8 %); Table 4.3). However, cyanobacteria and prochlorophytes dominated the surface phytoplankton community at both sites (Figure 4.3). The relatively high abundance of Hex and Chl *c1 c2* indicates a contribution from eukaryotic nanoflagellates to the surface phytoplankton community.

At the northern flanks of the North Atlantic subtropical gyre (35°N and 38°N), Fuc (13.9 % and 7.4 %, respectively), Chl *c1 c2* (9.2 % and 7.9 %, respectively) and

Hex (5.7 % and 13.3 %, respectively) were the most abundant pigments (Table 4.3). However, there were differences at the two sites; at 35°N, high [Fuc + Per] indicated the dominance of large eukaryotes, *i.e.* diatoms and dinoflagellates whereas at 38°N, high [But + Hex + Chl *b*] indicated that surface waters were dominated by eukaryotic nanoflagellates, *i.e.* chrysophytes, prymnesiophytes and chlorophytes (Figure 4.3)

In the northern subpolar region (45°N and 48°N), Hex (11.9 % and 9.4 %, respectively), Fuc (8.1 % and 8.8 %, respectively), Chl *c1 c2* (7.8 % and 8.8 %, respectively) and Chl *b* (at 45°N only; 5.3 %) were the most abundant pigments (Table 4.3). The high [But + Hex + Chl *b*] at these sites reflects the presence of significant contribution of eukaryotic nanoflagellates to the surface phytoplankton community (Figure 4.3).

The data presented above was compared to pigment data determined and interpreted by Dr. Victoria Hill (Southampton Institute of Oceanography) and Dr. Alex Poulton (Southampton Oceanography Centre). Overall, our interpretation of the dominant phytoplankton groups in the surface ocean agreed well between the two independent data sets, despite the methods of sample collection being completely independent (underway non-toxic seawater supply vs. discrete water samples from Niskin bottles). Unfortunately, the absolute pigment concentrations were not comparable (data not shown), probably due to the degradation of the internal standard during analysis by the author.

4.2.2. Latitudinal variation in DOC and DON: High Temperature Catalytic Oxidation (HTCO)

Seawater samples (ampoules, preserved with orthophosphoric acid) from 4 stations (AMT 10-10, -11, -12, -13) were analysed using the HTCO technique and depth

profiles constructed for DOC (Figure 4.4.a) and DON (Figure 4.4.b). Surface [DOC] (489 – 3632 μM) were extremely high for an open ocean environment (60 – 90 μM; see review by Benner, 2002), and depth profiles were incomparable to other studies (Sharp *et al.,* 2002), which show maximal [DOC] in the surface ocean, decreasing with depth. [DON] did not resemble concentrations determined by UV oxidation (UV = 1.017 HTCO + 14.706, R^2 = 0.0262, data not shown) and again, [DON] in the surface ocean (2.5 – 37 μM) were much higher than in other studies (3.5 to 7.5μM; see review by Benner, 2002). Although depth profiles in DON resembled those of other studies (Koike and Tupas, 1993; Hansell *et al.,* 1993), that is, maximum concentrations in the surface ocean with decreasing [DON] with depth, the large degree of variation with depth and the [DON] were suspect. Therefore, analyses of ampouled seawater samples for DOC and DON were abandoned.

Collection of seawater samples from open ocean environments for DOC and DON analysis is prone to contamination. The unclean ship environment and the lack of adequate cleaning facilities on-board (e.g. high temperature oven) introduce the risk of contamination of samples, as observed in this study.

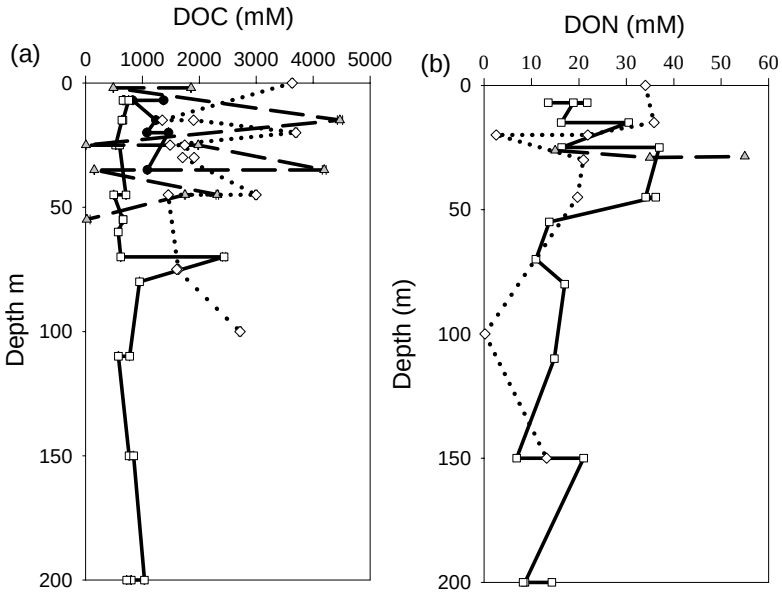

Figure 4.4. Depth variation (< 200m) in (a) dissolved organic carbon (DOC; μM) and (b) dissolved organic nitrogen (DON; μM) determined by high temperature catalytic oxidation for samples collected during AMT 10 (April-May, 2000) at stations 10 (black circle), 11 (white square), 12 (grey triangle) and 13(white diamond).

4.2.3. Comparison between DON concentrations analysed by UV oxidation and the HTCO technique

Surface seawater samples (amber bottles, stored at -20°C) were analysed by UV oxidation and by HTCO to determine [DON] ([DON_{UV}] and [DON_{HTCO}], respectively) and to compare the efficiency and reliability of the techniques. The relationship between [DON_{UV}] and [DON_{HTCO}] (DON_{HTCO} = 0.102 DON_{UV} + 4.04, R = 0.1, data not shown) was not significant (95 % confidence level). [DON_{HTCO}] were usually lower than [DON_{UV}]. It was impossible to know which method is more accurate in this case as reference materials (see section 2.3.3.2) were not analysed by both methods. Bacterial degradation and mishandling of samples may be responsible for the large variation of [DON]. For the purpose of this study, [DON_{UV}] was assumed more reliable as concentrations were comparable to surface [DON] concentrations analysed by nitrate determination and UV oxidation at Southampton Oceanography Centre (Dr. Richard Sanders, personal communication).

Recent international inter-calibration exercises (Sharp *et al.*, 2002) for DOC and DON, and comprehensive investigations into the methods for determination of DON (Bronk *et al.*, 2000) have revealed that despite the mechanical difficulties in operating the instrument used for high temperature oxidation and expense its it daily maintenance, it is the most precise and accurate method for the determination of oceanic DOC and DON. In agreement, the author would recommend the HTCO technique over UV oxidation as the preferred method, due to the consistent oxidation efficiency, detection limits, sample throughput and ability to simultaneously determine DON and DON.

4.2.4. Vertical and horizontal distribution of DON and DOP: UV oxidation

Overall, [DON] and [DOP] ranged from 1.33 ± 0.07 (mean ± error; 3 significant figures) to 11.97 ± 0.83 μM and 0.001 ± 7.50 × 10^{-5} μM to 0.54 ± 0.04 μM, respectively

along the AMT 10 transect (Figure 4.5 a and b, respectively). Both [DON] and [DOP] tended to be elevated in surface waters and decline with depth (Figure 4.5 a and b). Maximum [DON] were observed in the subsurface (15 to 25m and 65 to 75m) equatorial upwelling region (1.94°N, 9.34 ± 0.65 μM; 6.10°N, 7.28 ± 0.50 μM, respectively) and in the North Atlantic subtropical gyre (36°N, 11.97 ± 0.83 μM). Maximum [DOP] were also observed in the equatorial upwelling region (1.94°N, 0.54 ± 0.04 μM at 75m), in the south Atlantic subtropical gyre (14.18 °S, 0.35 ± 0.03 μM at 30m) and in the North Atlantic subtropical gyre (36°N, 0.24 ± 0.02 μM). The maxima [DON] and [DOP] do not always coincide (See appendix J for reassessment of the AMT 10 DON and DOP data).

The MLD was assessed in section 3.2.3 of chapter 3 and superimposed onto Figure 4.5, a and b (white and black dashed lines, respectively). The mixed layer should represent a layer in the surface ocean where biological and chemical properties are homogenous. However, the [DON] and [DOP] were not vertically or horizontally homogenous in the MLD. Examination of DON and DOP data published by Duarte *et al.,* (1999) also reveals a heterogeneous distribution in the surface layer (data not shown), despite using alternative methods of organic nutrient analysis. It is possible that fine scale processes may be producing DON or DOP, or indeed using them, although the timescale of this exudation or utilisation is probably less than the time required to mix the water column. However, since no rates of DON or DOP uptake or release were assessed in this study, the actual cause of such variation in the water column remains unknown.

Figure 4.5. Latitudinal (35°S-50°N) and depth (250m) variation in concentrations of (a) dissolved organic nitrogen (DON, μM) and (b) dissolved organic phosphorus (DOP, μM). Black circles indicate the depth of sampling. White dashed line represents the mixed layer depth (Hooker *et al.*, 2000). Note that data exists at 35.09°S and therefore the contours south of 25°S reflect the data at 35.09°S.

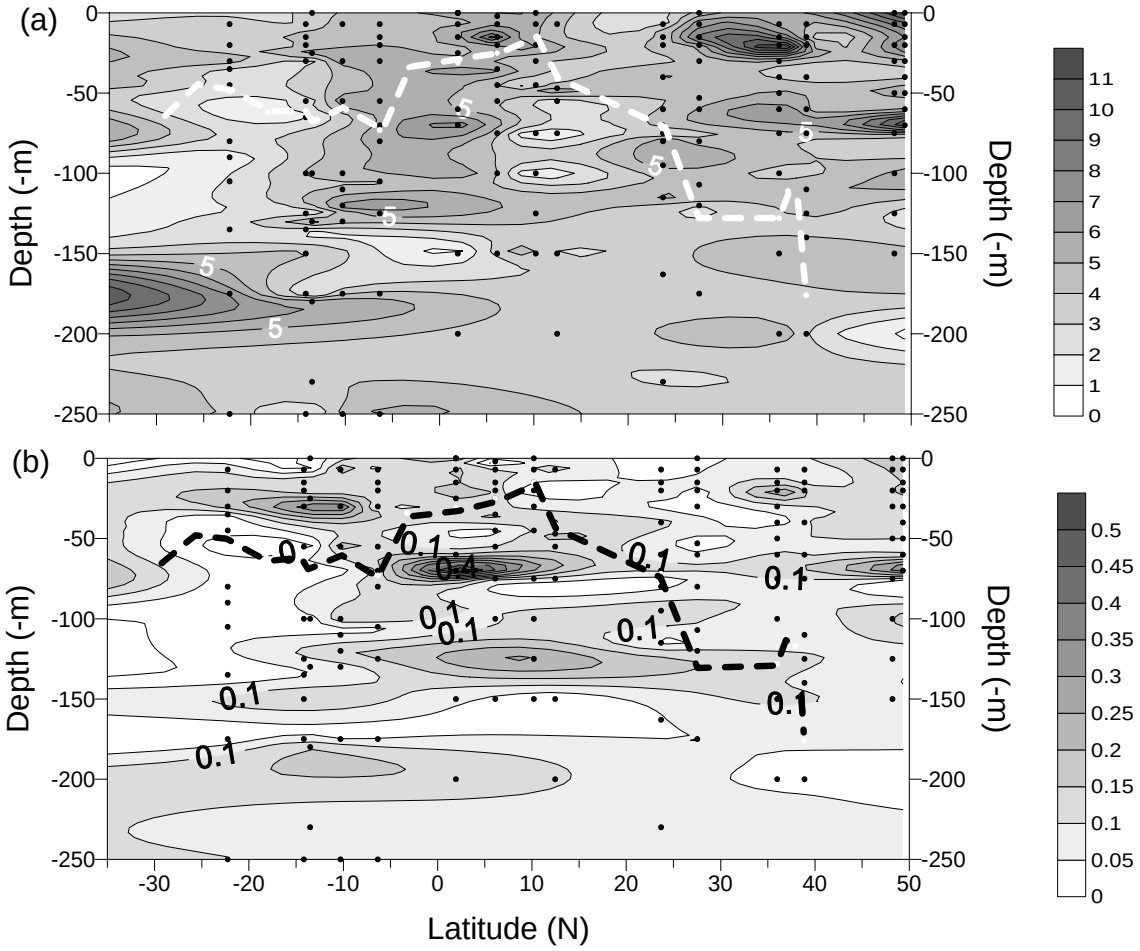

[DON] and [DOP] concentrations were depth averaged above the mixed layer depth (MLD) as defined by Hooker *et al.*, (2000) (Figure 4.6 a and b). Relatively high [DON] and [DOP] were observed at the southern (4.69 ± 0.31 μM and 0.11 ± 0.02 μM, respectively) and northern flanks (5.01 ± 0.33 to 5.48 ± 0.36 μM and 0.27 ± 0.02 to 0.43 ± 0.04 μM, respectively) of the south Atlantic subtropical gyre (Figure 4.6 a and b). [DON] and [DOP] both decreased into the centre of the gyre (3.32 ± 0.21 μM and 0.07 ± 0.01 μM, respectively) (Figure 4.6 a and b). DON accounted for 94 to 100 % of the

TDN pool whereas DOP was 67 to 100% of the TDP pool (Figure 4.7.a). The DON: DOP ratio increased from the southern (32) and northern (20) flanks into the centre of the gyre (45), with an exception at 6^{o}S, where the DON: DOP ratio increases to 43 (Figure 4.7.b).

Figure 4.6. Latitudinal variation (35°S-50°N) in (a) nitrate (NO_3^-, μM; white squares) and dissolved organic nitrogen (DON, μM; black squares) and (b) phosphate (PO_4^{3-}, μM; white circles) and dissolved organic phosphorus (DOP, μM) averaged above the mixed layer depth (Hooker *et al.*, 2000) during AMT 10.

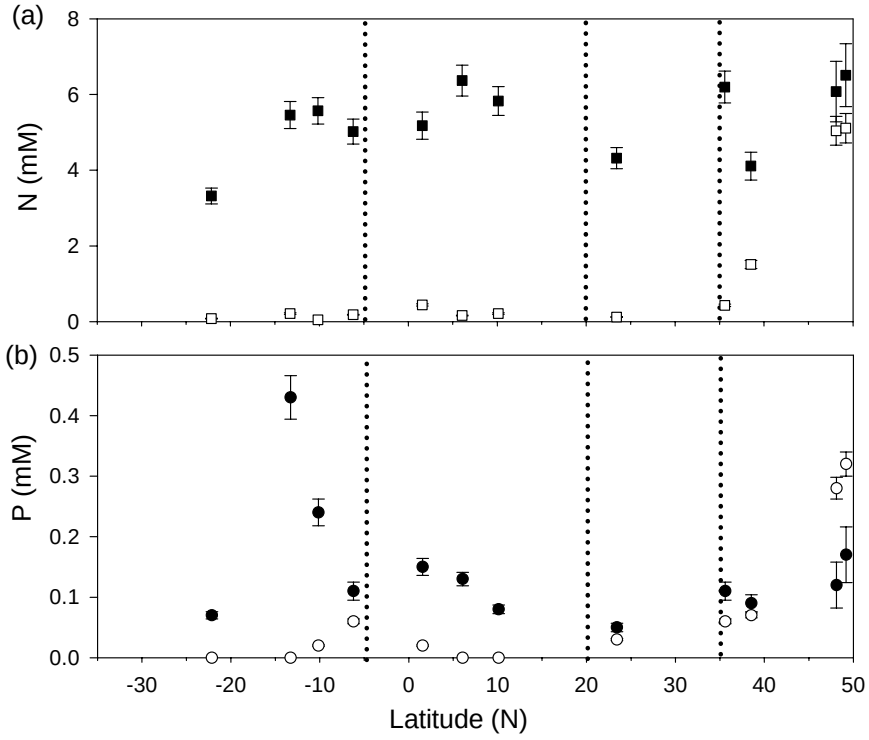

In the equatorial and coastal upwelling region, [DON] increased slightly northwards (1.56^{o} to 10.52^{o} N) from 5.39 ± 0.37 μM to 5.83 ± 0.38 μM. [DOP] decreased from 0.14 ± 0.02 μM to 0.07 ± 0.01 μM (Figure 4.6 a and b). Overall, DON accounted for 92 to 98 % of the TDN pool and DOP accounted for 83 to 100 % of the TDP pool (Figure 4.7 a). The DON: DOP ratio increased northwards from 38 to 84 (Figure 4.7.a). [DON] increased by only 18% in this region, whereas [DOP] decreased by 50%, possibly indicating a local source for DON but a sink for DOP.

Figure 4.7 Latitudinal variation (35°S to 50°N) in (a) contribution of dissolved organic nitrogen to total dissolved nitrogen (DON/TDN, %: black triangles) and contribution of dissolved organic phosphorus to total dissolved phosphorus (DOP/TDP, %; white triangle) and (b) DON:DOP ratio. DON, DOP, TDN and TDP are depth averaged above the mixed layer depth (Hooker *et al.,* 2000).

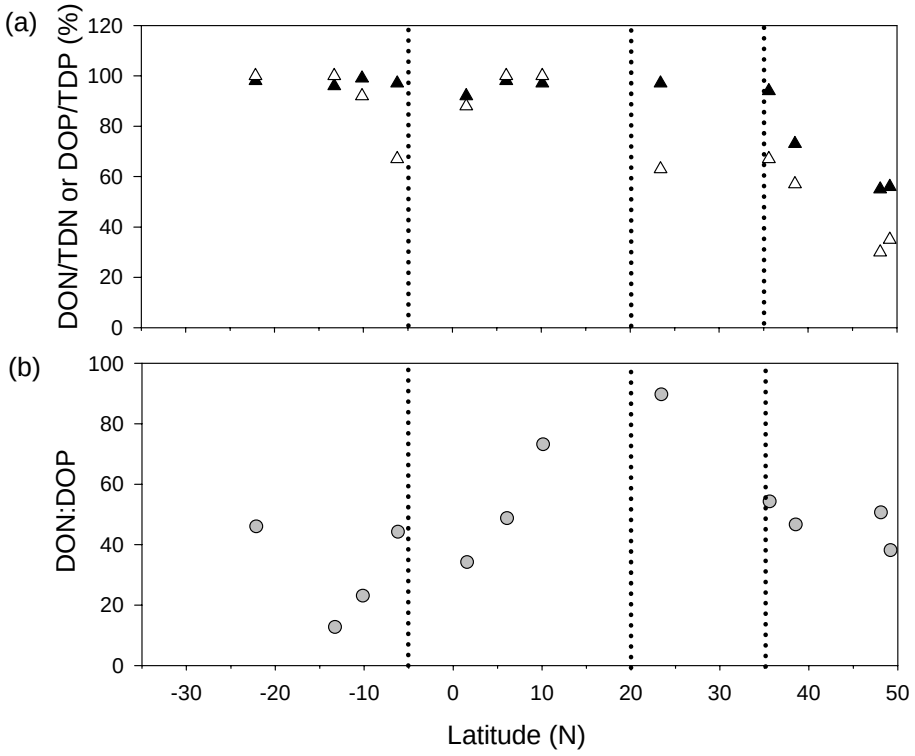

Unfortunately, the north Atlantic subtropical gyre was under-sampled due to severe weather conditions. [DON] and [DOP] (4.32 ± 0.28 μM and 0.05 ± 0.01 μM, respectively) were lower than in the surrounding regions (Figure 4.6 a and b). An increase in the DON: DOP ratio compared to the equatorial and coastal upwelling region and subpolar region is attributed to a significant decrease in [DOP] in the subtropical gyre, as no significant increase in DON was observed. DON and DOP were 89 % and 61 % of the TDN and TDP pools, respectively (Figure 4.7 a). The highest DON: DOP ratio (86) on the AMT-10 transect was observed in this region (Figure 4.7 b).

In the Subpolar region, [DON] and [DOP] ranged from 4.11 ± 0.37 to 6.51 ± 0.83 μM and 0.09 ± 0.014 to 0.17 ± 0.05 μM, respectively (Figure 4.6 a and b). Again, a greater than two-fold northward increase in [DOP] was observed in contrast to a 37 %

change in [DON]. Overall, DON accounted for 55 to 73% of the TDN pool whereas DOP accounted for 30 to 57 % of the TDP pool (Figure 4.7 a). There is a northwards decrease in DON: DOP ratio from 56 to 38 (Figure 4.7 b).

DON and DOP usually dominated (> 50%) the TDN and TDP pools in near surface waters (< 80 m) (Figure 4.8 a and b). With increasing depth, $NO_3^-$and PO_4^{3-} became more important. In contrast, DON and DOP constituted less than 50% of the TDN and TDP pools at depth (> 80m) in the equatorial and coastal upwelling region (Figure 4.8 a and b).

Figure 4.8 Latitudinal (35°S to 50°N) and depth (< 250m) variation in (a) percentage contribution of dissolved organic nitrogen to total dissolved nitrogen (DON/TDN) and (b) percentage contribution of dissolved organic phosphorus to total dissolved phosphorus (DOP/TDP).

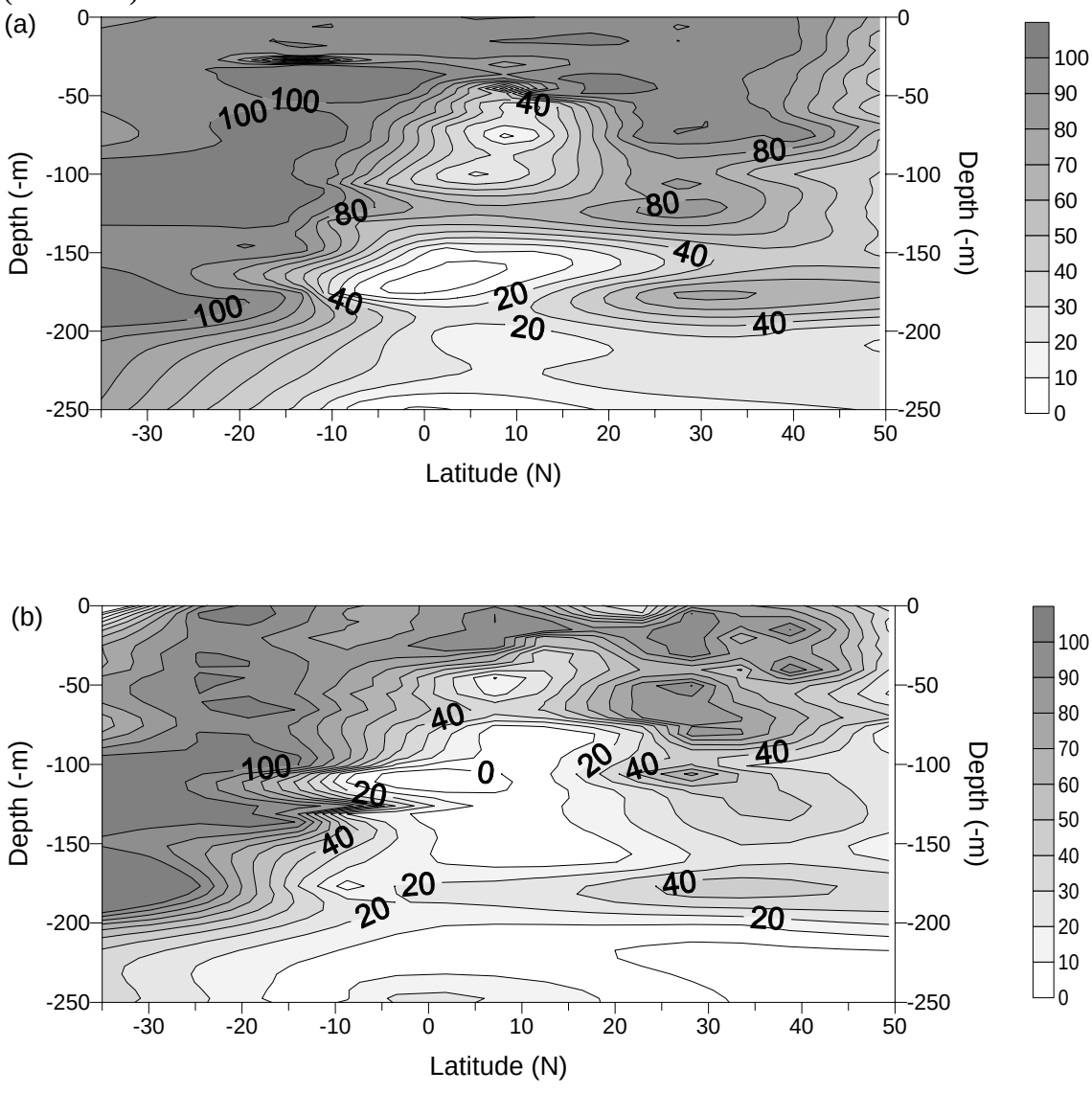

One CTD cast was deployed to 1000 m (AMT 10-7 at 13.51°S, 32.33°W). Depth profiles of [TDN] and [NO_3^-] and [TDP] and [PO_4^{3-}] are shown in Figure 4.9 a and b, respectively, the difference (TDN- NO_3^- and TDP- PO_4^{3-}) representing the [DON] and [DOP], respectively. TDN, NO_3^-, TDP and PO_4^{3-} increase significantly below 180m. [DON] were relatively high in the surface waters (< 180 m; 5.11 ± 0.30 μM to 6.97 ± 0.48 μM, mean ± 1 stdev, 5.58 ± 0.96, n=4) and decreased with depth (> 500 m; 1.96 ± 0.14 μM to 2.32 ± 0.16 μM, mean 2.15 μM, n=2) (Figure 4.9.a). In contrast, [DOP] were relatively high in surface waters (< 180 m; 0.01 ± 0.0005 μM to 0.37 ± 0.03 μM, 0.15 ± 0.15, n=4) but negligible at depth (>500 m; < 0.02 ± 0.001 μM) (Figure 4.9.b). Residual [DON] and [DOP] in surface waters (surface [DON] minus deep [DON], surface [DOP] minus deep [DOP], respectively) were 2.96 to 4.83 μM and 0.02 to 0.35 μM, respectively.

Figure 4.9. Depth variation (< 1000 m) in (a) nitrate (NO_3^-; black circles, dashed line) and total dissolved nitrogen (TDN; white circles, solid line) and (b) phosphate (PO_4^{3-}; black triangles, dashed line) and total dissolved phosphorus (TDP; white triangles, solid line) at station 7 (13.51°S, 32.33°W) during AMT 10 transect in the Atlantic Ocean. Error bars represent ± 1 coefficient of variation (CV).

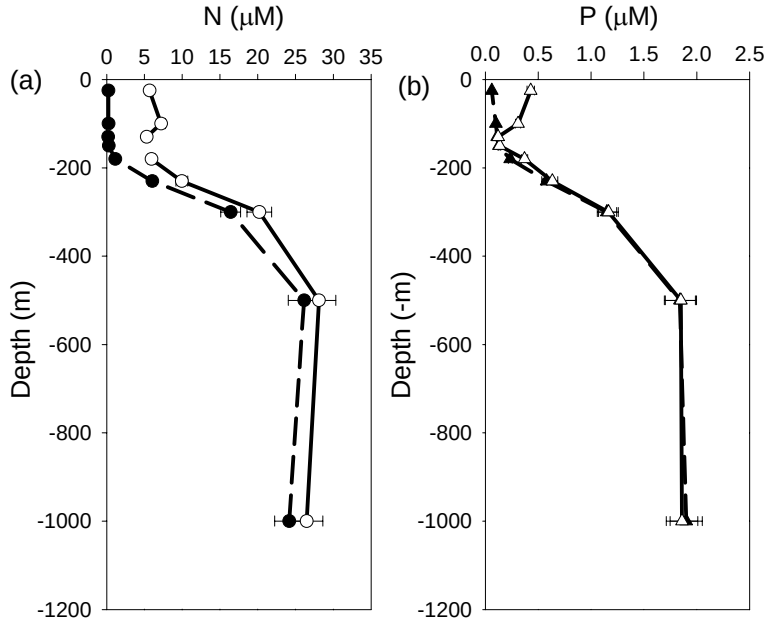

4.2.5. Latitudinal variation in dissolved free and total hydrolysable amino acids in the North Atlantic subtropical gyre

Dissolved free amino acid concentrations ([DFAA]), determined by the fluorimetric technique (Parsons *et al.*, 1984), ranged from 0.05 ± 0.01 to 0.34 ± 0.01 μM (Figure 4.10, a). [DFAA] were slightly elevated in the equatorial and coastal upwelling region off West Africa (0.16 to 0.34 μM between 6°S and 10°N), but relatively low (< 0.14 μM) over the remainder of the AMT 10 transect.

[DFAA] were converted to N using alanine (15.73% N) as a conversion factor (Cowie and Hedges, 1992) and found to range from 0.007 ± 0.001 to 0.054 ± 0.002 μM N. DFAA represented 0.15 to 0.57 % of the total DON_{UV} pool (Figure 4.10, b).

Total acid hydrolysable amino acid concentrations (THAA), determined by chromatographic techniques (Cowie and Hedges, 1992), ranged from 0.30 ± 0.05 μM to 1.28 ± 0.05 μM (Figure 4.10, a). High [THAA] (1.28 ± 0.05 μM) were observed in the subpolar region during AMT 10, otherwise [THAA] were relatively low (<0.46 μM) and uniform over the remainder of the transect.

[THAA] were re-calculated based on the percentage N content of each amino acid and ranged from 0.39 ± 0.06 μM N to 1.44 ± 0.09 μM N. THAA represented 3.63 to 9.86 % of the total DON_{UV} pool (Figure 4.10, b)

Figure 4.10. Latitudinal variation (35°S to 50°N) in surface (7m) concentrations of (a) dissolved free amino acids (DFAA, μM; black cirlces) and total hydrolysable amino acids(THAA, μM; white circles) and (b) the contribution (%) of DFAA (black circles) and THAA (white circles) to dissolved organic nitrogen (DON) determined by nitrate analysis prior to and after UV oxidation. Note the different vertical scales for DFAA and THAA. Vertical dotted lines broadly characterise oceanic regions (see Figure 4.2)

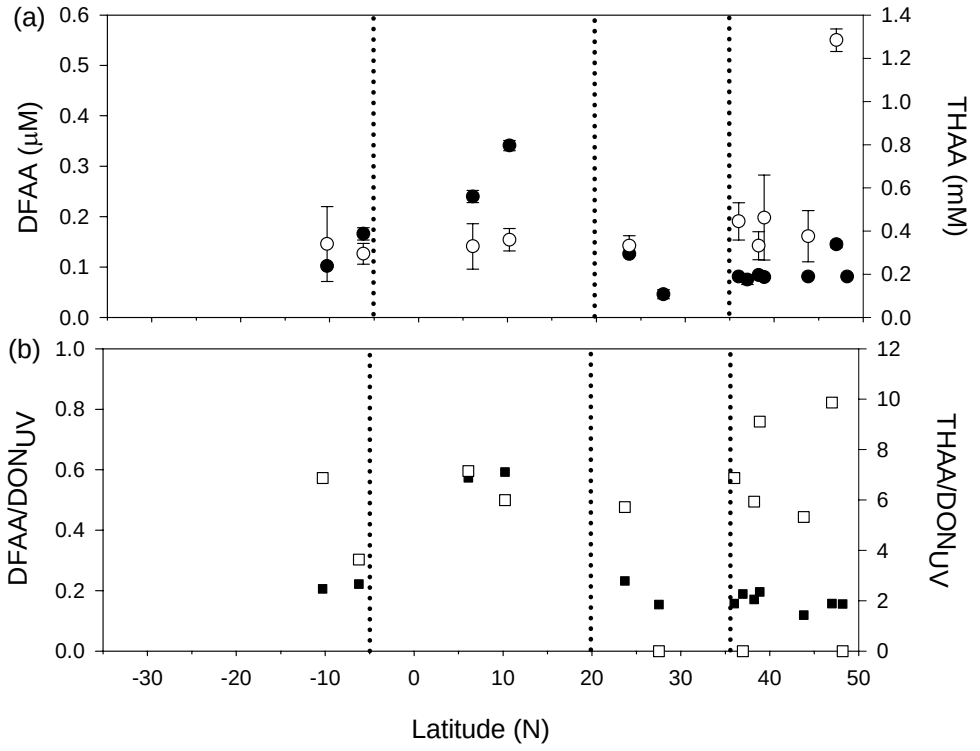

4.2.6. Stable isotopic composition of phytoplankton

Over the AMT 10 transect, the of $\delta^{15}N$ suspended particulate matter ($\delta^{15}N_{SPM}$) ranged from –3 ‰ to +6.89 ‰ (Figure 4.11, Table 4.2; page 144). The $\delta^{15}N_{SPM}$ was generally heavy (> 2.5 ‰) over much of the tropical and coastal upwelling zone between 5°S and 20°N (+3.3 to + 6.89 ‰; mean ± standard deviation, +4.81 ± 0.32‰; mean ± standard error), over the southern subtropical gyre between 35°- 6°S (+ 2.69 to + 6.03 ‰, + 4.09 ± 0.46 ‰) and in the northern subtropical gyre between 21°- 23°N (+ 3.60 to +6 .30 ‰, + 4.35 ± 0.75 ‰) and 33°-39°N (+ 2.66 to + 4.33 ‰, + 3.16 ± 0.41 ‰) (Figure 4.11). In contrast, two localised regions of isotopically light SPM (< 2.5 ‰) were observed in the oligotrophic northern subtropical gyre observed between 24°-

32°N (+ 1.84 to + 2.5 ‰,+ 2.25 ± 0.36 ‰) and at the northern end of the transect between 40°- 48°N (+ 1.3 to –3.0 ‰; –0.72 ± 0.52‰) (Figure 4.11), with an exception at 48°N (+ 4.0 ‰; see section 4.2.1.1).

Figure 4.11 Latitudinal variation in the stable isotope composition of suspended particulate organic nitrogen (δ^{15}N PON), ‰), collected from the underway seawater supply (7m; black circles) and daily CTD casts (7 to 55m: white circles) during AMT 10 in the Atlantic Ocean. Vertical dotted lines broadly characterise oceanic regions (see Figure 4.2)

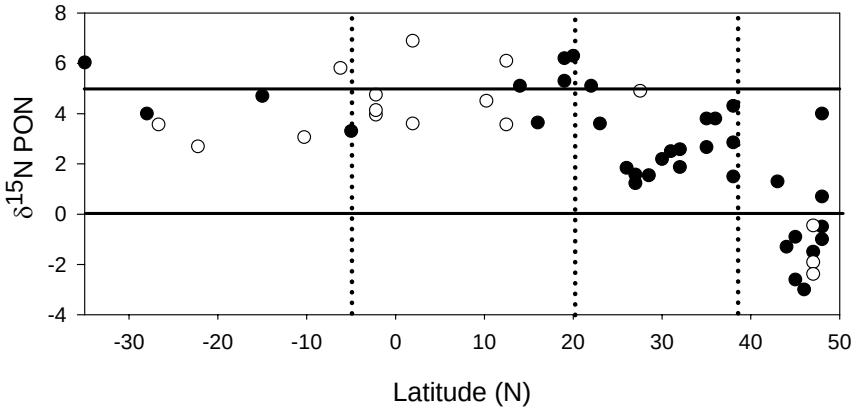

Over the south Atlantic subtropical gyre, isotopically heavy $\delta^{15}N\ PON_{SPM}$ (+ 6.03 $^{o}/_{oo}$) was observed at the southern flanks of the gyre and isotopically lighter $\delta^{15}N\ PON_{SPM}$ (+ 2.69 to + 4.70 ‰) in the centre of the gyre. Over the equatorial and coastal upwelling region, elevated $\delta^{15}N_{SPM}$ (+ 5.1 to + 6.3 ‰) coincided with peaks in chlorophyll *a* (Figure 3) at 13.72°N, 18.69°N and 20.64°N. In the north Atlantic subtropical gyre, $\delta^{15}N\ PON_{SPM}$ increased from +1.23 $^{o}/_{oo}$ on the eastern flanks to +4.3 $^{o}/_{oo}$ at the northern flanks of the gyre. The lightest isotopic signals were observed at the northern end of the AMT 10 transect (40°- 48°N; –0.72 ±0.52‰) and coincided with the onset of the spring bloom, the lightest signal being –3‰. Over the transect, these large variations in the isotopic signals reflect changes in the N sources and, where there was excess NO_3^- , the influence of biological isotopic fractionation.

4.3. DISCUSSION

4.3.1. Validity of sampling methods

4.3.1.1 Heterotrophic influence on stable nitrogen isotopic signals

There is a great deal of evidence in the literature to suggest that much of the subtropical Atlantic Ocean is heterotrophic, that is, the decomposition of organic matter due to biological respiration exceeds the production of organic matter through photosynthesis over small spatial and temporal scales (Fuhrman *et al*., 1989; Duarte *et al*., 2001; Robinson *et al*., 2002; del Giorgio and Duarte, 2003). In contrast to primary production, which tends to be both spatially and temporarily variable, respiration appears to be much less variable. This is because heterotrophic microorganisms can use a diversity of organic matter for respiration. Indeed much of the carbon demand in the open ocean is supported by DOC (Lefévre *et al.,* 1996; Karl *et al.,* 1998). This has implications on the biomass of heterotrophs versus autotrophs in the surface ocean, the former biomass exceeding the latter to create this net heterotrophic ecosystem. In a review by Cotner and Bibbanda (2002), the dominance of heterotrophs in the particulate organic carbon pool is outlined, being maximised in oligotrophic systems, which are dominated by dissolved organic rather than inorganic nutrients.

Suspended particulate matter (SPM) consists of a complex mix of autotrophs, heterotrophs and detrital material, all of which are inseparable filtering large volumes (> 200 L) of seawater from the non-toxic underway seawater supply or from Niskin bottles. Inclusion of higher trophic levels or detrital material in the SPM would enrich the ^{15}N to ^{14}N ratio of bulk SPM ($\delta^{15}N_{SPM}$) (Waser *et al.,* 2000), due to the phenomenon of isotopic enrichment with increasing trophic level (Minagawa and Wada, 1984). $\delta^{15}N_{SPM}$ collected on AMT 10 was heavier than 5 ‰ over much of the transect, suggesting a potential heterotrophic influence on the isotopic signals. Additionally, relatively high POC and PON concentrations were observed in the equatorial and

coastal upwelling regions and in the northern subtropical gyre, although Chl *a* concentrations were relatively low, possibly indicating post-bloom conditions and/or high grazing activity (Landry *et al*., 1995; Libby and Wheeler, 1997).

In the present study, the POC: PON ratio ranged from 3.82 and 21.51 for samples collected from the underway non-toxic supply (7m) and CTD (various depths; Figure 4.12i, a and ii, a, respectively). The POC: POC ratio is markedly different from the average molar ratio of oceanic plankton (phytoplankton and zooplankton), 6.6 (Redfield *et al.*, 1963), but in agreement with more recent views on C and N dynamics in the marine environment (C: N ratios of 8 to 14; Sambrotto *et al.*, 1993). POC and PON were significantly correlated (95% confidence level) for samples collected underway and from CTD casts (Figure 4.12i, a and ii, a, respectively).

A significant contribution of heterotrophs would be expected to introduce POC and PON to SPM, but not Chl *a*. The relationships between POC and PON, and Chl *a* (chlorophyll a data from sample taken from the underway non-toxic seawater supply), which indicates the relative contribution of particulate carbon or nitrogen to SPM, were significant (95% confidence level) for samples collected underway and from CTD casts (Figure 4.12i, b and c and ii, b and c), indicating that there was no significant input of POC and PON from heterotrophs. In addition, the ratio (slope) between POC and Chl *a* (87.10) and PON to Chl *a* (24.16) for samples collected underway (Figure 4.12i, b and c), was within the range cited for a healthy phytoplankton population (POC: Chl *a*, 10 to 200; Falkowski and Raven, 1997, more likely to be around 30-40; Patrick Holligan, personal communications) and in agreement with other studies in nutrient depleted waters of the Atlantic Ocean (Malone *et al.*, 1993; Maranon *et al.*, 2000), assuming a C: N ratio of 4. The POC: Chl *a* (265.17) and PON: Chl *a* (47.62) for samples collected

from the CTD were elevated in comparison to the underway samples (Figure 4.12ii, b and c), implying a heterotrophic influence.

If heterotrophic influence was responsible for the observed enriched $\delta^{15}N$ SPM, then one would expect a positive linear relationship between either the POC: chlorophyll *a* ratio and $\delta^{15}N$ SPM or PON: chlorophyll *a* ratio and $\delta^{15}N$ SPM (Waser *et al.*, 2000). However, this was not the case for samples collected underway (Figure 4.12i, c and d), the correlation coefficient (R; POC: Chl a vs. $\delta^{15}N$ PON=0.03 and PON: Chl a vs. $\delta^{15}N$ PON= -0.036, 95% confidence level), being less than the critical value (n=36, critical R of 0.325; Table A2, Miller and Miller, 1993). Samples collected from the CTD casts also showed a non-significant correlation between POC: Chl *a* (R=0.465) and PON: Chl *a* (R=0.38) and $\delta^{15}N$ SPM.

Figure 4.12. Correlation for (i) samples collected from the underway non toxic supply and (ii) samples collected from various depths from the CTD (7 to 55m), between (a) particulate organic carbon (POC) and particulate organic nitrogen (PON), (b), POC and chlorophyll *a* concentrations (Chl *a*; mg m^{-3}), (c) PON and Chl a, (d) the relationship between POC:Chl a ratio and the stable nitrogen isotope composition of PON (δ^{15}N PON) and (e) the relationship between PON:Chl a ratio and δ^{15}N PON. Regression analysis was performed at the 95% confidence level.

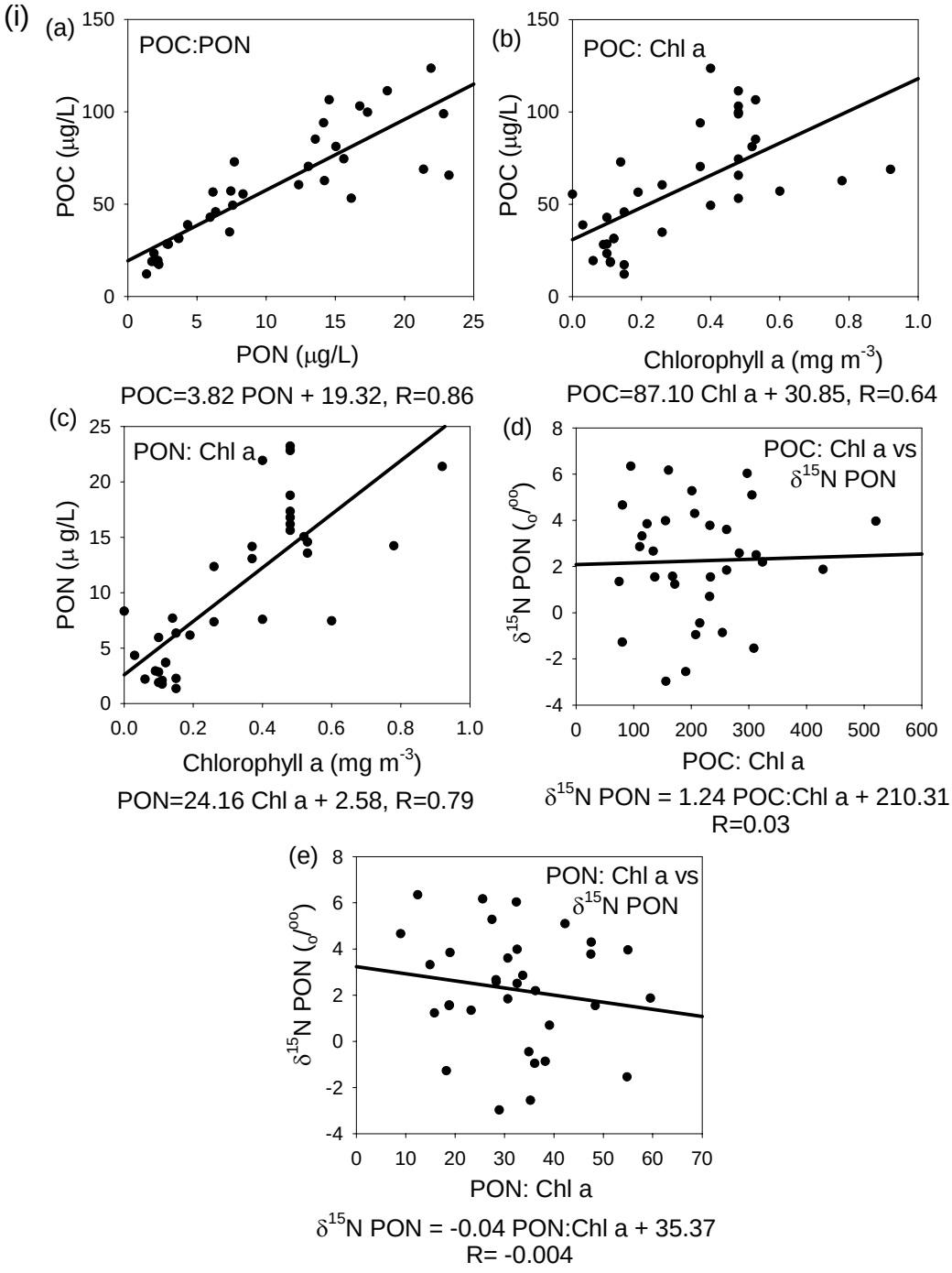

(ii)

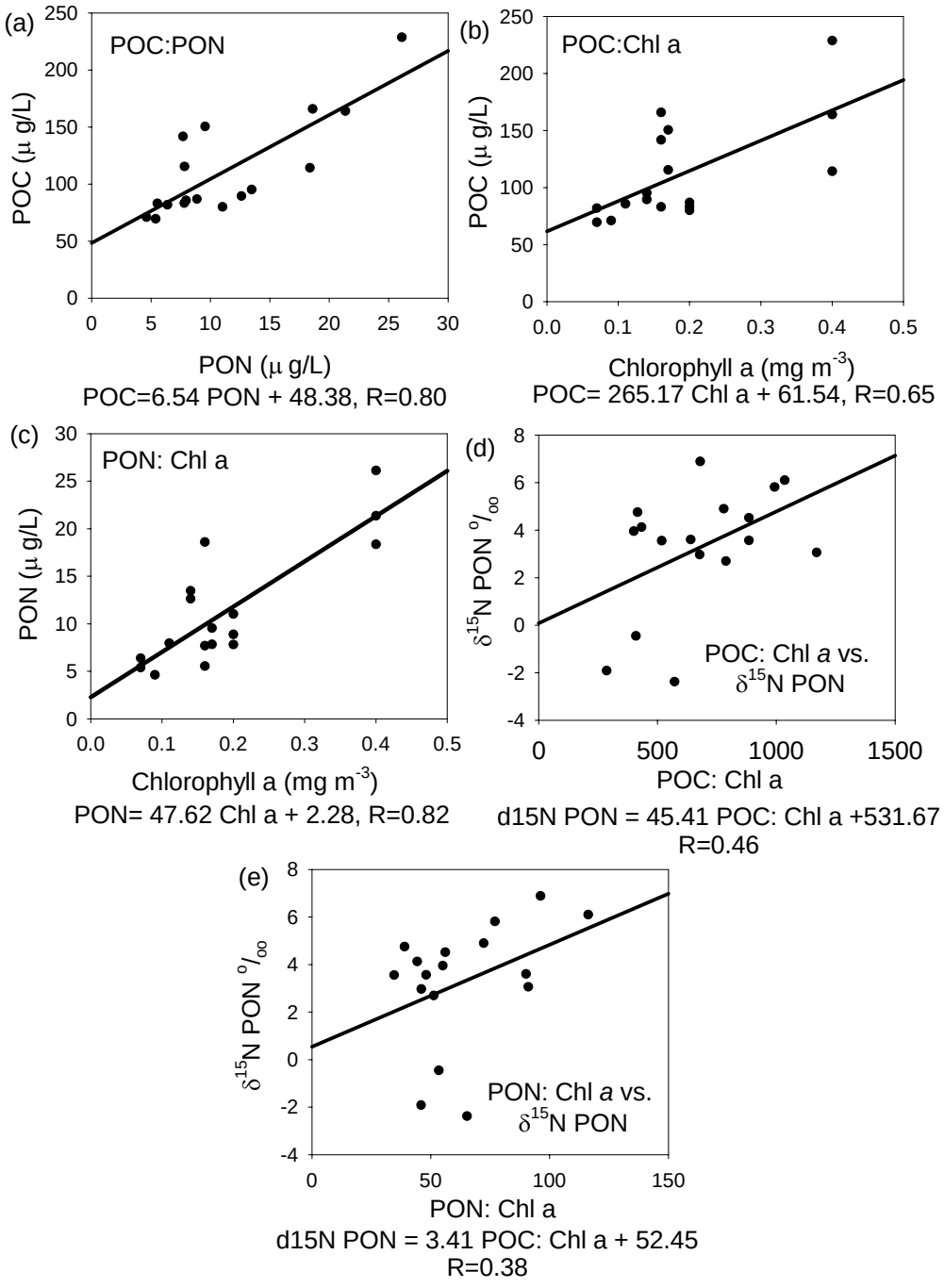
(a)
POC:PON
POC (μ g/L)
PON (μ g/L)
POC=6.54 PON + 48.38, R=0.80
(b)
POC:Chl a
POC (μ g/L)
Chlorophyll a (mg m-3)
POC= 265.17 Chl a + 61.54, R=0.65
(c)
PON: Chl a
PON (μ g/L)
Chlorophyll a (mg m-3)
PON= 47.62 Chl a + 2.28, R=0.82
(d)
δ15N PON o/oo
POC: Chl a vs. δ15N PON
POC: Chl a
d15N PON = 45.41 POC: Chl a +531.67
R=0.46
(e)
δ15N PON o/oo
PON: Chl a vs. δ15N PON
PON: Chl a
d15N PON = 3.41 POC: Chl a + 52.45
R=0.38

The distribution of sterols in the marine environment can be used to compare the relative contribution of zooplankton and phytoplankton to SPM (Wakeham and Canuel, 1988; Carpenter *et al.,* 1997; Volkman *et al.,* 1998). Specific sterols are used as biomarkers and are indicative of either zooplankton or phytoplankton origin (see review by Volkman *et al.,* 1998). Four filters were analysed (see Appendix I for methods and results) from 15°N, 16°N, 25°N and 48°N. The ratio of phytoplankton sterols to zooplankton sterols was greater than unity (16°N, 1.11; 25°N, 1.66; 48°N, 1.02; see Appendix I for data) for all samples except at 15°N (0.77). Cholesterol can be of zooplankton and phytoplankton origin (especially dinoflagellates), although it is usually a minor component of the later. Cholesterol can also represent living zooplankton plus detrital material and therefore, interpretation is subjective. In conclusion, although heterotrophic influence cannot be excluded from this data set, the author feels that sufficient biogeochemical evidence has been presented to show that the $\delta^{15}N$ of PON is sufficiently representative of the autotrophic community.

In N limited environments, phytoplankton utilise their N source to undetectable concentrations, resulting in no net isotopic fractionation (Altabet and McCarthy, 1985, Fogel and Cifuentes, 1993). Under such N-depleted conditions, it seems likely that zooplankton may also efficiently utilise their N source (i.e. phytoplankton) thus limiting fractionation during excretion. Small differences between the $\delta^{15}N$ of phytoplankton and zooplankton in the subtropical Atlantic have been observed (Montoya *et al*., 1992, Montoya *et al*., 2002), thus showing a weak association between size and $\delta^{15}N$. However, this absence of trophic level enrichment of ^{15}N has been attributed to variations in $\delta^{15}N$ through the seasonal production cycle and the differential turnover of N between phytoplankton and zooplankton.

4.3.1.2. Suspended versus sinking particulate matter

Sinking and suspended particles are operationally defined by the method of sample collection. Sinking particles are collected using sediment traps, which have inherent biases towards the size of particles they collect (Michaels *et al.*, 1990; Gust *et al*., 1992; Buesseler *et al.*, 1994; Buesseler, 1998). Suspended particles are sampled by filtration of large volumes of water, either from a ship's underway supply or by using *in situ* large volume pumps (*e.g*. Stand Alone Pumping System, SAPS), which may collect a negligible amount of sinking particles. Interactions between sinking and suspended particles are not well-understood and difficult to study. Studies of the stable isotopic composition of nitrogen in surface POM have found a general enrichment in sinking particles relative to suspended particles (see section 1.2.3.1; Altabet, 1988). Considering that the $\delta^{15}N$ of phytoplankton, whether sinking or suspended, is dependent on the $\delta^{15}N$ of the N source and isotopic fractionation, the observed difference in $\delta^{15}N$ POM raises an important question; what fraction of POM, sinking or suspended, accurately reflects the ambient nutrient dynamics of phytoplankton in the surface ocean?

The flux of "new" nitrogen from the deep ocean fuels "new " production in the euphotic zone, and under steady state conditions, this should be balanced by the export of PON from the euphotic zone to the deep ocean (Eppley and Peterson, 1979). Subsequently, stable isotopic mass balance for nitrogen would also be expected, that is, the $\delta^{15}N$ of nitrate from the deep ocean should be reflected in the $\delta^{15}N$ of POM being exported (sinking POM) from the euphotic zone (Altabet *et al.*, 1996), assuming a closed system. Indeed, a number of studies have reported that the $\delta^{15}N$ PON sinking out of the euphotic zone resembles the $\delta^{15}N$ of the original nitrate source (Altabet, 1988), an assumption also associated with paleo-oceanographic reconstruction of surface nutrient

dynamics in past ocean environments (Altabet and Francois, 1994). However, this scenario assumes two factors;

1.Nitrate from the deep ocean is the only "new" nitrogen source to the surface ocean. N_2 fixation, atmospheric inputs and possibly far field DON advection are considered "new" nitrogen sources by the modern oceanographic community. Thus, uptake and assimilation of these "new" sources will significantly influence the $\delta^{15}N$ of PON sinking from the euphotic zone.

2. Isotopic effects of new nitrogen sources are reflected in $\delta^{15}N$ of sinking particles, rather than $\delta^{15}N$ of suspended particles, which should not be used to deduce new sources of N to phytoplankton (Altabet, 1988). However, the significant negative linear relationship between the depth variation in nitrate concentrations and $\delta^{15}N$ of suspended particulate matter (Altabet and McCarthy, 1986; Saino and Hattori, 1987; Voss *et al.*, 1996; Rau *et al.,* 1998; Altabet, 2001) implies that suspended particles, as well as sinking, respond to inputs of nitrate from the deep waters to the surface ocean. Additionally, significant responses have been observed in $\delta^{15}N$ of suspended PON to "new" N inputs via N_2 fixation (Carpenter *et al.,* 1997; Carpenter *et al.,* 1999). In contrast, no light isotopic signals were observed in sediment traps at BATS during periods of significant N_2 fixation (Lipschultz *et al.,* 2002), possibly due to rapid remineralisation in surface waters.

Whereas sinking particles reflect the $\delta^{15}N$ of the N source minus isotopic fractionation effects, suspended particles are affected by other processes, such as uptake and assimilation of regenerated N and atmospheric N sources. As this study is primarily concerned with the relative influence of N sources to surface phytoplankton communities, collection of suspended particulate matter, which should reflect new as well as regenerated N sources, seems the most representative approach.

The relationship between the $\delta^{15}N$ of surface POM is also dependent on the flux rate. It has been found that in regions of high POM flux, such as in the equatorial upwelling region (Altabet, 2001) and during a spring bloom (Altabet *et al.*, 1991), the $\delta^{15}N$ PON of suspended particulate was similar to $\delta^{15}N$ PON of sinking particulate matter. This is probably due to high sinking rate of particles, allowing little time for degradation, and the high grazing activity during bloom conditions, a mechanism which is partly responsible for the exchange between sinking and suspended particles (Bishop, 1986; Allredge and Gotschalk, 1989).

4.3.2. Interpretation of stable nitrogen isotopic signals: isotopically light phytoplankton

4.3.2.1. Spring Bloom Region

In the northern flanks of the North Atlantic subtropical gyre (north of 38°N) and in the subpolar region (north of 45°N), the phytoplankton biomass during AMT 10 was high. Convection and lateral wind-driven transfer due to passing storms in this region (see section 3.3.1 and Figure 3.7) (Williams and Follows, 1998; Williams *et al.*, 2000) probably encouraged the entrainment of nutrients from the deep ocean into the euphotic zone, thus promoting primary production. However, the timing of the cruise coincided with the North Atlantic spring bloom. Chemotaxonomic data indicated that the bloom was dominated by chrysophytes, prymnesiophytes and chlorophytes. The north Atlantic spring bloom is usually dominated by diatoms with a succession to nanoflagellates in the later stages of the bloom (Bidigare *et al.*, 1990; Barlow *et al.*, 1993; Barlow *et al.*, 2002). Thus, our observations suggest that we observed the final stages of the spring bloom. Depth averaged [DON] and [DOP] in this region were the highest observed during the AMT 10 transect, and may be attributed to high grazing and sloppy feeding by zooplankton. Unfortunately, zooplankton biomass data is absent from this study.

The lightest isotopic signals for phytoplankton ($\delta^{15}N$ PON + 1.3 to –3.0 ‰) were also observed in this region. Such depleted values of $\delta^{15}N_{SPM}$ have been previously observed during spring bloom events (Altabet and Deuser, 1985; Altabet and McCarthy, 1985; Goering *et al*., 1990; Altabet *et al.,* 1991), where high nitrate concentrations (> 5 μM, this study) result in net isotopic fractionation during uptake and assimilation of the nitrogen source. Altabet *et al.,* (1991) estimated a fractionation factor (ε) of 8 to 9 ‰ during phytoplankton blooms in the North Atlantic. If similar conditions prevailed during AMT 10, this would probably imply an initial $\delta^{15}N$ composition of nitrate to be 5 - 6 ‰ (by application of the instantaneous product equation in an open system, see Introduction), which is similar to measured $\delta^{15}N$ NO_3^- of deep water in the Atlantic Ocean (Liu and Kaplan, 1989; Sigman *et al.,* 1997). During the post-bloom period, there is a good correlation between the decrease in ambient NO_3^- concentrations and the increase in the $\delta^{15}N$ of suspended PON, which reflects the increase in ^{15}N in the NO_3^- pool, due to the preferential uptake of $^{14}NO_3^-$ by phytoplankton (Saino and Hattori, 1985; Goering et al 1990; Altabet et al 1991; Nakatsuka et al., 1992). The $\delta^{15}N$ of NH^+_4 (Altabet 1988), the magnitude of the grazer-produced NH_4^+ pulse, the upward vertical diffusion of new NO_3^- (Nakatsuka *et al.* 1992) and the physiological state of the cells will be important in the determining the $\delta^{15}N$ of phytoplankton after the spring bloom (Waser *et al*. 1999).

4.3.2.2 Nitrogen fixation

Isotopically light phytoplankton nitrogen (1.23 to 1.84 ‰) observed in a localised region of the north Atlantic subtropical gyre (26°N to 28°N) implies uptake and assimilation of an isotopically light source of nitrogen, possibly regenerated N (i.e.

NH_4^+) or N derived from N_2 fixation (Mahaffey *et al.,* 2002). There is evidence to suggest that the latter was the dominant N source in this region, this is outlined below.

4.3.2.2.1. Species Abundance

Trichodesmium spp. is reported to be the most prolific and is undoubtedly the best studied N_2 fixing organism in the surface ocean (Glibert and Bronk, 1994; Capone *et al.,* 1997; Karl *et al.,* 1997; Mulholland and Capone, 1999; Hood *et al.,* 2000; Capone, 2001). *Trichodesmium* spp. were quantified during AMT-1 to -8 (1995 to 1999) and found to be most abundant (600 to 300 filaments per litre) between the equator and 15°N, variably and of intermediate abundance north of 20°N (20 to 400 filaments per litre) and almost absent (< 20 filaments) in the south Atlantic subtropical gyre (5°S to 30°S) (Figure 4.13; Tyrrell *et al.,* 2002). In this study, chemotaxonomic evidence from pigments implies that cyanobacteria and prochlorophytes dominate the surface phytoplankton community between 25°N and 10°S. Furthermore, phytoplankton counts during AMT 10 suggest that *Trichodesmium* were present between 2°S and 27°N (Alex Poulton, pers comm). During AMT 4 (spring cruise), *Trichodesmium* sp. was abundant at 28°N, at the same location where light $\delta^{15}N$ SPM were measured during AMT 10 (Figure 4.14). Similar abundances were observed during autumn cruises (AMT 3, 5 and 7; Figure 4.14), although *Trichodesmium* is normally considered to have a seasonally variable distribution (Karl *et a1*., 1995; Orcutt *et al.,* 2001).

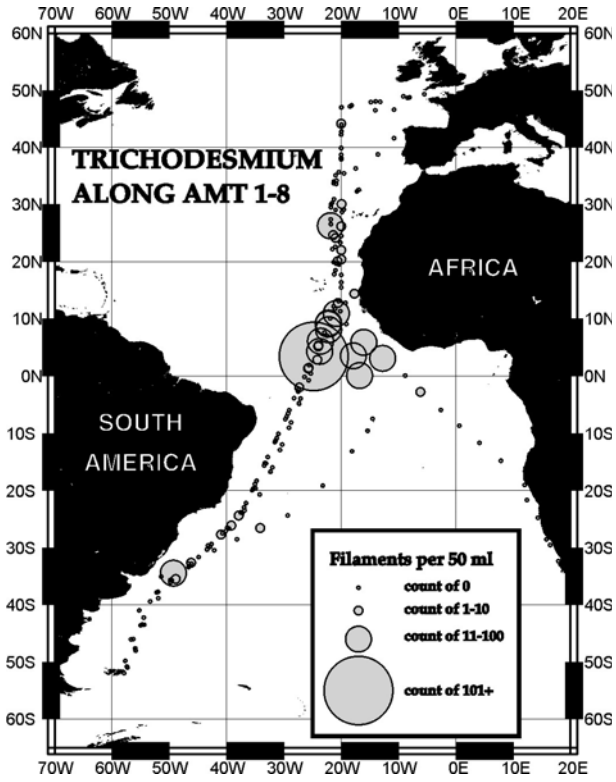

Figure 4.13. Concentrations of *Trichodesmium* filaments measured along 8 Atlantic Meridional Transect cruises. Filaments abundances are represented as successively larger circles for every 10 fold increase in filaments. Figure courtesy of Dr. Toby Tyrrell at Southampton Oceanography Centres (Tyrrell *et al.*, 2002).

Figure 4.14. Latitudinal variation (50°N to 50°S) in *Trichodesmium* filaments counts (filaments per litre) in the surface ocean (7m; black bars) and at the deep chlorophyll maximum (DCM; grey bars) during AMT 1 to 8. Note the different vertical scales. Figure courtesy of Dr. Toby Tyrrell at Southampton Oceanography Centres (Tyrrell *et al.*, 2002).

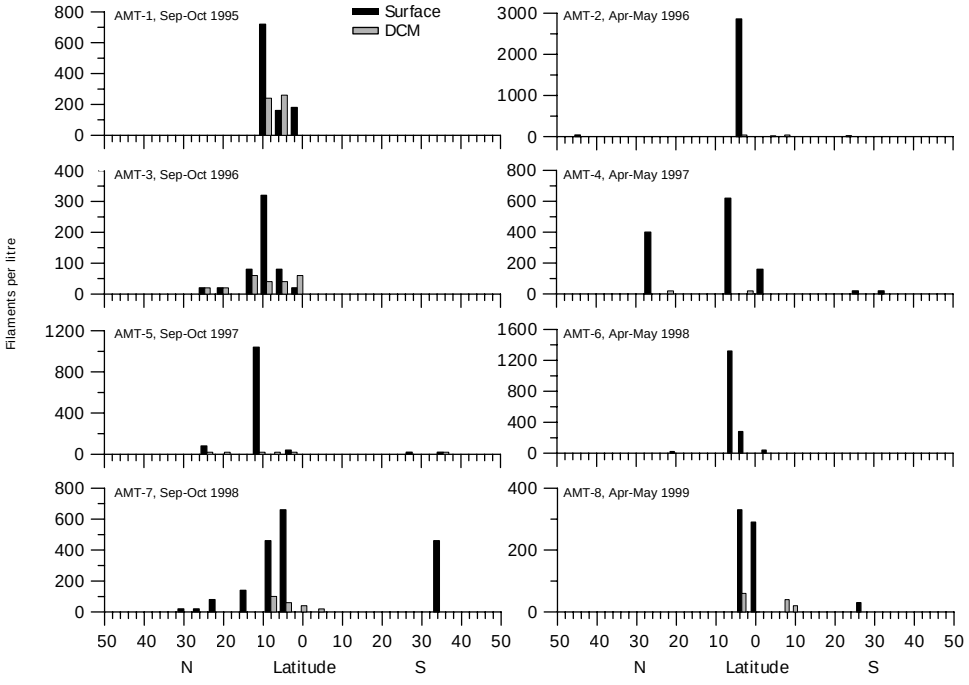

4.3.2.2.2. Iron

Iron (Fe) is essential for N_2 fixation due to the requirements of the nitrogenase enzyme complex (Raven, 1988; Raven *et al.,* 1998; Falkowski, 1997). Aeolian dust inputs are the major source of Fe to the open ocean (Prospero *et al.,* 1996). Although upwelling may deliver sufficient Fe to low dust areas (Bowie *et al.,* 2002), it is questionable whether sufficient iron is delivered to relieve iron limitation relative to nitrate elsewhere (Martin *et al.,* 1989; Vink and Measures, 2001; Bowie *et al.,* 2002). Additionally, the bioavailability of iron delivered to the surface ocean during dust deposition is not well understood (Johnson *et al.,* 1997; Jickells, 1999; Vink and Measures, 2001; Bowie *et al.,* 2002). Nevertheless, numerous studies suggest that iron may ultimately control the distribution of N_2 fixers in the global coastal and open ocean (Rueter *et al.,* 1992; Micheals *et al.,* 1996; Falkowski, 1997; Wu *et al.,* 2000; Berman-Frank *et al.,* 2001; Lenes *et al.,* 2001) promoting a community level (*i.e.* increase) rather than physiological response (Orcutt *et al.,* 2001).

The Trade Winds transport dust westwards from the Sahara Desert to the tropical and subtropical Atlantic and are responsible for the highest recorded particulate deposition to the surface oceans, with inputs of up to 18 mg m^{-2} yr^{-1} (Duce and Tindale 1991; Tegen and Fung 1995; Mahowald, 1999; Fung *et al.,* 2000). Between February and mid-April 2000, immediately before AMT 10, an anomalously strong injection of Saharan dust to between 20° and 40°N was observed, as independently suggested by SeaWiFS remotely sensed satellite images for the 28th February 2000 (Figure 4.15, a, left panel), atmospheric model output from 1999 to 2001 (Luo *et al.,* 2002, Figure 4.15, a, right panel) and aerosol index derived from total ozone mapping spectrometry for March and April, 2000 (TOMS; Figure 4.15, b and c respectively). The atmospheric transport model predicts the source, transport and wet and dry deposition of dust using NCEP/NCAR meteorological reanalysis from 1979 to 2000 (Zender *et al.,* 2002). The

model predictions of dust deposition are significantly correlated with the observed aerosol index from TOMS over the AMT 20°W transect, (correlation coefficient 0.6 at a 95% confidence level), as well as with *in situ* surface observations at Bermuda, Barbados and Miami (Luo *et al.*, 2002). The model predicts that the dust deposition is unusually high (twice the climatological monthly mean) from February to mid-April of 2000, recording twice the climatological monthly mean between 22°N and 35°N.

Figure 4.15. Independent evidence for an anomalous atmospheric dust event over the Sahara desert into the East Atlantic; (a) SeaWiFS satellite images for February 26th 2000 over the east Atlantic(source;http://seawifs.gsfc.nasa.gov/SEAWIFS/HTML/dust.html;left panel) and model predictions of wet and dry dust deposition along the 20°W transect between 1999 and 2001 (Luo et al., 2002; right panel) and (b) Total Ozone Mapping Spectrometer image of the aerosol index in (b) March and (c) April 2000 (source; http://toms.gsfc.nasa.gov/eptoms/ep.html).

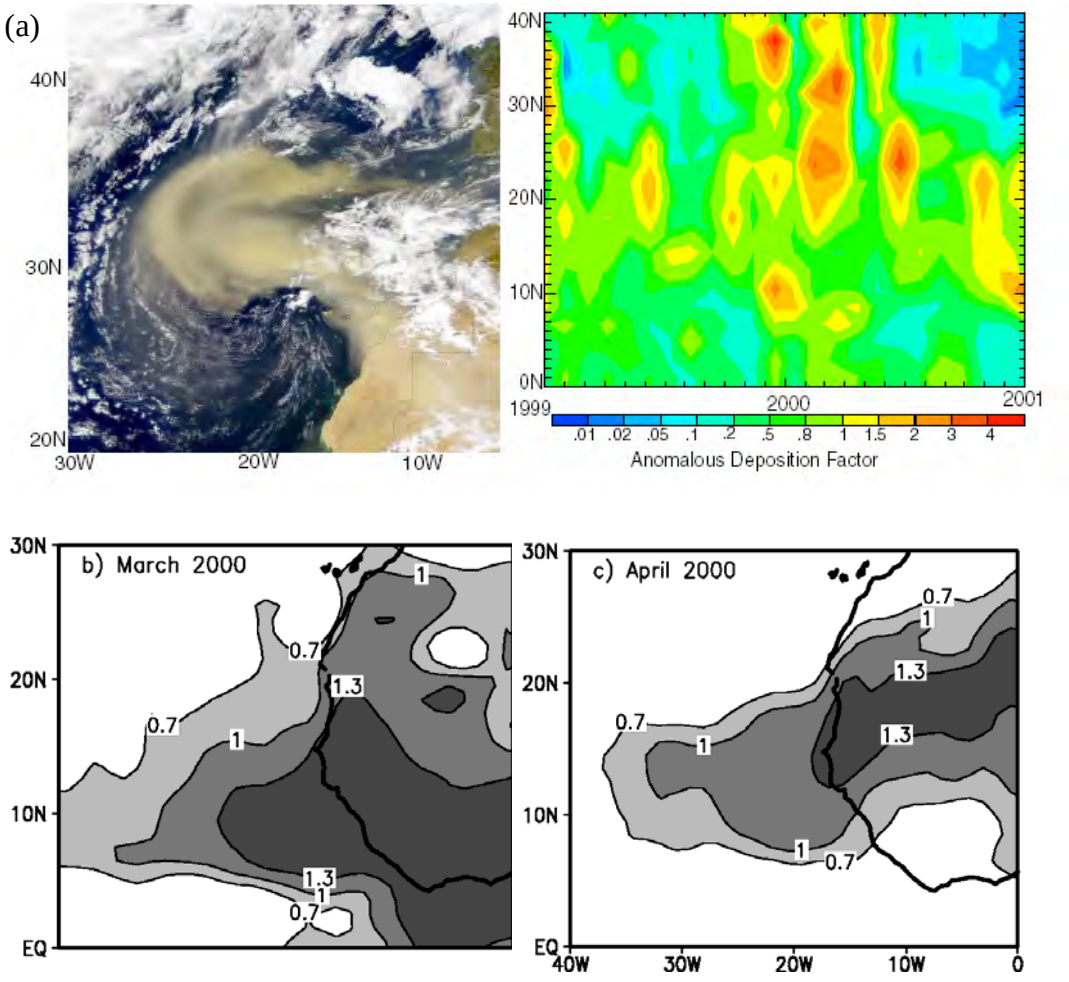

In view of the residence time of total and dissolved iron in the surface ocean (~200 and ~20 days, respectively; Jickells, 1999), and the response time of *Trichodesmium* (days to weeks; Lenes *et al.*, 2001), it is plausible that the atmospheric dust injection led to natural iron and phosphorus fertilisation. Hence, the atmospheric dust inputs may have been responsible for the biogeochemical signals observed between 27 April and 1 May during AMT 10.

Considerable daily and seasonal variability of dust input, both spatially and temporarily, is observed in this region (Mahowald, 1999; Fung *et al.,* 2000) due to the seasonal migration of Inter Tropical Convergence Zone. It is possible that the temporal and spatial distribution of N_2 fixers in this region is dependent upon the magnitude and supply of dust inputs from the Sahara. However, a number of studies have shown that there is no correlation between *Trichodesmium* abundance and ambient surface iron concentrations (Capone *et al.,* 1998, Sanudo-Wilhelmy *et al.,* 2001, Tyrrell *et al.,* 2002). Instead, the episodic nature of dust deposition and relatively short residence time of dissolved Fe (considered bioavailable) in surface waters (Jickells, 1999) demands consideration of the annual dust supply. Thus, simultaneous measurement of surface iron concentrations and N_2 fixation may be misleading.

4.3.2.2.3. Phosphorus

While N_2 fixers are independent of their ambient N conditions, they can be highly P-limited (Letelier and Karl, 1988, 1996; Karl, 1999; Sanudo-Wilhelmy *et al.,* 2001). *Trichodesmium* sp. has been shown to have a number of physiological and behavioural adaptations to cope with P stress and to allow it to exploit low P levels. In this study, NO_3^- and PO_{4-}^{3} concentrations were near detection limits in surface waters. However, an increase in [DON] and significant decrease in [DOP] was observed in the

region coincident with a region associated with N_2 fixation in the present study. [DON] exudation during N_2 fixation will be discussed later (see section 4.3.4.1.1.). During severe P limitation, *Trichodesmium* sp. have the ability to utilise DOP by induction of specific transport and hydrolytic enzymes, such as alkaline phosphatase (McCarthy and Carpenter 1979; Mulholland *et al.,* 2002), thus decreasing [DOP]. Mulholland *et al.,* (2002) found that alkaline phosphatase was inhibited when dissolved inorganic phosphate (DIP) was present and was activated in the presence of DOP. Overall, they found *Trichodesmium* sp. had the ability hydrolyse DOP and grow with DOP as its sole P source (Mulholland *et al.,* 2002). In general, the DOP pool is substantially larger than the DIP pools in oligotrophic environments, and so the enzyme, alkaline phosphatase, may relieve P stress under severe limitation on time scales of weeks to month (Benitez-Nelson and Karl, 2002). (A potential mechanism supplying DOP to subtropical gyres is discussed in section 4.2.5.1.).

Additional physiological adaptations include P-sparing strategies, for example, the ability to grow with altered P cell quota by reduction of intracellular nucleotide pools and lower nucleic acid content (Karl *et al.,* 2002) and efficient P recycling rates under P limitation. P-sparing may be responsible for slow growth rates observed in *Trichodesmium.*

Periodic vertical migrations, known as P-mining (Villareal and Carpenter, 1990; Karl *et al.,* 1992; Karl and Tien, 1997) and increased abundance correlated with shallow mixed layer (Orcutt *et al.,* 2001) may allow *Trichodesmium* spp. colonies to exploit deep P reserves. This behaviour may explain the relatively high abundance of *Trichodesmium* spp. in the tropical upwelling region of the Atlantic during eight AMT transects (Tyrrell *et al.,* 2002), where a shallow mixed layer is observed.

The conflicting interaction between P and Fe in controlling N_2 fixation is exemplified by comparing N_2 fixation in the Atlantic and Pacific Oceans. Wu *et al,* (2000) observed more depleted surface P pools in the Atlantic compared to the Pacific and attributed this observation to elevated inputs of Fe from Saharan dust driving high rates of N_2 fixation and drawing down P to very low levels. (Indeed, N_2 fixation was found to be directly correlated with cell phosphorus content, but not cellular iron in tropical Atlantic (Sanudo-Wilhelmy *et al.,* 2001)). In comparison, N_2 fixation in the Pacific is highly iron limited, due to the lack of arid deserts on its boundaries and large basin.

4.3.2.2.4. Contribution to surface N pool

N accumulation in oligotrophic environments where N is severely limited is unlikely and, in accord, no significant increase in [DON] was observed in the north Atlantic subtropical gyre in comparison to surrounding regions during AMT 10. Rapid recycling of recently exuded organic matter within *Trichodesmium* spp. colonies may add credence to this hypothesis. Bergman and Carpenter (1991) reported that not all filaments within a *Trichodesmium* colony have nitrogenase, the N_2 fixing enzyme, present. This implies that trichomes either operate individually within the colony and have the ability to activate nitrogenase depending on ambient N conditions, or that actively fixing filaments may provide a source of combined N to adjacent non-fixing filaments. Recycling of amino acids, specifically glutamine and glutamate, within colonies has been deemed an important nutritional strategy for these colonial organisms (Carpenter *et al.,* 1993; Capone *et al.,* 1994). Furthermore, Mulholland and Capone (1999) report that N_2 fixation, N release and N regeneration are tightly coupled, creating a highly efficient recycling ecosystem within the colonies themselves. Although *Trichodesmium* spp. may alleviate N limitation through fixation of N_2, retention of the recently exuded N within the colonies probably explains the lack of DON accumulation.

Nevertheless, other studies have observed net [DON] accumulation during *Trichodesmium* spp. blooms (Karl *et al.,* 1992; Lenes *et al.,* 2001), at least 25% of which are amino acids (Glibert and Bronk, 1994, Capone *et al.,* 1994). Subsequent regeneration of exuded amino acids by heterotrophic bacteria (Kirchman *et al.,* 1989) releases bioavailable N (probably NH_4^+) to the surrounding the phytoplankton community. Thus, DON accumulation preceding *Trichodesmium* blooms may be dependent on the efficiency of the heterotrophic recycling process. In addition, excessive DON exudation during "luxurious" N_2 fixation may require an acclimatisation period before efficient recycling occurs, thus allowing DON accumulation.

4.3.2.2.5. Independent climatological diagnostics – N*

The background and application of the quasi-conservative tracer, N*, has been previously discussed (see Section 3.5.3). During AMT 10, N* was greater than 2.52 over much of the North Atlantic subtropical gyre (Figure 4.16), indicating excess N, consistent with the proposal that N_2 fixation was the dominant N supplying process in this region. Such patterns are also observed in the latitudinal variation in the NO_3^-: PO_4^{3-} ratio (Figure 3.44). At this time of AMT 10, an anomalous input of atmospheric dust was transported from the Sahara, model prediction suggesting that the wet and dry deposition of dust was twice the climatological monthly mean (see section 4.3.2.2.2). Such a dust injection and possible iron fertilisation would be expected to fuel significant activity of N_2 fixers. However, comparison of N* and the NO_3^-:PO_4^{3-} ratio between AMT 10 and other Spring and Autumn transects suggests that excess N due to N_2 fixation was not considerably different during AMT 10. This implies that N_2 fixation was probably limited by another factor, such as phosphorus, thus impinging an upper bound on N_2

fixation in this local region. Studies in the West Atlantic, based on comparisons of nutrient dynamic (Wu *et al.,* 2000) and cellular iron and phosphorus quotas of *Trichodesmium* (Sanudo-Wilhelmy *et al.,* 2001) have concluded that N_2 fixation is PO_4^{3-} limited. In contrast, studies in the central Atlantic based on PO_4^{3-} uptake dynamics have concluded that PO_4^{3-} is not limiting (Canellas *et al.,* 2000). More recently, Ridame and Guieu (2002) suggest that Saharan dust is a significant source of PO_4^{3-} to the oligotrophic surface ocean, fuelling ~ 15 % of the integrated and total primary production in the mixed surface layer of the oligotrophic Mediterranean Sea. Therefore, the Saharan dust event observed in early 2000 may have not only caused iron, but also PO_4^{3-} fertilisation to this localised region. However, simultaneous determination of PO_4^{3-} and iron dissolution and uptake, and N_2 fixation rates would be required to deconvolute this scenario.

Figure 4.16. Latitudinal variation in N* ($N^*=0.87(NO_3^- -16PO_4^{-3} +2.9)$ μmol kg^{-1}) during AMT 10 in April-May 2000 in the Atlantic Ocean. The solid line represents the N* equivalent to the Redfield ratio of N:P (2.5 μmol kg^{-1}).

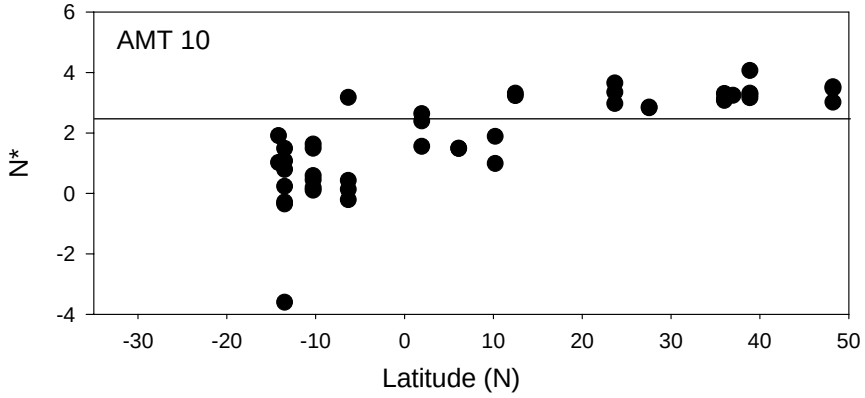

4.3.2.2.6. Direct observations versus biogeochemical techniques

Independent observations of N_2 fixation in the Atlantic, by direct counts (Tyrrell *et al.,* 2002) and stable isotopic techniques employed in this study, reveal a difference with respect to spatial distribution of N_2 fixers. Tyrrell *et al.,* (2002) found the highest concentrations of *Trichodesmium* spp. in the tropics during both spring and autumn

AMT transects (Figure 4.13), yet during AMT 10, PON isotopic signals were enriched (> 3 ‰) relative to the expect values of near 0‰ for N_2 fixation. In addition, we observe a localised region of isotopically light signals over the North Atlantic subtropical gyre (Figure 4.11) yet *Trichodesmium* spp. appears to be more abundant further north (Figure 4.13). There are a number of possible explanations for this.

Firstly, determination of *Trichodesmium* abundance using plankton tows, Niskin bottles and SCUBA divers has revealed significant discrepancies between sampling methods (Carpenter and Romans, 1991; Orcutt *et al.,* 2001; Tyrrell *et al.,* 2002). Tyrrell et al., (2002) suggested that *Trichodesmium* filament counts could vary by one order of magnitude depending on the method of collection (Figure 4.17). Furthermore, *Trichodesmium* spp. exist in a number of different but distinct morphologies, as free trichomes (Karl *et al.,* 1996) and as colonies, which may be arranged as puffs (radial arrangement) or tuffs (parallel arrangement) (Letelier and Karl, 1996; Orcutt *et al*, 2001). Obviously, accurate quantification of this species requires a trained eye and strict protocol. Thus, comparison of abundance, both spatially and temporally, may be subjective.

Figure 4.17. Distribution of Trichodesmium during AMT 8 as measured by (a) a plankton net hauled through the top 150-200m, (b) a Niskin bottle fired at 15m depth, (c) a bucket lowered into the water surface and (d) counts of filaments in a small volume of water taken from a Niskin bottle fired at 7m depth. Figure courtesy of Dr. Toby Tyrrell at Southampton Oceanography Centres (Tyrrell *et al.,* 2002).

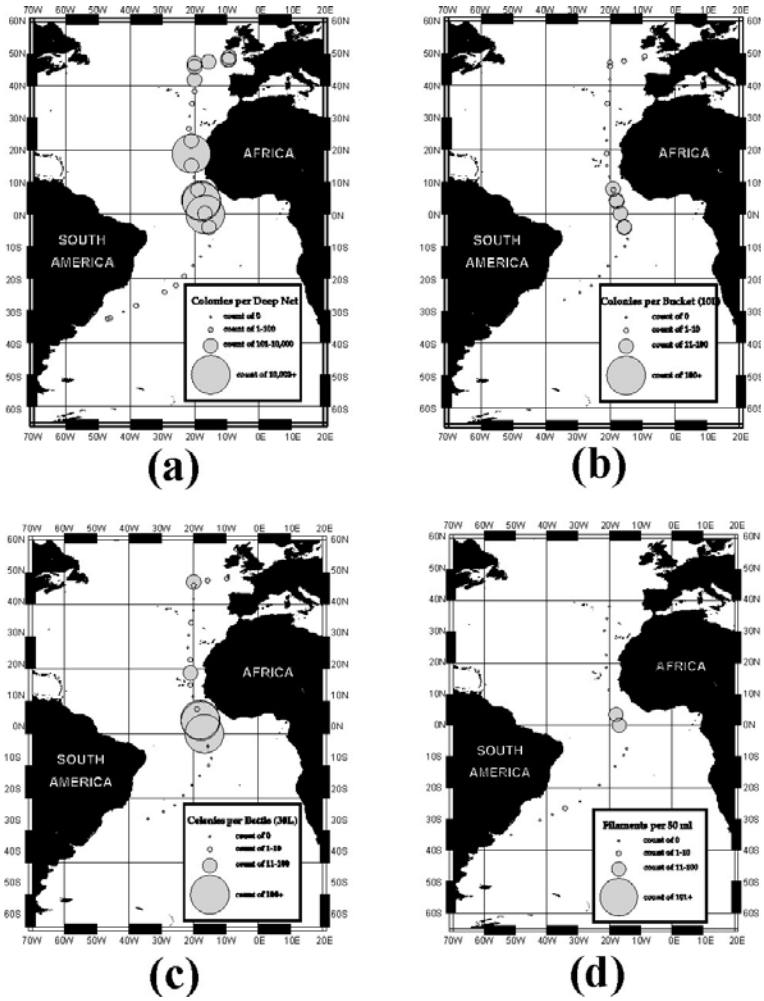

Oceanographic application of new epifluorescence, light microscopy and molecular probe techniques, especially the *nif*H primers specific to the N_2 fixing enzyme, nitrogenase, have revealed an array of marine N_2-fixing micro-organisms in the Atlantic and Pacific, previously undetected by traditional microscopy (Zehr and McReynolds, 1989; Bergman and Carpenter, 1991; Villareal, 1991; Bergman *et al.,* 1997; Zehr *et al.,* 1998, 2000; Falcon *et al.,* 2002). The zeaxanthin bearing pico-cyanobacteria, *Synechococcus* spp., is abundant in warm tropical oceans and recent evidence suggests it may have the ability to fix N_2 (Mitsui *et al.,* 1986). Since

Synechococcus spp. (as well as Prochlorococcus spp.), are reported to be few orders of magnitude more abundant than *Trichodesmium* (Zubkov *et al.*, 2000; Zehr *et al.*, 2000), their potential capacity to fix N_2 would have a significant ecological impact. Additionally, recent studies have identified a symbiotic heterocytous cyanobacterium *Richelia intracellularis* during an extensive bloom of the diatom *Hemiaulus hauckii* in the tropical Atlantic (Villareal, 1993; Carpenter *et al.*, 1999), reflecting the diversity of marine N_2 fixing micro-organisms. It is therefore not surprising that there are inconsistencies between direct observations and biogeochemical data (*i.e.* $\delta^{15}N$) considering our lack of knowledge on N_2 fixing species other than *Trichodesmium*, and accurate methods of detection.

McCarthy and Carpenter (1979) and Carpenter *et al.*, (1993) showed that *Trichodesmium* spp. doubling rates were greater than could be accounted for by N metabolism from N_2 fixation alone. Further investigations have revealed that *Trichodesmium* spp., and possibly other N_2 fixing organisms are not obligate N_2 fixers. Instead, they have the capacity to take up and assimilate combined N forms, such as ammonium, nitrate, and DON (Goering *et al.*, 1966; Saino and Hattori, 1978; Ohki *et al.*, 1986; Ohki *et al.*, 1991; Carpenter *et al.*, 1992; Capone *et al.*, 1994; Mulholland *et al.*, 1999; Mulholland and Capone, 1999;). Intriguingly, studies on *Trichodesmium* cultures and natural populations have revealed their ability to simultaneous fix N_2 and assimilate combined N (Mulholland *et al.*, 1999; Mulholland and Capone 1999; Orcutt *et al.*, 2001), which may explain how *Trichodesmium* can continue fixing N_2 during periods of rapid recycling (Mulholland *et al.*, 2001). Indeed, nitrate reductase, the enzyme required for nitrate utilisation, within *Trichodesmium* is induced by the presence of nitrate, (Goering *et al.*, 1966; Eppley *et al.* 1969), at concentrations greater than a specific threshold (~ 10μM N) after a period of acclimation (Mulholland and

Capone, 1999; Mulholland *et al*. 2001; Orcutt *et al*., 2001). This finding may explain the lack of light isotopic signals observed over the tropical equatorial region during AMT 10, as *Trichodesmium* populations may be utilising nitrate upwelled from the deep ocean. It is therefore important to note that presence of *Trichodesmium* in the water column does not imply active fixation of N_2.

Recent evidence suggests that N_2 fixation not only fuels autotrophic and microbial growth but affects higher trophic levels in the oceanic ecosystems. The $\delta^{15}N$ of zooplankton in regions of N_2 fixation (0.2 to 3.6 ‰; Montoya *et al.*, 2002) are found to be isotopically lighter than in regions where N_2 fixers are absent (5.5 to 8.9 ‰; Macko *et al.,* 1984; Fry 1988). This implies ^{15}N depleted organic nitrogen is being transferred to higher trophic levels and thus may be used an alternative tracer for N_2 fixation.

Although *Trichodesmium* spp. are capable of surviving on combined N sources, and indeed, it is energetically less expensive to do so, their ability to fix N_2 allows them to occupy a specific niche in the surface ocean in which they can out-compete other phytoplankton species in extreme oligotrophic environments.

4.3.3. Interpretation of stable nitrogen isotopic signals: isotopically heavy phytoplankton

4.3.3.1 Physical supply of nutrients to the surface ocean

Isotopically enriched $\delta^{15}N$ SPM (2.69 to 6.89 ‰) over a large part of the South Atlantic subtropical gyre, the equatorial region and part of the northern flanks of the North Atlantic subtropical gyre, implies uptake and assimilation of an isotopically heavy source of nitrogen, assuming that this parameter is a proxy for the isotopic composition of phytoplankton (see 4.3.1.1). The most likely source of N, which would explain this observation, is nitrate from the deep ocean (normally ~ 5 to 6 ‰; Liu and Kaplan, 1989; Sigman *et al.,* 1997), which is utilised by phytoplankton in a closed

system according to the instantaneous production equation (see section 1.2.2.3). The range in values may reflect some degree of isotopic fractionation or utilisation of other N sources (see section 4.3.5.2). However, explaining the high level of nitrate supply is problematic over the subtropical gyres since the wind system drives downwelling over the basin scale. Nevertheless, there are a number of physical mechanisms, from gyre- to fine-scale, which may permit such a nitrate injection.

4.3.3.2. Gyre scale processes

4.3.3.2.1. Convection

Convection is the depression of the surface mixed layer due to a combination of solar irradiance and atmospheric forcing (Williams and Follows, 2002), entraining nutrients into the euphotic zone and initiating a phytoplankton response (see section 3.3.1.1 for a full description; Follows and Dutkiewicz, 2002; Dutkiewicz *et al.*, 2001).

Convection is manifested by a deep mixed layer. However, during AMT 10, a convective supply is only likely to be significant in the northern latitudes, since elsewhere the diagnosed mixed layer was thin (<80m) and had low surface nitrate concentrations (<0.5μM) (Figs 4.1 and 4.2, b, respectively). In May 2000, convection and lateral wind-driven transfer were probably responsible for the elevated [NO_3^-] and [PO_4^{3-}] along the northern flanks of the subtropical gyre (Williams and Follows, 1998; Williams *et al.*, 2000). Indeed, the top 100m of the water column was near isothermal in a region where in late spring, post bloom stratification might have been expected (25° N to 46°N, Figure 4.1). The lack of seasonal stratification was attributed to strong mixing from the passage of storms that had broken down any early stratification in these waters. Average wind speed on AMT 10 was 29.5 knots (see Figure 3.7) compared to 19.5 knots on AMT 2, during which stratification was observed (Gallienne, 2000). The

localised occurrences of N_2 fixation in this region may have been due to the deleterious effects of the adverse wind, changing the vertical position of surface-dwelling communities (Orcutt *et al.,* 2001). In support, Walsh (1996) found N_2-fixation accounted for 34% of the new production during strong upwelling and 77% during weaker fluxes of nitrate at the Venezuelan upwelling system.

4.3.3.2.2. Ekman Transfer

Ekman transfer is the wind induced horizontal transport of the surface layer of the ocean (see section 3.3.1.2). Ekman transfer is important at the intergyre boundary of the North Atlantic and may transport 0.03 to 0.06 mol N m^{-2} yr^{-1} (Williams and Follows, 1998), comparable in magnitude to rates of N_2 fixation (see Chapter 5).

High physical variability is usually observed between the Falklands and Montevideo south of 32.80 °S (Aiken *et al.,* 2000, Gibb *et al.,* 2000). In April 2000, eddy activity extended north of Montevideo (to 29°S, 43°W) along the offshore edge of the tongue of warm water from the Brazil-Falklands Current Confluence Zone (BFCCZ) (Figure 4.18). Ekman transport was probably responsible for the slightly elevated concentrations of NO_3^- and chlorophyll *a* observed at the southern flanks of the south Atlantic subtropical gyre. Such mechanisms for transient nutrient supply have been proposed (McGillicuddy *et al.,* 1998) and observed (Metzler *et al.,* 1997) in oligotrophic regions. However, NO_3^- would be rapidly depleted over a horizontal scale of typically 500km by N-starved phytoplankton and thus, its limited penetration into the gyre cannot explain the isotopic signals observed in the centre of the gyre. Hansell and Waterhouse (1997) observed near zero nitrate concentrations in recently upwelled, advected water at 15°S in the equatorial Pacific, but increasing levels of DON. Indeed,

there is evidence to suggest that organic nutrients, *i.e.* DON, may be advected further into the gyre (Michaels *et al*., 1997; Abell *et al*., 2000)).

Figure 4.18 AVHRR composition of sea surface height anomaly for AMT 10 cruise track off Uruguay/Brazil shelf showing the extent of the eddy event at the southern flanks of the South Atlantic subtropical gyre (Gallienne, 2000).

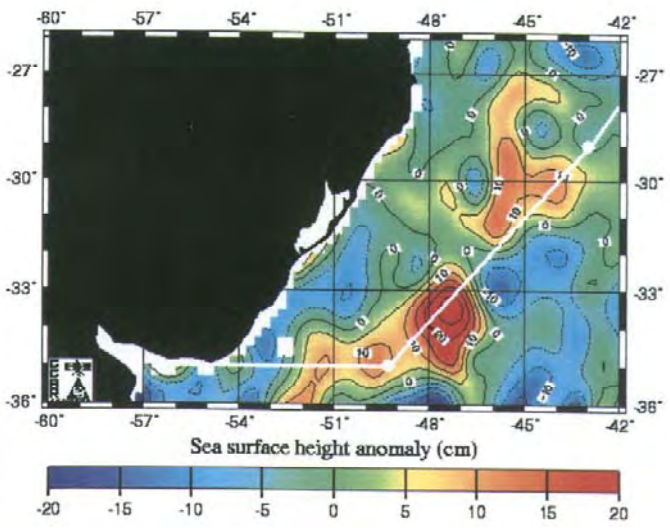

4.3.3.3. Fine scale processes

Gyre scale processes appear to be important in the transfer of nutrients in the northern latitudes, on a seasonal timescale or on the flanks of the subtropical gyres. Over the central part of the subtropical gyres, the NO_3^- might be supplied to phytoplankton through fine-scale transient upwelling from the deep ocean.

4.3.3.3.1 Eddies

A conceptual model describing the effects of fine-scale upwelling on a N-starved surface phytoplankton community in the open ocean is presented in Figure 4.19 (McGillicuddy *et al.*, 1997). Uplift of the nutricline into the euphotic zone would inject nutrients into the sun-lit surface ocean, promoting a phytoplankton response. Depression of the nutricline into the dark interior would not induce a biological response. The asymmetrical distribution of nutrients and light results in a net upward transport of nutrients and net production. This mechanisms may be excited by the

passage of mesoscale eddies (McGillicuddy and Robinson, 1997; Siegel *et al*., 1999) and planetary waves *(*Uz *et al.*, 2001), as well as through the development of sub-mesoscale frontal circulations (Mahadevan and Archer, 2000; Levy *et al.*, 2001).

Figure 4.19. Response of surface phytoplankton to uplift of nutricline into the nutrient depleted euphotic zone. Uplift of the nutricline promotes an ecosystem response and phytoplankton growth whereas depression of the nutricline results in no net ecosystem response. Such rectified inputs of nutrients may be initiated by fine-scale upwelling processes. Adapted from McGillicuddy and Robinson (1997).

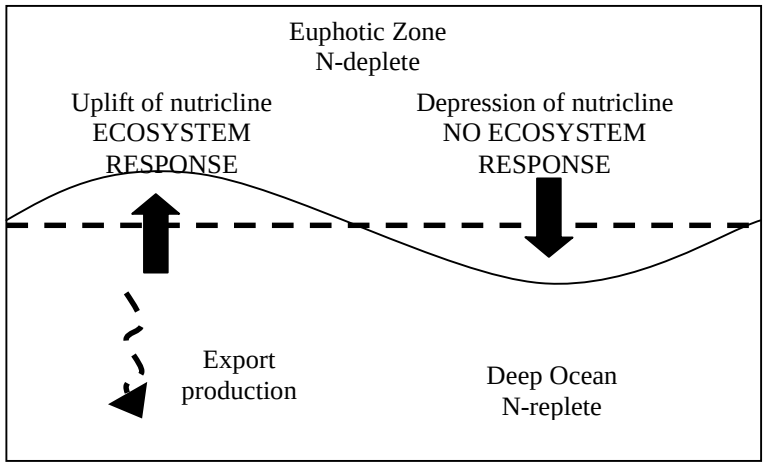

In contrast to previous studies relying on snapshots of hydrographic or remotely sensed data (McGillicuddy and Robinson, 1997; Siegel *et al*., 1999; Uz *et al.*, 2001), the view presented in this study is based upon the longer term isotopic signals of PON, which has a residence time in the euphotic zone lasting tens of days (Waser *et al.*, 2000). The isotopic signals (δ^{15}N PON) thus reflect nitrate utilisation integrated over the residence time for phytoplankton in the euphotic zone (Altabet and Francois, 1994).

In support of the findings of the present study, there have been a number of previous observations of phytoplankton response to eddy-induced nutrient injections to the surface ocean in the Sargasso Sea (BATS) and North Pacific subtropical gyre (HOTS) (Glover *et al.*, 1988; Metzler *et al*, 1997; McGillicuddy *et al.*, 1998, Letelier *et al.*, 2000). The nitrate supplied (27 nM, Glover *et al.*, 1988; 1.4 μM McGillicuddy *et al.*, 1998; 20 μM, Letelier *et al.*, 2000) was sufficient to induce a significant increase in

production. Glover *et al.,* (1988) observed a surface *Synechococcus* bloom 3 times more productive than previous observations in this region. McGillicuddy *et al.,* (1998) observed the highest chlorophyll *a* concentrations recorded to date at the BATS site. In contrast, Letelier *et al.,* (2000) observed a physiological rather than community response at the HOTS site in the subtropical Pacific, evident from an increase in cellular chlorophyll *a* efficiency. In the former two studies, a phytoplankton response was observed only a few days after the nutrient injection but persisted from 5 days, until nitrate was completely depleted (Glover *et al.,* 1988) to 30 days (McGillicuddy *et al.,* 1998), exemplifying the large temporal variability of such stochastic events. However, the delay in the response of phytoplankton to the nutrient injection implies that it is not the ambient nutrient concentration but rather the cellular nutrient concentrations that determine productivity. Indeed, this is supported by culture studies by Waser *et al.,* (1999), who found that the N status of the cells (N-starved or N-replete) determined the isotope kinetics of ammonium uptake, rather than the ammonium concentration. Additionally, the response of the microbial community to these vent scale phenomenon will also depend upon the frequency and duration of the pulse (Harris, 1980, Robarts *et al.,* 1998).

The response of N-starved phytoplankton to nutrient additions is also supported by nutrient addition experiments in central gyres (Graziano *et al.,* 1996; Dufour *et al.,* 1999), although the response of phytoplankton may be dependent on the pre-conditioning nitrogen source, the degree of nitrogen deficiency and the species composition (Dortch 1990; Dortch *et al.,* 1991; Cochlan and Harrison, 1991). Stochastic events are difficult to observe without moored instruments, as the time required for phytoplankton to remove nutrients (days) is less than that of the supply mechanism (weeks). Monthly sampling at HOTS site in the subtropical Pacific revealed 3 major

pulses of nitrate to the subtropical surface ocean in 9 years, which was attributed to eddy activity. However, the low frequency was more likely due to under-sampling (monthly) rather than a reflection of actual frequency of the events. Furthermore, the response of phytoplankton to nanomolar injections of nitrate emphasises the need for the detection of nutrients at nanomolar concentrations (Glover *et al.,* 1988), which was not available in the present study.

Nevertheless, how significant are these events? It has been speculated that stochastic eddy-induced production may represent a significant fraction of the annual production in the open ocean. McGillicuddy and Robinson (1997) and McGillicuddy *et al*., (1998) estimated eddies may supply 0.19 ± 0.1 to 0.35 ± 0.1 mol N m^{-2} yr^{-1}, respectively to the Sargasso sea, thus requiring 4 events per year to close the annual nitrogen budget at BATS. How realistic is this? At present, the frequency of such events is unknown.

In Chapter 3 of this study, apparent undulations in the MLD observed during AMT 3 and 5 were considered to reflect the choice of method used to define the MLD. However, alternative methods of defining the density gradient also revealed an undulating MLD. Although speculative, these vertical migrations in the MLD in a downwelling environment may be remnants of fine-scale upwelling processes.

4.3.3.4. Validation of the physical transfer of nitrate to the oligotrophic ocean

In the present study, the author concludes that surface phytoplankton (7m) communities respond to injections of nitrate from the deep ocean, although the mechanisms of supply are unclear. Here, it is assumed that the nitrate from the deep ocean has an isotopic composition of 5 to 6 ‰ and that this reaches the surface phytoplankton community and is utilised completely or with some degree of isotopic fractionation. However, there are a number of inconsistencies in this scenario. Maranon

et al., 2000 observed no significant change in the phytoplankton community structure with depth and concluded that surface samples represent the water column phytoplankton community. If this is true, it implies that nitrate from the deep ocean passes through a deep phytoplankton community, whilst its stable isotopic composition remains unaltered. Furthermore, the response of individual species to nutrient injections should be considered.

Chemotaxonomic and phytoplankton counts indicate that the cyanobacteria, *Synechococcus* spp. and *Prochlorococcus* spp. and small (< 5 μM) flagellates dominate the phytoplankton community in the tropical and subtropical Atlantic (this study, see Section 4.1.2.1; Gibb *et al.,* 2000; Barlow *et al.,* 2002), accounting for 70 to 90% of the total photosynthetic C biomass (Maranon *et al.,* 2000). *Prochlorococcus* spp. tend to be geographically limited to latitude 40°N to 40 °S, but are replaced by *Synechococcus* spp. in cooler waters (Zubkov *et al.,* 1998, 2000; Moore *et al.,* 2002). More importantly, there are significant differences in the vertical position of the genus depending on light and nutrient availability (Moore *et al.,* 1995; Moore and Chisholm, 1999). Low light-adapted *Prochlorococcus* spp. occupy a position deep in the water column have the ability to grow on regenerated N and nitrite, thus exploiting deep nitrite pools (Olson, 1981; Dore and Karl, 1996). High light-adapted *Prochlorococcus* spp. are restricted to surface waters (West *et al.,* 2001), and can grow at near maximal growth rates on regenerated N alone (Partensky *et al.,* 1999). Both *Prochlorococcus* spp. communities are unable to use nitrate for growth (Moore *et al.,* 2002). In contrast, *Synechococcus* spp. can grow on nitrate, nitrite and regenerated N (Glibert *et al.,* 1986; Paerl 1991; Lindell *et al.,* 1998; Collier *et al.,* 1999; DuRand *et al*., 2001), but tend to be limited to the surface layer of the ocean (Partensky *et al*., 1999, Barlow *et al.,* 2002). This layering appears to be common in the open ocean. Barlow *et al*., (2002) observed a dominance of

cyanobacteria, diatoms and prymnesiophytes in upper water column, diatoms and nanoflagellates in subsurface layers and green flagellates in the deep layers of the equatorial Atlantic. Such a layered community structure has important implications. Firstly, the isotopic signals ($\delta^{15}N$) observed in the surface ocean are not representative of the whole phytoplankton community in the water column in some regions of the Atlantic. Deep phytoplankton communities, adapted to lower light regimes and capable of utilising nutrient sources that are not available to surface communities, possibly of the same species, are suspected to have different $\delta^{15}N_{SPM}$. Secondly, the inability of deep *Prochlorococcus* communities to utilise nitrate would permit eddy-induced injection of nitrate to penetrate into the euphotic zone, without altering its isotopic composition. In conclusion, the heavy isotopic signals observed during AMT 10 may be attributed to the ability of surface dwelling *Synechococcus* spp. to utilise nitrate and their vast abundance in the open ocean.

The layered community structure of *Prochlorococcus* spp. and *Synechococcus* spp. is not ubiquitous in the open ocean and, therefore, there must be additional factors which result in the $\delta^{15}N$ of the surface community resembling that of deep nitrate. Over the period of an eddy event, the surface waters may resemble an open system with an infinite but low supply of nitrate to the surface populations. However, this may only last for one month after which the system would return to being closed. Nitrate in the euphotic zone would then be rapidly utilised by phytoplankton, returning the euphotic zone to oligotrophy. Hence, the $\delta^{15}N$ of the phytoplankton would resemble that of the deep $\delta^{15}N$ nitrate. The range in $\delta^{15}N$ PON observed in the present study may thus reflect the relative strength of eddy-induced nitrate supply or frequency of the eddy event. Indeed, Waser *et al.,* (2000) concluded that the subtropical Atlantic was an open rather than closed system.

4.3.3.5. Atmospheric source of nitrogen

The relative importance in atmospheric inputs of inorganic and organic nitrogen to the oligotrophic open ocean is controversial (Knap *et al.,* 1986; Fanning, 1989; Owens *et al.,* 1992; Cornell *et al.,* 1995), mainly due to under-sampling and the episodic nature of significant atmospheric events. Although some studies suggest atmospheric deposition is a significant source of N to the open ocean (Owens *et al.,* 1992), supplying 50% of the annual N requirement at BATS, others deem the N input insignificant (Knap *et al.,* 1986). However, recent evidence suggests that DON may represent a substantial fraction of N in rainwater, representing 2 to 84% of the total N deposited annually, of which 45 to 75 % is bioavailable (Seitzinger and Sanders, 1999)

The contribution of atmospheric N to the surface ocean and its biological incorporation could be assessed by considering the stable isotopic composition of atmospheric N species. However, the $\delta^{15}N$ of atmospheric inorganic and organic species is highly variable (Cornell *et al.,* 1995; Yeatman *et al.,* 2001; Yeatman *et al.,* 2001). The atmospheric $\delta^{15}N$ NO_3^- composition was from $+7 \pm 6‰$ and $-1 \pm 3‰$ for a coastal and open ocean site, respectively, whereas $\delta^{15}N$ NH_4^+ was $+ 6 \pm 6‰$ and $- 9 \pm 8$ ‰ for an open ocean and coastal site respectively (Yeatman *et al.,* 2001). Cornell *et al.,* (1995) found DON to be a significant component of atmospheric aerosols and in remote regions, being the dominant form of fixed N. However, the $\delta^{15}N$ DON ranged from – 8 ‰ to + 6 ‰ for 10 sites ranging from coastal to the open ocean. Thus, the range in $\delta^{15}N$ of atmospheric N species makes it impossible to determine their importance in the present study. In addition, the bioavailability of atmospheric DON is largely unknown.

4.3.3.6. F ratio and new nitrogen supplies

The *f* ratio is defined as the ratio between new production (fuelled by new N), to total production (production fuelled by regenerated N plus new production (Eppley and Peterson, 1979). Classically, primary production in oligotrophic regions is reported to be is fuelled by regenerated N (i.e. NH_4^+) and therefore, defined by a low *f* ratio (< 0.5; Dugdale, 1967; Eppley and Peterson, 1979; Glibert and McCarthy, 1984). Indeed, Eppley and Peterson (1979) set the canonical value of 0.06 for central gyres and 0.13 for transitional zones between subtropical and subpolar regimes; sediment trap studies in the Pacific Ocean (0.14; Martin *et al.,* 1989) and Sargasso Sea (Altabet *et al.,* 1986; 1988; 1989) support such estimates. In this study, isotopic enrichment of phytoplankton (δ^{15}N PON) over much of the south Atlantic subtropical gyre reflects the uptake of nitrate delivered from the deep ocean by a number of possible mechanisms. This contradicts the classic view of primary production in oligotrophic regions, as implied by the *f* ratio, and raises the question; can low *f* ratios and isotopically heavy phytoplankton be reconciled over subtropical gyres.

f ratios are measured by the addition of ^{15}N-labelled nitrate and ammonium to phytoplankton communities at 10% of the ambient nutrient concentrations, and subsequent isotopic analysis of PON to determine the uptake of ^{15}N-nitrate and ^{15}N ammonium. This is a particular challenge in oligotrophic regions, where nutrient concentrations are near the detection limits of chemiluminescent techniques. Addition of nanomolar concentrations of nitrate to oligotrophic waters can increase nitrate by up to 300 % of its ambient concentrations (Rees *et al.,* 1999; Donald *et al.,* 2001). Inhibition of nitrate uptake by ammonium is a well-cited phenomenon (Wheeler and Kokkinakis, 1990; Harrison *et al.,* 1996) but is dependent on high ammonium concentrations rather than the ratio of ammonium to nitrate (Wheeler and Kokkinakis, 1990; Tamminen, 1995). Rees *et al.,* (1999) observed no inhibition of nitrate uptake at

ammonium and nitrate concentrations of 58 nM and 7 nM, respectively, concentrations typical of oligotrophic gyres. Thus, it is questionable if the determination of *f* ratios in oligotrophic waters reliably reflects the nutrient conditions of the water column. Indeed, a well-cited relationship between *f* ratio and nitrate concentrations (Platt and Harrison, 1985; 1986; Harrison *et al.,* 1987) has recently been found to be untrue at the oligotrophic BATS site (Lipschultz, 2001)

There is a great deal of evidence to suggest that the definitions of "new" and "regenerated" N sources require major revision. Studies in the Pacific Ocean suggest that euphotic zone nitrification is a major source of nitrate or nitrite in the surface ocean (Dore and Karl, 1996), thus suggesting that nitrate is a recycled nutrient in stratified waters (Lipschultz, 2001). Exudation of N by N_2 fixers supports production of "new" ammonium (Karl *et al.,* 2002). It is also unclear whether horizontal advection of DON from productive regions into oligotrophic gyres constitutes new or regenerated N. Furthermore, the potential importance of direct assimilation of DON (Palenik and Morel, 1990; Bronk and Glibert, 1993; Berman and Chava, 1999), rapid ammonium cycling (Glibert *et al.,* 1982) and exclusion of atmospheric N inputs (aerosol or N_2 fixation) have raised additional controversy in definition of the *f* ratio.

A number of studies have observed high *f* ratios (> 0.5) in the oligotrophic Atlantic (Koeve *et al.,* 1993; Waser *et al.,* 2000; Donald *et al.,* 2001). Latitudinal variation in the depth-integrated *f* ratio in the Northeast Atlantic was found to increase from the eutrophic into the oligotrophic region and with depth (Donald *et al.,* 2001). This was attributed a shallow nutricline within the euphotic zone, together with enhanced light penetration, permitting nitrate-fuelled phytoplankton growth in an oligotrophic region. The surface (0-30m) *f* ratio was typically oligotrophic but the mixed layer depth integrated result showed that 37-50 % of primary production was

fuelled by nitrate (Donald *et al.,* 2001). Thus, determination of the ratio of new to total production in the surface ocean only misrepresents the water column and does not accurately reflect the nutrient dynamics, especially in oligotrophic regions.

Independent determination of nitrogen dynamics in the subtropical Atlantic ultimately expose the misinterpretation of *f* ratios in oligotrophic regions. Waser *et al.*, (2000) performed two transects between Newfoundland and the Canary Islands. The range in *f* ratio (0.05 to 0.54) implied that over most of the oligotrophic North Atlantic gyre, ammonium was the dominant source of N. However, $\delta^{15}N$ of phytoplankton was heavier (1.32 to 11.29 ‰, mean in spring and autumn, 3.23 and 5.76 ‰, respectively) than previous findings for phytoplankton growth on regenerated N (-2 to + 2 ‰) (Altabet, 1988; Villareal *et al.,* 1993) and indeed, no significant relationship was observed with either ambient ammonium concentrations or uptake rates. Overall, Waser *et al.,* (2000) concluded that nitrate was the dominant control on the $\delta^{15}N$ of phytoplankton, even in oligotrophic regions, and that growth on ammonium had little effect on the $\delta^{15}N$ of phytoplankton, possibly due to the small ammonium inventory relative to surface particulate matter.

Interestingly, the range in $\delta^{15}N$ of phytoplankton (1.84 to 6.89 ‰, excluding the spring bloom region) in the present study is overlaps the observations of Waser *et al.,* (2000; 1.32 to 11.29‰).

4.3.4. Dissolved organic nutrients

4.3.4.1. Latitudinal and depth variation in dissolved organic nitrogen and dissolved organic phosphorus

The vertical distributions of DON and DOP during AMT 10 were similar to those observed in other studies in the open ocean (Jackson and Williams, 1985; Libby and Wheeler, 1997; Vidal *et al.,* 1999; Karl *et al.,* 2001) with elevated concentrations at

the surface and a general decrease with depth. These vertical gradients are maintained by biological production of DON and DOP in surface waters, thus acting as a source, and microbial remineralisation to inorganic N and P in deeper waters, acting as a sink. Such gradients support a vertical flux of DON and DOP from the euphotic zone to the deep ocean. In the subtropical Atlantic, Vidal *et al.*, (1999) estimated that most of the upward flux in NO_3^- into the euphotic zone was exported downward as DON. (The fact that DON export often exceeded the input of NO_3^- implied another source of N to the surface ocean, probably from N_2 fixation). In contrast, DOP accounted for only 9% of the upward PO_4^{3-} flux. However, subsurface (> 50m) elevations in [DON] and [DOP] were also observed (i.e. equator), probably due to high primary production at the thermocline and grazing by zooplankton. Indeed, Vidal *et al.*, (1999) observed net upward flux of DON and DOP in the equatorial Atlantic due to this subsurface maximum.

The latitudinal variation in depth averaged [DON] during AMT 10 was inconclusive. A small increase in [DON] north of the equatorial region was observed, and could be explained by DON exudation by phytoplankton and subsequent horizontal advection of the recently upwelled water (Libby and Wheeler, 1997; Hansell and Waterhouse, 1997). Slightly elevated [DON] coincided with the northern spring bloom, again, due to DON exudation during luxury N consumption. Otherwise, no significant variations were observed.

In contrast, remarkable latitudinal variations in depth averaged [DOP] were observed along the AMT 10 transect, with elevated concentrations observed just south of the equatorial region, at the equator and in the northern subpolar gyre, again, coinciding with the spring bloom. Decreased [DOP] in the northern and southern subtropical gyre imply a possible sink of DOP, as suggested by other authors (Karl *et*

al., 2001, Abell *et al.,* 2000, see section 4.2.5.1). The dissimilarity in DON and DOP distributions implies that different processes are controlling their dynamics in the open ocean. These are discussed in terms of biological and physical controls on their distributions.

4.3.4.1.1. Biological control on DON and DOP

Numerous authors have suggested that biological production, recycling and remineralisation of DON and DOP are uncoupled (Harrison, 1983; Vidal *et al.,* 1999; Karl *et al.,* 2001). This is attributed to the differential biological reactivity or lability of DON and DOP: a substantial part of biologically-derived DON (exuded by phytoplankton and through microbial activity) in surface waters is refractory and therefore exported to deep ocean whereas, most of biologically-derived DOP is labile and recycled in the euphotic zone leading to negligible export to the deep ocean (Jackson and Williams 1985; Smith *et al.,* 1986; Vidal *et al.,* 1999; Karl *et al*., 2001). These differences in reactivity are attributed to the greater molecular complexity of the DON pool (Antia *et al.,* 1991, McCarthy *et al.,* 1997) compared to the DOP pool (Karl and Yanagi, 1997; Suzumura *et al.,* 1998; Kolowith *et al.,* 2001) and heterotrophic activity in the euphotic zone (Zubkov *et al.,* 2000).

In support of these arguments, refractory DON and DOP (defined by deep ocean concentrations), accounted for 2.14 μM (38%) and < 0.02 μM (< 5 %) of the surface DON and DOP pools, respectively, at one specific site in the Atlantic (AMT 10, station 7 at 13.51°S, 32.33°W). Changes in the labile and semilabile DON pools will be obscured by the presence of this considerable refractory pool, partially explaining the lack of significant latitudinal variation in DON. In contrast, variations in DOP reflect the dynamics of the biologically available DOP pools. In the subtropical North Pacific,

Abell *et al.,* (2000) also observed very little gradient in TON, but a distinct gradient in TOP.

N_2-fixing organisms are a significant source of DON, but are P limited (*Karl et al.,* 2001), thus leading to elevated surface DON, but possibly utilising surface DOP (see section 4.2.2.3.). N_2 fixation, along with differential recycling of DON and DOP (see above) overall amplifies the DON pool in the surface ocean but only drives exchange of P between inorganic and organic pools in Atlantic (Figure 4.20). Indeed, numerous studies suggest that the Atlantic is P rather than N limited (Wu *et al.,* 2000).

Figure 4.20. Schematics describing the biological control of the distribution of dissolved organic nitrogen (DON) and dissolved organic phosphorus (DOP).

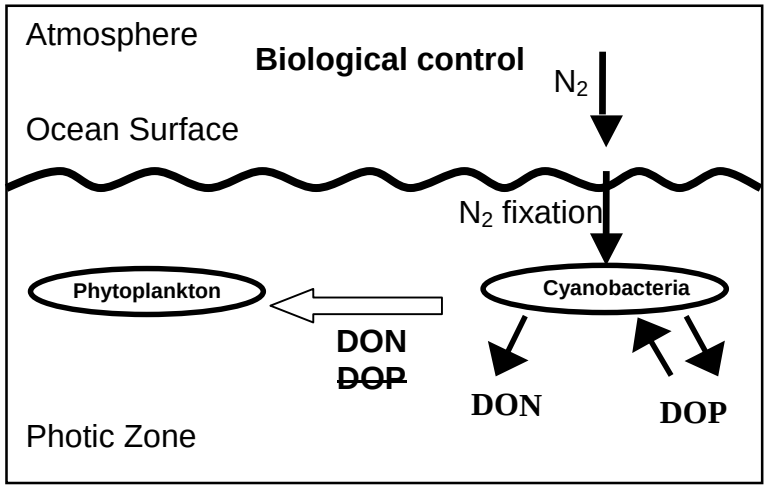

4.3.4.1.2. Physical process controlling DON and DOP

From data collected during AMT 10, it was concluded that there is a significant refractory DON pool in the deep ocean, but negligible DOP (see section 4.2.4). Time-varying upwelling at the equator and at the northern latitudes and subsequent horizontal advection of the water mass into the gyre, would transfer this DON pool to the surface subtropical ocean (Figure 4.21), thus maintaining the refractory DON in surface waters, without an equivalent DOP pool. Indeed, a net upward transfer of DON and DOP has

been observed in the equatorial Atlantic (Vidal *et al.,* 1999). Subsequent downwelling of DON and DOP from the surface subtropical ocean to the deep ocean (black block arrows; Figure 4.21) will transfer high DON to the deep ocean, but relatively (to Redfield) lower DOP, which is mostly remineralised in the surface ocean. Remineralisation of DON at depth maintains deep nitrate concentrations.

It is important to note the timescales involved in the vertical and horizontal transfer of DON and DOP. During the time period required to advect a water mass from the equator or subpolar region to the subtropics (~ 5 years), fine-scale, short lived upwelling events will also cause a flux of DON and DOP between the surface and deep ocean. More importantly, biological utilisation of organic nutrients (although relatively unknown) will remove DON and DOP from the surface ocean. Therefore, it is difficult to determine the source and sink of organic nutrients in these highly dynamic subtropical regions. Hansell and Carlson (2001) demonstrate the importance of convective overturning in controlling the vertical distribution of TOC and TON in the Sargasso Sea.

Figure 4.21. Schematics describing the physical control of the distribution of dissolved organic nitrogen (DON) and dissolved organic phosphorus (DOP) in the surface ocean (1000m). Large scale (thick arrows) and fine scale (thin arrows) vertical transfer of DON and DOP is represented.

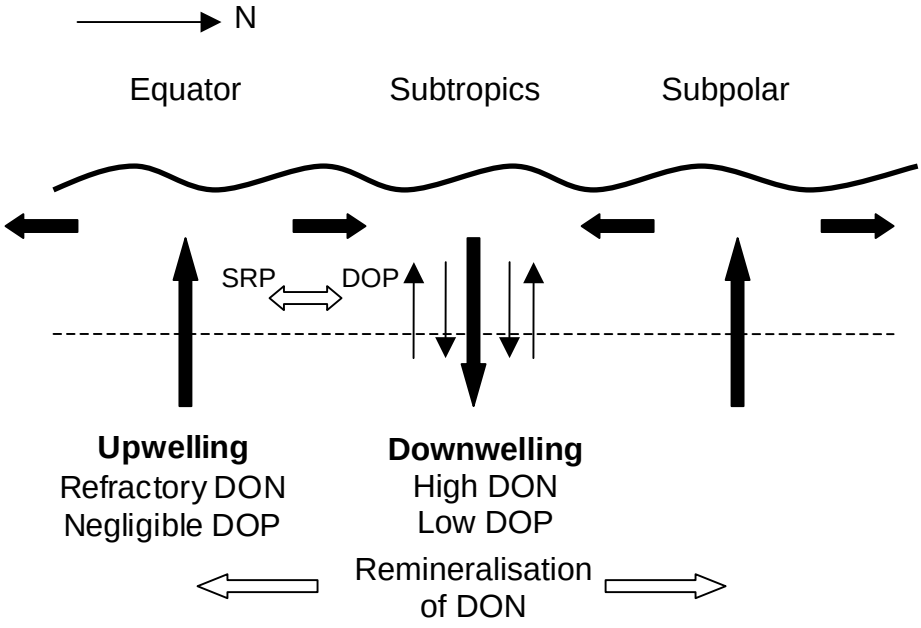

4.3.4.2. Molecular composition of DON

4.3.4.2.1. Amino acids

Concentrations of dissolved free amino acids [DFAA] and total hydrolysable amino acids [THAA] for the oligotrophic Atlantic during AMT 10 were similar to those observed previously in the North Atlantic (Kirchman *et al.*, 1994) and in the Northern Sargasso Sea (Kiel and Kirchman, 1999). Elevated concentrations of both DFAA and THAA in the equatorial and coastal upwelling region off West Africa and northern subpolar region coincided with regions of elevated productivity and probably reflected the active and passive release of DON, including sloppy feeding by grazers (Bronk, 2002).

If it is assumed that DFAA represents a labile fraction of the DON pool, then it would appear that labile DON accounts for < 0.57 % of the DON pool in the AMT 10 samples. However, DFAA does not accurately reflect labile DON for two reasons: 1) other compounds contribute to the labile DON pool, and 2) the release and uptake of DFAA by phytoplankton and bacteria are closely coupled (Fuhrman, 1990). and thus determination of [DFAA] does not represent the entire DFAA pool. Thus, rate measurements are required to determine the significance of amino acids in fuelling primary production.

As for DON, the THAA pool can also be divided into 3 pools (Keil and Kirchman, 1993): a protein with a bacterially mediated turnover time of hours to days, an abiotically glucosated protein and a nonproteinaceous pool which represents bound amino acids with unknown turnover time. During AMT 10, THAA represented less than 10% of the total DON pool. Unlike DFAA, the bioavailability of this pool is questionable as the recovery of protein and nonproteinaceous material using the standard acid hydrolysis method is unknown. Overall, Carlson and Ducklow (1996)

estimate that only 6 to 7 % of the DOM in surface waters can be considered reactive on the time scales of days to weeks, thus reiterating the magnitude of the refractory pool.

4.3.4.2.2. Stable isotopic composition of DON

Methodological difficulties and the complexity of the DON pool have hampered the routine and precise determination of $\delta^{15}N$ DON (see Appendix F). A number of analysts have attempted to determine $\delta^{15}N$ DON using various methods of DON isolation, conversion of DON to inorganic N species and estimation by isotopic mass balance (See Table 4.4). However, no method has yet been routinely and reproducibly developed.

As previous discussed, DON is exuded into the ocean through a number of mechanisms, including both passive and active (Bronk, 2002). However, when in the marine environment, it is somewhat difficult to determine the source, or more often, sources, of DON. Since the $\delta^{15}N$ of specific N sources or processes are distinct (e.g. deep ocean NO_3^- vs. N derived from N_2 fixation), it is assumed that the $\delta^{15}N$ DON will reflect the source of the DON or process involved in its formation. So far, there have been a number of attempts to determine the $\delta^{15}N$ DON (Table 4.6), using both bulk (Feuerstein *et al.*, 1997; Abell *et al.*, 1999) and size fractionated DON (Benner *et al.*, 1997). A number of interesting inferences can be made from the present literature values. Firstly, the $\delta^{15}N$ DON in regions associated with N_2 fixation is apparently isotopically light (-3 to + 2 ‰; Liu *et al.*, 1996; Abell *et al.*, 1999), which is not surprising considering atmospheric N_2 has a $\delta^{15}N$ composition of 0 ‰. This is clear evidence that N_2 fixed by N_2 fixers becomes incorporated in the organic nutrient pool, and maybe a useful tool in tracing this organic nitrogen through the microbial food chain.

Table 4.4. Referenced literature values for the stable isotopic composition of dissolved organic nitrogen (δ^{15}N DON; ‰) determined by both experimental and isotopic mass balance techniques.

SAMPLE	δ^{15}N DON (‰)	METHOD OF DETERMINATION	REF.
Mesocosm experiment	+ 4	Isotopic mass balance	1.
Laboratory cultures	Light	Isotopic mass balance	2.
Kuroshio current, Taiwan	-3 ± 0.2	Isotopic mass balance	* 3.
Culture: Flagellate Ciliate Bacteria	- 20 to + 5 - 5 to + 15 + 5 to + 8	Isotopic mass balance	4.
Pacific: surface deep Atlantic: surface deep Gulf of Mexico: surface deep	7.8 ± 0.8 8.0 ± 0.5 6.6 8.5 to 8.9 9.5 10.2	Tangential Flow ultrafiltration †	† 5.
Lake Superior Lake Michigan	9.9 to 11.0 ± 0.8 6.8 ± 0.2	Dialysis	6.
North Pacific subtropical gyre (12°N to 30°N)	+1.0 to + 2.0	Inorganic analysis and UV oxidation	‡ 7.

* Nitrogen fixers are abundant in Kuroshio water, hence isotopically light DON
† Ultrafiltration was through a 1000 Da membrane and therefore accounts for high molecular weight DON only. The retentate was dialysed, condensed by rotary evaporation and vacuum to a powder prior to isotopic analysis.
‡ Abell et al., (1999) concluded that DON was probably from N_2 fixation
1. Nakatsuka *et al.*, 1992
2. Montoya and McCarthy, 1995
3. Liu *et al.*, 1996
4. Hoch *et al.*, 1996
5. Benner *et al.*, 1997
6. Feuerstein *et al.*, 1997
7. Abell *et al.*, 1999

Benner *et al.*, (1997) determined the δ^{15}N DON in the surface waters and deep ocean of the Atlantic, Pacific and Gulf of Mexico (Table 4.4; Benner *et al.*, 1997) by isolating the DON pool greater than 1000 Da MWCO using tangential flow

ultrafiltration. In general, the found the $\delta^{15}N$ DON to be relatively isotopically heavy (6.6 to 10.2 ‰), possibly indicating that the organism which exuded this DON probably utilised a heavy source of N. More interestingly, they found that the $\delta^{15}N$ DON in the surface and deep ocean were marginally similar, implying that at least at the isotopic level, these DON pools were similar. Since DON in the deep ocean is assumed to represent the refractory DON pool, and its isotopic composition is similar to that in the surface ocean, this implies that DON isolated in the surface ocean (> 1000 Da MWCO), also represents the refractory DON, the more bioavailable molecules being less than 1000 Da. Nevertheless, a slight increase in $\delta^{15}N$ DON is observed between the surface and deep ocean, the lighter signal possibly originating from inclusion of a small fraction of the labile and semi-labile pool (Table 4.4). In agreement with Benner *et al*., (1997), Feuerstein *et al.,* 1997 also found the $\delta^{15}N$ DON to be isotopically heavy in Lake Superior and Lake Michigan, which are regions not associated with N_2 fixation. The isotopically heavy DON pool may not only reflect a refractory DON pool but also the source of N used by the organism which exuded this DON. Culture studies reveal a large range in the $\delta^{15}N$ DON, mostly being determined by isotopic mass balance in cultures (-20 to + 15 ‰; Hoch et al., 1996).

More speculatively, one would expect the $\delta^{15}N$ DON to become heavier as the DON ages, that is, as labile and semi-labile compounds are shunted into the more recalcitrant DON pool. However, this is not a uni-directional process, that is, recalcitrant DON may also be remineralised (albeit over long timescales) to more labile compounds. Until we have greater understanding of the dynamics of DON, the value the determination of $\delta^{15}N$ DON will not be fully appreciated.

4.3.5. How much Nitrogen?

4.3.5.1. Horizontal advection of N and P

The horizontal advection of inorganic and organic nutrients from productive upwelling regions into oligotrophic subtropical gyres is considered a potential N and P supplying process (Rintoul and Wunsch, 1991; Williams and Follows, 1998; Abell *et al.,* 2000; Lee and Williams, 2000). In particular, the horizontal advection of DON and DOP into subtropical gyres may be sufficient to relieve N stress in regions of not associated with N_2 fixation and meet the P requirements or at least relieve P stress for N_2 fixers (Abell *et al.,* 2000; Tyrrell *et al.,* 2002). In this section, horizontal Ekman transport of inorganic and organic nutrients is determined using data from AMT 10. Firstly, the flux of NO_3^-, PO_4^{3-}, DON and DOP is determined using climatological wind data and nutrient data collected during AMT 10. Secondly, the potential supply of nutrients is determined between stations based on flux calculations. Finally, export production sustained by these supplies of inorganic and organic nutrients are determined.

4.3.5.1.1. Determination of the flux and supply of nutrients

The horizontal Ekman flux of nutrients is assessed between stations on AMT 10, using the along track Ekman transport between 2 points, d1 and d2 (Figure 4.22).

Figure 4.22. Schematic representing a conceptual ocean basin depicting; consecutive stations d1 and d2, surface layer thickness, h (m), and meridional velocity (v). Convergence and divergence of water masses is indicated.

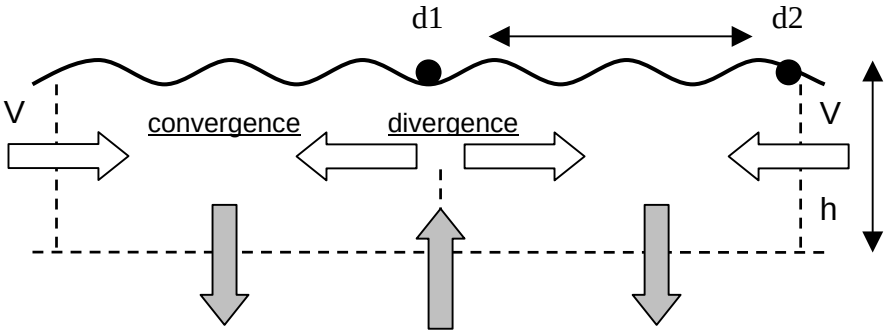

The total flux of nutrients at a station d is described by:

$$h_e v_e N_d \qquad \text{Eq. 4.1}$$

where the product h_e v_e, represents the horizontal Ekman volume flux (m^2s^{-1}) (where h_e is the thickness of the Ekman layer and v_e is the Ekman velocity, however, these terms are not separately diagnosed). The northwards Ekman volume flux is given by $h_e v_e = -\tau_x / (\rho f)$ where τ_x is the eastwards wind stress, f is the Coriolis parameter and ρ is the density. The Ekman volume flux is evaluated from wind vectors from NCEP Reanalysis data set (www.cdc.noaa.gov/cdc/data). The Ekman nitrate flux, $h_e v_e N_d$, is then evaluated using the nutrient concentrations, where N_d is the mean inorganic or organic nutrient concentrations (mmol N m^{-3}) in the surface layer collected during AMT 10. The supply of nutrients is given by the convergence of the horizontal Ekman fluxes between 2 stations, d_1 and d_2:

$$h_e \frac{\partial N}{\partial t} = \frac{\left(h_e v_e N_{d2} - h_e v_e N_{d1}\right)}{y_{d2} - y_{d1}} \qquad \text{Eq. 4.2}$$

A negative flux implies a southward flux of nutrients, whereas a positive flux implies a northward flux of nutrients. Where horizontal fluxes converge, such as over the subtropical gyres (Figure 4.22), nutrients are transported into the surface waters from both the northern and southern flanks. This horizontal nutrient supply can be either utilised by phytoplankton, leading to export production, or be lost through downwelling. Where horizontal fluxes diverge, such as in the equatorial upwelling region, nutrients are transported out of the surface layer, promoting upwelling of nutrients from the deep ocean. Hence, a net supply is only achieved in a downwelling zone when the convergence of the horizontal fluxes exceeds the nutrients being lost through downwelling. Conversely, there is only a net supply in an upwelling zone when the upwelling of nutrients exceeds the loss of nutrients in the surface layer from the

divergence of the horizontal fluxes. Here, the horizontal Ekman supply of nutrients is estimated providing an upper bound for the levels of export production in downwelling zones.

The horizontal flux (mmol N m^{-1} s^{-1}) and supply (mmol N m^{-2} y^{-1}) of NO_3^- and DON is shown in Figure 4.23i and ii, respectively, and the flux and supply of PO_4^{3-} and DOP is shown in Figure 4.24i and ii, respectively. There is a maximum horizontal flux of NO_3^- from the equator northwards at 5 °N (0.3 mmol N m^{-1} s^{-1}) and a southward flux of NO_3^- from ~ 50°N (0.25 mmol N m^{-1} s^{-1}) and from the equator at 5°S (0.25 mmol N m^{-1} s^{-1}; flux direction indicated by black arrows; Figure 4.23i, a). Overall, this pattern of leads to a net supply of NO_3^- over the northern flanks of the north Atlantic subtropical gyre (~ 45°N, ~ 10 mmol N m^{-2} y^{-1}), over the northern and southern equatorial regions (10°N and 10°S; ~ 20 mmol N m^{-2} y^{-1}).

Figure 4.23. Latitudinal variation (35°S to 50°N) in the (i) (a) flux of nitrate (NO_3^-; mmol N m^{-1} s^{-1}) and (b) supply of NO_3^- (mmol N m^{-2} y^{-1}) and (ii) (a) flux of dissolved organic nitrogen (DON; mmol N m^{-1} s^{-1}) and (b) supply of DON (mmol N m^{-2} y^{-1}) diagnosed from nutrient data collected during AMT 10 and the along track Ekman field (see Figure 3.24).

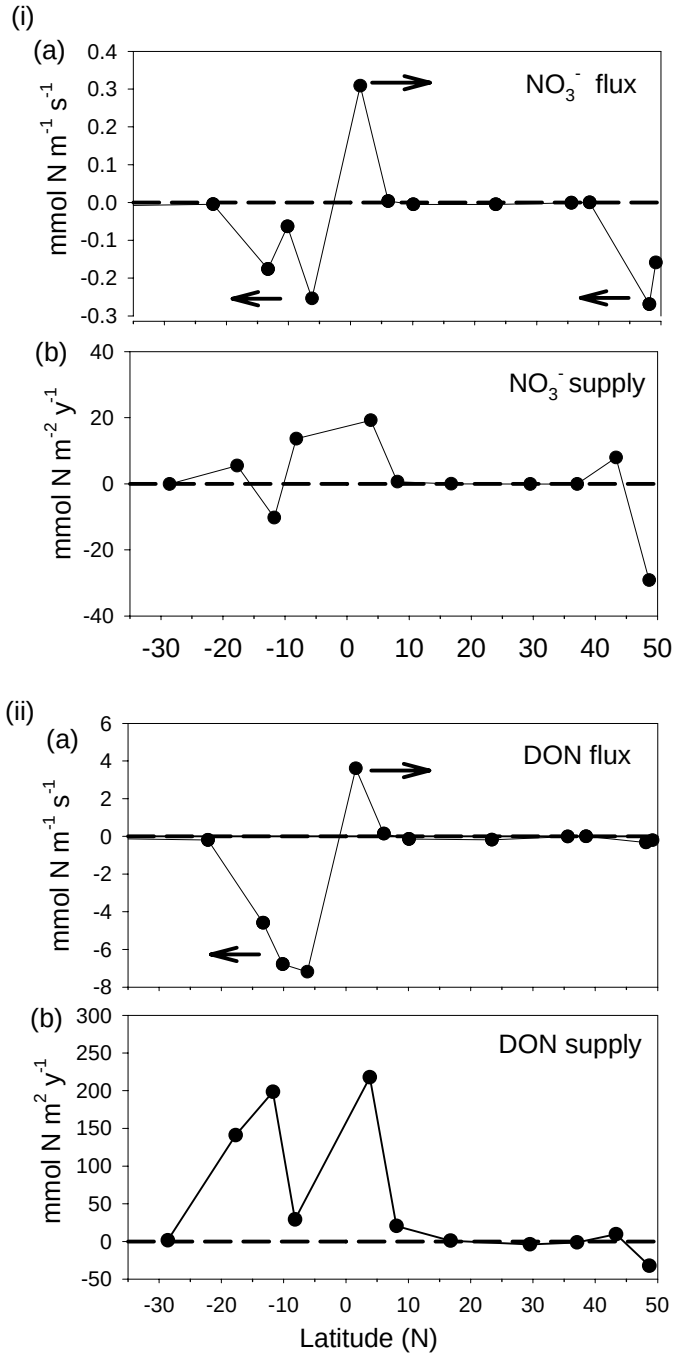

Figure 4.24. Latitudinal variation (35°S to 50°N) in the (i) (a) flux of phosphate (PO_4^{-3}; mmol P m^{-1} s^{-1}) and (b) supply of PO_4^{-3} (mmol P m^{-2} y^{-1}) and (ii) (a) flux of dissolved organic phosphorus (DOP; mmol P m^{-1} s^{-1}) and (b) supply of DOP (mmol P m^{-2} y^{-1}) diagnosed from nutrient data collected during AMT 10 and the along track Ekman field (see Figure 3.24)

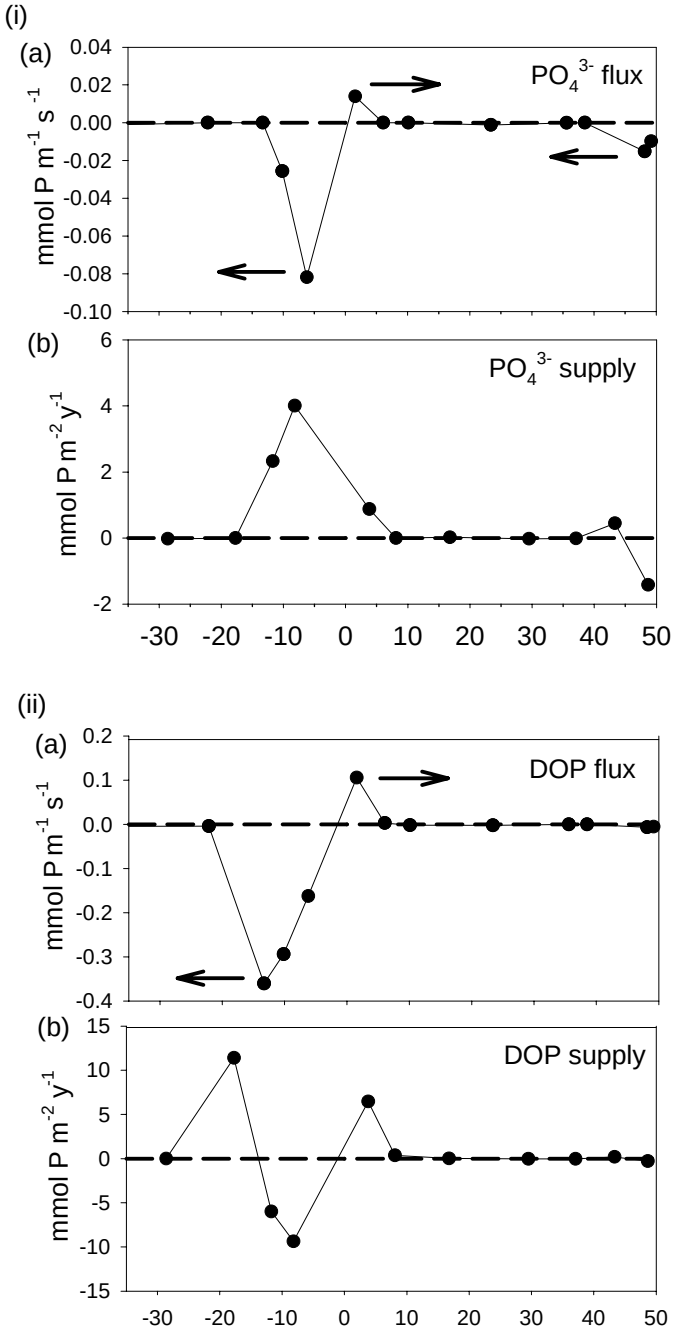

With respect to DON, there is a northward flux from the equator at 5°N (~ 4 mmol N m^{-1} s^{-1}) and a series of southward fluxes between 5 and 15°S, leading to a net supply of DON around the equatorial region (~ 200 mmol N m^{-2} y^{-1}) and south of 10°S into the southern subtropical gyre (~ 200 mmol N m^{-2} y^{-1}). Similar patterns are observed

for the transfer of PO_4^{3-} and DOP, with a net supply of PO_4^{3-} between the equator and 20°S (~ 4 mmol P m^{-2} y^{-1}) and around 40°N (0.05 mmol P m^{-2} y^{-1}), and a net supply of DOP around the equatorial region (6 mmol P m^{-2} y^{-1}) and into the south Atlantic subtropical gyre (12 mmol P m^{-2} y^{-1}).

The conversion of the N or P supplies diagnosed from the convergence of the along track flux to export of organic carbon from the surface to the deep ocean is described by:

$$h_e \frac{dC}{dt} = Rh_e \frac{dN}{dt} \qquad \text{Eq. 4.3}$$

where R is the Redfield ratio (C:N:P = 106:16:1; Redfield *et al.*, 1963) for the nutrient in question. The export production sustained by the flux of inorganic and organic nutrients is reported in Table 4.5.

NO_3^- sustained export production over the north and south Atlantic ranged from 0.4 to 0.98 g C m^{-2} y^{-1} and 0.04 to 1.38 g C m^{-2} y^{-1}, respectively, whereas DON sustained export production was generally higher, ranging from 0.1 to 14.30 g C m^{-2} y^{-1} and 0.06 to 15.69 g C m^{-2} y^{-1} (Table 4.5). The supply of PO_4^{3-} diagnosed along the AMT 10 track sustained 2.96 to 5.10 g C m^{-2} y^{-1} and 0.03 to 1.11 g C m^{-2} y^{-1} over the north and south Atlantic (Table 4.5). Over the south Atlantic, horizontal fluxes of DOP sustained 14.5 g C m^{-2} y^{-1} of export production, whereas in the north Atlantic, DOP fluxes sustained 0.44 to 8.21 g C m^{-2} y^{-1} (Table 4.5). Overall, the flux of organic nutrients tended to sustain greater export production than the flux of inorganic nutrients, in some cases, being equal to or more than the field determined rates of export production.

Table 4.5 Upper bounds for the export production (g C m^{-2} y^{-1}) sustained by the along track horizontal advection of nitrate (NO_3^-), dissolved organic nitrogen (DON), phosphate (PO_4^{3-}) and dissolved organic phosphate (DOP). Calculations are based on the flux of nutrients between stations during AMT 10 and the along track Ekman transport. The mid-station is the position between the 2 stations from which data was used to diagnose the flux, *i.e.* ((d2-d1/2)+d1). Estimates giving a significant supply and upper bound to export production are in bold.

	MID-STATION	NO_3^-	DON	PO_4^{3-}	DOP
South Atlantic Ocean	28.60°S	0	0.10	0	-0.01
	17.72°S	0.40	**10.41**	0	**14.5**
	11.74°S	-0.74	**14.30**	2.96	-7.63
	8.19°S	**0.98**	**2.10**	5.10	-11.92
North Atlantic Ocean	3.81°N	**1.38**	**15.69**	1.11	**8.21**
	8.09°N	0.04	**1.47**	0	0.44
	16.76°N	0	0.06	0.03	0
	29.50°N	-0.01	-0.29	-0.03	-0.05
	37.06°N	-0.01	-0.09	-0.01	-0.03
	43.32°N	0.57	0.69	0.57	0.24
	48.66°N	-2.11	-2.33	-1.80	-0.37

4.3.5.3. Discussion

Estimates of the horizontal supply of NO_3^- determined in this study (5 to 20 mmol N m^{-2} y^{-1}; Figure 4.23i, b), are in accord climatological with diagnostics by Williams and Follows (1998) over the North Atlantic (50 mmol N m^{-2} y^{-1}). However, horizontal advection of DON is up to one order of magnitude higher (~ 200 mmol N m^{-2} y^{-1}; Figure 4.23ii, b) than the NO_3^- supply over the southern subtropical gyre, adding credence to the importance of lateral advection of organic nutrients. Additionally, the supply of DOP (0.24 to 14.5 mmol P m^{-2} y^{-1}; Figure 4.24ii, b) into the subtropical

Atlantic are of a similar magnitude (or higher) to estimates in the subtropical Pacific (4.4 ± 1.0 mmol P m^{-2} y^{-1}; Abell *et al.*, 2000), where horizontal supplies of TOP are estimated to supply up to 40 % of the particulate P export. This supply of organic nutrients may be partly important in closing the N budget over the north Atlantic (Rintoul and Wunsch, 1991; Ganachaud and Wunsch, 2002).

In general, the supply of organic nutrients is higher than inorganic nutrients. This may be attributed to two factors. Firstly, the lifetime of NO_3^- (days) is much shorter than organic nutrients (months to years) in oligotrophic environments (Anderson and Williams, 1999). This is partially due to the molecular complexity of DON compared to NO_3^-, leading to the rapid uptake of NO_3^- compared to DON by phytoplankton. However, as illustrated in this study, only a small fraction (~ 10%; see section 4.3.4.1.1) of the DON pool may be available (directly or through microbial breakdown) to phytoplankton. Therefore, estimates of export production sustained by organic nutrients are an upper bound. Therefore, a true estimate of export production sustained by organic nutrients may be only 10% of the values shown in Table 4.5.

Secondly, not all nutrients supplied to the subtropical ocean by horizontal convergence will be utilised by phytoplankton, as a fraction will be downwelled or subducted as organic nutrients. Thus, the exported production estimated in this study again represents an upper bound for the possible level sustained by horizontal transfer, as losses were not considered.

Estimates of export production over the south Atlantic were generally higher than over the north Atlantic. This was probably due to the weak Ekman pumping field diagnosed over the north Atlantic compared to the south Atlantic for this particular 6 month period. Despite storm events being encountered during AMT 10 in the North Atlantic (see Figure 3.7), the 6-monthly averaged wind vector was relatively weaker.

Estimates of primary production in the subtropical Atlantic derived from satellite data (Sathyendranath *et al.*, 1995) and direct field measurements along the AMT transect (Maranon *et al.*, 2000) are ~ 100 g C m^{-2} y^{-1}. Assuming that only 10 % of the primary production leaves the euphotic zone, export production is estimated to be 10 g C m^{-2} y^{-1}. Therefore, export production sustained by the horizontal advection of DON and DOP from the flanks into the oligotrophic subtropical Atlantic Ocean represents from 2 % to greater than 100 % of the diagnosed export production. However, this is reduced to 0.2 to 10 % if the bioavailability of DON is considered, an even less if losses through downwelling and subduction are included.

4.3.5.4. How much new Nitrogen?

In order to estimate the contribution of N to phytoplankton from N sources discussed in the present study, a simple two-member mixing model was applied. Here, it was assumed that the $\delta^{15}N$ of phytoplankton is in equilibrium with the N source, according to the instantaneous product equation (Eq. 1.8, section 1.2.2.3). Conservative choices were made for a heavy-isotopic source of 5 ‰, representing NO_3^- from the deep ocean (Liu and Kaplan, 1989; Sigman *et al.*, 1997) and a light-isotopic source of 0 ‰, representing N from either from N_2 fixation, ammonium or DON (Figure 4.25; Altabet 1988; Carpenter *et al.*, 1997; Abell *et al.*, 1999, respectively).

Figure 4.25. Schematic representing a two-member mixing model, where an isotopically heavy source of N, 5‰ ,represents nitrate from the deep ocean and an isotopically light source of N, 0 ‰, represents a N from N_2 fixation, recycled nitrogen and DON.

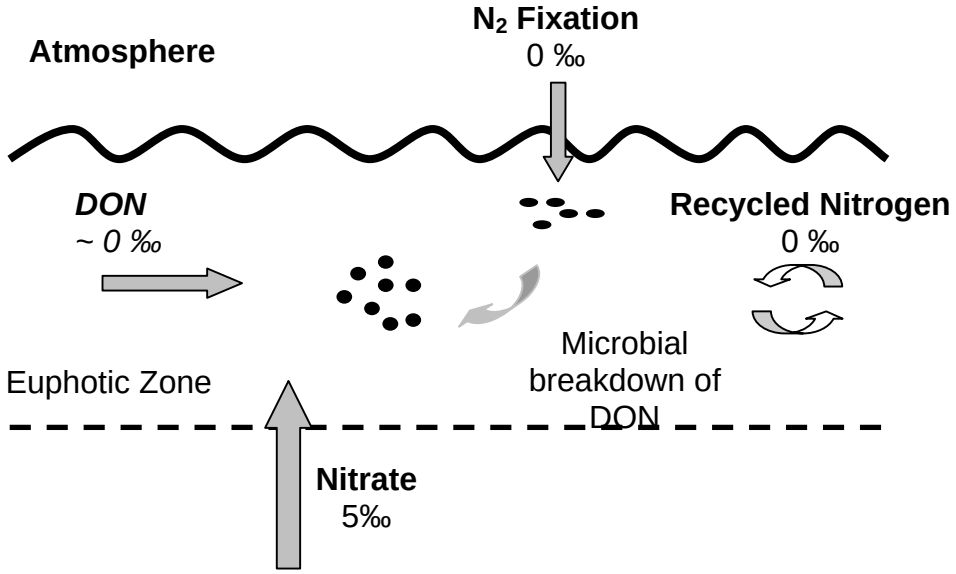

Using the mean δ^{15}N PON for each oceanic region, the relative importance of the two end member N sources was calculated by isotopic mass balance (Table 4.6), as defined by:

$$\%\ \text{heavy source} = \frac{\text{mean}\ \delta^{15}\text{N PON}}{5} \times 100\,\% \qquad \text{Eq. 4.4}$$

This two-member model was only applicable to oligotrophic regions where no net isotopic fractionation is expected, i.e. in a closed system.

Table 4.6. Mean δ^{15}N PON ± 1 standard deviation (σ), number of observations (n) and the percentage of nitrate supporting primary production, calculated using the two-end member isotope model, where there is a light source of N (0‰) and a heavy source of N (5 ‰) for 5 latitude bands in oceanic regions in the Atlantic Ocean.

OCEANIC REGION	LATITUDE	MEAN δ^{15}N PON ± 1 σ	N	% NITRATE
South Atlantic subtropical gyre	36°S to 6°S	4.06 ± 0.46	8	82
Equatorial and coast upwelling region	5°S to 23°N	4.75 ± 0.3	16	95
North Atlantic subtropical region	24°N to 32°N 33°N to 38°N 39°N to 48°N	2.25 ± 0.36 3.16 ± 0.41 - 0.72 ± 0.52	9 6 13	45 63 na

The heavy isotopic signals over the southern subtropical gyre, the tropics and parts of the northern subtropical gyre suggest that the nitrate supply accounts, respectively, for 82 %, 95 % and 63% of the N uptake by phytoplankton (Table 4.6). In contrast, nitrate supplies only 45% of the nitrate requirement in the north Atlantic subtropical region, implying either N_2 fixation, ammonium or DON may represent 55% of the N demand of phytoplankton in this localised area. Considering the additional evidence suggesting that N_2 fixation was an important N supplying pathway in this region during AMT10, 55% of the N demand was probably through N_2 fixation.

This model is crude as it assumes that the $\delta^{15}N$ of deep ocean nitrate is constant over the Atlantic basin. There is evidence to suggest that N_2 fixation would lower the $\delta^{15}N$ of nitrate (Liu *et al.*, 1996). Also, a $\delta^{15}N$ of nitrate of 5 ‰ has been chosen as a conservative estimate from literature values (Liu and Kaplan, 1989, Sigman *et al.*, 1997, Waser *et al.*, 2000), yet some $\delta^{15}N$ PON are more enriched than 5‰. This may imply utilisation of atmospheric N of heavy isotopic composition (see section 4.3.3.5).

4.4 Conclusions: Analysis of the AMT 10 Transect

1. During AMT 10, 4 distinct ocean regions were sampled, the oligotrophic, subtropical gyres of the north and south Atlantic, the productive equatorial and coastal upwelling region off northwest Africa, and the eutrophic north Atlantic subpolar region, in which a phytoplankton bloom was observed.

2. The phytopigment distribution during AMT 10 revealed a dominance of prokaryotic picoplankton over much of the north Atlantic, being succeeded by eukaryotic nanoflagellates north of 35°N.

3. [DON] and [DOP] concentrations determined during AMT 10 were found to be highest in surface waters and decrease with depth. DON concentrations in the deep

ocean (1000m) represented ~ 30 ‰ of that found in the surface ocean, whereas negligible DOP was found in the deep ocean, reflecting differential recycling of N and P in the water column.

4. Whereas [DON] did not vary significantly over the Atlantic during AMT 10, striking changes in the [DOP] were observed, possibly reflecting the addition of DON to the surface nutrient pool through N_2 fixation, without a similar input of DOP. In addition, physical processes transporting DON and DOP from the deep to the surface ocean may also explain the differences in their distribution.

5. Although DON dominated the total dissolved nitrogen pool (60 to 100%), the labile and semi-labile DON pools accounted for < 1 % and < 10 % of the DON pool, respectively, as implied by the contribution of dissolved free and total hydrolysable amino acids to the organic N pool, respectively. This confirms that a large part of the DON pool is refractory, that is, unavailable to phytoplankton over short timescales (weeks to months).

6. Light stable nitrogen isotopic signals of PON over part of the north-eastern Atlantic Ocean imply a localised region of N_2 fixation. This is supported by phytopigment, organic nutrient and N* data. During AMT 10, a significant input of dust from the Sahara was observed, and it is speculated that this dust storm may have caused iron, or possibly phosphorus fertilisation in this region, stimulating N_2 fixation, which may supply 50% of the N requirement in this region.

7. Heavy stable nitrogen isotopic signals of PON over much of the AMT 10 transect imply that phytoplankton were utilising a heavy source of N. Gyre- and fine-scale upwelling of isotopically heavy nitrate from the deep ocean and utilisation of this N source with negligible isotopic fractionation may explain this observation. Indeed,

fine-scale upwelling of nitrate may supply up to 95% of the N requirement in the subtropical Atlantic along the AMT 10 transect.

8. Estimates of the horizontal Ekman transfer of inorganic and organic nutrients revealed that the supply of DON and DOP from productive regions into the oligotrophic subtropical gyres may fuel greater export production than inorganic nutrients. However, the relatively unknown lability of the organic nutrient pools adds doubt to such estimates.

5.1. Conclusions

The deep ocean represents a potential long-term sink for atmospheric carbon dioxide. An understanding of the nutrient supply and thus, biologically mediated export of particulate organic matter from the surface ocean in such vast areas is fundamental if we are to monitor the response of the oceans to climate change (del Giorgio and Duarte, 2002). Subtropical gyres account for 60% of the surface area of the world's oceans and Emerson *et al.*, (1997) have estimated that these vast downwelling regions are responsible for up to 40% of the global ocean uptake of carbon.

In Part One of Chapter 3 of this study, the seasonal and interannual variability in sea surface properties (< 250 m; temperature, salinity and density) was assessed for Spring and Autumn Atlantic Meridional transects since 1995. In addition, derived parameters, such as the mixed layer depth, the Ekman pumping field and ocean boundaries were determined. The asymmetrical seasonal variation in the physical structure of the Atlantic was more prominent than the interannual variability. The large subtropical gyre structures were a dominant and persistent feature throughout, whereas the equatorial region and coastal upwelling region exhibited both seasonal and interannual variability, upwelling generally being stronger and more prominent in Spring than Autumn. Convection and Ekman transport were found to strongly influence the distribution of phytoplankton through the supply of nutrients. While convection is important over the high latitudes, Ekman transport is of greater influence over the flanks of the subtropical gyre. Sea surface properties did not correlate well with the atmospheric anomaly, the North Atlantic Oscillation, which tends to influence the western more than the eastern Atlantic Ocean. Additionally, assessment of the seasonal and interannual variability in the ocean boundaries was hampered by changes in the cruise tracks and inherent problems in defining the boundaries.

In the Part Two of Chapter 3, inorganic nutrient data from AMT cruises since 1995 and organic nutrient data from AMT 10 was used to attempt to reconcile which nutrient, N or P, limited primary production over the Atlantic. The complementary, although dependent, use of nitrate to phosphate (NO_3^-: PO_4^{3-}) ratios and N* allowed inferences to be made regarding which processes controlled the nutrient dynamics in the north and south Atlantic. In the north Atlantic, elevated NO_3^-: PO_4^{3-} ratios and elevated N* (> 2.5 μmol kg^{-1}) implied a region of excess N. In the south Atlantic and over the equatorial region, relatively low NO_3^-: PO_4^{3-} ratios and low N* values (< 2.5 μmol kg^{-1}) reflect P limitation. This pattern may be controlled, in part, by the prevalence of N_2 fixation in the north Atlantic and the absence of N_2 fixation in the south Atlantic, the latter being attributed to the lack of significant aeolian iron inputs. However, the shortfalls and alternative explanations for differential distribution of N and P, and interpretation of N* were also addressed. Whilst there is theoretical evidence to suggest that iron inputs regulate primary production and in turn, influence both the N and P cycle (Cullen, 1999; Falkowski, 1997), some authors believe that N limits present day productivity whereas P limits productivity over geological time (Tyrrell, 1999). However, this is difficult to reconcile considering the long residence time of phosphorus (50,000 years; Van Cappelan and Ingel, 1994), its burial rate in comparison to inputs (~ 1%; Broecker and Peng, 1983), the relatively short residence time (5000 years; McElroy, 1983) and the fast throughput of N (Toggweiler, 1999). The residence time of iron is still unclear and the subject of debate (Johnson *et al.*, 1997; Toggweiler, 1999).

In Chapter 4, the study focused on delineating three potential sources of N to phytoplankton in the surface ocean along the Atlantic Meridional Transect during spring 2000: N_2 fixation by cyanobacteria, the supply of nitrate from the deep ocean by gyre and fine scale processes, and the lateral advection of organic nutrients. Independent

biogeochemical proxies namely, $\delta^{15}N$ of phytoplankton, organic nutrient concentrations, pigment biomarkers and the relationship between nitrate to phosphate, have been used as tools to determine the distribution and relative importance of these processes, as well as postulating on the basin-scale nutrient dynamics.

The supply of nitrate from the deep ocean, possibly by Ekman transport and convection over the flanks of the gyres and eddy inducing mechanisms over the subtropical gyre, is the most dominant and widespread N source observed during AMT 10. Such mechanisms have the potential to challenge the traditional view of the open ocean being environments where phytoplankton productivity is maintained, albeit at low levels (Maranon *et al.,* 2000), by regenerated N over yearly timescales. Evidence from the literature suggests that surface phytoplankton populations respond to new N injections at a community level, thus having the potential to drawdown C as a result of these short and stochastic events (Glover *et al.,* 1988, McGillicuddy *et al.,* 1998; Letelier *et al.,* 2000). Climatological studies and geochemical diagnostics estimate that fine-scale upwelling, by whatever mechanism, can supply up to 0.35 mol N m^{-2} y^{-1} (Table 5.1). If each process is averaged, the sum of the total supply of N by these physical processes is ~ 0.48 mol N m^{-2} y^{-1} (Table 5.1), which is almost equivalent to the geochemical estimates of export production (~ 0.5 mol N m^{-2} y^{-1}; see Table 1.1). From direct observations in the subtropical Pacific, eddy pumping events are estimated to enhance primary production by ~ 20 % (Falkowski *et al.,* 1991). Nevertheless, it is important to note that not only does these stochastic upwelling events supply inorganic nitrogen to the surface ocean, but they also supply dissolved inorganic carbon. Therefore, the potential for these upwelling events to drive the biological pump, that is, to remove atmospheric carbon, is somewhat reduced.

Table 5.1 Estimates of supply of N (mol N m^{-2} y^{-1}) to the surface Atlantic by physical processes of convection, diapycnal and isopycnal mixing, Ekman transport and mesoscale eddies. References (Refs.) for each flux are shown.

PROCESS	METHOD OF ESTIMATION	RATE OF N SUPPLY (mol N m^{-2} y^{-1})	REFERENCES.
Convection	O_2 production Nitrate uptake Climatological model	0.17 ± 0.05 0.09 ± 0.04 0.1 ± 0.2	1. 1. 2.
Diapycnal mixing	Microstructure	0.05 ± 0.01 < 0.015	3. 4.
Isopycnal mixing		< 0.03	4.
Ekman transport	Climatological model	0.03-0.06	5.
Mesoscale eddies		0.19 ± 0.1 0.35 ± 0.1 0.3 0.24 ± 0.1	6. 7. 8. 4.
Total supply of process means		**0.48**	

1. Michaels *et al.,* (1994)
2. Williams et al., (2000)
3. Lewis *et al.,* (1986)
4. Siegel *et al.,* (1999)
5. Williams and Follows (1998)
6. McGillicuddy and Robinson (1997)
7. McGillicuddy *et al.,* (1998)
8. Oschillies and Garcon (1998)

On the gyre scale, the horizontal advection of DON and DOP was the second largest potential source of N and P to the subtropical gyres. Whilst horizontal gradients in DON did not conclusively support significant lateral advection and concomitant export production, horizontal gradients in and lateral transport of DOP are apparently much more important to the oligotrophic Atlantic. However, the potential of lateral advection is complicated by the differential bioavailability of DON and DOP. This study concluded that ~ 35% of DON is refractory and less than 10% may be bioavailable on time-scales of days to weeks. This means that ~ 55 % of the DON pool is uncharacterised and of unknown reactivity. In contrast, from determination of the deep (1000m) DOP concentrations, only 17 % of surface DOP was considered refractory, implying that 83 % of DOP may be available and thus may sustain greater

export production over Atlantic. However, the bioavailability of different DOP fractions was not assessed.

Independent biogeochemical proxies implied that N_2 fixation was a significant process in a localised region of the eastern North Atlantic subtropical gyre, which had apparently been affected by an anomalous dust input, possibly inducing natural iron and/or phosphorus fertilisation of the surface ocean. N_2 fixation is reported to cause significant inputs of new N to the North Atlantic surface ocean, daily areal estimates ranging from 1.4 ± 0.47 µmol N m^{-2} day^{-1} (Carpenter and McCarthy, 1975) to 2100 µmol N m^{-2} day^{-1} (Carpenter and Romans, 1991; Table 5.2).

Table 5.2. Nitrogen fixation rates (µmol N m^{-2} day^{-1}) by *Trichodesmium* colonies over the North Atlantic. Rates were determined by the acetylene reduction method (AR) and mass balance using ^{15}N isotope techniques nitrogen to phosphate diagnostics (N*). Adapted from Lipschultz *et al*, (2002) and Capone (2001).

NITROGEN FIXATION RATE µMOL N M^{-2} DAY^{-1}	LOCATION	METHOD OF RATE DETERMINATION	REFERENCE
41 ± 7.6	0°-24°N	Mass balance (^{15}N) ‡	1.
1.4 ± 0.47	27°-34°N	Acetylene reduction†	2.
6.2 ± 4.0 77 ± 9.7	22°-36°N 12°-22°N	Acetylene reduction†	3.
0.29 ± 0.13	30°N	Acetylene reduction†	4.
2100	< 30°N	Mass balance	5.
278 ± 129 73 ± 22	NE Caribbean 14°-22°N	Acetylene reduction†	6.
197		Mass balance (N*)	7.
15-75	32°N	Acetylene reduction†and mass balance (^{15}N) ‡	8.

† see Capone (1993)
‡ see Montoya *et al.*, (1996)
1. Goering et al., (1966)
2. Carpenter and McCarthy (1975)
3. Carpenter and Price (1977)
4. McCarthy and Carpenter (1979)
5. Carpenter and Romans (1991)
6. Capone et al., (1997)
7. Gruber and Sarmiento (1997)
8. Orcutt et al., (2001)

During an extensive bloom of the diatom *Hemiaulus hauckii* containing the endosymbiont N_2-fixer *Richelia intracellularis* in the tropical Atlantic, CO_2 uptake rates

were high (1.15 g C m^{-2} d^{-1}; Carpenter *et al*. 1999) in comparison to typical open-ocean productivity rates for this region (0.33 to 0.8 g C m^{-2} d^{-1}; Michaels *et al.* 1994). Indeed, N_2-fixation has been cited to be the "missing" term contributing to the apparent imbalance in the current elemental budgets of the ocean (Sambrotto *et al* 1993, Codispoti 1995, Michaels *et al.,* 1996, Gruber and Sarmiento 1997), despite being orders of magnitude smaller than the nitrate supply from the deep ocean (Table 5.1).

The processes of N supply assessed in this study are important over different time scales. Mechanisms inducing fine scale upwelling are short-term stochastic events, which induce short-lived increases in primary production. Indeed, a simulation model comparing the response of a pelagic phytoplankton community to pulsed nutrient supply versus a constant supply, found that injections of nutrients maintained a photosynthetically efficient, complex trophic structure which was eradicated under constant nutrient supply (Wiegert and Penas-Lado, 1995). Horizontal advection of DON and DOP be expected to would act over timescales of years. However, the bioavailability of the DON and DOP must ultimately control their importance as nutrient pools; at present, there is little or no direct evidence for their uptake by autotrophs. In contrast, N_2 fixation has been reported to be responsible for the ecological changes observed since the mid-1980's over the northern subtropical Pacific. At station ALOHA, Karl *et al.,* (1997, 1999, 2001) have observed a greater than 200% increase in primary production, 33 to 100 % increase in chlorophyll *a*, with a simultaneous halving in soluble reactive phosphate and dissolved silica pools. Such dramatic changes have been attributed to increased stratification of the surface water, causing a decrease in the flux of inorganic nutrients from the deep ocean. The decreased supply of inorganic nutrients allows N_2 fixers to out-compete other phytoplankton species. In turn, the exudation of DON by N_2 fixers has resulted in an ecosystem shift

from eukaryotes, *e.g.* dinoflagellates to picoeukaryotes, *e.g. Prochlorococcus*, which have the ability to utilise DON exuded by N_2 fixers (Moore *et al.*, 2002). Thus, the increase in primary production is attributed to the biological sequestration of N_2 in an otherwise N depleted environment. Estimates from this "ecosystem shift hypothesis" infer that primary production has doubled due to the ecosystem shift, increasing the biological pump by 32% (Emerson *et al.*, 1997). However, one questions if our increased knowledge regarding the picoplankton community and their relevance in nutrient cycling as led to more intense investigations into this newly founded microscopic community, or it this dramatic ecosystem shift is real. Further observations over decadal timescales will allow this ecosystem shift hypothesis to be tried and tested.

Although the transition from a nitrate-based to a DON based nutrient supply may shift N into the microbial food web rather than into new production (Bronk and Ward, 1999; Cotner and Biddanda, 2002), DON derived from N_2 fixation constitutes a new source of N, thus having the potential to fuel export production.

Over the AMT 10 transect, a localised input of N from N_2 fixation appears small, compared to fine scale transient upwelling of nitrate or lateral advection of DON over large areas of the subtropical and tropical Atlantic. However, the temporal response of N_2 fixers and their subsequent effects on the global C cycle, has potentially more importance with respect to the long term ecosystem structure. While stochastic mechanisms transport not only nitrate to the surface ocean but also carbon (as dissolved inorganic carbon and DOC, which is highly refractory (Hansell and Carlson, 2001), resulting in zero net export of carbon (McGillicuddy *et al.*, 1998), N_2 fixation draws down atmospheric N_2 and C, thus causing a net drawdown of CO_2. Indeed, Hood *et al.*, (2000) estimate that N_2 fixation is responsible for ~ 14 % of the export of organic carbon.

Our increased knowledge of N sources and N recycling means that the nature of new and regenerated nutrients needs to be reassessed to determine the important processes that ultimately fuel new production. Figure 5.1 represents the recently devised N cycle (Lipschultz *et al.,* 2002). There is great uncertainty regarding their relative importance, as shown by the range in supply rates in Tables 5.1 and Table 5.2. If the total physical supplies of N (0.48 mol N m^{-2} y^{-1}), the mean N_2 fixation rate in the Atlantic (0.015 to 0.05 mol N m^{-2} y^{-1}) and contribution of DON (see section 4.3.5.1.1; 0.004 to 0.2 mol N m^{-2} y^{-1}, note the latter value represents an upper bound) are realistic, then N inputs to the surface ocean almost equal to or possibly exceed the export production estimated over the subtropical Atlantic (see Table 1.1). This implies that either the N budget can be closed, geochemical estimate of export production are inaccurate, or more than likely, the temporal and spatial variability and errors of estimating the N sources, as proposed in this study, are not yet understood. In addition, the accumulation of N as DON and our lack of knowledge on the composition of this dissolved pool adds complexity to closing the N budget.

In conclusion, the spatial variations observed during this study, together with the variations observed during other studies in oligotrophic environments (Karl *et al.*, 2000, Karl *et al.*, 2001, Lipschultz, 2001), challenge the traditional view of oligotrophic gyres or “ocean deserts” as being monotonous, steady-state environments. Instead, these vast regions are highly dynamic on a spatial and temporal scale, and may support changing phytoplankton communities, which have the potential to respond to climate change, or influence the drawdown of atmospheric carbon.

Figure 5.1. Schematic of the traditional and recently recognised pathways (*) for the supply of nitrogen to surface phytoplankton populations. Adapted from Lipschultz *et al.*, 2002.

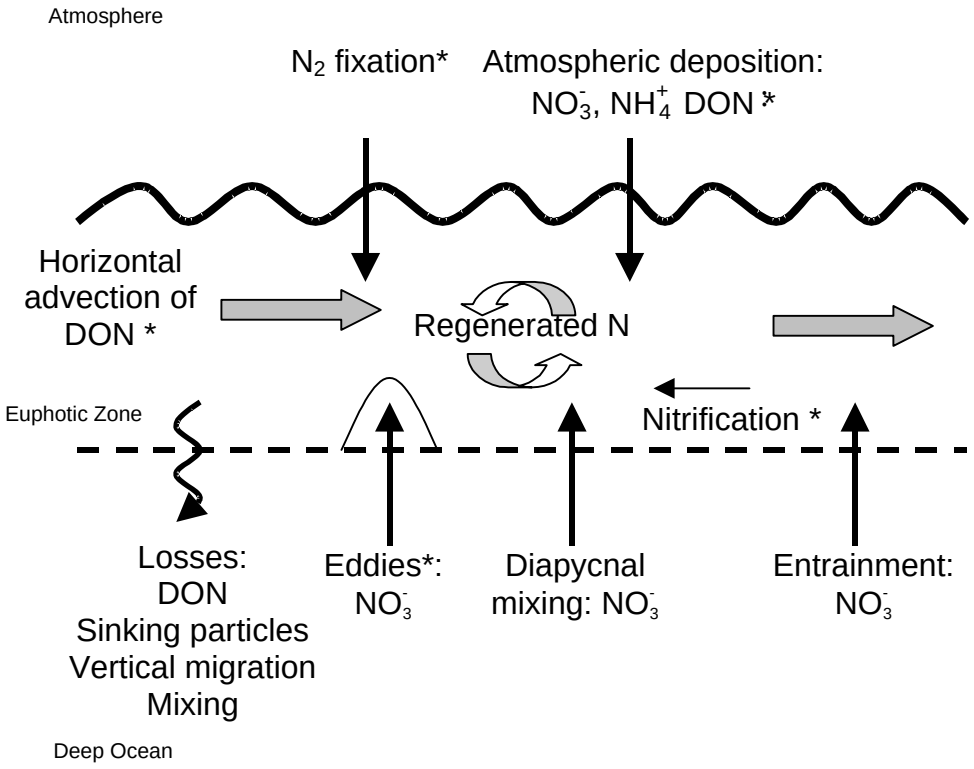

In section 1.2.4.2 of this thesis, four aims and objectives were outlined. Overall, the objectives were accomplished, despite methodological problems:

1. Seasonal and interannual variability in sea surface T, S, σ_t and MLD were examined to assess the physical structure of the Atlantic since 1995. The convective and Ekman transport of nutrients were compared to phytoplankton biomass, illustrating the strong links between physics and biology. Gyre and fine scale frontal regions were identified using sea surface properties, the Ekman pumping field and the along track density gradients.

2. The distribution of nitrate and phosphate in the surface (250m) ocean from 9 AMT cruises was assessed. Spatial gradients in the concentrations of nitrate and phosphate, as well as the nitrate to phosphate ratio, were greater than the temporal

gradients. The quasi-conservative parameter, N*, was assessed and revealed N limitation in the south Atlantic but N limitation in the north Atlantic, varying seasonally between Spring and Autumn AMT cruises.

3. The latitudinal variation in DON and DOP were assessed during AMT 10. Whereas [DON] did not vary significantly over the Atlantic during AMT 10, striking changes in the [DOP] were observed, implying DOP may be a more important far field nutrient than DON. Stable N isotope signals revealed only localised region of N_2 fixation in the north-eastern Atlantic, possibly being fuelled by atmospheric dust inputs from the Sahara. Over most of the AMT 10 transect, heavy stable nitrogen isotopic signals revealed that nitrate was the dominant nutrient source to phytoplankton, possibly being supplied by fine- and gyre-scale upwelling.

4. The potential of horizontal Ekman transfer of inorganic and organic nutrients was assessed, revealing that the supply of DON and DOP may fuel greater export production than inorganic nutrients, if the entire DON and DOP is bioavailable.

5.2. Future work

The results and discussion, which have evolved from this study, have revealed gaps in our knowledge of the nutrient dynamics of the open ocean and have raised a number of ideas for future work:

1. In this study, the influence of detrital material and higher trophic levels on the phytoplankton $\delta^{15}N$ signature was questioned. However, the isolation and stable nitrogen isotope analysis of chlorophyll *a* (representing an autotrophic tracer; Sachs *et al.*, 1999) would exclude such biases, allowing the $\delta^{15}N$ signature to be studied.

2. In light of the range of nutrient uptake dynamics between phytoplankton groups and species (i.e. nitrate vs. DON utilisation, see section 4.3.3.4.), the $\delta^{15}N$ of accessory pigments may also allow insights into species-specific N dynamics. In addition, depth profiles of the isotopic signals of phytoplankton may give better insight into the nutrient dynamics of surface dwelling phytoplankton and those that thrive at the base of the mixed layer.

3. Isotopically light phytoplankton can be fuelled by N_2 fixation, regenerated nutrients and possibly DON. In order to distinguish regions of N_2 fixation, the $\delta^{15}N$ of subsurface nitrate would be a more useful tool, as isotopically light nitrate can only be created through remineralisation of isotopically light PON exported from the surface ocean. A number of methods for the determination of $\delta^{15}N$ of nitrate such as the "passive ammonia diffusion method" (Sigman *et al.,* 1997) and the "denitrifier method" (Sigman *et al.,* 2001) have been developed and could be applied (Pantoja *et al.,* 2002).

4. The composition of DON and its bioavailability are complex, and thus stable isotopic analysis of the bulk DON pool would be inconclusive. However, it may be insightful to isolate and concentrate the more readily available fractions of DON, possibly amino acids, for subsequent isotopic analysis. This would be especially applicable in regions of N_2-fixers, which are known to readily exude significant quantities of amino acids.

5. At present, we have little knowledge regarding the uptake and assimilation of naturally occurring DON. Stable isotopic composition of the labile fractions of DON may also yield insights into its bioavailability and utilisation by specific algal groups, assessed by isotopic analysis of both dissolved and particulate organic pools.

6. From this study, relatively large variations in DOP were observed. Thus, it would be interesting to perform a transect of alkaline phosphatase assays to identify

specific regions of P limitation in the Atlantic. In addition, the composition of DOP, e.g. phospholipids, may give insight into this relatively unstudied organic nutrient pool.

7. On a global scale, it would be interesting to devise a method to study the frequency and strength of fine-scale upwelling events over scales of 100 to 200 km. One possible method for this would be to deploy a basin scale array of sensors to measure nanomolar nutrient concentrations, temperature and salinity in the mid-euphotic zone for a period of time (e.g. 2 years). This may lead to significant advances in our understanding of these stochastic events, not only on a temporal scale but also on a spatial scale.

Tables

Figures

References

Abell, J., Devol, A., Emerson, S., 1999. Isotopic composition of dissolved organic nitrogen in the subtropical North Pacific. *Abstracts of Papers of the American Chemical Society*, **218**, 1.

Abell, J., Emerson, S. and Renaud, P., 2000. Distributions of TOP, TON and TOC in the North Pacific subtropical gyre: Implications for nutrient supply in the surface ocean and remineralisation in the upper thermocline. *Journal of Marine Research*, **58**, 203-222.

Aebischer, N.J., Coulson, J.C., Colebrook J.M., 1999. Parallel long-term trends across four marine trophic levels and weather. *Nature*, **347** (6295), 753-755.

Agusti, S., Duarte C.M., 1999. Phytoplankton chlorophyll a distribution and water column stability in the central Atlantic Ocean. *Oceanologica Acta*, **22** (2), 193-203.

Aiken, J., Rees, N., Hooker, S., Holligan, P., Bale, A., Robins, D., Moore, G., Harris, R. and Pilgrim, D., 2000. The Atlantic Meridional Transect: overview and synthesis of data. *Progress in Oceanography*, **45**, 257-312.

Allredge, A. L. and Gotschalk, C. C., 1989. Direct observations of the mass flocculation of diatom blooms: characteristics, settling velocities, and formation of diatom aggregates. *Deep-Sea Research*, **36**, 159-171.

Altabet, M. A. 1988. Variations in nitrogen isotopic composition between sinking and suspended particles: implications for nitrogen cycling and particle transformation in the open ocean. *Deep-Sea Research*, **35**, (4), 535-554.

Altabet, M.A., 1996. Nitrogen and carbon isotopic tracers of the source and transformation of particles in the deep sea. In: *Particle Flux in the Ocean*. Edited by: Ittekot, V., Schafer, O., Honjo, S. and Depetris, P.J. Wiley, 155-184.

Altabet, M.A., 2001. Nitrogen isotopic evidence for micronutrient control of fractional NO_3^- utilisation in the equatorial Pacific. *Limnology and Oceanography*, **46**, (2), 368-380.

Altabet, M. A. and Deuser, W. G. 1985. Seasonal variations in natural abundance of ^{15}N in particles sinking to the deep Sargasso Sea. *Nature*, **315**, 218-219.

Altabet, M. A. and McCarthy, J. J. 1985. Temporal and spatial variations in the natural abundance of ^{15}N in PON from a warm-core ring. *Deep-Sea Research*, **32**, (7), 755-772.

Altabet, M. A. and McCarthy, J. J., 1986. Vertical patterns in ^{15}N natural abundance in PON from the surface waters of warm-core rings. *Journal of Marine Research*, **44**, 185-201.

Altabet, M. A and Small, L. F., 1990. Nitrogen isotope ratios in fecal pellets produced by marine zooplankton. *Geochimica et Cosmochimica Acta*, **54**, 155-163.

Altabet, M. A., Deuser, W. G., Honjo, S. and Christian, S. 1991. Seasonal and depth-related changes in the source of sinking particles in the North Atlantic. *Nature*, **354**, 136-139.

Altabet, M. A. and Francois, R., 1994. Sedimentary nitrogen isotopic ratios as a recorder for surface ocean nitrate utilisation. *Global Biogeochemical Cycles*, **8**, (1), 103-116.

Anderson, G. C., 1969. Subsurface chlorophyll maximum in the Northeast Pacific Ocean. *Limnology and Oceanography*, **14**, 386-391.

Anderson T. R. and Williams P. J. L., 1999. A one-dimensional model of dissolved organic carbon cycling in the water column incorporating combined biological-photochemical decomposition. *Global Biogeochemical Cycles*, **13** (2), 337-349.

Antia N.J., Harrison P.J. and Oliveira L., 1991. The role of dissolved organic nitrogen in phytoplankton nutrition, cell biology and ecology. *Phycologia*, **30** (1), 1-89.

Archer, D., Petzler, E. T. and Kirchman, D. L., 1997. A timescale of DOC production in equatorial Pacific surface waters. *Global Biogeochemical Cycles*, **11**, (3), 435-452.

Armstrong, F. A. J., Williams, P. M. and Strickland, J. D. H., 1966. Photo-oxidation of organic matter in seawater by ultraviolet radiation, analytical and other applications. *Nature*, **211**, 481-483.

Barlow R.G., Mantoura R.F.C., Gough M.A., Fileman T.W., 1993. Pigment signatures of the phytoplankton composition in the northeastern Atlantic during the 1990 spring bloom. *Deep-Sea Research I*, **40,** (1-2), 459-477.

Barlow, R.G., Cummings, D.G. and Gibb, S.W., 1997. Improved resolution for mono- and divinyl chlorophylls a and b and zeaxanthin and lutein in phytoplankton extracts using reverse phase C-8 HPLC. *Marine Ecology-Progress Series*, **161**, 303-307.

Barlow , R.G., Aiken, J., Holligan, P.M., Cummings, D.G., Maritorena, S. and Hooker, S., 2002. Phytoplankton pigment and absorption characteristics along meridional transects in the Atlantic Ocean. *Deep-Sea Research I*, **47**, 637-660.

Bates, N. R., 2001. Interannual variability of oceanic CO_2 and biogeochemical properties in the Western North Atlantic subtropical gyre. *Deep-Sea Research II*, **48**, 1507-1528.

Benitez-Nelson C.R., 2000. The biogeochemical cycling of phosphorus in marine systems *Earth-Science Reviews*, **51** (1-4), 109-135.

Benitez-Nelson C.R., Karl D.M., 2002. Phosphorus cycling in the North Pacific Subtropical Gyre using cosmogenic P-32 and P-33. *Limnology and Oceanography*, **47** (3), 762-770.

Benner, R., 2002. Chemical Composition and Reactivity. In: *Biogeochemistry of marine dissolved organic matter*. Edited by: Hansell, D. A. and Carlson, C. A., Academic Press, San Diego, 59-90.

Benner, R., Bibbanda, B., Black, B. and McCarthy, M., 1997. Abundance, size distribution, and stable carbon and nitrogen isotopic compositions of marine organic matter isolated by tangential-flow ultrafiltration. *Marine Chemistry*, **57**, 243-263.

Bergman, B., Carpenter, E.J., 1991. Nitrogenase confined to randomly distributed trichomes in the marine cyanobacterium *Trichodesmiu thiebautii*. *Journal of Phycology*, **27** (2), 158-165.

Bergman B., Gallon J.R., Rai A.N., Stal L.J., 1997. N-2 fixation by non-heterocystous cyanobacteria. *FEMS Microbiology Reviews*, **19** (3), 139-185.

Berman, T., Chava, S., Kaplan, B. and Wynne, D., 1991. Dissolved organic substrates as phosphorus and nitrogen sources for axenic batch cultures of freshwater green algae. *Phycologia***, 30**, 339-345.

Berman, T. and Chava, S., 1999. Algal growth on organic compounds as nitrogen sources. *Journal of Plankton Research*, **21**, 1391-1421.

Berman-Frank, I., Cullen, J. T., Shaked, Y., Sherrell, R. M. and Falkowski, P. G., 2001. Iron availability, cellular iron quotas, and nitrogen fixation in *Trichodesmium*. *Limnology and Oceanography*, **46**, (6), 1249-1260.

Bidigare R.R., Marra J., Dickey T.D., Iturriaga R., Baker K.S., Smith R.C., Pak H., 1990. Evidence for Phytoplankton succession and chromatic adaptation in the Sargasso Sea during Spring 1985. *Marine Ecology-Progress Series*, **60** (1-2), 113-122.

Bigeleisen, J., 1952. The effect of isotopic substitution on the rates of chemical reactions. *Journal of Chemical Physics*, **20**, 823-828.

Bishop J.K.B., 1986. The correction and suspended particulate matter calibration of sea tech transmissometer data. *Deep-Sea Research Part A*, **33** (1), 121-134.

Bjorkman, K., Thomason-Bulldis, A. L. and Karl, D. M., 2000. Phosphorus dynamics in the Norht Pacific subtropical gyre. *Aquatic Microbiology*, **22**, 185-198.

Bjørnsen, P. K., 1988. Phytoplankton exudation of organic matter: Why do healthy cells do it? *Limnology and Oceanography*, **33**, 151-155.

Bowie, A.R., Whitworth, D.J., Acterberg, E.P., Mantoura, R.F.C. and Worsfold, P.J., 2002. Biogeochemistry of Fe and other trace elements (Al, Co, Ni) in the upper Atlantic. *Deep-Sea Research I*, **49**, 605-636.

Bronk, D.A., 2002. Dynamics of DON. In: *Biogeochemistry of Marine Dissolved Organic Matter*. Edited by: Hansell, D.A. and Carlson, C.A. Academic Press, San Diego, 153-250.

Bronk, D. A. and Glibert, P. M. 1991. A ^{15}N tracer method for the measurement of dissolved organic nitrogen release by phytoplankton. *Marine Ecology-Progress Series*, **77**, 171-182.

Bronk, D. A. and Glibert, P. M. 1993. Applications of ^{15}N tracer method to study dissolved organic uptake during spring and summer in Chesapeake Bay. *Marine Biology*, **115**, 501-508.

Bronk, D.A., Glibert, P.M. and Ward, B.B. 1994. Nitrogen uptake, dissolved organic nitrogen release and new production. *Science*, **265**, 1843-1846.

Bronk, D. A. and Ward, B. B. 1999. Gross and net nitrogen uptake and DON release in the euphotic zone of Monterey Bay, California. *Limnology and Oceanography*, **44**, (3), 573-585.

Bronk, D. A., Lomas, M. W., Glibert, P. M., Schukert, K. J. and Sanderson, M. P., 2000. Total dissolved nitrogen analysis: comparison between the persulfate, UV and high temperature oxidation methods. *Marine Chemistry*, **69**, 163-178.

Buesseler K.O., 1998. The decoupling of production and particulate export in the surface ocean. *Global Biogeochemical Cycles*, **12** (2), 297-310.

Buesseler K.O., Michaels A.F., Siegel D.A., Knap A.H., 1994. A 3-Dimensional time-dependent Approach to calibrating sediment trap fluxes. *Global Biogeochemical Cycles*, **8** (2), 179-193.

Canellas, M., Agusti, S. and Duarte, C. M. 2000. Latitudinal variability in phosphate uptake in the Central Pacific. *Marine Ecology-Progress Series*, **194**, 283-294.

Capone, D.G., 1993. Determination of nitrogenase activity in aquatic samples using the acetylene reduction procedure. In: *Handbook of Methods in Aquatic Microbial Ecology*. Edited by: Kemp, P.F.F, Sherr, B.F., Sherr, E.B., Cole, J.J., Lewis Press, Boca, 621-631.

Capone, D. G., Ferrier, M. D. and Carpenter, E. J., 1994. Amino acid cycling in colonies of the planktonic marine cyanobacterium *Trichodesmium thiebautii*. *Applied and Environmental and Microbiology*, **60**, (11), 3989-3995.

Capone, D.G., Zehr, J.P., Paerl, H. W., Bergman, B. and Carpenter, E. J. 1997. *Trichodesmium*, a globally significant marine cyanobacterium. *Science*, **276**, (5316), 1221-1229.

Capone, D.G., Subramaniam, A., Montoya, J. P., Voss, M., Humborg, C., Johansen, A. M., Siefert, R. L. and Carpenter, E. J., 1998. An extensive bloom of the N_2-fixing cyanobacterium *Trichodesmium erythraeum* in the central Arabian Sea. *Marine Ecology-Progress Series*, **172**, 281-292.

Capone, D. G., 2001. Marine nitrogen fixation: what's the fuss? *Current Opinions in Microbiology*, **4**, (3), 341-348.

References

Carpenter, E.J., 1983. Nitrogen fixation by marine *Oscillatoria (Trichodesmium*) in the World's Oceans. In: *Nitrogen in the Marine Environment*. Edited by: Carpenter, E. J. and Capone, D. G. Academic press, New York, 65-105.

Carpenter, E.J. and McCarthy, J. J. ,1975. Nitrogen fixation and uptake of combined nitrogenous nutrients by *Oscillatoria (Trichodesmium) thiebantii* in the western Sargasso Sea. *Limnology and Oceanography*, **20**, 389-401.

Carpenter, E.J. and Price, C. C., 1977. Nitrogen fixation, distribution, and production of *Oscillatoria (Trichodesmium*) spp. in the western Sargasso and Caribbean Seas. *Limnology and Oceanography*, **22**, 60-72.

Carpenter, E.J. and Romans, K., 1991. Major role of the cyanobacterium *Trichodesmium* in nutrient cycling in the North Atlantic Ocean. *Science*, **254**: 1356-1358.

Carpenter, E.J., Bergman, B., Dawson, R., Siddiqui, P.J.A., Soderback, E. and Capone, D.G., 1992. Glutamine synthetase and nitrogen cycling in colonies of the marine diazotrophic cyanobacteria *Trichodesmium* spp. *Applied and Environmental Microbiology*, **58**, (9), 3122-3129.

Carpenter, E.J. and Capone, D.G., 1992. Nitrogen fixation in *Trichodesmium* blooms. In: *Marine pelagic cyanobacteria: Trichodesmium and other diazotrophs*. Edited by: Carpenter, E.J., Capone, D.G and Reuter, J.G., Kluwer Academic Publishers, Dordrecht, 211-217.

Carpenter E.J., O'Neil J.M., Dawson R., Capone D.G., Siddiqui P.J.A., Roenneberg T, Bergman B, 1993. The tropical diazotrophic phytoplankter *Trichodesmium* - Biological characteristics of two common species. *Marine Ecology-Progress Series*, **95** (3), 295-304.

Carpenter, E. J., Harvey, H. R., Fry, B. and Capone, D. G. 1997. Biogeochemical tracers of marine cyanobacterium *Trichodesmium*. *Deep-Sea Research*, **44**, (1), 27-38.

Carpenter, E. J., Montoya, J. P., Burns, J., Mulholland, M. R. Subramaniam, A., Capone, D. G. 1999. Extensive bloom of a N_2-fixing diatom/cyanobacterial association in the tropical Atlantic Ocean. *Marine Ecology-Progress Series*, **185**, 273-283.

Carlsson, P., Segatto, A.Z. and Graneli, E., 1993. Nitrogen bound to humic matter of terrestrial origin-A nitrogen pool for coastal phytoplankton? *Marine Ecology-Progress Series*, **97**, 105-116.

Carlson, C.A., 2002. Production and Removal Processes. In: *Biogeochemistry of marine dissolved organic matter*. Edited by: Hansell, D.A. and Carlson, C.A., Academic Press, San Diego, 91-153.

Carlson C.A., Ducklow H.W., 1996. Growth of bacterioplankton and consumption of dissolved organic carbon in the Sargasso Sea. *Aquatic Microbial Ecology*, **10,** (1), 69-85.

Cavender-Bares, K.K., Karl, D.M. and Chisholm, S.W., 2001. Nutrient gradients in the western North Atlantic Ocean: Relationship to microbial community structure and comparison to patterns in the Pacific Ocean. *Deep-Sea Research I*, **48**, (11), 2373-2395.

Cayan, D. R., 1992. Latent and sensible heat flux anomalies over the Northern oceans: driving the seas surface temperature. *Journal of Physical Oceanography*, **22**, 859-881.

Checkley, D. M. Jr. and Miller, C. A., 1989. Nitrogen isotope fractionation by oceanic zooplankton. *Deep-Sea Research*, **36**, (10), 1449-1456.

Chen, W., Zhao, Z., Koprivnjak, J.F. and Perdue, E.M., 2002. A mechanistic study of the high temperature oxidation of organic matter in a carbon analyser. *Marine Chemistry*, **78**, 185-196.

Christian, J.R., Lewis, M.R. and Karl, D.M., 1997. Vertical fluxes of carbon, nitrogen and phosphorus in the North Pacific subtropical gyre near Hawaii. *Journal of Geophysical Research*, **102** (C7), 15667-15677.

Christie, W.W., 1982. Esterification of Fatty Acids in Adipose-Tissue. *Journal of the Science of Food and Agriculture*, **33** (8), 809-809.

Cifuentes, L. A., Fogel, M. L., Pennock, J. R. and Sharp, J. H., 1989. Biogeochemical factors that influence the stable nitrogen isotope ration of dissolved ammonium in the Delaware Estuary. *Geochimica et Cosmochimica acta*, **53**, 2713-2721.

Cline, J. D. and Kaplan, I. R. 1975. Isotopic fractionation of dissolved nitrate during denitrification in the eastern tropical Pacific Ocean. *Marine Chemistry*, **3**, 271-299.

Cochlan, W.P. Harrison, P.J., 1991. Inhibition of nitrate uptake by ammonium and urea in the eukaryotic picoflagellate *Micromonas Pusilla* (Butcher) Manton-Et-Parke. *Journal Of Experimental Marine Biology And Ecology*, **153** (2): 143-152 1991

Codispoti, L.A. 1995. Is the ocean losing nitrate? *Nature*, **376**, 724.

Collier, J.L., Brahamsha, B., and Palenik, B., 1999. The marine cyanobacterium, *Synechococcus* sp. WH 7805 requires urease (urea amindohydrolase, EC 3.5.1.5) to utilise urea as a nitrogen source: molecular-genetic and biochemical analysis of the enzyme. *Microbiology*, **145**, 447-459.

Cotner, J.B. and Biddanda, B.A., 2002. Small players, large role: Microbial influence on biogeochemical processes in pelagic aquatic ecosystems. *Ecosystems*, **5**, 105-121.

Cornell, S., Rendell, A. and Jickells, T., 1995. Atmospheric inputs of dissolved organic nitrogen to the oceans. *Nature*, **376,** 243-246.

Cowie, G.L. and Hedges, J.I., 1992. Improved amino acid quantification in environmental samples: charge-matched recovery standards and reduced analysis time. *Marine Chemistry*, **37**, 223-238.

Crutzen, P.J., 1981. Atmospheric chemical processes of the oxides of nitrogen, including nitrous oxide. In: *Denitrification, Nitrification and Atmospheric Nitrous Oxide*. Edited by: Delwiche, C.C., Wiley Interscience, New York, 17-44

Cullen, J.J., 1982. The deep chlorophyll maximum: comparing profiles of chlorophyll a. *Canadian Journal of Fisheries and Aquatic Sciences*, **39**, 791-803.

Cullen, J.J., 1999. Iron, nitrogen and phosphorus in the ocean. *Nature*, **402**, 372.

del Giorgio, P. A. and Duarte, C. M., 2002. Respiration in the open ocean, *Nature*, **420**, 379-384

Delaney, M.L., 1998. Phosphorus accumulation in marine sediments and the oceanic phosphorus cycle. *Global Biogeochemical Cycles*, **12** (4), 563-572.

Delwiche, C.C., 1970. The nitrogen cycle. *Sciencitific American*, **223**, 136-147

Deutsch, C., Gruber, N., Key, R. M and Sarmiento, J. L., 2000. Denitrification and N_2 fixation in the Pacific Ocean. *Global Biogeochemical Cycles*, **15,** (2), 483-506.

Dickson, R., Lazier, J., Meinke, J., Rhines, P. and Swift, J., 1996. Long-tern coordinated changes in convective activity of the North Atlantic. *Progress in Oceanography*, **38**, 214-295.

Donald K.M., Joint I., Rees A.P., Woodward E.M.S., Savidge G., 2001. Uptake of carbon, nitrogen and phosphorus by phytoplankton along the 20 degrees W meridian in the NE Atlantic between 57.5 degrees N and 37 degrees N. *Deep-Sea Research Part II*, **48,** (4-5), 873-897.

Dore, J.E., Karl, D.M., 1996. Nitrification in the euphotic zone as a source for nitrite, nitrate, and nitrous oxide at Station ALOHA. *Limnology and Oceanography*, **41,** (8), 1619-1628.

Dortch, Q., 1990. The interaction between ammonium and nitrate uptake in phytoplankton. *Marine Ecology-Progress Series*, **61,** (1-2), 183-201.

Dortch, Q., Thompson, P.A., Harrison P.J., 1991. Variability in nitrate uptake kinetics in *Thalassiosira Pseudonana (Bacillariophyceae). Journal of Phycology*, **27**, (1), 35-39.

Downing, J. A., 1997. Marine nitrogen:phosphorus stoichiometry and the global N:P cycle. *Biogeochemistry*, **37**, 237-252.

Duarte, C.M., Arístegui, J., González, N., Agustí, S. and Anadón, R., 2001. Evidence for a heterotrophic subtropical NE Atlantic. *Limnology and Oceanography*, **46**, 425-428.

Duce, R.A., Tindale, N.W., 1991. Atmospheric transport of iron and its deposition in the ocean. *Limnology and Oceanography*, **36** (8), 1715-1726.

Duce, R.A., Tindale, N., Zhuang, G., 1991. Atmospheric iron and its impact on marine biological productivity and chemical cycling. *Abstracts of Papers of the American Chemical Society*, **201,** 20.

Dufour, P., Charly, L., Bonnet, S. and Garcia, N., 1999. Phytoplankton nutrient control in the oligotrophic South Pacific subtropical gyre (Tuamotu Archipelago). *Marine Ecology-Progress Series*, **179**, 285-290.

Dugdale, R.C., 1967. Nutrient limitation in the sea: dynamics, identification and significance. *Limnology and Oceanography*, **12,** 685-695.

Dugdale, R.C. and Goering J.J., 1967. Uptake of new and regenerated forms of nitrogen in primary productivity. *Limnology and Oceanography*, **12**, 196-206.

DuRand, M.D., Olson, R.J. and Chisholm, S.W., 2001. Phytoplanton population dynamics at the Bermuda Atlantic time-series station in the Sargasso Sea, *Deep-Sea Research II*, **48**, 1983-2003.

Dutkiewicz, S., Follows, M., Marshall, J. and Gregg W.W., 2001. Interannual variability of phytoplankton abundances in the North Atlantic. *Deep-Sea Research Part II-Topical Studies in Oceanography*, **48** (10), 2323-2344.

Ebdon, D., 1985. *Statistics in Geography: A Practical Approach*. Blackwell publishers.

Emerson, S., Quay, P, Karl, D., Winn, C., Tupas, L. and Landry, M., 1997. Experimental determination of organic carbon flux from open-ocean surface waters. *Nature*, **389**, 951-954.

Eppley, R.W. and Peterson B.J.,1979. Particulate organic matter flux and planktonic new production in the deep ocean. *Nature*, **282**, 677-680.

Evans, R.D., Bloom, A.J., Sukrapanna, S.S. and Ehleringer, J.R., 1996. Nitrogen isotope composition of tomato (*Lycopersion esculentum* Mill. Cv. T-5) grown under ammonium or nitrate nutrition. *Plant Cell Environment*, **19**, 1317-1323.

Falcon, L.I., Cipriano, F., Chistoserdov, A.Y., and Carpenter, E.J., 2002. Diversity of diazotrophic unicellular cyanobacteria in the tropical North Atlantic Ocean. *Applied and Environmental microbiology*, **68** (11), 5760-5764.

Falkowski, P.G., 1983. Enzymology of nitrogen assimilation. In: *Nitrogen in the Marine Environment.* Edited by: Carpenter, E. J. and Capone, D. G., Academic press, New York, 839-869.

Falkowski, P. G., 1997. Evolution of the nitrogen cycle and its influence on the biological sequestration of CO2 in the ocean. *Nature*, **387**, 272-275.

Falkowski, P.G. and Raven, J.A., 1997. Photosynthesis and primary production in nature, in Aquatic photosynthesis, edited by P.G. Falkowski and J.A. Raven, Capital City Press, New York, 193-228.

Falkowski, P. G., Ziemann, D., Kolber, Z. and Bienfang, P. K. 1991. Role of eddy pumping in enhancing primary production in the ocean. *Nature*, **352**, (6330), 55-58

Fanning, K. A., 1989.Nutrient Provinces in the Sea: Concentration Ratios, Reaction Rate Ratios, and Ideal Covariation. *Journal of Geophysical Research*, **97**, (c4), 5693-5712.

Feuerstein, T. P., Ostrom, P. H. and Ostrom, N. E., 1997. Isotopic biogeochemistry of dissolved organic nitrogen: A new technique and isolation. *Organic Geochemistry***, 27**, 363-370.

Fogel, M. L. and Cifuentes, L. A. 1993. Isotope fractionation during primary production. In: *Organic Geochemistry*. Edited by: Engel, M. H., Macko, S. A., Plenum Press, New York, 73-98.

Follmi, K. B., 1996. The phosphorus cycle, phosphogenesis and marine phosphate-rich deposits. *Earth-Science Reviews*, **40** (1-2), 55-124.

Follows M. and Dutkiewicz, S., 2002. Meteorological modulation of the North Atlantic spring bloom *Deep-Sea Research Part II*, **49** (1-3), 321-344.

Fraga, F., 2001. Phytoplankton biomass synthesis: application to deviations from Redfield stoichiometry. *Scientia Marine*, **65**, (S2), 153-169.

Fraga, F., Rios, A. F., Perez, F. F. Estrada, M. and Marrase, C., 1999. Effect of upwelling pulses on excess carbohydrate synthesis as deduced from nutrient, carbon dioxide and oxygen profiles. *Marine Ecology-Progress Series*, **189**, 65-75.

Fuhrman, J.A., Sleeter, T.D., Carlson, C. A. and Proctor, L.M., 1989. Dominance of bacterial biomass in the Sargasso Sea and its ecological implications. *Marine Ecology-Progress Series*, **57**, 207-217.

Fuhrman, J. A, 1990. Dissolved free amino acid cycling in an estuarine outflow plume. *Marine Ecology-Progress Series*, **66**, 197-203.

Fuhrman, J. A., 1999. Marine viruses and their biogeochemical and ecological effects. *Nature*, **399**, 541-548.

Fung, I. Y., Meyn, S. K., Tegen, I., Doney, S. C., John, J. G. and Bishop, J. K. B., 2000. Iron supply and demand in the upper ocean. *Global Biogeochemical Cycles*, **14,** (2), 697-700.

Fry, B., 1988. Food web structure on Georges Bank from stable C, N and S isotopic compositions. *Limnology and Oceanography*, **33**, 1182-1190.

Ganachaud, A. and Wunsch, C., 2002. Oceanic nitrate and oxygen transports and bounds on export production during the World Ocean Circulation Experiment. *Global Biogeochemical Cycles*, **16**, (4), 1057, doi:10.1029.

Gallienne, 2000. Atlantic Meridional Transect 10. Cruise Report. Plymouth Marine Laboratory.

Ganeshram, R. S., Pedersen, T. F., Calvert, S. E., and Murray, J. W., 1995. Large changes in oceanic nutrient inventories from glacial to interglacial periods. *Nature*, **376**, 755-758.

Gieskes, W. W., Kraay, G.W. and Tijssen, S. B., 1978. Chlorophylls and their degradation products in the deep pigment maximum layer of the tropical North Atlantic. *Netherlands Journal of Sea Research* **12**, 195-204.

Gibb, S. W., Barlow, R. G., Cummings, D. G., Rees, N. W., Trees, C. C., Holligan, P. and Sugget, D., 2000. Surface phytoplankton pigment distributions in the Atlantic Ocean: an assessment if basin scale variability between 50°N and 50°S. *Progress in Oceanography*, **45**, 339-368.

del Giorgio P. A. and Duarte C. M., 2002. Respiration in the open ocean. *Nature*, **420** (6914), 379-384.

Glibert, P. M., 1982. Regional studies of daily, seasonally and size fractionation variability in ammonium remineralisation, *Marine Biology Berlin*, **70**, 209-222.

Glibert, P. M. and McCarthy, J. J. 1984. Uptake and assimilation of ammonium and nitrate by phytoplankton - indexes of nutritional-status for natural assemblages. *Journal Of Plankton Research*, **6**, (4), 677-697.

Glibert, P.M., Kana, T. M., Olson, R. J., Kirchman, D. L. and Alberte, R. S. 1986. Clonal comparisons of growth and photosynthetic responses to nitrogen availability in marine *Synechococcus* spp.. *Journal of Experimental Marine Biology and Ecology*, **101**, (1-2), 199-208.

Glibert, P.M. and Bronk, D. A. 1994. Release of Dissolved Organic Nitrogen by Marine Diazotrophic Cyanobacteria, *Trichodesmium* spp. *Applied and Environmental Microbiology*, **60**, (11), 3996-4000.

Glover, H. E., Prezelin, B. B., Campbell, L., Wyman, M. and Garside, C. A., 1998. Nitrate-dependent *Synechococcus* bloom in surface Sargasso sea-water. *Nature*, **331**, (6152), 161-163.

Goering, J., Dugdale, R. C. and Menzel, D. W., 1966. Estimates of in-situ rates of nitrogen uptake by *Trichodesmium* sp. in the tropical Atlantic Ocean. *Limnology and Oceanography*, **11**, 614-620.

Goering, J., Alexander, V. and Haubenstock, N., 1990. Seasonal variability of stable carbon and nitrogen isotope ratios of organisms in a north Pacific bay. *Estuarine Coastal and Shelf Science*, **30**, (3), 239-260.

Goldman., J. C., McCarthy, J. J., and Peavey, D. G., 1979. Growth rate influence on the chemical composition of phytoplankton in oceanic waters. *Nature*, **279**, 210-215.

Graziano, L. M., LaRoche J. and Geider, R.J.,1996. Physiological responses to phosphorus limitation in batch and steady-state cultures of *Dunaliella tertiolecta* (chlorophyta): a unique stress protein as an indicator of phosphate deficiency. *Journal of Phycology*, **32,** (5), 825-838.

Gruber, N. and Sarmiento, J. L. 1997. Global patterns of marine nitrogen fixation and denitrification. *Global Biogeochemical Cycles*, **11**, (2), 235-266.

Guillard, R. R. L. and Ryther, J. H., 1962. Studies of marine planktonic diatoms. I. *Cyclotella nana* Hustedt and *Detonula confervacea* Cleve. *Canadian Journal of Microbiology*, **8**, 229-239.

Gust, G., Byrne, R. H., Bernstein, R. E., Betzer, P. R., Bowles, W., 1992. Particle fluxes and moving fluids - experience from synchronous trap collections in the Sargasso Sea. *Deep-Sea Research Part A*, **39**, (7-8a), 1071-1083.

Handley, L. L. and Raven, J. A., 1992. The use of natural abundance of nitrogen isotopes in plant physiology and ecology. *Plant Cell Environment*, **15**, 965-985.

Hansell, D. A., Williams, P. M. and Ward, B.B., 1993. Measurements of DOC and DON in the southern California Bight using oxidation by high-temperature combustion. *Deep-Sea Research Part I*, **40**, (2), 219-234.

Hansell, D.A. and Waterhouse, T. Y. 1997. Controls on the distribution of organic carbon and nitrogen in the eastern Pacific. *Deep-Sea Research*, **44**, (5), 843-857.

Hansell, D. A. and Carlson, C. A. 2001, Biogeochemistry of total organic carbon and nitrogen in the Sargasso Sea: control by convective overturn, *Deep-Sea Research Part II*, **48**, (8-9), 1649-1667.

Harris, G. P., 1980. Temporal and spatial scales in phytoplankton ecology. Mechanisms, methods, models and management. *Canadian Journal of Fisheries and Aquatic Sciences*, **37**, 877-900.

Harrison, W. G., 1983. Nitrogen in the Marin Environment: Use of isotopes. In: *Nitrogen in the Marine Environment*. Edited by: Carpenter, E. J. and Capone, D. G., Academic press, New York., 763-809.

Harrison, W.G., Platt, T. and Lewis, M. R., 1987. F-ratio and its relationship to ambient nitrate concentration in coastal waters. *Journal Of Plankton Research*, **9,** (1), 235-248.

Harrison, W. G., Harris, L. R., and Irwin, B. D., 1996. The kinetics of nitrogen utilisation in the oceanic mixed layer: Nitrate and ammonium interactions and nanomolar concentrations. *Limnology and Oceanography*, **41**, 16-32.

Herut, B., Collier, R. and Krom, M. D., 2002. The role of dust in supplying nitrogen and phosphorus to the southeast Mediterranean. *Limnology and Oceanography*, **47**, (3), 870-878.

Heywood, K. J. and King, B. A., 1996. WOCE Section A23 Cruise Report. *University of East Anglia Cruise Report Series*, No. 1.

Hoch, M. P., Fogel, M. L. and Krichman, D. L., 1992. Isotope fractionation during ammonium uptake by marine bacterium. *Limnology and Oceanography*, **37,** 1447-1459.

Hoch, M. P., Fogel, M. I., and Kirchman, D.L., 1994. Isotope fractionation during ammonium uptake by marine microbial assemblages. *Geomicrobiology Journal*, **12**, (2), 113-127.

Hoch, M. P., Snyder, R. A., Cifuentes, L. A. and Coffin, R. B., 1996. Stable isotope dynamics of nitrogen recycled during interactions among marine bacteria and protists. *Marine Ecology-Progress Series*, **132**, 229-239.

Hoering, T. C. and Ford, H. T., 1960. The isotope effects in the fixation of nitrogen by the Azotobacter. *Journal of the American Chemical Society*, **82**, 376-378.

Hood, R. R., Michaels, A. F. and Capone, D. G. 2000. Answers sought to the enigma of marine nitrogen fixation. *EOS, Transactions, American Geophysical Union*, **81**, (13), 137-139.

Hooker, S. B., Rees, N. W. and Aiken, J., 2000. An objective methodology for identifying oceanic provinces. *Progress in Oceanography*, **42**, 313-338.

Horrigan, S. G., Montoya, J. P., Nevins, J. L. and McCarthy, J. J. 1990. Natural isotopic composition of dissolved inorganic nitrogen in the Chesapeake Bay. *Estuarine, coastal and shelf sea science*, **30**, 393-410.

Howard, J.B. and Rees, D.C., 1996. Structural basis of biological nitrogen fixation. *Chemical Reviews*, **96,** (7), 2965-2982.

Howarth, R. W., Marino, R., Lane, J. and Cole, J. J. 1988. Nitrogen fixation in freshwater, estuarine and marine ecosystems. 1. Rates and importance. *Limnology and Oceanography*, **33**, (4), 669-687.

Hurrell, J. W., 1995. Decadal trends in the North Atlantic Oscillation: regional temperatures and precipitation. *Science*, **269**, 676-679.

Jackson, G. A. and Williams, P. M. 1985. Importance of dissolved organic nitrogen and phosphorus to biological nutrient cycling. *Deep-Sea Research*, **32**, (2), 223-235.

Jeffrey, S. W., Mantoura, R. F. C. and Bjornland, T. 1997. Data for the identification of 47 key phytoplankton pigments. In: *Phytoplankton pigments in oceanography*. Edited by: Jeffrey, S. W., Mantoura, R. F. C. and Wright, S. W., UNESCO Publishing, 449-559

Jenkins, W. J., 1982. Oxygen utilisation rates in North Atlantic subtropical gyre and primary production in oligotrophic systems. *Nature*, **300**, 246-248.

Jenkins, W. J., 1988. Nitrate flux into the photic zone near Bermuda. *Nature*, **331**, 521-523

Jenkins, W. J., 1998. Studying subtropical thermocline ventilation and circulation using tritium and He-3. *Journal of Geophysical Research-Oceans*, **103,** (C8), 15817-15831.

Jenkins, W. J. and Goldman, J. C., 1985. Seasonal oxygen cycling and primary production in the Sargasso Sea. *Journal of Marine Research*, **43**, 465-491.

Jenkins, W.J. and Wallace, D., 1992. Tracer based inferences of new primary production in the sea. In: *Primary Productivity and Biogeochemical Cycles in the Sea*. Edited by: Falkowski, P.G. and Woodhead, A.D., Plenum Press, New York, 299-316.

Jickells, T. J., The inputs of dust derived elements to the Sargasso Sea; a synthesis, *Marine Chemistry*, **68**, (5-14), 1999.

Johnson, K. S., Gordin, R. M. and Coale, K. H., 1997. What controls dissolved iron concentrations in the world ocean? *Marine Chemistry*, **57**, 137-161.

Jorgensen, N. O. G., Kroer, N. and Coffin, R. B., 1994. Utilisation of dissolved nitrogen by Heterotrophic bacterioplankton: effect of substrate C/N ratio. *Applied Environmental Microbiology*, **60**, 4124-4133.

Karl, D. M., 1999. A sea of change: Biogeochemical variability in the North Pacific Subtropical Gyre. *Ecosystems*, **2,** (3), 181-214.

Karl, D. M., Tien, G., Dore, J. and Winn, C. D., 1993. Total dissolved nitrogen and phosphorus concentrations at United-States-JGOFS station ALOHA - Redfield reconciliation. *Marine Chemistry*, **41**, (1-3), 203-208.

Karl, D. M., Letelier, R., Hebel, D., Tupas, L., Dore, J., Christian, J. and Winn, C., 1995. Ecosystem changes in the north Pacific subtropical gyre attributed to the 1991-92 El-Nino *Nature*, **373**, (6511), 230-234.

Karl, D.M., Christian, J.R., Dore, J.E., Hebel, D.V., Letelier, R.M., Tupas, L.M. and Winn, C.D., 1996. Seasonal and interannual variability in primary production and particle flux at station ALOHA. *Deep-Sea Research Part II,* **43**, (2-3), 539-568.

Karl, D. M., Letelier, R., Tupas, L., Dore, J., Christian, J. and Hebel, D. 1997. The role of nitrogen fixation in the biogeochemical cycling in the subtropical North Pacific Ocean. *Nature*, **388**, 533-538.

Karl, D. M. and Tien, G., 1997. Temporal variability in dissolved phosphorus concentrations in the subtropical North Pacific Ocean. *Marine Chemistry*, **56,** (1-2), 77-96.

Karl, D. M. and Yanagi, K., 1997. Partial characterisation of the dissolved organic phosphorus pool in the oligotrophic North Pacific Ocean. *Limnology and Oceanography*, **42**, (6), 1398-1405.

Karl, D. M., Hebel, D. V., Bjorkman, K. and Letelier, R. M., 1998. The role of dissolved organic matter release in the productivity of the oligotrophic North Pacific Ocean. *Limnology and Oceanography*, **43**, (6), 1270-1286.

Karl, D. M., 1999. A sea of change, Biogeochemical variability in the North Pacific subtropical gyre. *Ecosystems*, **2**, 181-214.

Karl, D. M., Bidigare, R. R., Letelier, R. M., 2001. Long-term changes in plankton community structure and productivity in the North Pacific Subtropical Gyre: The domain shift hypothesis. *Deep-Sea Research II*, **48**, 1449-1470.

Karl, D. M. and Bjorkman, K.M., 2001. Phosphorus cycle in seawater: dissolved and particulate pool inventories and selected phosphorus fluxes. *Methods in Microbiology*, **30**, 239-270.

Karl, D. M., Michaels, A., Bergman, B., Capone, D., Carpenter, E., Leterlier, R., Lipschultz, F., Paerl, H., Sigman, D., and Stal, L., 2002. Dinitrogen fixation in the world's oceans. *Biogeochemistry*, **57/58**, 47-98.

Kerherve, P., Minagawa, M., Heussner, S. and Monaco, A., 2001. Stable isotopes ($^{13}C/^{12}C$ and $^{15}N/^{14}N$) in settling organic matter of the northwestern Mediterranean Sea: biogeochemical implications. *Oceanologica Acta*, **24**, S77-S85.

Kiel, R. G. and Kirchman, D. L., 1993. Dissolved combined amino acids, Chemical form and utilisation by marine bacteria. *Limnology and Oceanography*, **38**, 1256-1270.

Kiel, R. G. and Kirchman, D. L., 1999. Utilisation of dissolved protein and amino acids in the northern Sargasso Sea. *Aquatic Microbial Ecology*, **18**, 293-800.

Kirchman, D. L., Henry, D. L. and Dexter, S. C., 1989. Adsorption of proteins to surfaces in seawater. *Marine Chemistry*, **27**, 201-217.

Kirchman, D. L., Suzuki, Y., Garside, C. and Ducklow, H. W., 1991. High turnover rates of dissolved organic carbon during a spring phytoplankton bloom. *Nature*, **352**, 612-614.

Kirchman, D. L., Ducklow, H. W., McCarthy, J. J. and Garside, C., 1994. Biomass and nitrogen uptake by heterotrophic bacteria during the spring bloom in the North Atlantic Ocean. *Deep-Sea Research II*, **41**, 879-895.

Kirkwood, D. S., 1995. Nutrients: practical notes on their determination in seawater. In: *ICES techniques on Marine Environmental Sciences Report 17*. International Council for the Exploration of the Seas, Copenhagen, 25 pp.

Koeve, W., Eppley, R. W., Podewski, S. and Zeitzschel., B., 1993. An unexpected nitrate distribution in the tropical North-Atlantic at 18-degrees-N, 30-degrees-W-implications for new production. *Deep-Sea Research Part II*, **40**, (1-2), 521-536.

Koike, I. and Tupas, L., 1993. Total dissolved nitrogen in the northern north pacific assessed by a high-temperature combustion method. *Marine Chemistry*, **41**, (1-3), 209-214.

Kolowith, L. C., Ingall, E. D. and Benner, R., 2001. Composition and cycling of marine organic phosphorus. *Limnology and Oceanography*, **46**, (2), 309-320.

Knap, A., Jickells, T., Pszenny, A. and Galloway, J., 1986. Significance of atmospheric-derived fixed nitrogen on productivity of the Sargasso Sea. *Nature*, **320**, 158-160.

Knapp, A. N and Sigman, D. M, 2003. Stable isotopic composition of dissolved organic nitrogen from surface waters of BATS, paper presented at American Society of Limnology and Oceanography conference, Salt Lake City, Utah, USA.

Kroer, N., Jorgensen, N. O. G. and Coffin, R. B., 1994. Utilisation of dissolved nitrogen by heterotrophic bacterioplankton: a comparison of 3 ecosystems. *Applied environmental Microbiology*, **60**, 4116-4123.

Lampert, W. 1978. Release of dissolved organic carbon by grazing zooplankton. *Limnology and Oceanography*, **23**, 831-834.

Laws, E. A. and Bannister, T.T, 1980. Nutrient and light limited growth of *Thalassiosira fluviatilis* in continuous culture, with implications for phytoplankton growth in the ocean. *Limnology and Oceanography*, **25**, 457-473.

Le Bouteiller, A., 1986. Environmental control of nitrate and ammonium uptake by phytoplankton in the Equatorial Atlantic Ocean. *Marine Ecology-Progress Series*, **30**, 167-179.

Lee, M-M and Williams, R. G., 2000. The role of eddies in the isopycnic transfer of nutrients and their impact on biological production. *Journal of Marine Research*, **58**, (6), 895-917.

Lefévre, D., Denis, M., Lambert, C. E. and Miguel, J.-C., 1996. Is DOC the main source of organic matter remineralisation in the ocean water column? *Journal of Marine Systems*, **7**, 281-291.

Lenes, J. M., Darrow, B. P., Cattrall, C., Heil, C. A., Callaham, M., Vargo, G. A., Byrne, R. H., Prospero, J. M., Bates, D. E., Fanning, K. A. and Walsh, J. J., 2001. Iron fertilisation and the *Trichodesmium* response on the West Florida Shelf. *Limnology and Oceanography*, **46**, (6), 1261-1277.

Letelier, R. M. and Karl, D. M. 1996. Role of *Trichodesmium* spp. in the productivity in the subtropical North Pacific Ocean. *Marine Ecology Progress Series*, **133,** (1-3), 263-273.

Letelier, R. M., Dore, J. E., Winn, C. D. and Karl, D. M., Seasonal and interannual variations in photosynthetic carbon assimilation at Station ALOHA. *Deep-Sea Research II*, **43**, (2-3), 467-490.

Letelier, R. M., Karl, D. M., Abbott, M. R., Flament, P., Freilich, M., Lukas, R. and Strub, T., 2000. Role of late winter mesoscale events in the biogeochemical variability of the upper water column of the north pacific subtropical gyre. *Journal of Geophysical Research-Oceans*, **105**, (C12), 28723-28739.

Levy, M., Klein, P. and Treguier, A-M., 2001. Impact of sub-mesoscale physics on production and subduction of phytoplankton in an oligotrophic regime. *Journal of Marine Research*, **59**, 535-565.

Lewis, M. R., Harrison, W. G., Oakey, N. S., Herbert, D. and Platt, T., 1986. Vertical nitrate fluxes in the oligotrophic ocean: *Science*, **234**, 870-873.

Libby, P. S. and Wheeler, P.A., 1997. Particulate and dissolved organic nitrogen in the central and eastern equatorial Pacific. *Deep-Sea Research* I, **44**, (2), 345-361.

Lindell, D., Padan, E., and Post, A. F., 1998. Regulation of NTC A expression and nitrite uptake in the marine *Synechococcus* spp. Strain WH 7803. *Journal of Bacteriology*, **180**, 1878-1886.

Lipschultz, F. A., 2001. Time-series assessment of the nitrogen cycle at BATS. *Deep-Sea Research Part II*, **48**, (8-9), 1897-1924.

Lipshultz, F. and Owens, N. J. P., 1996. An assessment of nitrogen fixation as a source of nitrogen to the North Atlantic Ocean. *Biogeochemistry*, **35**, 261-274.

Lipschultz, F., Bates, N.R., Carlson, C.A. and Hansell, D.A., 2002. New production in the Sargasso sea: history and current status. *Global Biogeochemical Cycles*, **16**, (1), art no. 1001.

Liu, K-K and Kaplan, I. R., 1989. The eastern tropical Pacific as a source of ^{15}N-enriched nitrate in seawater off southern California. *Limnology and Oceanography*, **34**, (5), 820-830.

Liu, K-K, Su, M-J., Hseuh, C-R. and Gong, G-C., 1996. The nitrogen isotopic composition of nitrate in the Kuroshio Water Northeast of Taiwan: evidence of nitrogen fixation as a source of isotopically light nitrate. *Marine Chemistry*, **54**, 273-292.

Loh, A. N. and Bauer, J. E. 2000. Distribution, partitioning and fluxes of dissolved and particulate organic C, N and P in the eastern North Pacific and Southern Oceans. *Deep-Sea Research I*, **47**, 2287-2316.

Longhurst, A., Sathyendranath, S., Platt, T. and Caverhill, C., 1995. An estimate of global primary production in the ocean from satellite radiometer data. *Journal of Plankton Research*, **17,** (6), 1245-1271.

Luo, C., Mahowald, N. and Zender, C. Mineral aerosol climatology from a 22-year Simulation. Submitted to *Tellus*, 2002.

McCarthy, J.J. and Carpenter, E. J., 1979. *Oscillatoria* (*Trichodesmium*) *thiebautii* (Cyanophyta) in the central North Atlantic Ocean. *Journal of Phycology*, **15,** 75-82.

McClain, C. R. and Firestone, J., 1993. An investigation of Ekman upwelling in the North Atlantic. *Journal of Geophysical Research-Oceans*, **98**, (C7), 12327-12339.

McCarthy, J. J., Garside, C., Nevins, J. L., and Barber, R. T., 1996. New production along 140^{o}W in the equatorial Pacific during and following the 1992 El Nino event. *Deep-Sea Research 11*, **43**, 1065-1093.

McCarthy, M., Pratum, T., Hedges, J. and Benner, R., 1997. Chemical composition of dissolved organic nitrogen in the ocean. *Nature*, **390**, 150-153.

McElroy, M.B., 1983. Marine biological controls on atmospheric CO_2 and climate. *Nature*, **302**, 328-329.

McGillicuddy, D. J. Jr and Robinson, A. R. 1997. Eddy-induced nutrient supply and new production in the Sargasso Sea. *Deep-Sea Research* I, **44**, (8), 1427-1450.

McGillicuddy, D. J., Robinson, A.R., Siegel, D. A., Jannasch, H. W., Johnson, R., Dickeys, T., McNeill, J., Michaels, A. F. and Knap, A. H., 1998. Influence of mesoscale eddies on new production in the Sargasso Sea. *Nature*, **394**, 263-266.

McGillicuddy, D. J., Johnson, R., Siegel, D.A., Michaels, A.F., Bates, N.R. and Knap, A.H., 1999. Mesoscale variations of biogeochemical properties in the Sargasso Sea. *Journal Of Geophysical Research-Oceans*, **104,** (C6), 13381-13394.

Macko, S. A., Fogel, M., L., Hare, P. E., and Hoering, T. C., 1987. Isotopic fractionation of nitrogen and carbon in the synthesis of amino acids by microorganisms. *Chemical Geology*, **65**, 79-92.

Mague, T. H., Friberg, E., Hughes, D. J. and Morris, I. 1980. Extracellular release of carbon by marine phytoplankton: a physiological approach. *Limnology and Oceanography*, **25**, 262-279.

Mahadevan. A. and Archer, D., 2000. Modelling the impact of fronts and mesoscale circulation on the nutrient supply and biogeochemistry of the upper ocean. *Journal of Geophysical Research*, **105**, 1209-1225.

Mahaffey, C. Williams, R. G., Wolff, G. A., Mahowald, N., Anderson, W., and Woodward, M.. Isotopic signals of Nitrogen Fixation over the eastern North Atlantic. Submitted to *Geophysical Research Letters*, 2002.

Mahowald, N., Kohfeld, K., Hansson, M., Balkanski, Y., Harrison, S.P., Prentice, I.C., Schulz, M. and Rodhe, H., 1999. Dust sources and deposition during the last glacial maximum and current climate: A comparison of model results with paleodata from ice cores and marine sediments. *Journal of Geophysical Research-Atmospheres*, **104**, (D13), 15895-15916.

Malone, T. C., Pike, S. E. and Conley, D. J., 1993. Transient variations in phytoplankton productivity at the JGOFS Bermuda time-series station. *Deep-Sea Research Part I,* **40,** (5), 903-924.

Mann, K. H and Lazier, J. R. N., 1996. Vertical structure of the open ocean: Biology of the Mixed layer. In: *Dynamics of Marine Ecosystems, Biological and Physical interactions in the ocean*, 2nd edition. Edited by: Mann, K. H and Lazier, J. R. N., Blackwell Science, 56-98.

Maranon, E. and Holligan, P. M., 1999. Photosynthetic parameters of phytoplankton from 50 degrees N to 50 degrees S in the Atlantic Ocean. *Marine Ecology-Progress Series*, **176,** 191-203.

Maranon, E., Holligan, P. M., Varela, M, Mouino, B. and Bale, A. J., 2000. Basic-scale variability of phytoplankton biomass, production and growth in the Atlantic Ocean. *Deep-Sea Research* 1, **47**, 825-857.

Mariotti, A., Germon, J. C., Hubert, P., Kaiser, P., Letolle, R., Tardieux, A. and Tardieux, P., 1981. Experimental determination of nitrogen kinetic isotope fractionation: Some principles; illustration for the denitrification and nitrification processes. *Plant Science*, **62**, 413-430.

Marshall, J. and Schott, F., 1999. Open-ocean convection: observations, theory and models. *Review of Geophysics*, **37**, 1-64.

Martin., J. H., Gordon, R. M., Fitzwater, S. and Broenkow, W. W., 1989. VERTEX: phytoplankton iron studies in the Gulf of Alaska. *Deep-Sea Research*, *1*, **36**, 649-680.

Menzel, D.W and Vaccaro, R. F., 1964. The measurement of dissolved organic and particulate carbon in sea water. *Limnology and Oceanography*, **9,** 138-142.

Metzler, P. M., Glibert, P. M. Gaeta, S. A. and Ludlam, M. 1997. New and regenerated production in the South Atlantic off Brazil. *Deep-Sea Research*, **44**, 363-384

Micheals, A. F., Silver, M.W., Gowing, M. M. and Knauer, G. A., 1990. Cryptic zooplankton swimmers in upper ocean sediment traps. *Deep-Sea Research Part A*, **37,** (8), 1285-1296. 0

Micheals, A. F., Bates, N. R., Buesseler, K. O., Carlson, C. A. and Knap, A. H. 1994. Carbon cycle imbalances in the Sargasso Sea. *Nature*, **372**, 537-540.

Micheals, A. F., Olson, D., Sarmiento, J. L., Ammerman, J. W., Fanning, K., Jahnke, R., Knap, A. H., Lipschultz, F. and Prospero, J. M., 1996. Inputs, losses and transformations of nitrogen and phosphorus in the pelagic North Atlantic Ocean. *Biogeochemistry*, **35**, 181-226.

Miller, C. A. and Glibert, P. M., 1998. Nitrogen excretion by the calanoid copepod *Acartia tonsa*: Results from Mesocosm experiments. *Journal of Plankton Research*, **20**, 1767-1780.

Miller, J. C. and Miller, J. N., 1993. *Statistics for Analytical Chemistry*. 3rd Edition. Ellis Horwood Limited.

Millero, F. J., Chen, C. T., Bradshaw, A. and Schleicher, K., 1980. A new high pressure equation of state for seawater. *Deep-Sea Research*, **27**, 255-264.

Minagawa, M. and Wada, E. 1984. Stepwise enrichment of ^{15}N along food chains: further evidence and the relation between $\delta^{15}N$ and animal age. *Geochimica et Cosmochimica Acta*, **48**, 1135-1140.

Minagawa, M. and Wada, E. 1986. Nitrogen isotope ratios of red tide organisms in the east china sea: a characterisation of biological nitrogen fixation. *Marine Chemistry*, **19**, 245-259.

Mitsui, A., Kumazawa, S., Takahashi, A., Ikemoto, H., Cao, S. and Arai T., 1986. Strategy by which nitrogen-fixing unicellular cyanobacteria grow photoautotrophically. *Nature*, **323,** (6090), 720-722.

Moore, L.R., Goericke, R. and Chisholm, S. W., 1995. Comparative physiology of *Synechococcus* – influence of light and temperature on growth, pigments, fluorescence and absorptive properties. *Marine Ecology-Progress Series*, **116**, (1-3), 259-275.

Moore, L.R. and Chisholm, S. W., 1999. Photophysiology of the marine cyanobacterium *Prochlorococcus*: Ecotypic differences among cultured isolates. *Limnology and Oceanography*, **44**, (3), 628-638.

Moore, L.R., Post, A.F., Rocap, G. and Chisholm, S.W., 2002. Utilization of different nitrogen sources by the marine cyanobacteria *Prochlorococcus* and *Synechococcus*. *Limnology and Oceanography*, **47,** (4), 989-996.

Montoya, J. P., Wiebe, P. H. and McCarthy, J. J. 1992. Natural abundance of ^{15}N in particulate nitrogen and zooplankton in the Gulf Stream region and warm-core ring 86A. *Deep-Sea Research*, **39**, (1), S 363-S 392.

Montoya, J. P. and McCarthy, J. J. 1995. Isotopic fractionation during nitrate uptake by phytoplankton grown in continuous culture. *Journal of Plankton Research*, **17**, (3), 439-464.

Montoya, J.P., Voss, M., Kaehler, P. and Capone, D.G. 1996. A simple, high-precision, high-sensitivity tracer assay for N_2 fixation. *Applied and environmental microbiology*, **62**, (3), 986-993.

Montoya, J. P., Carpenter, E. J. and Capone, D. G., 2002. Nitrogen fixation and nitrogen isotope abundances in zooplankton of the oligotrophic North Atlantic. *Limnology and Oceanography*, **47**, (6), 1617-1628.

Mulholland, M. R. and Capone, D. G. 1999. Nitrogen fixation, uptake and metabolism in natural and cultured populations of *Trichodesmium* spp. *Marine Ecology Progress Series*, **188**, 33-49.

Mulholland, M. R., Ohki, K. and Capone, D. G., 1999. Nitrogen utilization and metabolism relative to patterns of N_2 fixation cultures of *Trichodesmium* NIBB1067. *Journal of Phycology*, **35**, 977-988.

Mulholland, M. R. and. Capone, D. G., 2000. The physiology of the marine N_2 fixing cyanobacteria *Trichodesmium*. *Trends in Plant Science*, **5,** 148-153.

Mulholland, M. R., K. Ohki and D. G. Capone. 2001. Nutrient controls on nitrogen uptake and metabolism by natural populations and cultures of *Trichodesmium* (Cyanobacteria). *Journal of Phycology*, **37**, 1001-1009.

Mulholland, M. R., Floge, S., Carpenter, E. J., and Capone, D. G., 2002. Phosphorus dynamics in cultures and natural populations of *Trichodesmium* spp.. *Marine Ecology-Progress Series*, **239**, 45-55.

Murphy, J., and Riley, J.P., 1962. A modified single solution method for the determination of phosphate in natural waters. *Analytica Chimica Acta*, **27**, 31-36.

Nakatsuka, T., Handa, N., Wada, E. and Wong, C. S. 1992. The dynamic changes of stable isotopic ratios of carbon and nitrogen in suspended and sedimented particulate organic matter during a phytoplankton bloom. *Journal of Marine Research*, **50**, 267-296.

Nakatsuka, T. and Handa, N. 1997. Reconstruction of Seasonal Variation in Nutrient Budget of a Surface Mixed Layer Using $\delta^{15}N$ of Sinking Particle Collected by a Time-Series Sediment Trap System. *Journal of Oceanography*, **53**, 105-116.

Nakatsuka, T., Handa, N., Harada, N., Sugimoto, T. and Imaizumi, S. 1997. Origin and decomposition of sinking particulate organic matter in the deep water column inferred from the vertical distributions of its $\delta^{15}N$, $\delta^{13}C$ and $\delta^{14}C$. *Deep-Sea Research*, **44**, (12), 1957-1979.

Napolitano, G. E., 1994. The relationship of lipids with light and chlorophyll measurements in fresh-water algae and periphyton. *Journal of Phycology*, **30**, (6), 934-950.

Ohki, K., Reuter, J. G. and Fujita, Y., 1986. Cultures of the pelagic Cyanophytes *Trichodesmium erythraeum* and *T. thiebautii* in synthetic medium. *Marine Biology*, **91**, 9-13.

Ohki, K, Zehr, J. P., Falkowski, P. G. and Fujita, Y., 1991. Regulation of nitrogen fixation by different nitrogen sources in the marine non-heterocystous cyanobacterium, *Trichodesmium* sp. NIBB1067. *Archives of Microbiology*, **156,** 335-337.

Olson, R. J., 1982. ^{15}N tracer studies of the primary nitrite maximum. *Journal of Marine Research*, **39,** 203-226.

Orcutt, K. M., Lipschultz., F., Gundersen, K., Arimoto, R., Michaels, A. F., Knap, A. H. and Gallon, J. R., 2001. A seasonal study of the significance of N_2 fixation by *Trichodesmium* spp. at the Bermuda Atlantic Time-series Study (BATS) site. *Deep-Sea Research II*, **48**, 1583-1608.

Ormazagonzalez, F. I. and Statham, P.J.A., 1996. A comparison of methods for the determination of dissolved and particulate phosphorus in natural waters. *Water Research*, **30**, (11), 2739-2747.

Oschlies, A. and Garcon, V., 1998. Eddy-induced enhancement of primary production in a model of the North Atlantic Ocean. *Nature*, **394**, 266-269.

Owens, N.J.P., 1987. Natural variations in N-15 in the marine environment. *Advances in Marine Biology*, **24,** 389-451.

Owens, N. J. P and Rees, A. P., 1989. Determination of N-15 at submicrogram levels of nitrogen using automated continuous-flow isotope ratio mass-spectrometry. *Analyst*, **114**, (12), 1655-1657.

Owens, N. J. P., Galloway, J. N. and Duce, R. A., 1992. Episodic atmospheric nitrogen deposition to oligotrophic oceans. *Nature*, **357**, 397.

Paerl, H. W., 1985. Enhancement of marine primary production by nitrogen-enriched acid-rain. *Nature*, **315,** (6022), 747-749.

Paerl, H. W., 1991. Ecophysiological and trophic implications of light-stimulated amino-acid utilization in marine picoplankton. *Applied and Environmental Microbiology*, **57,** (2), 473-479.

Palenik, B. and Morel, F. M. M., 1990. Amino acid utilisation by marine phytoplankton: A novel mechanism. *Limnology and Oceanography*, **35**, 260-269.

Palenik, B. and Henson, S. E., 1997. The use of amides and other organic nitrogen source by the phytoplankton *Emiliana huxleyi*. *Limnology and Oceanography*, **42**, 1544-1551.

Pantoja, S., Repeta, D.J., Sachs, J.P. and Sigman, D.M., 2002. Stable isotope constraints on the nitrogen cycle of the Mediterranean Sea water column. *Deep-Sea Research Part I*, **49**, (9), 1609-1621.

Parsons, T. R., Maita, Y. and Lalli, C. M., 1984. *A manual of chemical and biological methods for seawater analysis*. Pergamon Press, Oxford, England.

Partensky, F. Hess, W. R., Vaulot. D., 1999. *Prochlorococcus*, a marine photosynthetic prokaryote of global significance. *Microbiology and Molecular Biology Reviews*, **63**, (1), 106.

Peltzer, E.T., Fry, B., Doering, P.H, McKenna, J.H., Norrman, B. and Zweifel, U.L., 1996. A comparison of methods for the measurement of dissolved organic carbon in natural waters. *Marine Chemistry*, **54** (1-2), 85-96.

Pennock, J. R., Velinsky, D. J., Ludlam, J. M. and Sharp, J. H., 1996. Isotopic fractionation of ammonium and nitrate during uptake by *Skeletonema costatum*: implications for $\delta^{15}N$ dynamics under bloom conditions. *Limnology and Oceanography*, **41**, (3), 451-459.

Pingree, R., Pugh. P., Holligan, P. and Forster, G., 1975. Summer phytoplankton blooms and red tides along tidal fronts in the approaches to the English Channel. *Nature*, **258**, 672 - 677.

Planas, D., Agusti, S., Duarte, C. M., Granata, T. C. and Merino, M. 1999. Nitrate uptake and diffusive supply in the Central Atlantic. *Limnology and Oceanography*, **44**, (1), 116-126.

Platt, T. and Harrison, W. G., 1985. Biogenic fluxes of carbon and oxygen in the ocean. *Nature*, **318**, (6041), 55-58.

Platt, T., and Harrison, W. G., 1986. Reconciliation of carbon and oxygen fluxes in the upper ocean. *Deep-Sea Research Part A*, **33,** (2), 273-276

Platt, T. and Sathyendranath, S., 1988. Oceanic primary production - estimation by remote-sensing at local and regional scales. *Science*, **241**, (4873), 1613-1620.

Polovina, J.J., G.T. Mitchum and G.T. Evans. 1995. Decadal and basin-scale variation in mixed layer depth and the impact on biological production in the Central and North Pacific, 1960-88. *Deep Sea Research*, **42,** (10), 1701-1716.

Proctor, L. M. and Fuhrman, J. A. 1991. Roles of viral infection in organic particle flux. *Marine Ecology-Progress Series*. **69**, 133-142.

Prospero, J. M., Barrett, K., Church, T., Dentener, F., Duce, R. A., Gallowat, J. N., Levy II, H., Moody, J. and Quinn, P., 1996. Atmospheric deposition of nutrients to the North Atlantic Basin. *Biogeochemistry*, **35**, 27-73.

Qian, Y., Kennicutt, M. C., Scalbergm J., Macko, S. A., Bidigare, R. R. and Walker, J., 1996. Suspended particulate organic matter (SPOM) in Gulf of Mexico Estuaries: Compound-specific isotope analysis and plant pigment compositions. *Organic geochemistry*, **24,** (8-9), 875-888.

Raven, J. A., 1988. The iron and molybdenum use efficiencies of plant-growth with different energy, carbon and nitrogen-sources. *New Phytologist*, **109**, (3), 279-287.

Raven, J. A., 1998. The twelfth Tansley Lecture. Small is beautiful: the picophytoplankton *Functional Ecology,* **12**, (4), 503-513.

Rau, G. H., Low, C., Pennington, J. T., Buck, K. R. and Chavez, F. P., 1998. Suspended particulate nitrogen $\delta^{15}N$ versus nitrate utilisation: observations in Monterey Bay, California. *Deep-Sea Research II*, **45**, 1603-1616.

Redfield, A. C.,. Ketchum, B. H and Richards, F. A., 1963. The influence of organisms on the composition of seawater. In: *The Sea*. Edited by: Hill, M. N., Interscience, New York, 26-77.

Rees, A., Woodward, M. and Joint, I. 1999. Measurement of nitrate and ammonium uptake at ambient concentrations in oligotrophic waters of the North-East Atlantic Ocean. *Marine Ecology-Progress Series*, **187**, 295-300.

Rhee, G.-Y., 1978. Effects of N:P atomic ratios and nitrate limitation on algal growth, cell composition, and nitrate uptake. *Limnology and oceanography*, **23,** 10-25.

Ridame, C. and Guieu, C., 2002. Saharan input of phosphate to the oligotrophic water of the open western Mediterranean Sea. *Limnology and Oceanography*, **47,** (3), 856-869.

Rintoul, S. R. and Wunsch C. 1991. Mass, heat, oxygen and nutrient fluxes and budgets in the North Atlantic Ocean. *Deep-Sea Research*, **38**, S355-S377.

Robarts, R.D., Waiser, M.J., Hadas, O., Zohary, T. and MacIntyre, S., 1998. Relaxation of phosphorus limitation due to typhoon-induced mixing in two morphologically distinct basins of Lake Biwa, Japan. *Limnology And Oceanography*, **43,** (6), 1023-1036.

Robins, D. B. and Aiken, J., 1996. The Atlantic Meridional Transect: An oceanographic research programme to investigate physical, chemical, biological and optical variables of the Atlantic Ocean. *Underwater Technology*, **21,** (4), 8-14.

Robinson, C., Serret, P., Tilstone, G., Teira, E., Zubkov, M.V., Rees, A.P. and E.M.S. Woodward, 2002. Plankton respiration in the Eastern Atlantic Ocean. *Deep-Sea Research I*, **49**, (5), 787-813.

Rudnik, D. L. and Martin, J. P., 2002. On the horizontal density ration in the upper ocean. *Dynamics of Atmospheres and Oceans*, **36**, (1-3), 3-21.

Ryther, J.H. and Dunstan, W. M., 1971. Nitrogen, phosphorus and eutrophication in the coastal marine environment. *Science*, **171**, 1008-1013.

Sachs, J. P., Repeta, D. J. and Goericke, R. 1999. Nitrogen and carbon isotopic ratios of chlorophyll from marine phytoplankton. *Geochimica et Cosmochimica Acta*, **63,** (7), 1431-1441.

Saino, T., 1992. ^{15}N and ^{13}C natural abundance in suspended particulate organic matter from a Kuroshio warm-core ring. *Deep-Sea Research*, **39**, S347-S362.

Saino, T. and Hattori, A. 1978. Diel variation in nitrogen fixation by a marine blue-green alga. *Trichodesmium thiebautii*. *Deep-Sea Research*, **25**, 1259-1263.

Saino, T. and Hattori, A. 1980. ^{15}N natural abundance in oceanic suspended particulate matter. *Nature*, **283**, 752-754.

Saino, T. and Hattori, A., 1985. Variation in ^{15}N natural abundance of suspended organic matter in shallow oceanic water. In: *Marine and estuarine geochemistry*. Edited by: Sigleo, A. C and Hattori, A., Lewis, Chelsea, MI, 1-13.

Saino, T. and Hattori, A. 1987. Geographical variation of the water column distribution of suspended particulate organic nitrogen and its ^{15}N natural abundance in the Pacific and its marginal seas. *Deep-Sea Research*, **34**, (5/6), 807-827.

Sakshaug, E and O. Holm-Hansen, 1977. Chemical composition of *Skeletonema costatus* (Grev.) Celve and *Pavlova* (Monochrysis) *lutheri* (Droop) Green as a function of nitrate-, phosphate-, and iron-limited growth. *Journal of Experimental Marine Biology and Ecology*, **29**, 1-34.

Sambrotto, R. N., Savidge, G., Robinson, C., Boyd, C., Takahashi, T., Karl, D. M., Langdon, C., Chipman, D., Marra, J. and Codispoti, L., 1993. Elevated consumption of carbon relative to nitrogen in the surface ocean. *Nature*, **363**, 248-250.

Sanders, R. and Jickells, T., 2000. Total organic nutrients in Drake Passage. *Deep-Sea Research*, **47**, 997-1014.

Sanudo-Wilhelmy, S. A., Kustka, A. B., Gobler, C. J., Hutchins, D. A., Yang, M., Lwiza, K., Burns, J., Capone, D. G., Raven, J. A. and Carpenter, E.J., 2001. Phosphorus limitation of nitrogen fixation by *Trichodesmium* in the central Atlantic Ocean. *Nature*, **411**, (6833), 66-69, 2001.

Sarmiento, J. L., Thiele, G., Key, R. M. and W. S. Moore, 1990. Oxygen and nitrate new production and remineralisation in the North Atlantic subtropical gyre. *Journal of Geophysical Research*, **95**, (C10), 303-315.

Sathyendranathan, S., Longhurst, R. S. A., Caverhill, C. M. and Platt, T., 1995. Regionally and seasonally differentiated primary production in the North Atlantic. *Deep-Sea Research 1*, **42**, 1772-1802.

Scranton. M. I., 1983. Gaseous nitrogen compounds in the marine environment. In: *Nitrogen in the Marine Environment*. Edited by: Carpenter, E. J. and Capone, D. G., Academic press, New York, 37-65.

Seitzinger, S. P. and Sanders, R. W., 1999. Atmospheric inputs of dissolved organic nitrogen stimulate estuarine bacteria and phytoplankton. *Limnology and Oceanography*, **44**, (3), 721-730.

Selner, K. G. and Nealley, E. W., 1997. Diel flucuations in dissolved free amino acids and monosaccharides in Chesapeake Bay dinoflagellate blooms. *Marine Chemistry*, **56**, 193-200.

Sharp, J. H., 1973. Total organic carbon in seawater-comparison of measurements using persulphate oxidation and high temperature combustion. *Marine Chemistry*, **1**, 211-229.

Sharp, J.H., 1977. Extracellular production of organic matter by marine phytoplankton: Do healthy cells do it? *Limnology and Oceanography*, **22,** 381-399.

Sharp, J.H., 1983. The distribution of dissolved inorganic and organic nitrogen in the sea. In: *Nitrogen in the Marine Environment*. Edited by: Carpenter E. J. and Capone, D. G., Academic Press, New York, 1-35.

Sharp, J. H., Peltzer, E. T. and Alperin, M. J., 1993. Measurement of dissolved organic-carbon and nitrogen in natural waters-procedures subgroup report. *Marine Chemistry*, **41**, (1-3), 37-49.

Sharp, J. H., Rinker, K. R., Savidge, K. B., Abell, J., Benaim, J.Y., Bronk, D., Burdige, D..J., Cauwet, G., Chen, W.H., Doval, M.D., Hansell, D., Hopkinson, C., Kattner, G., Kaumeyer, N., McGlathery, K.J., Merriam, J., Morley, N., Nagel, K., Ogawa, H., Pollard, C., Pujo-Pay, M., Raimbault, P., Sambrotto, R., Seitzinger, S., Spyres, G., Tirendi, F., Walsh, T.W. and Wong, C.S., 2002. A preliminary methods comparison for measurement of dissolved organic nitrogen in seawater. *Marine Chemistry*, **78,** (4), 171-184.

Siegel, D.A., McGillicuddy, D.J. and Fields, E.A., 1999. Mesoscale eddies, satellite altimetry, and new production in the Sargasso Sea. *Journal Of Geophysical Research-Oceans*, **104**, (C6), 13359-13379.

Sigman, D.M., Altabet, M. A., Michener, R., McCorkle, D. C., Fry, B. and Holmes, R. M., 1997. Natural abundance-level measurement of the nitrogen isotopic composition of oceanic nitrate: an adaptation of the ammonium diffusion method. *Marine Chemistry*, **57**, 227-242.

Sigman, D. M., Casciotti, K. L., Andreani, M., Barford, C., Galanter, M. and Böhlke, J. K., 2001. A bacterial method for the nitrogen isotopic analysis of nitrate in seawater and freshwater. *Analytical Chemistry*, **73**, 4145-4153.

Smith, S. V., Kimmerer, W. J. and Walsh, T. W., 1986. Vertical flux and biogeochemical turnover regulate nutrient limitation of net organic production in the North Pacific gyre. *Limnology and Oceanography*, **31**, 161-167.

Smith, D. C., Simon, M., Alldredge, A. L. and Azam, F., 1992. Intense hydrolytic enzyme activity on marine aggregates and implications for rapid particle dissolution. *Nature*, **359**, 139-141.

Spitzer, W. S. and Jenkins, W. J., 1989. Rates of vertical mixing, gas exchange, and new production; estimates from seasonal gas cycles in the upper ocean near Bermuda. *Journal of Marine Research*, **47,** 169-196.

Spokes, L. J., Yeatman, S. G., Cornell, S. E. and Jickells, J. D., 2000. Nitrogen deposition to the eastern Atlantic Ocean. The importance of south-easterly flow. *Tellus***, 52B**, 37-49.

Spyres, G., Nimmo, M., Worsfold, P. J., Acterberg, E. P and Miller, A. E. J., 2000. Determination of dissolved organic carbon in seawater using high temperature catalytic oxidation techniques. *Trends in analytical chemistry*, **19,** (8), 498-505.

Sterner, R. W. and Grover, J. P., 1998. Algal growth in warm temperate reservoirs: kinetic examination of nitrogen, temperature, light and other nutrients. *Water research*, **32**, (12), 3539-348.

Sugimura, Y. and Suzuki Y. 1988. A HTCO method for the determination of non-volatile DIC in seawater by direct-injection of a liquid sample. *Marine Chemistry*, **24**, 105-131.

Suttle, C. A. 1994. The significance of viruses to mortality in aquatic microbial communities. *Microbial Ecology*, **28**, 237-243.

Suzumura, M., Ishikawa, K., and Ogawa, H., 1998. Characterisation of dissolved organic phosphorus in coastal seawater using ultrafiltration and phosphohydrolytic enzymes. *Limnology and Oceanography*, **43**, 1553-1564.

Taguchi, S., Ditullio, G. R., Tintore, J. and Ladona, E. G., 1988. Physiological characteristics and production of mixed layer and chlorophyll maximum phytoplankton in the Caribbean Sea and western Atlantic Ocean. *Deep-Sea Research*, **35,** 1363-1377.

Tamminen, T., 1995. Nitrate and ammonium depletion rates and preferences during a Baltic spring bloom. *Marine Ecology-Progress Series*, **120**, (1-3), 123-133.

Tanoue, E., 1992. Vertical-distribution of dissolved organic-carbon in the north pacific as determined by the high-temperature catalytic-oxidation method. *Earth And Planetary Science Letters*, **111,** (1), 201-216.

Tegen, I. and Fung, I., 1995. Contribution to the atmospheric mineral aerosol load from land-surface modification. *Journal Of Geophysical Research-Atmospheres*, **100**, (D9), 18707-18726.

Tett, P., Heaney, S. I., and Droop, M. R., 1985. The Redfield ration and phytoplankton growth rate. *Journal of the Marine biological Association of the United Kingdom*, **65**, 487-504.

Toggweiler, J. R., 1999. Oceanography - An ultimate limiting nutrient. *Nature*, **400**, (6744), 511-512.

Touratier, F., Field, J. G. and Moloney, C. L., 2001. A stoichiometric model relating growth substrate quality (C: N: P ratios) to N: P ratios in the products of heterotrophic release and excretion. *Ecological Modelling*, **139**, (2-3), 265-291.

Tyrrell, T., 1999. The relative influences of nitrogen and phosphorus on oceanic primary production. *Nature*, **400**, 525-530.

Tyrrell T., E. Marañón, A. Poulton, A. R. Bowie, D. S. Harbour and E. M. S. Woodward, 2002. Large-scale latitudinal distribution of *Trichodesmium* spp. in the Atlantic Ocean, *Journal of Plankton research, in press.*

Uz, B. M., Yoder, J. A. and Osychny, V., 2001. Pumping of nutrients to ocean surface waters by the action of propagating planetary waves. *Nature*, **409**, (6820), 597-600.

Valderrama, J. C., 1981. The simultaneous analysis of total nitrogen and total phosphorus in natural-waters. *Marine Chemistry*, **10**, (2), 109-122.

Van Cappelan, P and Ingel, E. D., 1994. Benthic phosphorus regenerationm net primary production, and oceanic anoxia: A model of the coupled marine biogeochemical cycles of carbon and phosphorus. *Paleooceanography*, **9**, 677-692.

Vidal, M., Duarte, C. M. and Agusti, S. 1999. Dissolved organic nitrogen and phosphorus pools and fluxes in the central Atlantic Ocean. *Limnology and Oceanography*, **44**, (1), 106-115.

Villareal, T.A. 1991. Nitrogen-fixation by the cyanobacterial symbiont of the diatom genus *Hemiaulus*. *Marine Ecology-Progress Series*, **76**, (2), 201-204.

Villareal, T.A. 1993. Abundance of the giant diatom *Ethmodiscus* in the southwest Atlantic Ocean and central Pacific gyre. *Diatom Research*, **8,** (1), 171-177.

Villareal, T.A. and E.J. Carpenter. 1990. Diel buoyancy regulation in the marine diazotrophic cyanobacterium *Trichodesmium thiebautii* Ehr. *Limnology and Oceanography*, **35,** (8), 1832-1837.

Villareal, T.A., Altabet, M.A. and Culver-Rymsza, K., 1993. Nitrogen transport by vertically migrating diatoms mats in the North Pacific Ocean. *Nature*, **363**, 709-712.

Vink, S. and Measures, C. I., 2001. The role of dust deposition in determining surface water distributions of Al and Fe in the South West Atlantic, *Deep-Sea Research, II*, **48,** 2787-2809, 2001.

Volkman, J. K., Barrett, S. M., Blackburn, S, I., Mansour, M. P., Sikes, E. L. and Gelin, F., 1998. Microalgal biomarkers: A review of recent research developments. *Organic Geochemistry*, **29**, (5), 1163-1179.

Voss, M., Altabet, M. A. and Bodungen, B. V., 1996. $\delta^{15}N$ in sedimenting particles as indicator of euphotic-zone processes. *Deep-Sea Research*, **43**, (1), 33-47.

Wada, E., 1980. Nitrogen isotope fractionation and its significance in biogeochemical processes occurring in marine environments. In: *Isotope Marine Chemistry*. Edited by: Goldberg, E. D., Japan, 375-398.

Wada, E. and Hattori, A., 1976. Natural Abundance of ^{15}N in particulate organic matter in the North Pacific Ocean. *Geochimica et Cosmochimica Acta*, **40**, 249-251.

Wada, E. and Hattori, A., 1978. Nitrogen isotope effects in the assimilation of inorganic nitrogenous compounds by marine diatoms. *Geomicrobiology Journal*, **1**, 85-101.

Wada, E., Terasaki, M., Kabaya, Y., and Nemoto, T., 1987. ^{15}N and ^{13}C abundance in the Antarctic Ocean with emphasis on the biogeochemical structure of the food web. *Deep-Sea Research*, **34**, 829-841.

Wakeham, S. G. and Canuel, E. A., 1988. Organic geochemistry of particulate matter in the eastern tropical north Pacific-Ocean - implications for particle dynamics. *Journal of Marine Research*, **46,** (1), 183-213.

Wallace, J. M., Smith, C. and Bretherton, C. S., 1992. Singular value decomposition of wintertime sea-surface temperature and 500-mb height anomalies. *Journal of Climate*, **5**, (6), 561-576.

Walsh, J. J. 1996. Nitrogen fixation within a tropical upwelling ecosystem: Evidence for a Redfield budget of carbon/nitrogen cycling by the total phytoplankton community. *Journal of Geophysical Research*, **101**, (C9), 20607-20616.

Walsh, J.J., Rowe, G. T., Iverson, R. L. and McIlroy, C. P., 1981, Biological export of shelf carbon is a sink of the global CO_2 cycle. *Nature*, **291**, 196-201.

Wangersky, P. J., 1993. Dissolved organic-carbon methods – A critical review. *Marine Chemistry*, **41**, (1-3), 61-74.

Waser, N. A., Harrison, P. J., Nielsen, B., Calvert, S. E. and Turpin, D. H.,1998. Nitrogen isotope fractionation during the uptake and assimilation of nitrate, nitrite, ammonium and urea by marine diatom. *Limnology and Oceanography*, **43**, (2), 215-224.

Waser, N. A., Yu, Z., Yin, K., Nielsen, B., Harrison, P. J., Turpin, D. and Calvert, S. E. 1999. Nitrogen isotopic fractionation during a simulated diatom spring bloom: importance of N-starvation in controlling fractionation. *Marine Ecology-Progress Series*, **179**, 291-296.

Waser, N. A. D., Harrison, W. G., Head, E. J. H., Nielsen, B., Lutz, V. A. and Calvert, S. E. 2000. Geographic variations in the nitrogen isotope composition of surface particulate nitrogen and new production across the North Atlantic Ocean. *Deep-Sea Research*, **47,** 1207-1226.

Welschmeyer, N. A., 1994. Fluorometric analysis of chlorophyll-a in the presence of chlorophyll-b and pheopigments. *Limnology and Oceanography*, **39,** (8), 1985-1992.

West, N. J., Schonhuber, W. A., Fuller, N. J., Amann, R. I., Rippka, R., Ost, A. F., and Scanlan, D. J., 2001. Closely related *Prochlorococcus* genotypes show remarkably different depth distributions in two oceanic regions as revealed by in situ hybridisation using 16 S r RNA-targeted oligonucleotides. *Microbiology*, **147**, 1731-1744.

Wheeler, P. A. and Kokkinakis, S. A., 1990. Ammonium recycling limits nitrate use in the oceanic subarctic Pacific. *Limnology and Oceanography*, **35**, (6), 1267-1278.

Wiegert, R. G. and Penaslado, E., 1995. Nitrogen-pulsed systems on the coast of Northwest Spain. *Estuaries*, **18**, (4), 622-635.

Williams, R. G. and Follows, M. J., 1998. Eddies make ocean deserts bloom. *Nature*, **394**, 228-229.

Williams, R. G., McLaren, A. J. and Follows, M. J. 2000. Interannual variability in export production implied by changes in convection over the North Atlantic. *Global Biogeochemical Cycles*, **14**, 1299-1313.

Williams, R.G. and Follows, M.J., 2002. Physical transport of nutrients and the maintenance of biological production. In: *Ocean Biogeochemistry: a JGOFS synthesis*. Edited by: M. Fasham. Springer. In press.

Wolff, G., Boardman, D., Horsfall, I., Sutton, I., Davis, N., Chester, R., Ripley, M., Lewis, A., Rowland, S. J., Patching, J., Ferrero, T., Lambshead P. J. D. and Rice, A., 1995. The Biogeochemistry of Sediments from the Madeira Abyssal Plain - Preliminary Results. *International Revue ges. Hydrobiologie*, **80,** (2), 333-349.

Woodward, E. M. S. and Rees, A. P., 2001. Nutrient distributions in an anticyclonic eddy in the northeast Atlantic Ocean, with reference to nanomolar ammonium concentrations, *Deep Sea Res., II*, **48**, 775-793.

Wu, J., Calvert, S. E. and Wong, C. S. 1997. Nitrogen isotope variations in the subarctic Northeast Pacific: relationships to nitrate utilisation and trophic structure. *Deep-Sea Research*, **44**, (2), 287-314.

Wu, J., Sunda, W., Boyle, E. A. and Karl, D. M., 2000. Phosphate depletion in the Western North Atlantic Ocean. *Science*, **289**, 759-761.

Yeatman, S. G., Spokes, L. J., Dennis, P. F., and Jickells, T. D., 2001. Comparisons of aerosol nitrogen isotopic composition at two polluted coastal sites. *Atmospheric Environment*, **35**, (7), 1307-1320.

Zehr, J. P. and McReynolds, L. A., 1989. Use of degenerate oligonucleotides for amplification of the nifh gene from the marine cyanobacterium *Trichodesmium thiebautii*. *Applied and Environmental Microbiology*, **55**, (10), 2522-2526.

Zehr, J. P., Mellon, M. T. and Zani, S. 1998. New nitrogen-fixing micro-organisms detected in oligotrophic oceans by amplification of nitrogenase (nifH) Genes. *Applied and Environmental Microbiology*, **64,** (9), 3444-3450.

Zehr, J. P., Carpenter, E. J. and Villareal, T. A., 2000. New perspectives on nitrogen-fixing microorganisms in tropical and subtropical oceans. *Trends In Microbiology*, **8**, (2), 68-73.

Zender, C. S., H. Bian, and D. Newman, The mineral Dust Entrainment and Deposition (DEAD) model: Description and 1990's dust climatology, submitted to *Journal of Geophysical Research*, 2002.

Zubkov, M. V., Sleigh, M. A., Tarran, G. A., Burkill, P. H. and Leakey, R. J.G., 1998. Picoplanktonic community structure on an Atlantic Transect from 50 degrees N to 50 degrees S. *Deep-Sea Research Part I*, **45**, (8), 1339-1355.

Zubkov, M. V., Sleigh, M. A., Burkhill, P. H. and Leakey, R. J. G., 2000. Picoplankton community structure on the Atlantic Meridional Transect: a comparison between seasons. *Progress in Oceanography*, **45,** 369-386

Appendix A

Atlantic Meridional Transect cruise details and cross sections of temperature, salinity and density

Table A1. Cruise number, departure and arrive port and dates of Atlantic Meridional Transects between 1995 and 2000 on board the RRS James Clark Ross.

CRUISE	DEPARTED	DATE	ARRIVED	DATE
AMT 1	UK	21/09/95	Port Stanley	24/10/95
AMT 2	Port Stanley	22/04/96	UK	28/05/96
AMT 3	UK	20/09/96	Port Stanley	24/10/96
AMT 4	Port Stanley	21/04/97	UK	27/05/97
AMT 5	UK	14/09/97	Port Stanley	17/10/97
AMT 6	Cape Town	15/05/98	UK	15/06/98
AMT 7	UK	14/09/98	Port Stanley	25/10/98
AMT 8	Port Stanley	24/04/99	UK	07/06/99
AMT 9	UK	15/09/99	Montevideo	13/10/99
AMT 10	Montevideo	12/04/00	UK	07/05/00
AMT 11	UK	11/09/00	Montevideo	13/10/00

Figure A1. Latitudinal and depth variation in (a) temperature (°C), (b) salinity and (c) density (kg m^{-3}) during AMT 1

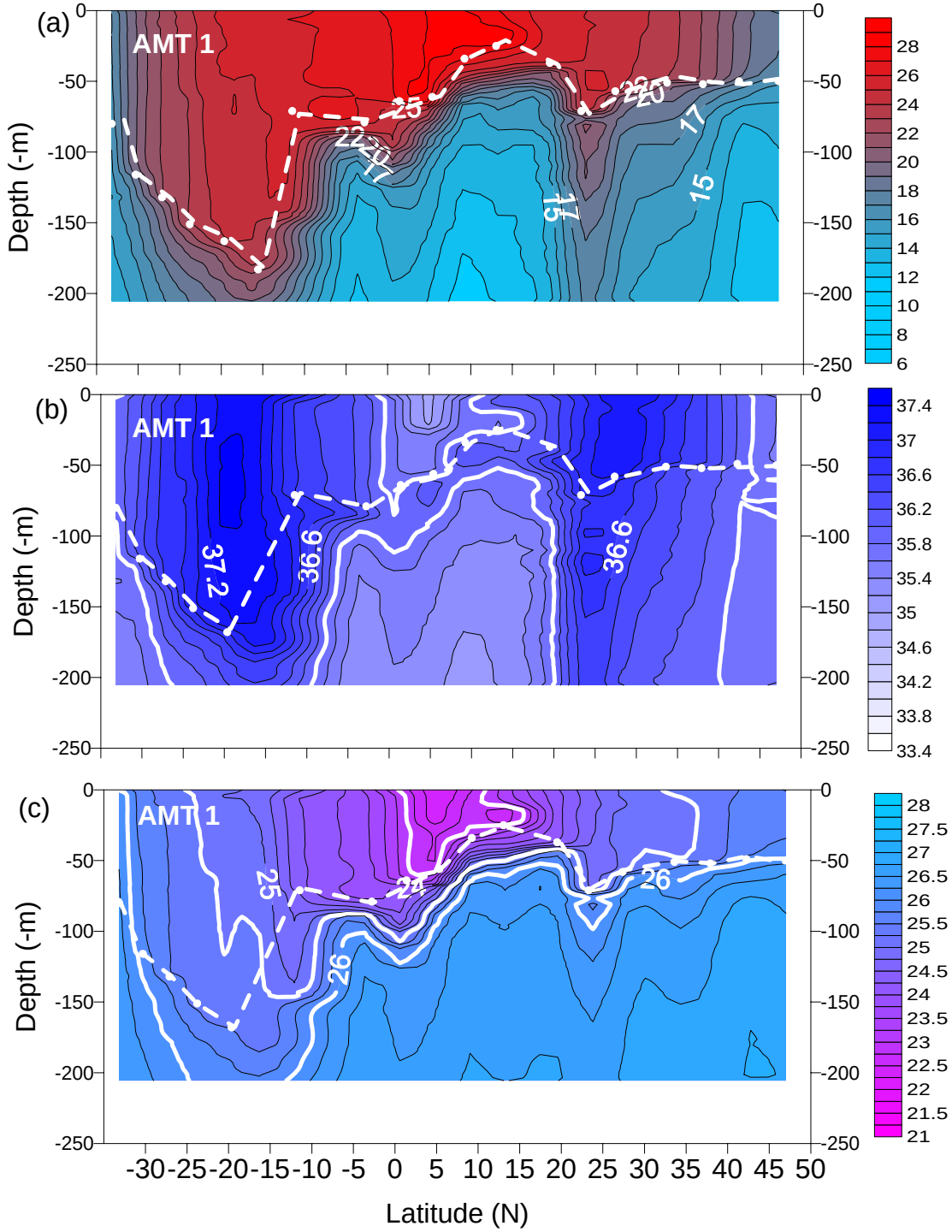

Figure A2. Latitudinal and depth variation in (a) temperature (°C), (b) salinity and (c) density (kg m^{-3}) during AMT 2

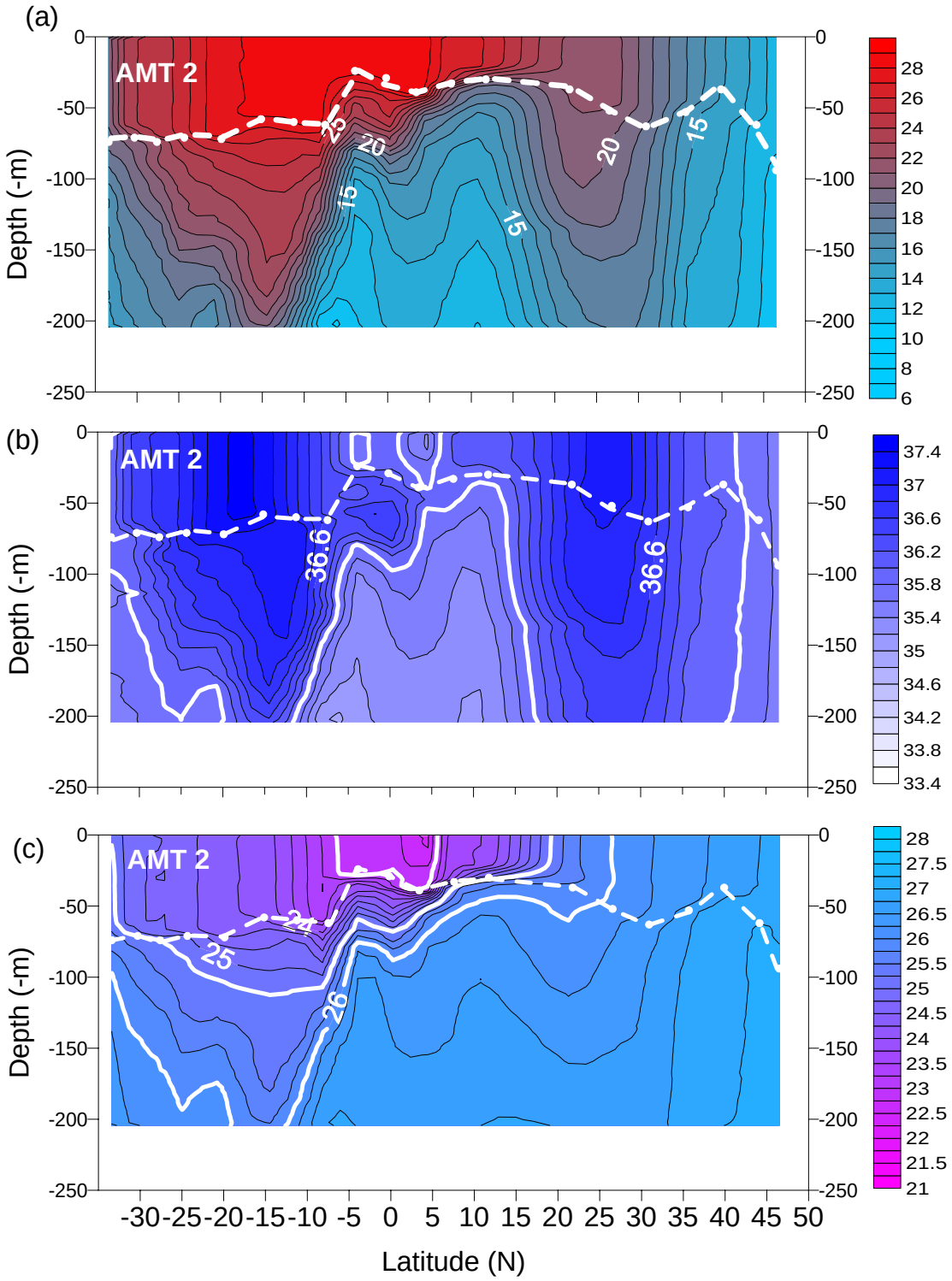

Figure A3. Latitudinal and depth variation in (a) temperature (°C), (b) salinity an(c) density (kg m^{-3}) during AMT 3

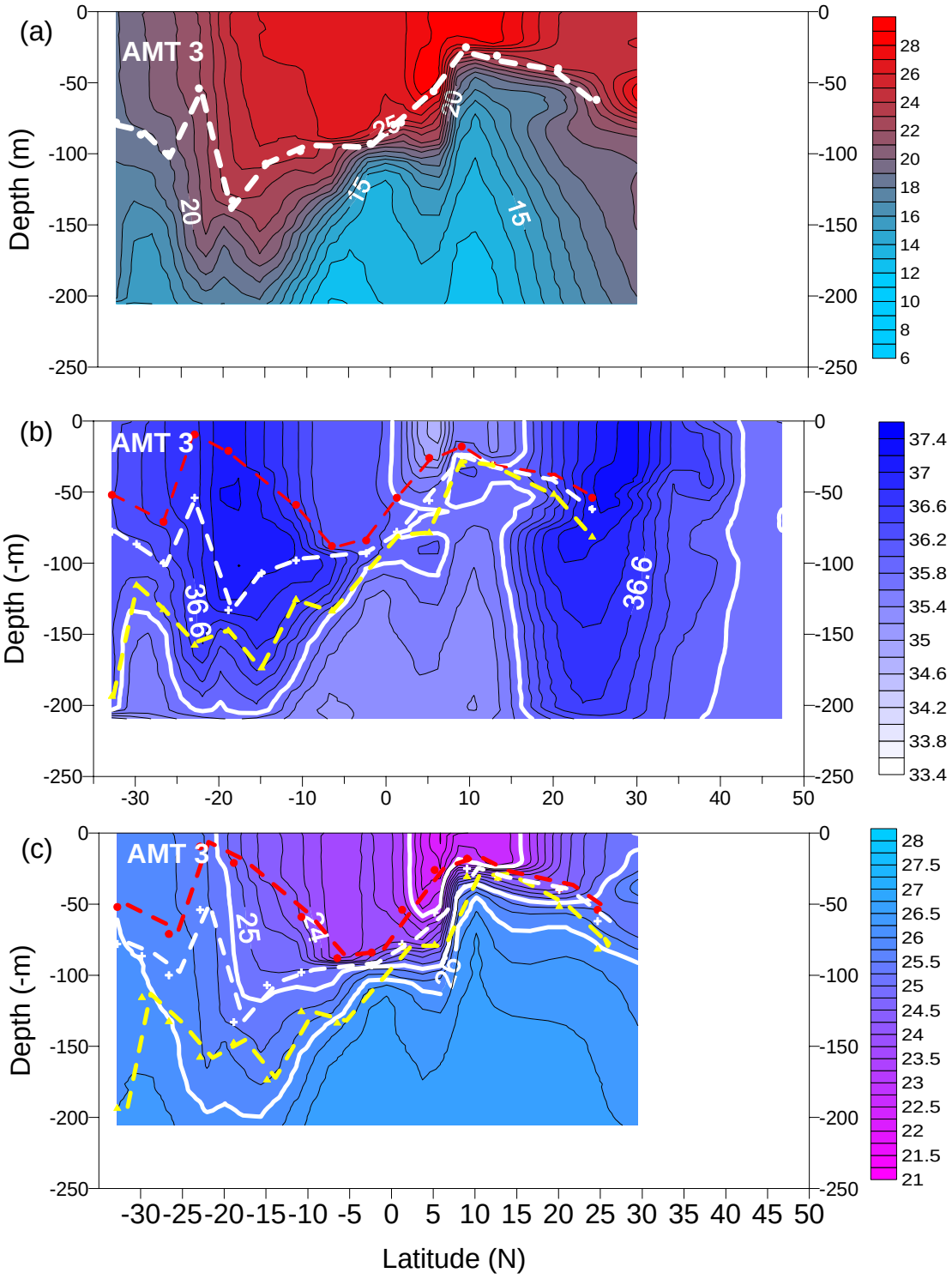

Figure A4. Latitudinal and depth variation in (a) temperature (°C), (b) salinity and (c) density (kg m^{-3}) during AMT 4

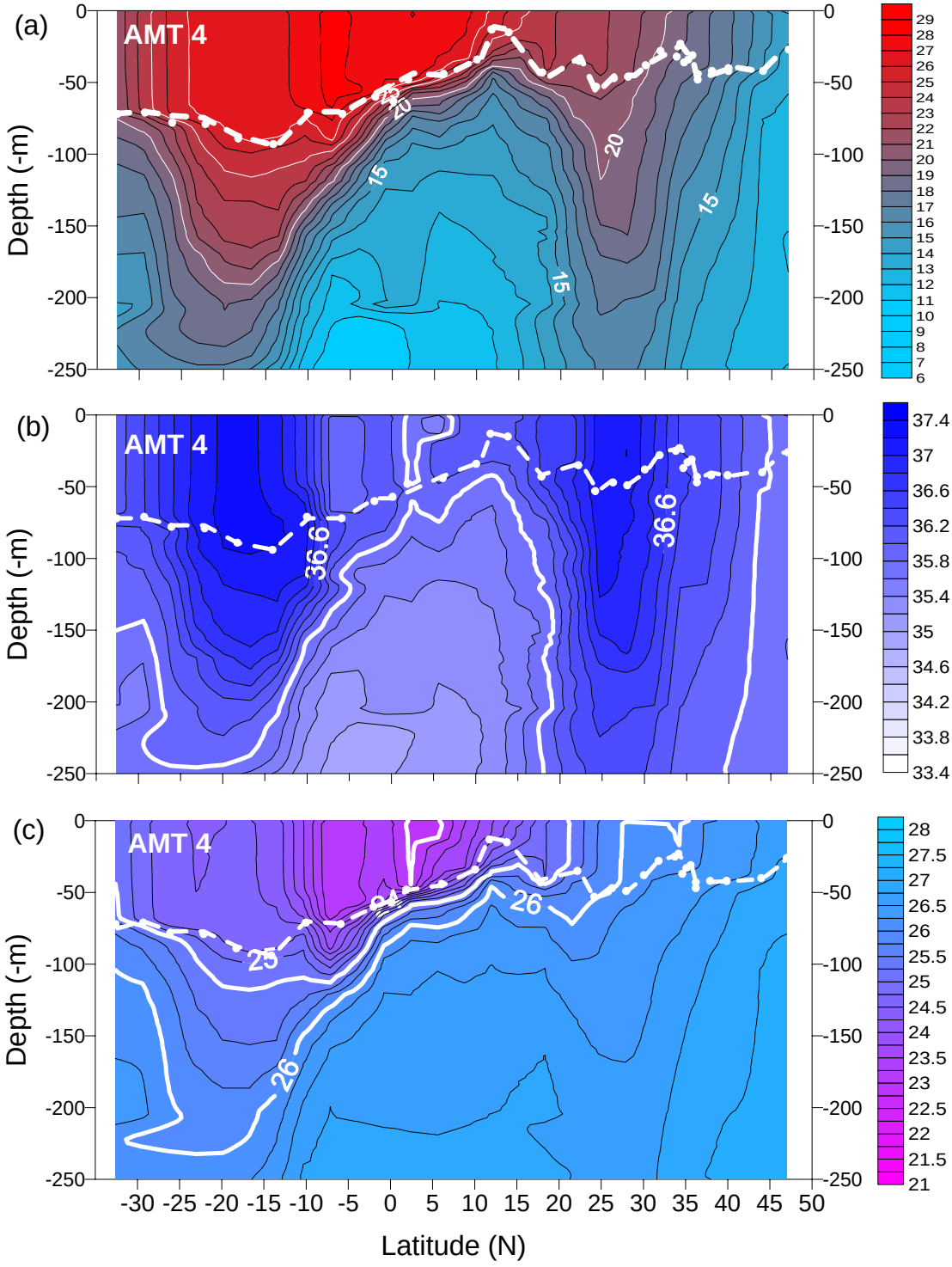

Figure A5. Latitudinal and depth variation in (a) temperature (°C), (b) salinity and (c) density (kg m^{-3}) during AMT 5

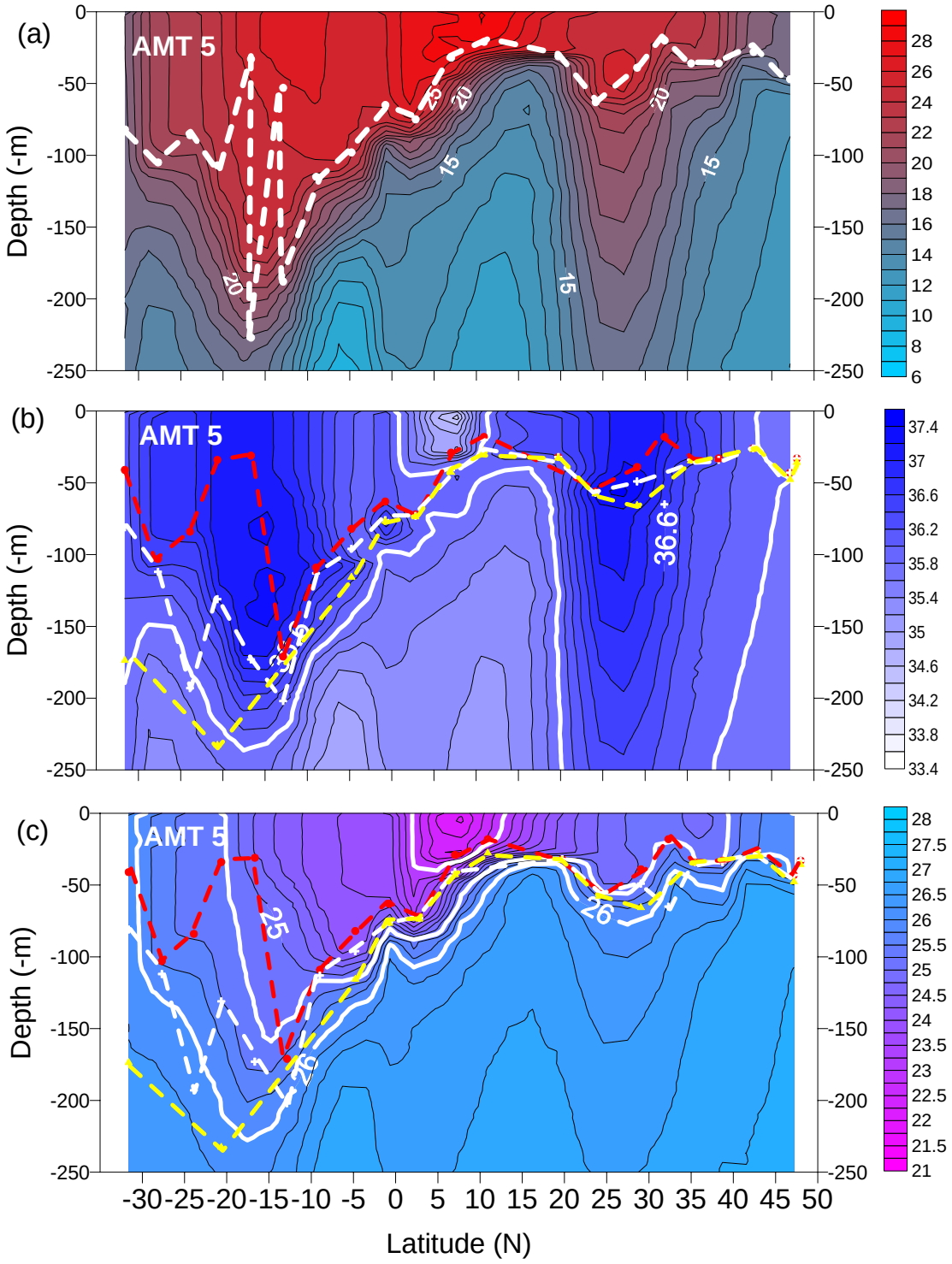

Figure A6. Latitudinal and depth variation in (a) temperature (°C), (b) salinity and (c) density (kg m^{-3}) during AMT 6

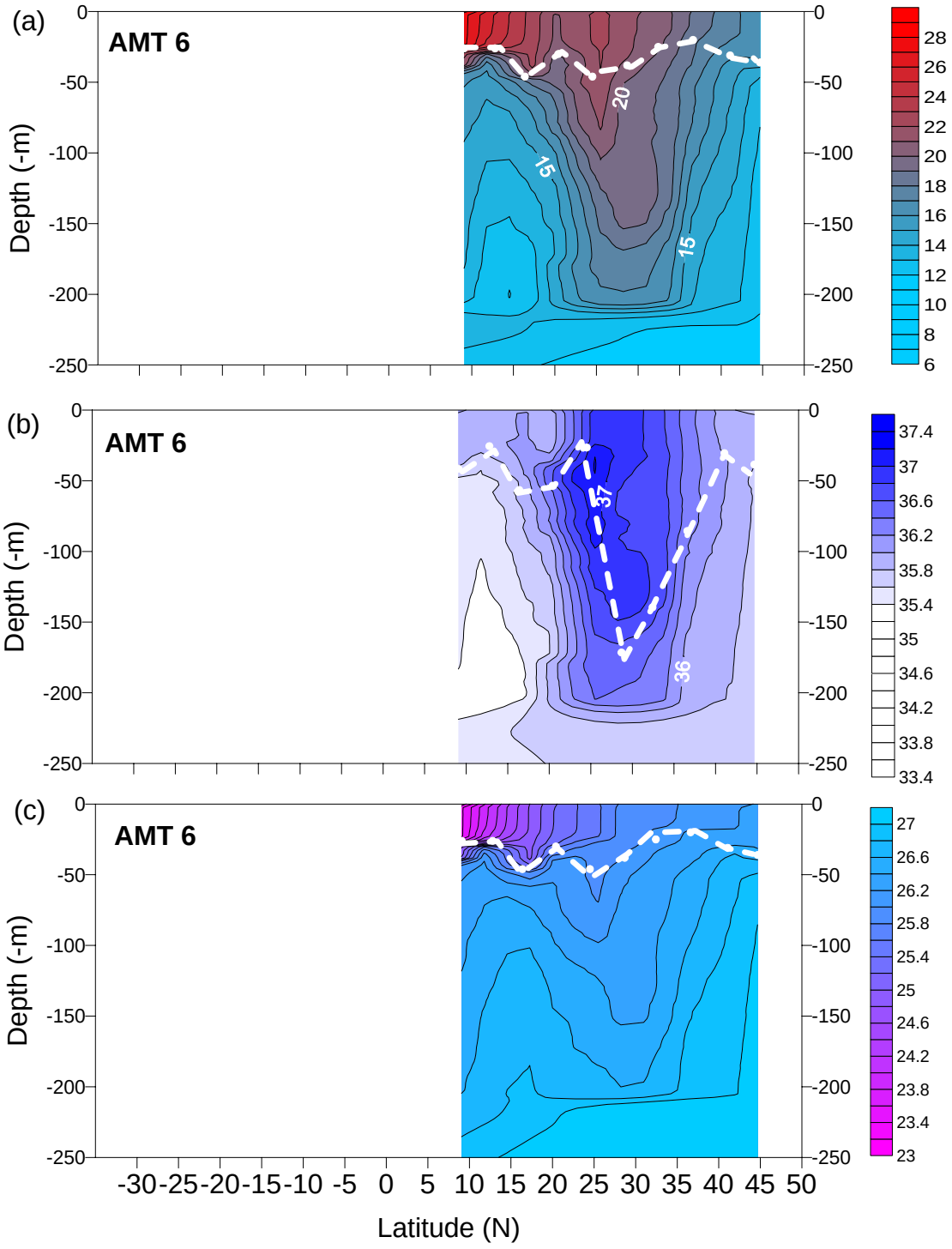

Figure A7. Latitudinal and depth variation in (a) temperature (°C), (b) salinity and (c) density (kg m^{-3}) during AMT 7

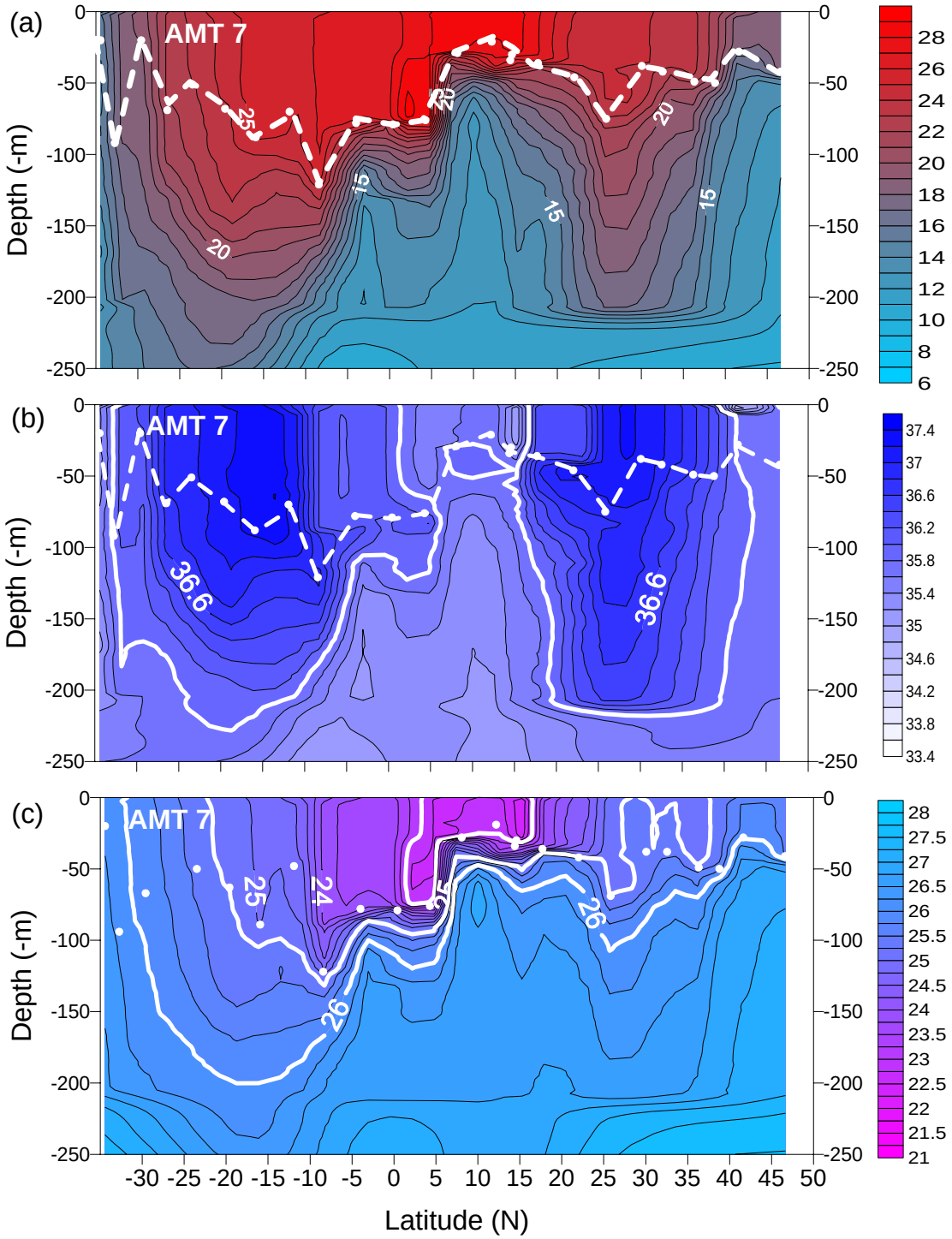

Figure A8. Latitudinal and depth variation in (a) temperature (°C), (b) salinity and (c) density (kg m^{-3}) during AMT 8

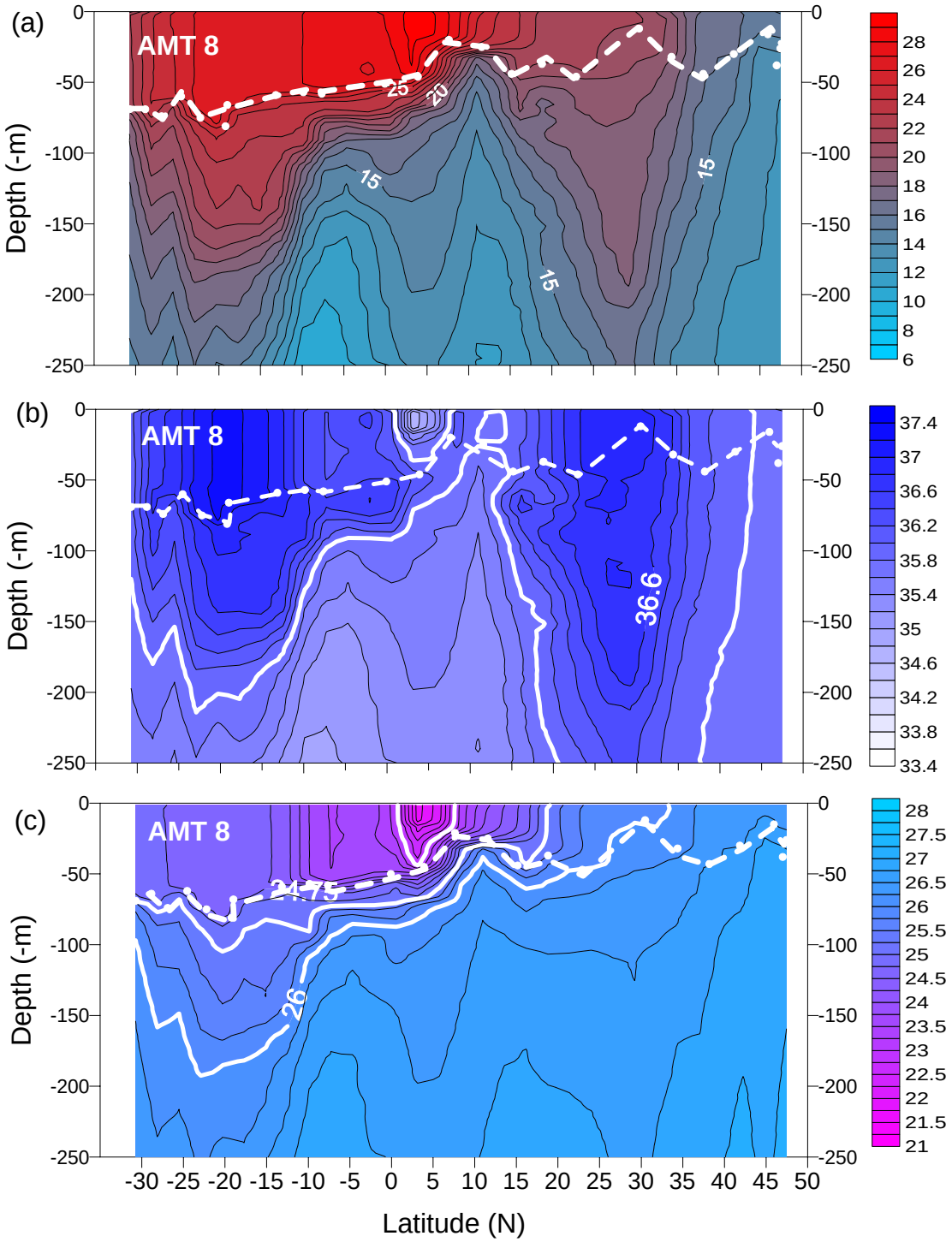

Figure A9. Latitudinal and depth variation in (a) temperature (°C), (b) salinity and (c) density (kg m^{-3}) during AMT 9

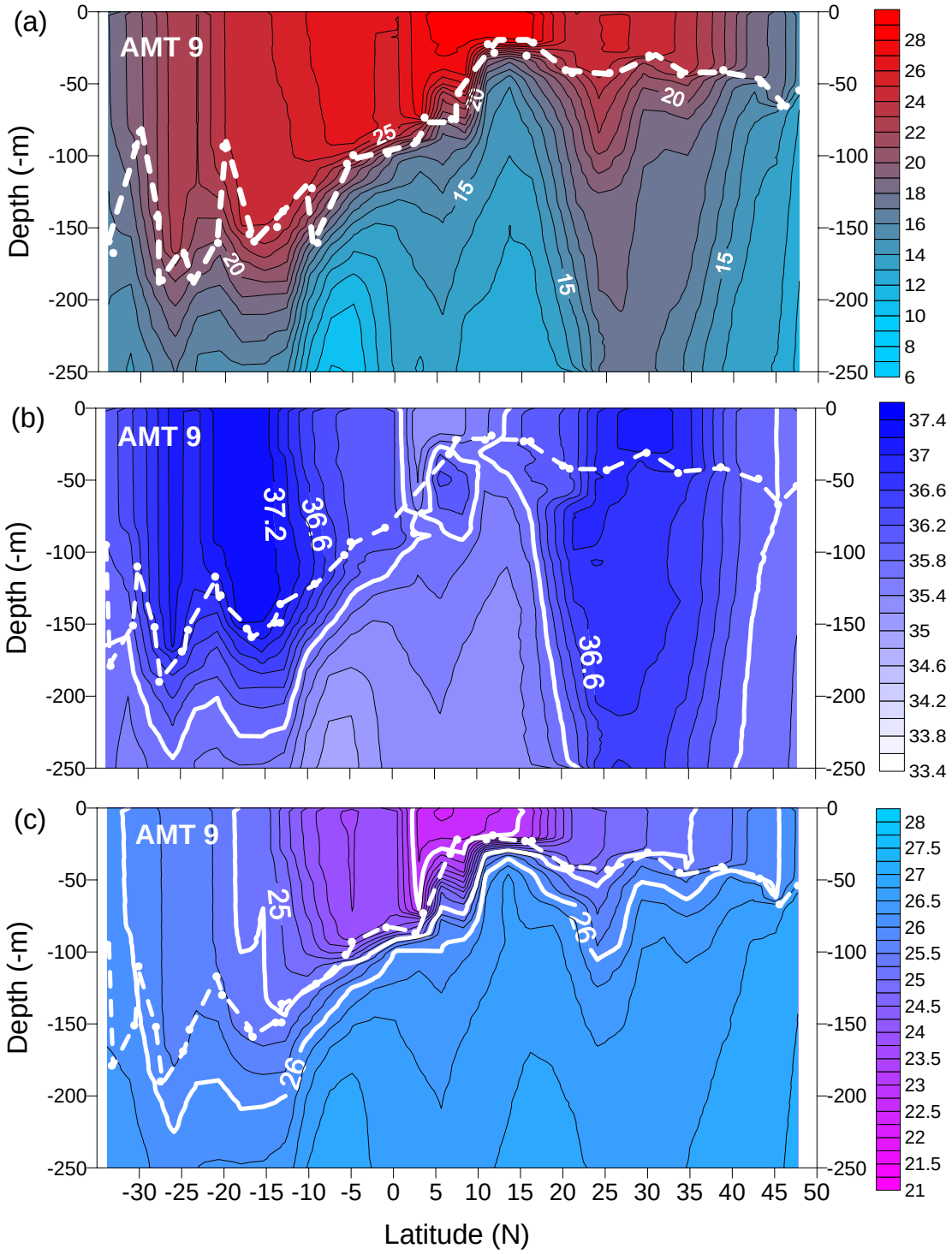

Figure A10. Latitudinal and depth variation in (a) temperature (°C), (b) salinity and (c) density (kg m^{-3}) during AMT 10

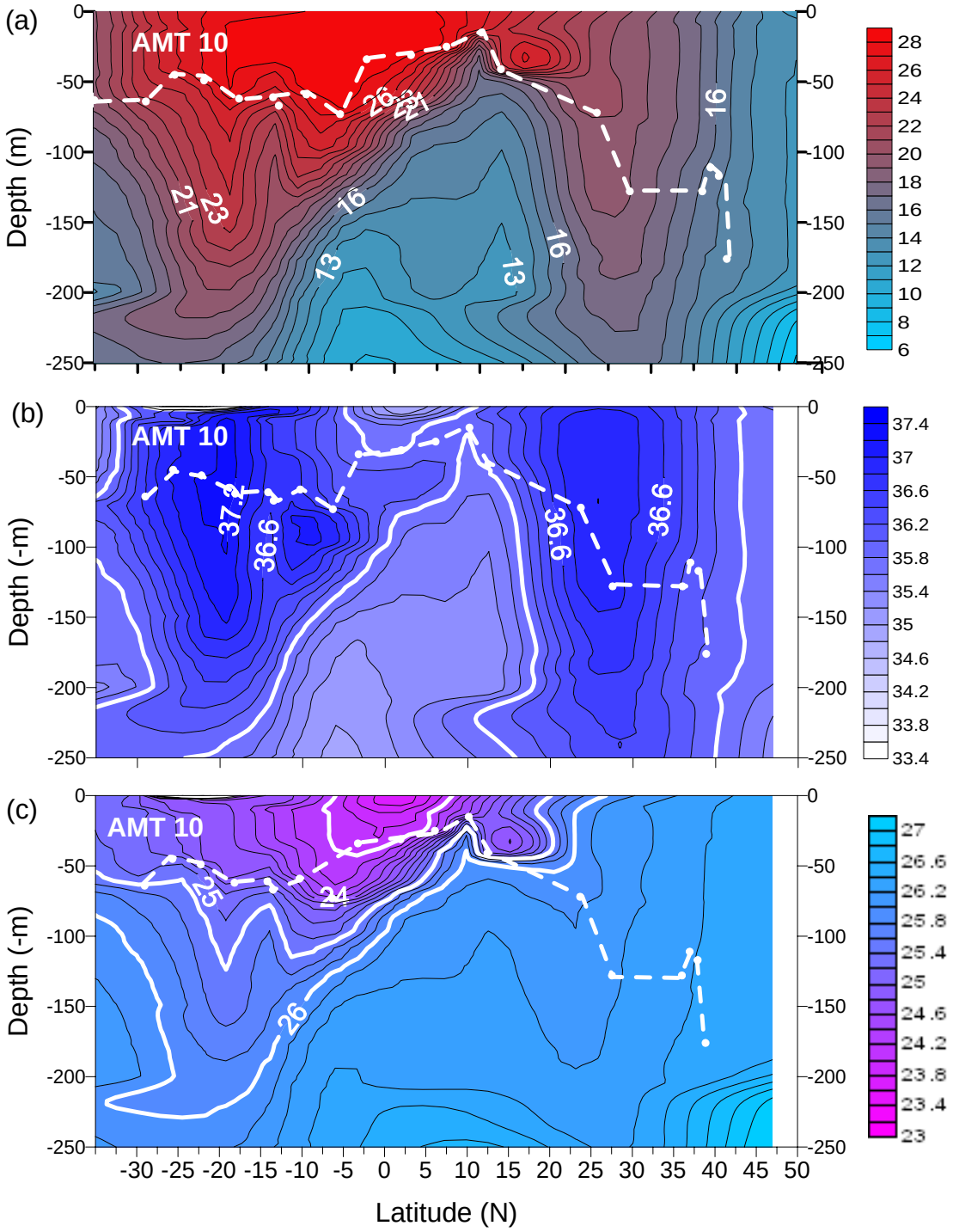

Figure A11. Latitudinal and depth variation in (a) temperature (°C), (b) salinity and (c) density (kg m^{-3}) during AMT 11

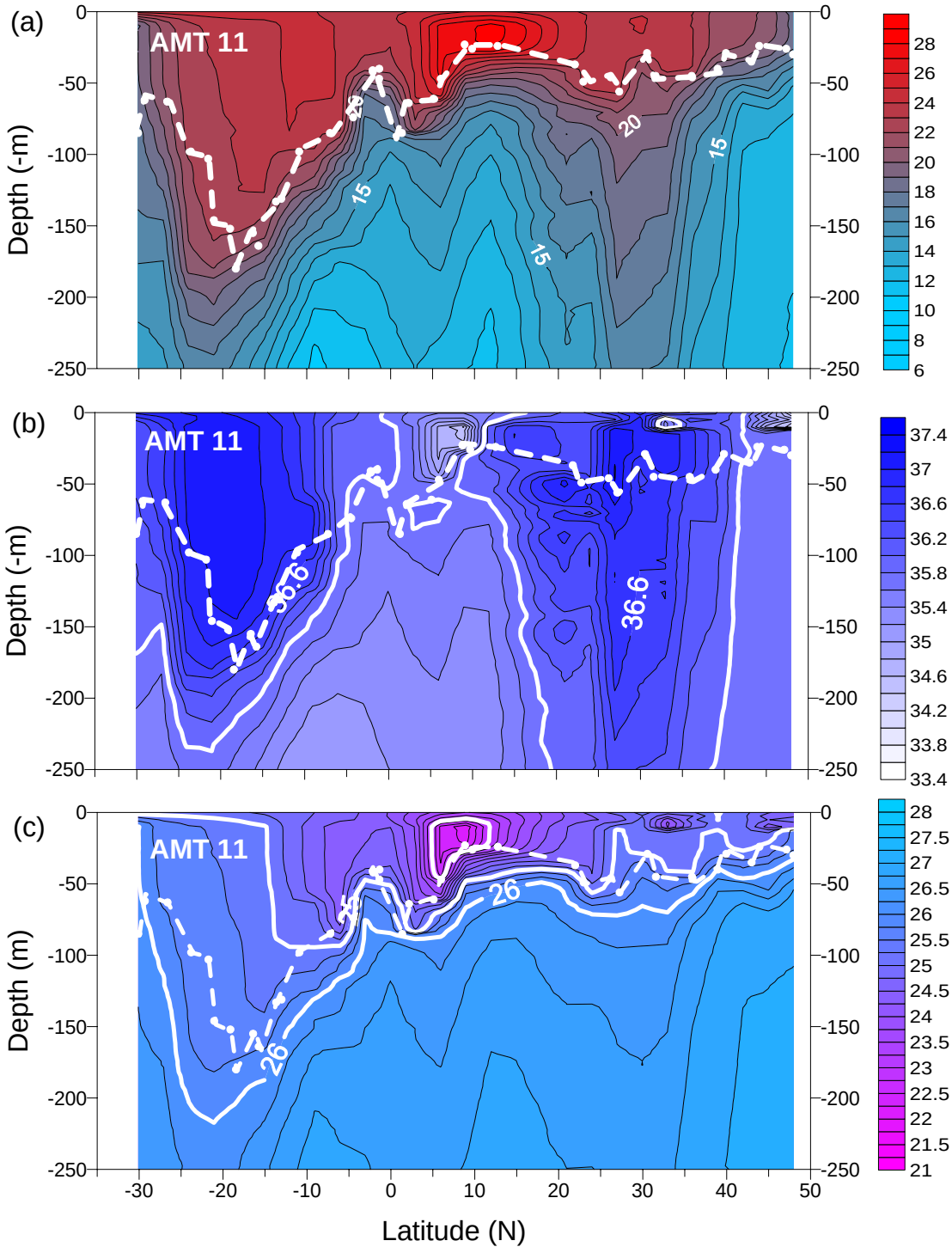

Appendix B

Station and sample log tables for AMT 10

Table B1. Sample Log for collection of filtered seawater samples in ampoules (~ 8 mL) and bottles (~ 100 mL) for DOC, DON and DOP analysis.

STATION NUMBER	DATE	LOCAL TIME	LATIT (N)	LONG (W)	DEPTH (M)	AMPOULES (~ 8 ML)	BOTTLES (~ 100ML)
1	13/04/2000	1000	-35.087	-42.924	200	AMT-10/1/200a/b/c/	AMT-10/1/200/d
					150	AMT-10/1/150a/b/	AMT-10/1/150/c
					75	AMT-10/1/75a/b/	AMT-10/1/75/c
					50	AMT-10/1/50a/b/	AMT-10/1/50/c
					45	AMT-10/1/45a/b/	AMT-10/1/45/c
					40	AMT-10/1/40a/b/	AMT-10/1/40/c
					25	AMT-10/1/25a/b/	AMT-10/1/25/c
					25	AMT-10/1/25a/b/	AMT-10/1/25/c
					15	AMT-10/1/15a/b/	AMT-10/1/15/c
					7	AMT-10/1/7a/b/	AMT-10/1/7/c
					7	AMT-10/1/7a/b/c/	AMT-10/1/7/d/
	14/04/2000	No station due to weather					
2	15/04/2000	1000	29.094	43.028	200	AMT-10/2/200a/b/c/	AMT-10/2/200/d/
					150	AMT-10/2/150a/b/	AMT-10/2/150/c
					130	AMT-10/2/130a/b/	AMT-10/2/130/c
					90	AMT-10/2/90a/b/	AMT-10/2/90/c
					75	AMT-10/2/75a/b/	AMT-10/2/75/c
					60	AMT-10/2/60a/b/	AMT-10/2/60/c
					45	AMT-10/2/45a/b/	AMT-10/2/45/c
					20	AMT-10/2/20a/b/	AMT-10/2/20/c
					15	AMT-10/2/15a/b/	AMT-10/2/15/c
					7	AMT-10/2/7a/b/	AMT-10/2/7/c
3	16/04/2000	No second CTD cast due to technical problems					
4	17/04/2000	1000	-22.25	-36.841	250	AMT-10/4/250a/b/c/	AMT-10/4/250/d/
					175	AMT-10/4/175a/b/	AMT-10/4/175/c
					135	AMT-10/4/135a/b/	AMT-10/4/135/c
					105	AMT-10/4/105a/b/	AMT-10/4/105/c
					90	AMT-10/4/90a/b/	AMT-10/4/90/c
					80	AMT-10/4/80a/b/	AMT-10/4/80/c
					45	AMT-10/4/45a/b/	AMT-10/4/45/c
					35	AMT-10/4/35a/b/	AMT-10/4/35/c
					30	AMT-10/4/30a/b/	AMT-10/4/30/c
					20	AMT-10/4/20a/b/	AMT-10/4/20/c
					15	AMT-10/4/15a/b/	AMT-10/4/15/c
					7	AMT-10/4/7a/b/c/	AMT-10/4/7/d
5	18/04/2000	No second CTD cast					
6	19/04/2000	1000	-14.189	-32.647	250	AMT-10/6/250a/b/c/	AMT-10/6/250/d/

					175	AMT-10/6/175a/b/	AMT-10/6/175/c
					150	AMT-10/6/150a/b/	AMT-10/6/150/c
					135	AMT-10/6/135a/b/	AMT-10/6/135/c
					125	AMT-10/6/125a/b/	AMT-10/6/125/c
					100	AMT-10/6/100a/b/	AMT-10/6/100/c
					65	AMT-10/6/65a/b/	AMT-10/6/65/c
					55	AMT-10/6/55a/b/	AMT-10/6/55/c
					30	AMT-10/6/30a/b/	AMT-10/6/30/c
					20	AMT-10/6/20a/b/	AMT-10/6/20/c
					15	AMT-10/6/15a/b/	AMT-10/6/15/c
					7	AMT-10/6/7a/b/c/	AMT-10/6/7/d/
7	19/04/2000	1600	-13.513	-32.327	1000	AMT-10/7/1000a/b/c/	AMT-10/7/1000/d/
deep station					500	AMT-10/7/500a/b/	AMT-10/7/500/c
					300	AMT-10/7/300a/b/	AMT-10/7/300/c
					230	AMT-10/7/230a/b/	AMT-10/7/230/c
					180	AMT-10/7/180a/b/	AMT-10/7/180/c
					150	AMT-10/7/150a/b/	AMT-10/7/150/c
					130	AMT-10/7/130a/b/	AMT-10/7/130/c
					100	AMT-10/7/100a/b/	AMT-10/7/100/c
					25	AMT-10/7/25a/b/c/	AMT-10/7/25/d/
8	20/04/2000		-10.285	-30.819	250	AMT-10/8/250a/b/c/	AMT-10/8/250/d/
					175	AMT-10/8/175a/b/	AMT-10/8/175/c
					130	AMT-10/8/130a/b/	AMT-10/8/130/c
					120	AMT-10/8/120a/b/	AMT-10/8/120/c
					110	AMT-10/8/110a/b/	AMT-10/8/110/c
					100	AMT-10/8/100a/b/	AMT-10/8/100/c
					60	AMT-10/8/60a/b/	AMT-10/8/60/c
					55	AMT-10/8/55a/b/	AMT-10/8/55/c
					30	AMT-10/8/30a/b/	AMT-10/8/30/c
					20	AMT-10/8/20a/b/	AMT-10/8/20/c
					7	AMT-10/8/7a/b/c/	AMT-10/8/7/d/
9	21/04/2000	1000	-6.206	-28.593	250	AMT-10/9/250a/b/c/	AMT-10/9/250/d/
					175	AMT-10/9/175a/b/	AMT-10/9/175/c
					125	AMT-10/9/125a/b/	AMT-10/9/125/c
					105	AMT-10/9/105a/b/	AMT-10/9/105/c
					80	AMT-10/9/80a/b/	AMT-10/9/80/c
					70	AMT-10/9/70a/b/	AMT-10/9/70/c
					55	AMT-10/9/55a/b/	AMT-10/9/55/c
					30	AMT-10/9/30a/b/	AMT-10/9/30/c
					20	AMT-10/9/20a/b/	AMT-10/9/20/c
					15	AMT-10/9/15a/b/	AMT-10/9/15/c
					7	AMT-10/9/7a/b/c/	AMT-10/9/7/d/
10	22/04/2000	1000	-2.225	-27.09	250	AMT-10/10/250a/b/c/	AMT-10/10/250/d/

					175	AMT-10/10/175a/b/	AMT-10/10/175/c
					100	AMT-10/10/100a/b/	AMT-10/10/100/c
					60	AMT-10/10/60a/b/	AMT-10/10/60/c
					55	AMT-10/10/55a/b/	AMT-10/10/55/c
					50	AMT-10/10/50a/b/	AMT-10/10/50/c
					40	AMT-10/10/40a/b/	AMT-10/10/40/c
					35	AMT-10/10/35a/b/	AMT-10/10/35/c
					25	AMT-10/10/25a/b/	AMT-10/10/25/c
					20	AMT-10/10/20a/b/	AMT-10/10/20/c
					15	AMT-10/10/15a/b/	AMT-10/10/15/c
					7	AMT-10/10/7a/b/c/	AMT-10/10/7/d/
11	23/04/2000	1000	-1.99	-25.25	200	AMT-10/11/200a/b/c/	AMT-10/11/200/d/
					150	AMT-10/11/150a/b/	AMT-10/11/150/c
					110	AMT-10/11/110a/b/	AMT-10/11/110/c
					80	AMT-10/11/80a/b/	AMT-10/11/80/c
					70	AMT-10/11/70a/b/	AMT-10/11/70/c
					60	AMT-10/11/60a/b/	AMT-10/11/60/c
					55	AMT-10/11/55a/b/	AMT-10/11/55/c
					45	AMT-10/11/45a/b/	AMT-10/11/45/c
					25	AMT-10/11/25a/b/	AMT-10/11/25/c
					15	AMT-10/11/15a/b/	AMT-10/11/15/c
					7	AMT-10/11/7a/b/c/	AMT-10/11/7/d/
12	24/04/2000	1000	6.105	-23.44	200	AMT-10/12/200a/b/c/	AMT-10/12/200/d/
					150	AMT-10/12/150a/b/	AMT-10/12/150/c
					100	AMT-10/12/100a/b/	AMT-10/12/100/c
					75	AMT-10/12/75a/b/	AMT-10/12/75/c
					55	AMT-10/12/55a/b/	AMT-10/12/55/c
					45	AMT-10/12/45a/b/	AMT-10/12/45/c
					35	AMT-10/12/35a/b/	AMT-10/12/35/c
					25	AMT-10/12/25a/b/	AMT-10/12/25/c
					20	AMT-10/12/20a/b/	AMT-10/12/20/c
					15	AMT-10/12/15a/b/	AMT-10/12/15/c
					7	AMT-10/12/7a/b/	AMT-10/12/7/c
					2	AMT-10/12/2a/b/c/	AMT-10/12/2/d/
13	25/04/2000	1000	10.209	-21.651	200	AMT-10/13/200a/b/c/	AMT-10/13/200/d/
					150	AMT-10/13/150a/b/	AMT-10/13/150/c
					100	AMT-10/13/100a/b/	AMT-10/13/100/c
					75	AMT-10/13/75a/b/	AMT-10/13/75/c
					45	AMT-10/13/45a/b/	AMT-10/13/45/c
					30	AMT-10/13/30a/b/	AMT-10/13/30/c
					25	AMT-10/13/25a/b/	AMT-10/13/25/c
					20	AMT-10/13/20a/b/	AMT-10/13/20/c
					15	AMT-10/13/15a/b/	AMT-10/13/15/c

					7	AMT-10/13/7a/b/	AMT-10/13/7/c
					0	AMT-10/13/0a/b/c/	AMT-10/13/0/d/
14	26/04/2000	midnight	12.466	-20.655	200	AMT-10/14/200a/b/c/	AMT-10/14/200/d/
					150	AMT-10/14/150a/b/	AMT-10/14/150/c
					75	AMT-10/14/75a/b/	AMT-10/14/75/c
					55	AMT-10/14/55a/b/	AMT-10/14/55/c
					47	AMT-10/14/47a/b/	AMT-10/14/47/c
					40	AMT-10/14/40a/b/	AMT-10/14/40/c
					7	AMT-10/14/7a/b/c/	AMT-10/14/7/d/
	27/05/2000	No station due to weather					
15	28/04/2000	1430	23.695	-21.55	230	AMT-10/15/230a/b/c/	AMT-10/15/230/d/
					163	AMT-10/15/163a/b/	AMT-10/15/163/c
					115	AMT-10/15/115a/b/	AMT-10/15/115/c
					95	AMT-10/15/95a/b/	AMT-10/15/95/c
					80	AMT-10/15/80a/b/	AMT-10/15/80/c
					75	AMT-10/15/75a/b/	AMT-10/15/75/c
					70	AMT-10/15/70a/b/	AMT-10/15/70/c
					60	AMT-10/15/60a/b/	AMT-10/15/60/c
					40	AMT-10/15/40a/b/	AMT-10/15/40/c
					20	AMT-10/15/20a/b/	AMT-10/15/20/c
					15	AMT-10/15/15a/b/	AMT-10/15/15/c
					7	AMT-10/15/7a/b/c/	AMT-10/15/7/d/
16	29/04/2000	2200	27.537	-21.97	250 spiked	AMT-10/16/250a-g	
					175	AMT-10/16/175a/b/	AMT-10/16/175/c
					120	AMT-10/16/120a/b/	AMT-10/16/120/c
					107	AMT-10/16/107a/b/	AMT-10/16/107/c
					95	AMT-10/16/95a/b/	AMT-10/16/95/c
					80	AMT-10/16/80a/b/	AMT-10/16/80/c
					60	AMT-10/16/60a/b/	AMT-10/16/60/c
					53	AMT-10/16/53a/b/	AMT-10/16/53/c
					30	AMT-10/16/30a/b/	AMT-10/16/30/c
					20	AMT-10/16/20a/b/	AMT-10/16/20/c
					15	AMT-10/16/15a/b/	AMT-10/16/15/c
					7	AMT-10/16/7a/b/c/	AMT-10/16/7/d/
	30/04/2000	Call into Madeira					
17	01/05/2000	1600	35.997	-20.013	200	AMT-10/17/200a/b/c/	AMT-10/17/200/d/
					150	AMT-10/17/150a/b/	AMT-10/17/150/c
					100	AMT-10/17/100a/b/	AMT-10/17/100/c
					75	AMT-10/17/75a/b/	AMT-10/17/75/c
					60	AMT-10/17/60a/b/	AMT-10/17/60/c

					50	AMT-10/17/50a/b/	AMT-10/17/50/c
					40	AMT-10/17/40a/b/	AMT-10/17/40/c
					30	AMT-10/17/30a/b/	AMT-10/17/30/c
					20	AMT-10/17/20a/b/	AMT-10/17/20/c
					15	AMT-10/17/15a/b/	AMT-10/17/15/c
					7	AMT-10/17/7a/b/c/	AMT-10/17/7/d
18	01/05/2000	2200	36.961	-19.999	200	AMT-10/18/200a/b/c/	AMT-10/18/200/d
					150	AMT-10/18/150a/b/	AMT-10/18/150/c
					100	AMT-10/18/100a/b/	AMT-10/18/100/c
					75	AMT-10/18/75a/b/	AMT-10/18/75/c
					60	AMT-10/18/60a/b/	AMT-10/18/60/c
					50	AMT-10/18/50a/b/	AMT-10/18/50/c
					40	AMT-10/18/40a/b/	AMT-10/18/40/c
					30	AMT-10/18/30a/b/	AMT-10/18/30/c
					20	AMT-10/18/20a/b/	AMT-10/18/20/c
					15	AMT-10/18/15a/b/	AMT-10/18/15/c
					7	AMT-10/18/7a/b/c/	AMT-10/18/7/d
19	02/05/2000	O400	37.916	-20	135	AMT-10/19/135a/b/c/	
					101	AMT-10/19/101a/b/c/	
					65	AMT-10/19/65a/b/c/	
					71	AMT-10/19/71a/b/c/	
					63	AMT-10/19/63a/b/c/	
					51	AMT-10/19/51a/b/c/	
					47	AMT-10/19/47a/b/c/	
					35	AMT-10/19/35a/b/c/	
					23	AMT-10/19/23a/b/c/	
					9	AMT-10/19/9a/b/c/	
20	02/05/2000	1000	38.878	-19.999	200	AMT-10/20/200a/b/c/	AMT-10/20/200/d/
					140	AMT-10/20/140a/b/	AMT-10/20/140/c
					125	AMT-10/20/125a/b/	AMT-10/20/125/c
					110	AMT-10/20/110a/b/	AMT-10/20/110/c
					75	AMT-10/20/75a/b/	AMT-10/20/75/c
					60	AMT-10/20/60a/b/	AMT-10/20/60/c
					40	AMT-10/20/40a/b/	AMT-10/20/40/c
					30	AMT-10/20/30a/b/	AMT-10/20/30/c
					20	AMT-10/20/20a/b/	AMT-10/20/20/c
					15	AMT-10/20/15a/b/	AMT-10/20/15/c
					7	AMT-10/20/7a/b/c/	AMT-10/20/7/d/
	03/05/2000	1320	43.942	-20	7m uw	AMT10/UW/a/b/c	
					spiked 50ul	AMT10/UW/50/a/b/c	
					spiked 100ul	AMT10/UW/100/a/b/c	
					spiked 150ul	AMT10/UW/150/a/b/c/	

21	04/05/2000	O600	46.998	-20.001	182	AMT-10/21/182a/b/c/	AMT-10/21/182/d/
					131	AMT-10/21/131a/b/c/	AMT-10/21/131/d
					65	AMT-10/21/65a/b/c/	AMT-10/21/65/d
					58	AMT-10/21/58a/b/c/	AMT-10/21/58/d
					45	AMT-10/21/45a/b/c/	AMT-10/21/45/d
					40	AMT-10/21/40a/b/c/	AMT-10/21/40/d
					35	AMT-10/21/35a/b/c/	AMT-10/21/35/d
					15	AMT-10/21/15a/b/c/	AMT-10/21/15/d
					7	AMT-10/21/7a/b/c/	AMT-10/21/7/d
22	05/05/2000	1000	48.7	-12.83	150	AMT-10/22/150a/b/c/	AMT-10/22/150/d/
					125	AMT-10/22/125a/b/c/	AMT-10/22/125/d
					100	AMT-10/22/100a/b/c/	AMT-10/22/100/d
					75	AMT-10/22/75a/b/c/	AMT-10/22/75/d
					50	AMT-10/22/50a/b/c/	AMT-10/22/50/d
					40	AMT-10/22/40a/b/c/	AMT-10/22/40/d
					30	AMT-10/22/30a/b/c/	AMT-10/22/30/d
					20	AMT-10/22/20a/b/c/	AMT-10/22/20/d
					7	AMT-10/22/7a/b/c/	AMT-10/22/7/d/
23	06/05/2000	1000	49.324	-6.016	90	AMT-10/23/90/a/b/c	AMT-10/23/90/d/
					80	AMT-10/23/80/a/b/c	AMT-10/23/80/d/
					70	AMT-10/23/70/a/b/c	AMT-10/23/70/d/
					60	AMT-10/23/60/a/b/c	AMT-10/23/60/d/
					50	AMT-10/23/50/a/b/c	AMT-10/23/50/d/
					40	AMT-10/23/40/a/b/c	AMT-10/23/40/d/
					30	AMT-10/23/30/a/b/c	AMT-10/23/30/d/
					15	AMT-10/23/15/a/b/c	AMT-10/23/15/d/
					7	AMT-10/23/7/a/b/c	AMT-10/23/7/d/
					0 spiked	AMT-10/23/0/50/a/b	
						AMT-10/23/0/100/a/b	
						AMT-10/23/0/150/a/b	

Table B2. Sample log for collection of filtered seawater sample (2 L) for analysis of molecular composition of DON.

SAMPLE NUMBER	DATE	LOCAL TIME	STATION NUMBER	LATITUDE (N)	LONGITUDE (W)	VOLUME (L)
1	20/04/2000	1000	8	-10.2850	-30.8190	2
2	21/04/2000	1000	9	-6.2060	-28.5930	2
3	25/04/2000	1000	13	10.2090	-21.6510	2
4	26/04/2000	1000		18.5510	-21.0350	2
5	28/04/2000	1430	15	23.6950	-21.5500	2
6	29/04/2000	2200	16	27.5370	-21.9700	2
7	01/05/2000	2200	18	36.9610	-19.9990	2
8	02/05/2000	1000		38.2410	-20.0000	2
9	02/05/2000	1000	20	38.8760	-19.9990	2
10	03/05/2000	1134		43.8240	-20.0000	2
11	04/05/2000	O600	21	46.9980	-20.0110	2
12	05/05/2000	10	22	48.1950	-12.8830	2

Table B3. Sample log for collection of particulate matter by filtration of seawater from the underway seawater supply at 7m for analysis of POC, PON, phytopigments and δ^{15}N PON.

FILTER NUMBER	DATES	TIME (GMT)	LATITUDE (N)	LONGITUDE (W)	VOLUME (L)	TOTAL Vol (L)
1	13/04/2000	1100	-35.092	-50.590	60	60
		1150	-35.089	-49.361	60	120
		1620	-32.082	-46.927	60	180
2	15/04/2000	1140	-29.095	-43.028	60	60
		1430	-28.863	-42.840	60	120
		1730	-28.421	-42.409	60	180
3	17/04/00 to	1250	-22.250	-36.841	60	60
	20/04/2000	1400	-22.029	-36.696	60	120
		1830	-21.290	-36.197	60	180
	18/04/2000	1050	-18.382	-34.633	60	240
		1610	-17.785	-34.248	60	300
		2130	-16.801	-33.879	60	360
	19/04/2000	1150	-14.188	-32.647	60	420
		1630	-13.583	-32.354	60	480
		2130	-12.874	-32.015	60	540
		O200	-12.075	-31.165	60	600
		O520	-11.452	-31.357	60	660
	20/04/2000	1010	-10.515	-30.919	60	720
		1210	-10.285	30.819	60	800
4	20/04/00 to	O200	-7.943	-29.720	60	60
	23/04/2000	1230	-6.206	-29.593	120	180
		1320	-6.151	-28.904	60	240

		1350	-6.012	-28.838	60	300
		1530	-5.728	-28.707	60	360
		1900	-5.074	-28.257	80	440
		2220	-4.476	-28.133	60	500
		2330	-4.216	-28.014	60	560
		OO40	-4.006	-27.919	60	620
		240	-3.668	-27.764	60	680
		1120	-2.225	-27.090	60	740
		1830	-1.049	-26.340	60	800
		OO20	0.000	-26.200	60	860
		1210	1.990	-25.250	60	920
5	24/04/2000	1100	6.101	-23.440	120	120
		1320	6.363	-23.331	60	180
		1510	6.635	-23.211	80	260
		2250	8.074	-22.585	80	340
		OO30	8.349	-22.462	60	400
		O150	8.539	-22.379	60	460
		O230	8.723	-22.302	60	520
		O430	9.017	-22.177	60	580
		O700	9.510	-21.961	60	640
6	26/04/2000	1220	14.368	-20.371	60	60
		1310	14.545	-20.301	80	140
		1330	14.590	20.394	60	200
7	26/04/2000	1840	15.567	-20.454	60	60
		2050	16.004	-20.457	60	120
		2100	16.041	-20.460	60	180
		2120	16.091	20.465	20	200
8	26/04/2000	1010	18.551	-21.035	60	60
		1330	19.181	-21.082	60	120
		1400	19.243	-21.059	40	160
9	26/06/2000	1400	19.243	-21.059	20	20
		1540	19.476	-21.099	20	40
		1700	19.705	-21.136	60	100
		1710	19.739	-21.115	20	120
10	27/04/2000	1710	19.739	-21.115	40	40
		1910	20.203	-21.120	80	120
		2220	20.648	-21.234	40	160
11	27/04/2000	2220	20.648	-21.234	20	20
		O810	22.429	-21.270	40	60
		O840	22.501	-21.279	60	120
		O900	22.592	-21.290	60	180

12	28/04/2000	1410	23.604	-21.543	60	60
		1500	23.699	-21.556	140	200
13	28/04/2000	1650	23.848	-21.346	60	60
		1800	24.072	-21.592	20	80
		1850	24.297	-21.381	60	140
		2130	24.835	-21.676	60	200
14	29/04/2000	O308	26.056	-21.808	60	60
		O330	26.169	-21.819	60	120
		O414	26.301	-21.833	60	180
		O517	26.599	-21.866	20	200
15	29/04/2000	O555	26.655	-21.873	80	80
		O619	26.752	-21.882	40	120
		O932	27.268	-21.578	60	180
		1000	27.537	-21.972	20	200
16	29/04/2000	1000	27.537	-21.972	120	120
		1224	27.458	-21.445	80	200
17	29/04/2000	1415	28.034	-21.197	60	60
		1912	28.562	-20.593	60	120
		2140	29.376	-20.165	60	180
		2156	29.429	-20.113	20	200
18	30/04/2000	O246	30.278	-19.275	60	60
		O455	30.656	-18.897	60	120
		O536	30.772	-18.785	60	180
		O549	30.813	-18.745	20	200
19	30/04/2000	O926	31.423	-18.123	60	60
		1001	31.524	-18.028	60	120
		1829	31.599	-17.953	60	180
20	30/04/2000	1305	32.047	-17.507	60	60
		1324	32.099	-17.485	60	120
		1420	32.266	-17.284	60	180
21	30/04/2000	1842	32.656	-17.195	60	60
		1904	32.683	-17.269	60	120
		1936	32.725	-17.378	20	140
22	01/05/2000	1936	32.725	-17.378	20	20
		1302	35.479	-19.570	60	80
		1334	35.792	-19.784	60	140

23	01/05/2000	1534	35.942	-19.958	60	60
		1600	35.997	-20.013	100	160
		1811	36.219	-19.998	20	180
24	02/05/00	2200	36.961	-19.999	140	140
		OO28	37.252	-19.999	40	180
25	02/05/2000	O640	38.241	-20.000	80	80
		O728	38.397	-20.003	60	140
26	02/05/2000	O926	38.801	-19.999	60	60
			38.876	-19.999	80	140
27	02/05/2000	1453	38.876	-19.999	40	40
			39.563	-20.000	60	100
28	03/05/2000	O941	43.217	-20.000	60	60
		1001	43.281	-20.000	60	120
		1134	43.585	-19.999	60	180
		1240	43.824	-20.000	20	180
29	03/05/2000	1326	43.962	-20.000	60	60
		1416	44.132	-20.000	60	120
		1711	44.694	-19.999	40	160
30	03/05/2000	2101	45.448	-20.000	60	60
		2121	45.513	-20.002	60	120
		2147	45.599	-20.003	20	140
31	04/05/2000	2147	45.599	-20.003	40	40
		2237	45.763	-20.003	20	60
		O200	46.451	-19.999	60	120
		O245	46.552	-19.995	40	160
32	04/05/2000	O518	46.998	-20.011	140	140
		O702	47.015	-19.893	40	180
33	04/05/2000	O702	47.015	-19.893	40	40
		1334	47.310	-18.161	60	100
		1432	47.411	-17.587	60	160
34	04/05/2000	2104	47.411	-17.587	20	20
		2144	47.674	-15.998	60	80
		2234	47.699	-15.723	60	140
		23.38	47.759	-15.504	60	200
35	05/05/2000	O857	48.195	-12.883	120	120
		1120	48.269	-12.436	20	140
36	05/05/2000	1110	48.269	-12.436	40	40
		1305	48.357	-11.904	60	100
		14.13	48.412	-11.58	60	160

Appendix C

Chromatograms and sample table from the analysis of nitrate and phosphate

Figure C1. Chromatograms from the analysis of (a) nitrate and (b) phosphate analysis using a Skalar San^{plus} segmented flow autoanalyser and Skalar sampler 1000 autosampler. Output from FlowAccess Software. Note the stable baseline during nitrate analysis and noisy baseline during phosphate analysis

(a)

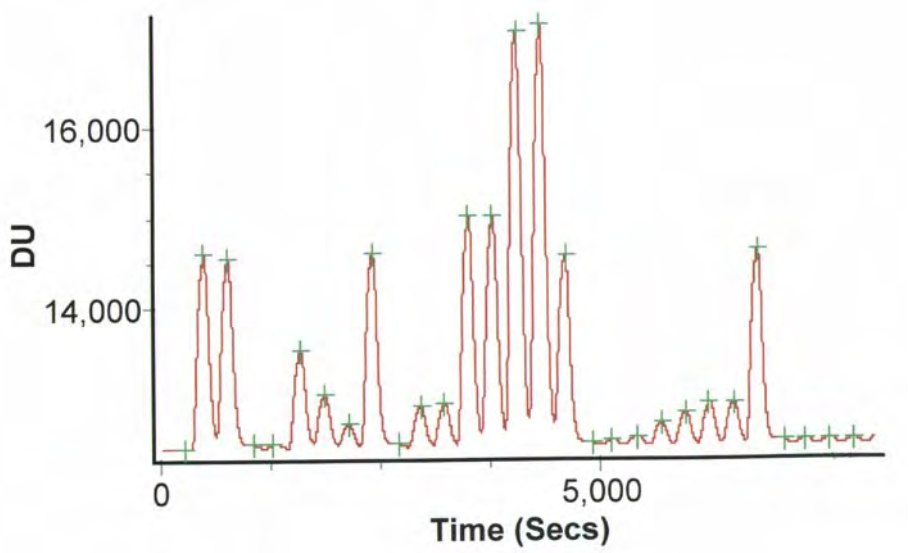

(b)

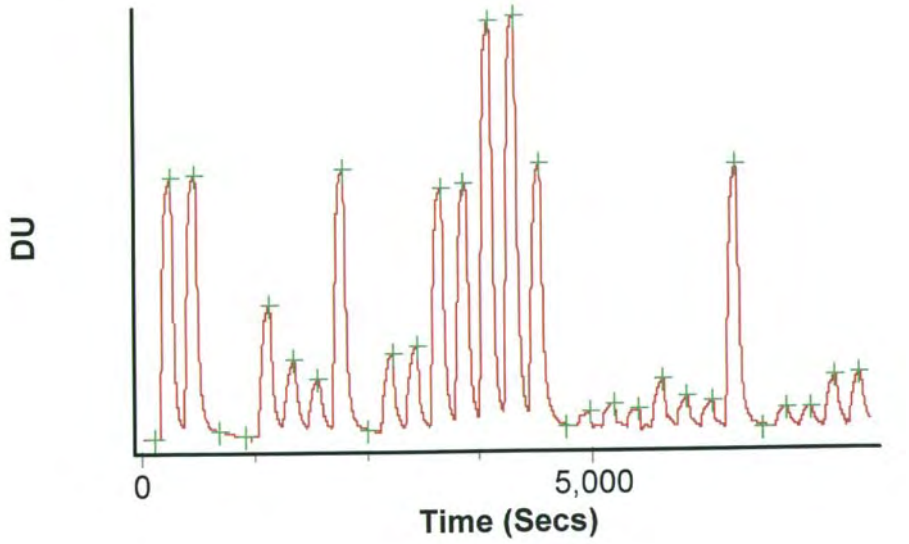

Table C1. Typical FlowAccess sample table including the position of the sample in the auto-analyser, the type of sample (T=Tracer, D=Drift, W=Wash, S=standard, U=unknown), identity (std1-4, see Table 2.4 in methods; asw=artificial seawater) and external dilution factor.

Position	Type	Identity	External DilFactor
	Needle 1		
1	T	Tracer std4	1.0000
2	D	Drift std4	1.0000
3	W	Asw	1.0000
4	W	Asw	1.0000
5	S3	Std3	1.0000
6	S2	Std2	1.0000
7	S1	Std1	1.0000
8	D	Tracer std4	1.0000
9	W	Drift std4	1.0000
10	U	Sample name	1.0000
11	U	Sample name	1.0000
12	U	Sample name	1.0000
13	U	Sample name	1.0000
14	U	Sample name	1.0000
15	U	Sample name	1.0000
16	U	Sample name	1.0000
17	U	Sample name	1.0000
18	D	Tracer std4	1.0000
19	W	Drift std4	1.0000
20	U	Sample name	1.0000

Appendix D

Recipe for Artificial Seawater

Table D1. Chemicals and instructions for preparation of artificial seawater (following method by Guillard and Ryther, 1962). All solutions to be prepared in Milli-Q water.

CHEMICAL	MASS IN VOLUME (g)
ASW BASE	**g per L**
Sodium chloride	23.38
Potassium chloride	0.75
Magnesium sulphate, 7 hydrate	4.93
Magnesium chloride, 6 hydrate	4.07
Calcium chloride, 6 hydrate	2.19
Sodium hydrogen carbonate	0.17
Boric Acid	0.025
NUTRIENTS[1]	**g per 100 L**
Sodium nitrate	7.5
Sodium hydrogen phosphate, hydrate	0.565
Ammonium chloride	2.65
TRACE ELEMENTS[2]	**g per 100 mL**
Copper sulphate, 5 hydrate	0.98
Zinc sulphate, 7 hydrate	2.2
Cobalt chloride, 6 hydrate	1.0
Manganese chloride, 4 hydrate	18
Sodium molybdate, 2 hydrate	0.63
TRACE METAL[3]	**g per 1 L**
Iron chloride, 6 hydrate +	3.15
Ethylenediaminetetraacetic acid (EDTA) disodium salt	4.36
VITAMIN PRIMARY STOCK[4]	**mg per 1 mL**
Biotin	0.1 mg
Vitamin B_{12}	1

[1] Add 1 mL of each nutrient to ASW base
[2] Add 1 mL of each trace element to the trace metal solution
[3] Volume to be adjusted to 1 L after addition of trace elements.
[4] To prepare a working vitamin stock, add 1 mL biotin stock, 1 mL Vitamin B_{12} and 20 mg of Thiamine HCl and adjust volume to 100 mL.

To prepare final artificial seawater solution, add 1 mL of the each of the nutrients, 1 mL of the trace metal working solution and 0.5 mL of the vitamin working solution to the ASW and adjust the volume to 1 L.

Appendix E

Chromatogram from phytoplankton pigment analysis

Figure E1. Typical pigment chromatogram produced by the software ChromQuest from the analysis of phytopigments from particulate matter collected during AMT 10. See Table 2.9 for pigment abbreviations.

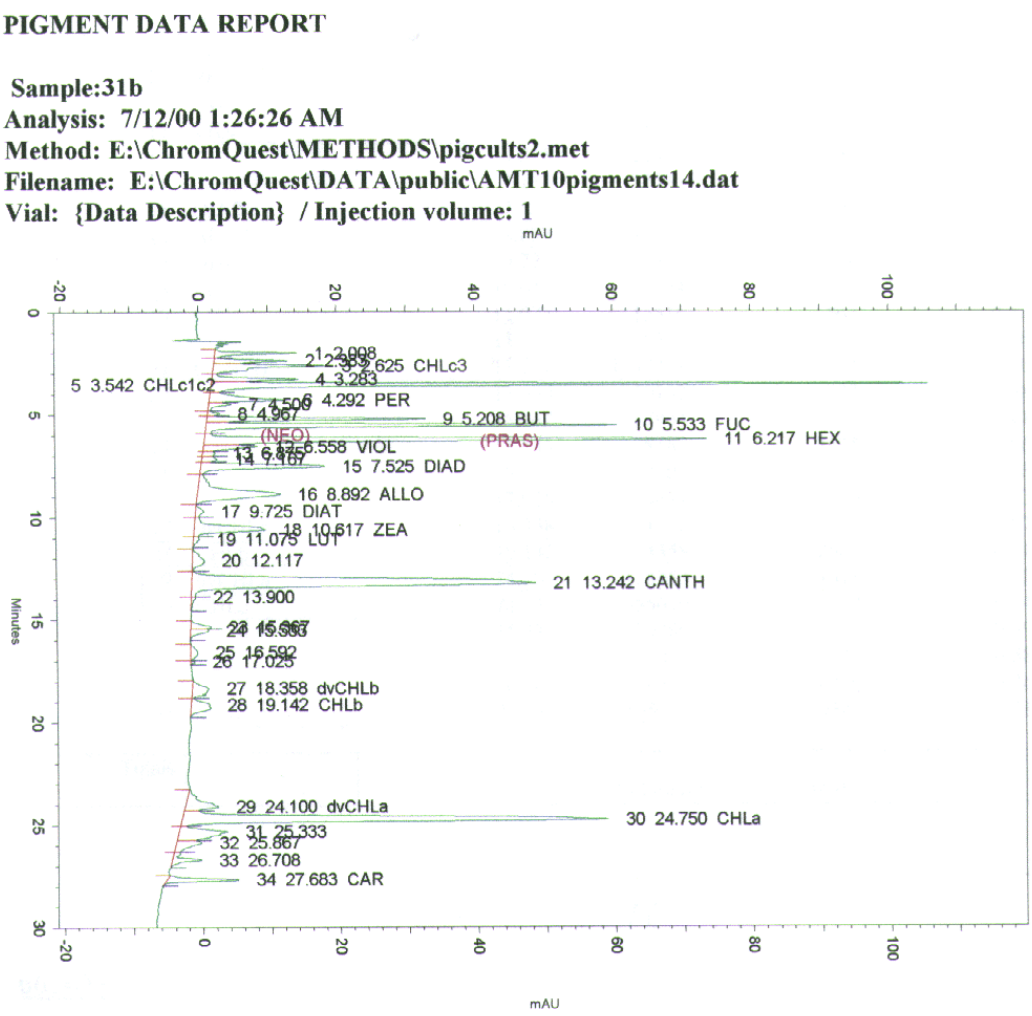

Appendix F

Methods for stable nitrogen isotopic composition of DON

F. 1. Introduction

In order to augment the source and sink approach adopted in the present study, the intention was to include the stable nitrogen isotopic composition of dissolved organic nitrogen (δ^{15}N DON). Although there are a number of methods in the literature (Benner *et al*. 1997, Abell 2000), they were considered to be unsuitable for this study.

Tangential-flow ultrafiltration was employed by Benner *et al.* 1997 to isolate dissolved organic material from seawater in the Atlantic and Pacific Ocean, through a filter of 1000 Da molecular weight cut off (MWCO). Considering labile and semi-labile DON is considered to be of low molecular weight (e.g. urea, amino acids, peptides, nucleotides, alkylamines), this procedure excluded the pools of interest in this study. In addition, recovery of organic matter by ultrafiltration is poor (10-50%) due to the organic molecules adhering to the membrane and possibly bacterial degradation during the procedure (Jones, pers. comms.). It was therefore deemed unsuitable for open ocean samples were DON concentrations are low, thus requiring excessive volumes of seawater for filtration.

The stable nitrogen isotopic composition of nitrate (δ^{15}N NO_3^-) (Sigman *et al*. 1997, Sigman *et al*. 2001) was employed by Abell (2000) to analyse the δ^{15}N NO_3^- prior to and after 20 hours UV oxidation (δ^{15}N TDN). Using isotopic mass balance, the δ^{15}N DON was calculated from the δ^{15}N NO_3^-, δ^{15}N TDN and mass of each nitrogen pool. In the oligotrophic ocean, NO_3^- concentrations tend to be below detection and therefore the isotopic contribution to the total nitrogen pool can be assumed to be insignificant. However, during the AMT 10 transect, a wide range of oceanic regimes were sampled, including productive bloom regions where NO_3^- concentrations exceeded 5 μM, thus contributing significantly to the total nitrogen isotopic composition. Also, as exemplified in section 2.2.2.1., the time required to UV oxidise DON to NO_3^- is questionable. Isotopic fractionation during the UV oxidation procedure was not assessed.

It was therefore necessary to consider alternative methods to determine the δ^{15}N DON. The primary aim was to isolate and concentrate DON from seawater. The stable nitrogen isotopic analysis is a routine and relatively simple procedure.

F 1.1. Isolation and desalination of organic nutrients by dialysis

F 1.1.1 Principle of operation

A seawater sample was concentrated by rotary evaporation, desalinated by dialysis, freeze-dried and analysed by EA-IRMS to determine the δ^{15}N DON. This method follows that developed by Feuerstein *et al*. (1997).

F 1.1.2. Concentration of seawater sample by rotary evaporation

During rotary evaporation, both temperature and negative pressure (30 psi) were used to concentrate 1000mL of seawater to less than 200mL. 1000mL of seawater was poured into a clean round bottom flask (rbf.), and connected to the condenser. A splash head unit was placed between the rbf and condenser to prevent condensed water re-entering the rbf after evaporation. The rbf was immersed in a water bath at ~ 40^{o}C and rotated rapidly to prevent bumping. Cold water (~ 5 to 6^{o}C) was pumped through the condenser and to promote condensation, the temperature of the waste vessel was maintained below 0^{o}C with ice, salt and acetone (dry ice). A vacuum of ~ 30 psi was applied. Up to 4 hours rotary evaporation were required to concentrate one litre of seawater to less than 200mL. A number of problems were considered:

1. The relatively high temperature (40^{o}C) and time required for concentration of the seawater sample (4-5 hours) meant the sample was more susceptible to bacterial degradation. This was not quantified.
2. The condensed sample was difficult to handle due to the high salt content. It was necessary to transfer using a spatula rather than a pipette.

F 1.1.3. Desalination by dialysis

Desalination was necessary to ensure exclusion of all inorganic nitrogen-containing salts, which may interfere with stable nitrogen isotopic analysis of DON. Cellulose-ester (CE) dialysis tubing (Spectrum Laboratories Inc., 8mm (0.2 mL/cm) and 16mm (0.81 mL/cm) flat width) with a 100 Dalton molecular weight cut off (MWCO) was used to desalinate the seawater sample. The membrane was stored in 0.1 % sodium hydroxide at < 4^{o} C to prevent bacterial growth.

The efficiency of desalination and recovery of organic matter was tested using the tripeptide GAY (glycine-alanine-tyrosine) and BSA in artificial seawater, and a coastal (Oban Lough, Scotland) and open ocean (AMT10-18) seawater sample (Table F 1).

Table F 1. Sample description, concentration (μM) and nitrogen content (μg) of the intial solution used to test the efficiency of desalination and DON isolation.

SAMPLE	SOURCE	INITIAL CONCENTRATION (μM)	NITROGEN CONTENT (μg N)
BSA	Standard	10	140
GAY	Standard	10	140
Coastal seawater	Oban	7.97 ± 1.42	111.58
Open Ocean seawater	North Atlantic (AMT10-18)	10.38 ± 1.93	145.32

Strips of membrane (20 cm) were soaked in Milli-Q water for 1 hour prior to use. The membrane was sealed at one end (Spectrum dialysis clips) and the concentrated seawater sample poured directly into the dialysis bag. The dialysis bag was filled to ~ 2 cm from the top, sealed with a dialysis clip and immersed in a 5 L beaker of Milli-Q. This procedure was repeated until the entire condensed sample had been transferred to dialysis tubes. To ensure quantitative transfer, the rbf was rinsed (> 3 x 10mL) with Milli-Q and washes transferred to a dialysis tube.

Two to three tubes were immersed in a 5L beaker of Milli-Q water, 2 to 3 beakers being required per sample. To prevent bacterial degradation, the beakers were stored in a fridge at 4-6^{o}C. To promote diffusion and maintain the concentration gradient between the contents of the dialysis tube and surrounding medium (Milli-Q), the beakers were constantly stirred using a magnetic stirrer and the Milli-Q water was changed 4 times per day throughout the dialysis period. Desalination by dialysis was performed for 264 hours (~ 9 days), as recommended by Feuerstein *et al* (1997). After 9 days, the dialysed sample was quantitatively (3 x Milli-Q) transferred from the dialysis tube to an rbf and the volume reduced, by rotary evaporation, to ~ 50mL. The sample was frozen and freeze-dried to dryness.

F. 1.1.4. Results

F.1.1.4.1. Removal of inorganic salts

To ensure complete removal of inorganic salts, salinity was measured prior to (30.23 psu) and after dialysis (< 1 psu) for an open ocean seawater sample (AMT10-18) using an AutoSal Model 8400 (Plessey Environmental Systems). Less than 3 % of the initial salts remained after 264 hours, confirming that dialysis efficiently removed inorganic salts from the sample.

F.1.1.4.2. Removal of Nitrate

Nitrate (NO_3^-) concentration was measured prior to and after dialysis for a high DIN solution and an open ocean seawater sample (AMT10-18) using the Technicon Auto-Analyser II segmented flow 1 channel NO_3^- analyser. For the high NO_3^- solution, 99.91% of the NO_3^- was removed (initial, 0.25mM, final, 0.17 and 0.216 μM). However, the initial DIN for AMT10-18 was below detection prior to dialysis.

F.1.1.4.3. Recovery of dissolved organic nitrogen

In order to investigate recovery of the dialysis procedure for dissolved organic nitrogen, total nitrogen analysis was performed on initial and final freeze-dried samples using a Carlo Erba Instruments NC 2500 elemental analyser. The results are shown in Table A2. Recovery of organic nitrogen could not be quantified for BSA as the material adhered to the glass when concentrated and could not be removed without detergent. Recovery of the tri-peptide GAY was between 7 and 15%. Overall, recovery of organic nitrogen was less than 23%.

Table F2. Percentage (%) recovery of the tripeptide, GAY (glycine-alanine-tyrosine) after 9 days of dialysis against Milli-q water. Initial concentration, 10 μM.

SAMPLE	INITIAL N CONTENT (μg)	FINAL N CONTENT (μg)	% RECOVERY (FINAL/INITIAL) X 100
GAY – 19/06/01	140	20.81	14.86
GAY – 20/07/01	140	10.44	7.6
GAY – 23/07/01	140	32.12	22.94
GAY – 23/07/01	140	6.84	4.88
GAY – 01/08/01	140	18.70	13.35

Low recovery of DON by dialysis may have been due to bacterial degradation during the dialysis period or loss of DON during transfer of the sample (rbf to dialysis tubes, dialysis tubes to freeze-drier). It was noted than during sealing of the tubes using the dialysis clips, small holes would appear around the clips, only noticed by the leaking of saltwater into the fresh water medium. Despite great care when handling the bags and discarding of damaged bags, this could not be prevented and may have contributed to the poor recovery observed. This procedure proved difficult to replicate and problems such as bursting of dialysis bags, rigidity of the membrane when in contact with salt and

time required to process one sample (at least 10 days from preparation to isotopic analysis) made it unsuitable for a large suite of samples.

In conclusion, although dialysis through a 100 Dalton cellulose ester membrane can efficiently remove inorganic salts from seawater, organic nitrogen was poorly retained.

F.1.2. ISOLATION OF DON BY ADSORPTION

F.1.2.1 Activated carbon

The use of high purity activated carbon to adsorb organic matter has been previously described (Jeffery 1969, Liska *et al* 1989, Nouri *et al* 2002) and applied extensively throughout the chemical and water purifying industry (Vitolo and Seggiani, 2002, Matsui *et al* 2002). Previous recovery of DOM ranges from 25 to 90 % (Jeffrey 1969, Kerr and Quinn 1975, 1980).

Activated carbon (AC) was employed in the present study to investigate its potential to adsorb dissolved organic matter from seawater. Chemviron activated carbon was chosen due to its physical properties (Table F3), low metal content and production from high quality bitumous coal (Lee 1998).

Table F3. Properties and Specification of Chemviron Granular Activated Carbon (source: data provided by Chemviron Carbon).

PROPERTY	SPECIFICATION
Total surface Area	950 –1050 m^2 /g
Apparent density	0.5 – 0.52 g /ml
Real density	2.0 – 2.2 g /ml
Specific heat at 100^oC	1 kJ / kg / K
Iron (acid soluble)	150 ppm max
PH	5.0 – 8.0

F.1.2.1.1. Purification of Activated carbon

Pre-sieved carbon (mesh 1 mm) was stirred for ~ 1 hour in 10 % hydrochloric acid (Analar grade) in order to remove adsorbed metals which can catalyse chemical reactions of adsorbed organics. Following 3 consecutive rinses with 10% HCl and more than 10 rinses with Milli-Q water, the activated carbon was dried in an oven for 24 hours.

To remove organic matter, the dried activated carbon was placed in an in-house built quick-fit quartz glass tube (80cm long, 1.5cm diameter) and heated in a tubular furnace (Carbolite furnaces Ltd, model CTF 12/75) at 850^oC for 8 hours under a

continuous stream of helium. After 8 hours, the activated carbon was cooled slowly and helium flow was maintained to prevent re-adsorption of nitrogen. The activated carbon was immediately transferred to pre-combusted (450^{o}C for > 4 hours) glass ampoules, which were sealed using a butane flame and metal forceps.

F.1.2.1.2. Results

Previous studies recommend a ratio of 0.31-0.78 mg activated carbon per 1 μM DOC (Lee 1998). This equates to 40mg of activated carbon per litre of open ocean seawater, where typical DON concentrations do not exceed 10μM (0.14 mg N). Total nitrogen analysis was performed on activated carbon prior to and after purification using a Carlo Erba Instruments NC 2500 elemental analyser. The total nitrogen content of the mass of activated carbon required for efficient adsorption (40 mg) after purification was found to be at least 20% of the organic nitrogen in one litre of open ocean water (Table F4). Repeated attempts to remove the carbon-bound organic matter by solvent extraction, increased high temperature purification time and different storage vessels (see Table F4) proved unsuccessful.

Table F4. The percentage nitrogen (%N, ± 1 standard deviation) adsorbed to activated carbon after purification and the mass (mg) of nitrogen on the mass of activated carbon (40 mg) to efficiently adsorb 140 μg of organic nitrogen from seawater.

DATE	TREATMENT	STORAGE	% N	N (mg) CONTENT IN 40 mg AC
20/11/01	850^{o}C 4 hours	Ampoule	0.38 ± 0.08	0.15 ± 0.032
26/11/01	850^{o}C 4 hours	jar	0.051 ± 0.002	0.02 ± 0.00008
		Ampoule	0.059 ± 0.004	0.024 ± 0.008
		Ampoule	0.058 ± 0.02	0.024 ± 0.01
		Ampoule	0.057	0.022
05/12/01	850^{o}C 4 hours		0.14 ± 0.006	0.27 ± 0.01
			0.15 ± 0.026	0.3 ± 0.05
08/01/02	Solvent extraction 850^{o}C 4 hours		0.60 ± 0.03	0.24 ± 0.006
			0.63 ± 0.07	0.25 0.0012

In conclusion, despite being a simple procedure to follow, the organic nitrogen content of the activated carbon was sufficiently high to represent a significant isotopic signal of unknown origin.

F.1.2.2. Clays minerals

The interaction between clay minerals and organic matter has been well studied, both in the marine (Gordon and Millero 1985, Kirchman *et al.* 1989, Henrichs and Sugai, 1993, Keil *et al.* 1994, Hedges and Keil 1999) and terrestrial environments

(Greenland 1971, Jardine *et al*. 1989). The adsorption of low molecular weight dissolved organic nitrogen, namely amino acids, onto clay mineral surfaces has been thoroughly investigated (Carter et al 1978, Hedges and Hare, 1987, Henrichs and Sugai, 1993). In this study, the adsorptive characteristics of clays were employed to investigate their potential to extract organic matter from open ocean seawater samples.

F.1.2.2.1. Purification of clays

The alumino-silicate clay, montmorillonite ($Al_4SiO_5(OH)_4$), was used throughout this study. Montmorillonite was ground to a fine powder using a mortar and pestle and heated to 400^oC overnight to remove organic nitrogen compounds. Montmorillonite was stored in pre-combusted (450^oC, > 4 hours) sealed quartz ampoules until use. Initial total nitrogen concentrations (determined using a Carlo Erba Instruments NC 2500 elemental analyser) were low (0.0096% dry weight). Using a ratio of 500mg of clay per litre of seawater sample, the organic nitrogen content of the clay accounted for less than 10% of the organic nitrogen in one litre of open ocean water.

F. 1.2.2.2. Procedure

All adsorption experiments were performed in duplicate. To investigate the adsorption efficiency of montmorillonite, 500mL artificial seawater containing 10μM of the tri-peptide (GAY), coastal seawater (Oban lough, Scotland) and open ocean seawater (AMT 10-18) were mixed with 0.25 g of purified montmorrilonite for 24 hours. Conditions were altered to investigate the effects of inorganic salts, temperature and pH on adsorption efficiency (Table F 2.5).

The percentage adsorbed was assessed by determination of initial nitrate concentrations and final total dissolved nitrogen (TDN) after 12 hours UV oxidation (See section 2.3.2.1. for details of instrument and techniques employed).

The presence of nitrate and ammonium in the GAY solution appeared to act as a competitor for the active sites on the carbon as more organic matter was adsorbed onto the carbon in the absence of inorganic nitrogen (32.8% compared to 13.4 and 19.1%). Organic nitrogen concentrations were greater for the coastal and open ocean seawater samples after treatment with montmorillonite, suggesting the clay may have been a source of contamination or analysis was total nitrogen was inaccurate, the former being more plausible.

Table F 2.5. Results from adsorption experiments between 10 μM GAY in a artificial seawater, coastal seawater and open ocean seawater and 25mg of Montmorillonite. Conditions, treatment and percentage (%) of nitrogen adsorbed (1 d.p.) is noted

DATE	SAMPLE	CONDITIONS	TREATMENT	% ADSORBED
08/01/02	10 μM GAY	Nitrate: 0 Ammonium: 0	Room temperature Stir: 24 hours	32.8
09/01/02	10 μM GAY	Nitrate: 1 μM Ammonium: 0.1 μM	Room temperature Stir: 24 hours	13.4
12/01/02	10 μM GAY	Nitrate: 1 μM Ammonium: 0.1 μM	Room temperature Stir: 24 hours pH: 3	19.1
31/01/02	Coastal water Oban Lough	Nitrate: 5.08 μM	Room temperature Stir: 24 hours	106.3
01/02/01	Coastal water Oban Lough	Nitrate: 5.08 μM	Room temperature Stir: 24 hours	62
13/02/02	Open ocean seawater (AMT10-18)	Nitrate: 0.58 μM	Temperature ~ 4^{o}C Stir: 24 hours	118.8

In conclusion, despite adsorption of organic matter by clay minerals being a well documented procedure, it was deemed unsuitable for open ocean samples were concentrations of organic nitrogen are low and thus contamination would actively compete with natural organic nitrogen in seawater.

Appendix G

Preparation of Amino Acid mixed standard solution and a typical chromatogram

G 1. Preparation of amino acid stock solutions and mixed standard

Individual amino acid primary stock solutions (2 mM) were prepared by in 100 mL (the mass depending of the amino acid (Table G1)). Stocks were divided into small vials and stored in the freezer (< 0°C). Individual vials of primary stock amino acid were defrosted for ~ 1 hour prior to use.

A mixed working stock amino acid solution (final concentration, 20 μM) was prepared by adding 100 μL of each primary stock and adjusting the volume to 1 mL. The mixed working stock was diluted with water (HPLC grade) to concentrations of 5, 8 12 and 15 μM to determine the response factors at different concentrations.

Table G1. Amino acids, their abbreviation, molecular weight and mass (g) required in 100 mL to prepare a final stock of 2 mM.

AMINO ACID	ABBREVIATION	MOLECULAR WEIGHT	MASS (g) IN 100 mL
β-alanine	BALA	89.09	0.0178
α-amino adipic acid	AAAA	161.15	0.0322
γ-amino adipic acid	GABA	103.12	0.0206
Arganine	ARG	210.67	0.0421
Aspartic Acid	ASP	133.10	0.0266
Fluorophenylalanine	FPHE	183.18	0.0366
Glutamic acid	GLU	147.13	0.0294
Glycine	GLY	75.06	0.0150
Histidine	HIS	209.63	0.0419
Hydroxylysine	HLYS	198.5	0.0397
Isoleusine	ILE	131.17	0.0263
Leusine	LEU	131.17	0.0263
Lysine	LYS	182.65	0.0365
Methionine	MET	149.20	0.0298
Ornithine	ORN	168.62	0.0337
Phenylalanine	PHE	165.19	0.0330
Serine	SER	105.09	0.0210
Threonine	THR	119.12	0.0238
Tyrosine	TYR	181.19	0.0362
Valine	VAL	117.15	0.0234

Figure G1. Chromatogram of a typical mixed amino acid standard (Cowie and Hedges, 1993).

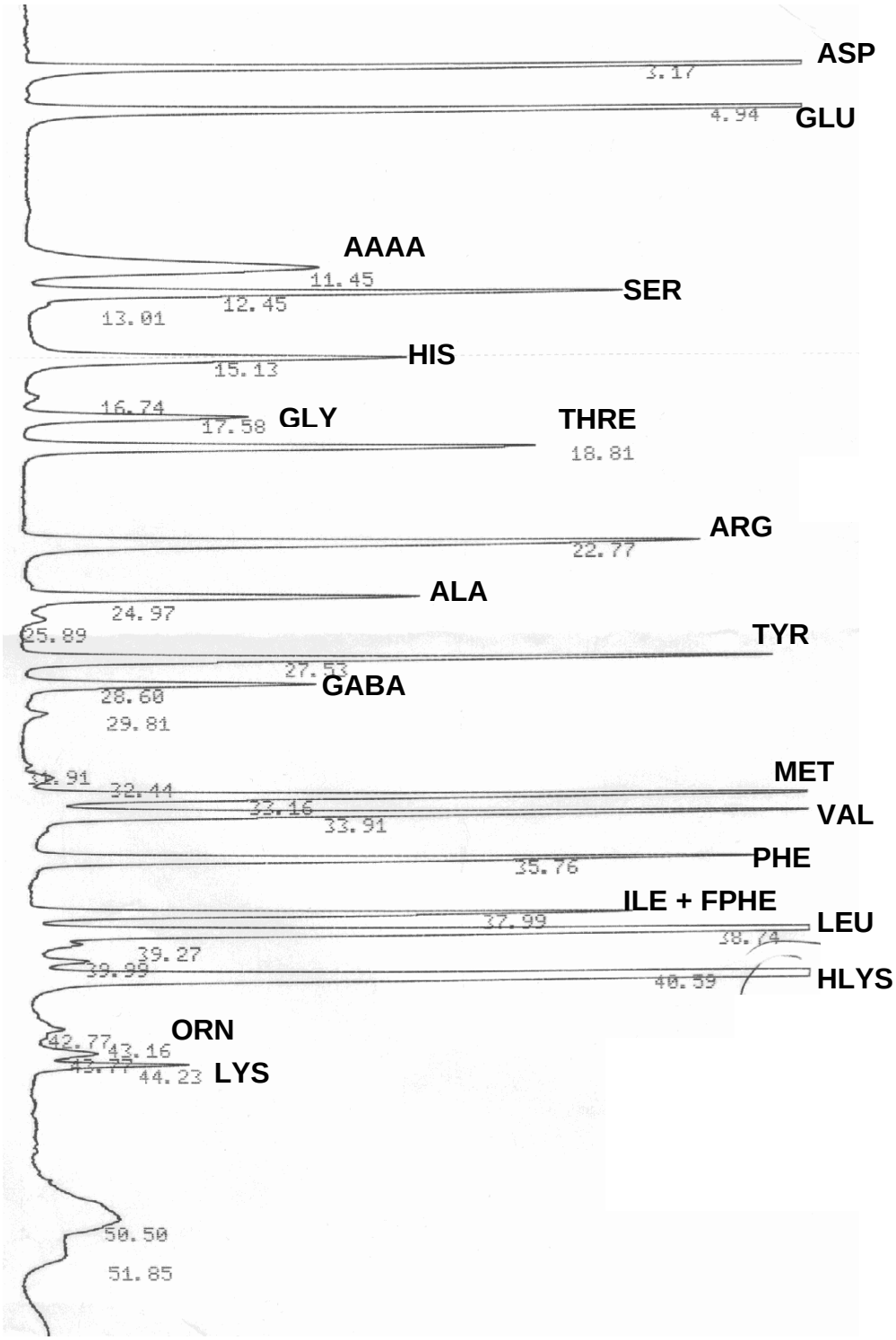

Appendix H

Ekman pumping field over the Atlantic during AMT 1-11

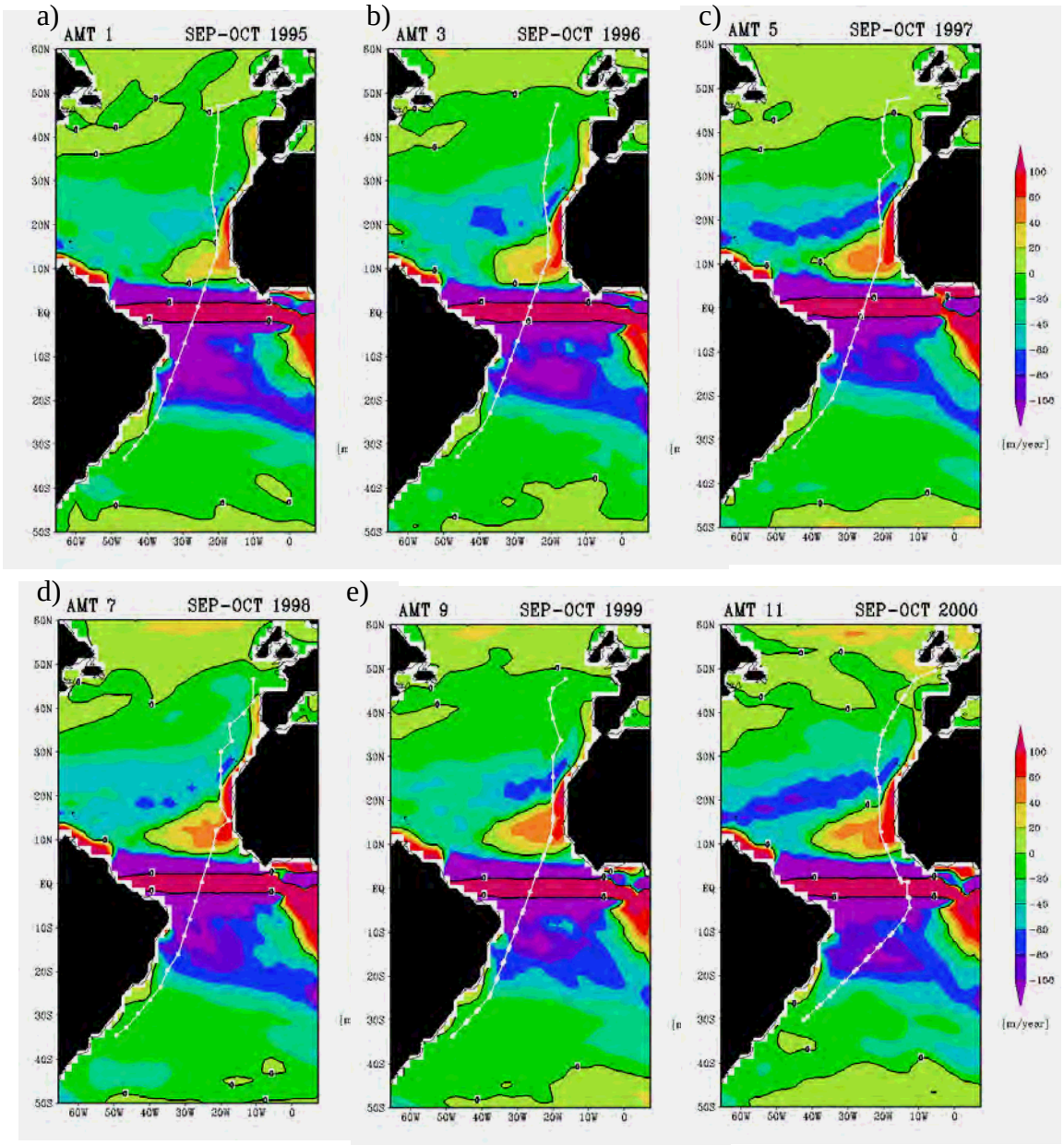

Figure H1. Ekman pumping field (m y^{-1}) for the Atlantic Ocean in Autumn corresponding to the period of Autumn AMT cruises: (a) AMT 1, (b) AMT 3, (b) AMT 5, (c) AMT 7, (d) AMT 9, (e) AMT 10.

Figure H2. Ekman pumping field (m y^{-1}) for the Atlantic Ocean in Autumn corresponding to the period of Autumn AMT cruises: (a) AMT 2, (b) AMT 4, (b) AMT 6, (c) AMT 8, (d) AMT 10.

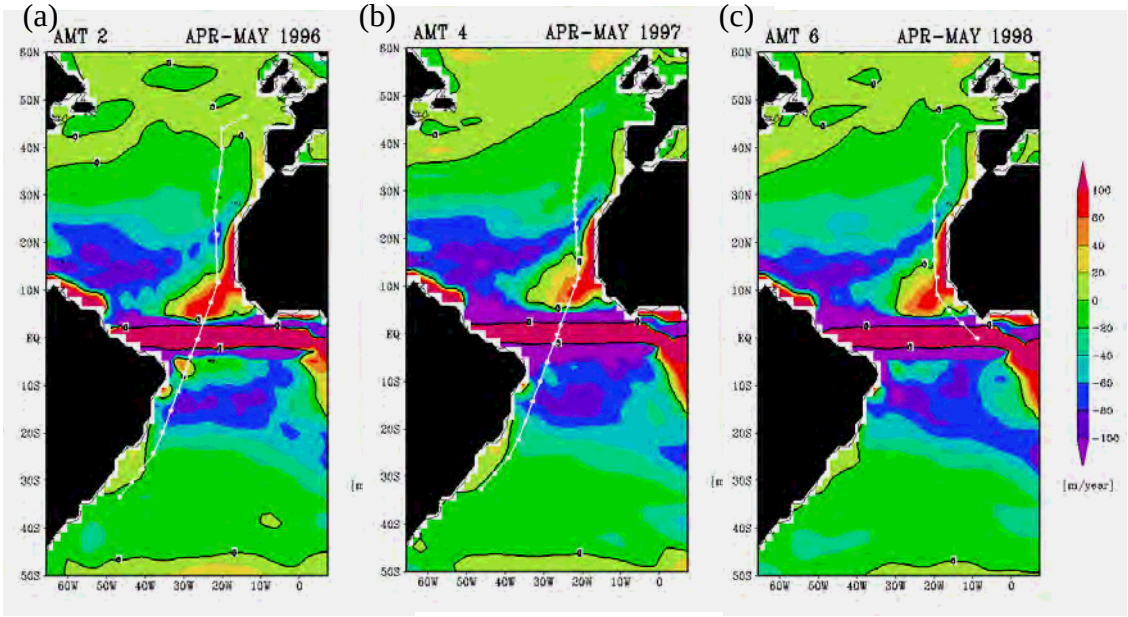

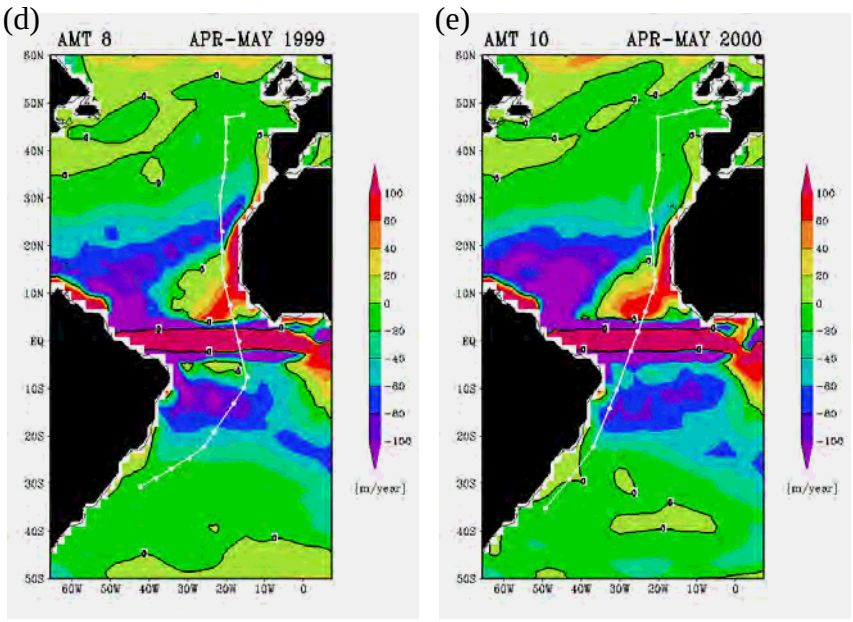

Appendix I

Method for lipid analysis

I 1. Lipid extractions

Lipid extractions (Wolff *et al.,* 1995) and analysis were performed on four samples of particulate organic matter (POM) collected from the underway non-toxic seawater supply during AMT 10 (Sample # 7, 8, 16 and 37; see Appendix B, Table B3 for sample locations). The purpose was to assess the contribution of zooplankton relative to total POM. All vials and glassware was pre-extracted in dichloromethane (DCM), dried and combusted at 450°C for > 4 h. Solvents used were pre-distilled using Soxhlet extraction.

I 1.1.Extractions

From each sample, a 13mm diameter disc was cut and weighed (~ 1.5 g) and placed into a glass fibre extraction thimble. 100 μL of the standard, cholestane (final mass of 2 μg) was added and the sample plus standard extracted (24 h) using dichloromethane (DCM) with 10 % methanol (MeOH). The extract was reduced to dryness under vacuum and the material resuspended in a small volume of DCM. This was passed through an in-house prepared column of anhydrous sodium sulphate, into a pre-weighed vial. The DCM and material was reduced to dryness and weighed.

Methylation was performed according to Christie (1982). After redissolving the extract in DCM, approximately half the volume was removed and transferred into 5 mL reaction vials with Teflon lined lids. The extract was reduced to dryness, after which 2 mL of methanolic acetyl chloride was added (prepared by slow addition of acetyl chloride and methanol over ice). After ~ 12 hours reaction time (40°C in the dark), the solution was reduced to dryness, redissolved in a small volume of DCM and transferred to a 2 mL vial.

I 1.2. Analysis of lipids by Gas chromatography-mass spectrometry (GC-MS)

Methylated extracts were derivatised (*bis*-trimethylsilyltrifluoroacetamide; BSFTA, 1% TMS; 30-50 μL; 40°C; 0.5-1h) and analysed using a Trace 2000 Series gas chromatograph., fitted with an on-column injector and a fused high temperature silica column (60 m × 0.25 mm i.d.; 5% phenyl/95% methyl polysiloxane equivalent phase). Operating conditions and identification of sterols and fatty acids were followed according to Kiriakoulakis *et al*., 2002. Data was processes using the Xcalibur software. Quantificat80

ion of lipids was performed by comparison of the sample peak areas with the standard peak areas. A spread sheet, devised by Dr. Kiriakoulakis, was used to calculate final concentrations as:

$$\text{conc}(\text{ngL}^{-1}) = \left(\frac{A_{\text{lipid}}}{A_{\text{standard}}}\right) \times M_{\text{standard}} \times RF_{\text{standard}} \times \left(\frac{M_{\text{sample}}}{M_{\text{extract}}}\right) \Big/ V_{\text{filtered}}(1 - WF) \times 1000$$

where A_{lipid} and A_{standard} are the peak areas of the lipid and standard respectively, M_{standard}, M_{sample} and M_{extract} are the masses of standard (2 μg), sample and extract after methylation, respectively. RF_{standard} is the response factor of each lipid compared to the internal standard, V_{filtered} is the volume of seawater filtered and WF is the weight to area ratio (18.2; accounts for the mass of the filter overestimating the mass of lipids). The ratio lipids indicative of zooplankton to phytoplankton was calculated (Table H1).

Table I 1. Results from Lipid analysis of sample numbers 7, 8, 16 and 37 (see Table B3 for positions). The source, zooplankton or phytoplankton, lipid, retention time of compound, area of peak, response factor (RF) of sterol compared to cholestane and final concentrations (ng L^{-1}) and the zooplankton to phytoplankton lipid ratio are included.

FILTER NUMBER	SOURCE	COMPOUND	RETENTION TIME	AREA	RF cholestane	CONC Ng L^{-1}	Z/P RATIO
7	zoop	D5,22 C27 sterol	60.02	44176744	1.41	10.61	0.77
	zoop	D5,22 C27 sterol	60.48	259410400	1.41	62.30	
	zoop	D22 C27 sterol	60.74	24127918	1.41	5.79	
	zoop	cholesterol	61.51	1426450663	1.61	391.63	
	zoop	cholestanol	61.71	66229732	1.16	13.08	
	diatom	D5,22 C28 sterol	62.45	667890382	1.41	160.41	
	diatom	D22 C28 sterol	62.69	81790340	1.41	19.64	
	dinoflag	4 methyl c28 sterol	63.78	53799532	1.27	11.61	
	dinoflag	methyl cholesterol	63.97	216363383	1.61	59.40	
	phytop	4 methyl c28 d22	64.77	77496048	1.33	17.49	
	diatoms	D5, 22 C29 sterol	65.51	39358597	1.41	9.45	
	algae	ethyl cholesterol	66	258319618	1.61	70.92	
	algae	ethyl cholestanol	66.27	44516658	1.16	8.79	
	dinoflag	dinosterol	66.61	66793127	1.40	15.89	
8	zoop	D5,22 C27 sterol	60.02	8926960	1.41	2.86	1.11
	zoop	D5,22 C27 sterol	60.47	85146479	1.41	27.28	
	zoop	D22 C27 sterol	60.73	8415667	1.41	2.70	
	zoop	cholesterol	61.46	321992854	1.61	117.92	
	zoop	cholestanol	61.69	28477997	1.16	7.50	
	diatom	D5,22 C28 sterol	62.42	270630748	1.41	86.70	
	diatom	D22 C28 sterol	62.68	31912830	1.41	10.22	

	dinoflag	4 methyl c28 sterol	63.78	35019264	1.27	10.08	
	dinoflag	methyl cholesterol	63.97	5635856	1.61	2.06	
	phytop	4 methyl c28 d22	64.77	49150488	1.33	14.80	
	diatoms	D5, 22 C29 sterol	65.6	2893162	1.41	0.93	
	algae	ethyl cholesterol	66	106109605	1.61	38.86	
	algae	ethyl cholestanol	66.27	22254971	1.16	5.86	
	dinoflag	dinosterol	66.61	19816317	1.40	6.29	
16	zoop	D5,22 C27 sterol	60.01	43988284	1.41	6.47	1.66
	zoop	D5,22 C27 sterol	60.46	81067042	1.41	11.93	
	zoop	D22 C27 sterol	60.72	15308230	1.41	2.25	
	zoop	cholesterol	61.43	201326409	1.61	33.86	
	zoop	cholestanol	61.67	26112986	1.16	3.16	
	diatom	D5,22 C28 sterol	62.41	262543822	1.41	38.62	
	diatom	D22 C28 sterol	62.67	67989354	1.41	10.00	
	dinoflag	4 methyl c28 sterol	63.78	31709236	1.27	4.19	
	dinoflag	methyl cholesterol	63.97	2194478	1.61	0.37	
	phytop	4 methyl c29	64.76	42223325	1.33	5.84	
	diatoms	D5, 22 C29 sterol	65.46	94523000	1.41	13.91	
	algae	ethyl cholesterol	65.99	94523000	1.61	15.90	
	algae	ethyl cholestanol	66.26	31916297	1.16	3.86	
	dinoflag	dinosterol	66.61	22243992	1.40	3.24	
37	zoop	D5,22 C27 sterol	60.04	36479831	1.41	9.73	1.02
	zoop	D5,22 C27 sterol	60.5	236583658	1.41	63.12	
	zoop	D22 C27 sterol	60.71	24706702	1.41	6.59	
	zoop	cholesterol	61.48	556458541	1.61	169.72	
	zoop	cholestanol	61.7	23381922	1.16	5.13	
	diatom	D5,22 C28 sterol	62.45	613607426	1.41	163.72	
	diatom	D22 C28 sterol	62.69	41257953	1.41	11.01	
	dinoflag	4 methyl c28 sterol	63.78	80275198	1.27	19.25	
	dinoflag	methyl cholesterol	63.94	26988485	1.61	8.23	
	phytop	D5, 22 C29 sterol	64.61	52974927	1.41	14.13	
	diatoms	D5, 22 C29 sterol ?	65.52	22207519	1.41	5.93	
	algae	ethyl cholesterol	66.01	110972991	1.61	33.85	
	algae	ethyl cholestanol	66.27	7457613	1.16	1.64	
	dinoflag	dinosterol	66.62	5315755	1.40	1.41	

Appendix J

Removal of outliers for DON and DOP data set

J 1. Method for outlier exclusion

In order to investigate the outlying data within the DON and DOP data set, a correlation between DON and DOP was plotted for each station in all oceanic regions. The station was rejected if the R value was less than 0.5 (non-significant relationship) or if the slope of the regression (DON: DOP ratio) was less than 5. A list of the stations excluded are shown in Table J1. Note that 5 out of the 6 stations rejected are in the equatorial region.

Table J1. Station number, latitude (°N), longitude (°S), date, slope and R value associated with AMT 10 stations rejected from the data set.

Station number	Latitude (°N)	Longitude (°S)	date	slope	R value
8	-10.29	30.82	20/04/00	6.21	0.48
9	-6.34	28.99	21/04/00	1.53	0.03
11	1.94	25.26	23/04/00	19.44	1.34
12	6.10	23.45	24/04/00	-0.32	$6\ e^{-5}$
13	10.20	21.65	25/04/00	-66.1	0.66
16	23.53	21.96	29/04/00	-14.35	0.08

Regression analysis was performed on the DON DOP data with the outlying stations excluded (Figure J1).

Figure J1. Regression analysis between DON and DOP data collected during AMT 10, with outliers excluded.

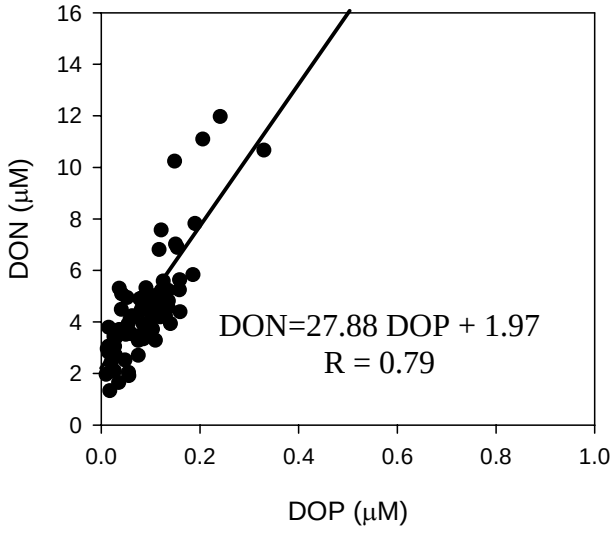

Both the slope (27.88) and R value (0.79) have increased when the outlying stations were removed (Table J1). In order to assess the distribution of DON and DOP, contour plots were re-drawn (Figure J2, a and b, respectively).

Figure J2. Latitudinal variation (35°S to 50°N) and depth (250m) variation in concentrations of (a) dissolved organic nitrogen (DON, µ) and (b) dissolved organic phosphorus (DOP, µM). Black circles indicate the depth of sampling. The white area indicates a region of no data.

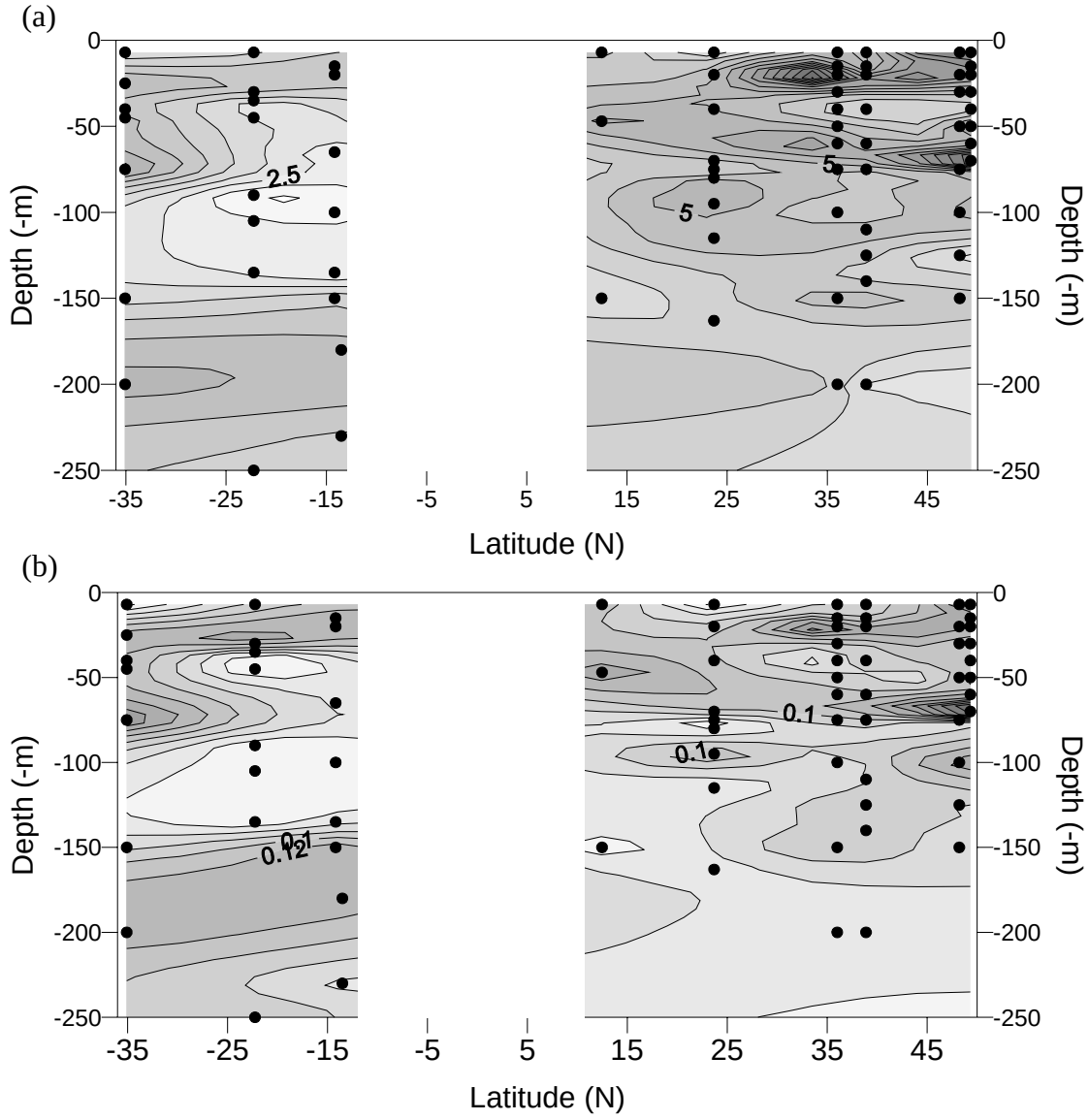

Despite assessing the AMT 10 DON and DOP data carefully, the only data to be excluded from the data set was in the equatorial Atlantic. At present, the author is uncertain why the data from this region is unusual.